Molecular mechanisms of cell wall lipid transport in *Mycobacterium tuberculosis*

by Nabiela Moolla

A thesis submitted to The University of Birmingham for the degree of Doctor of Philosophy

Institute of Infection and Microbiology

School of Biosciences

College of Life and Environmental Sciences

The University of Birmingham

September 2019

Abstract

Presently, Tuberculosis (Tb), caused by *Mycobacterium tuberculosis* (Mtb), remains a global health threat, particularly with the emergence of drug-resistant strains and HIV and Tb co-infection that challenges the current Tb treatment. Preventative measures and several anti-Tb drugs target the lipids of the mycobacterial outer membrane consisting of mycolic acids amongst an array of glycolipids. In Mtb, there are thirteen outer membrane lipid transporters designated mycobacterial membrane protein large (MmpL) proteins. These proteins are also involved in heme acquisition and possibly drug resistance and nitrosative stress adaptation, contributing to mycobacterial survival and pathogenesis. MmpL proteins are structurally and phylogenetically classed as resistance-nodulation-division (RND) transporters that use protonmotive force (PMF) to mediate substrate translocation. Unlike their RND counterparts in Gram-negative bacteria the structure and mechanisms of these transporters in Mycobacteria are yet to be determined. This work aimed to investigate the mechanism of three transport systems: MmpL3, MmpL7 and DrrABC (encoded by *mmpL3*, *mmpL7* and *drrABC* genes) using molecular modelling, genetics and lipid and protein biochemistry. *mmpL3* is essential for trehalose monomycolate (TMM) transport. While *mmpL7* is required for the export of two structurally related lipids, phthiocerol dimycocerosates (PDIM) and phenolic glycolipids (PGL). With the use of different membrane extraction agents, we were able to identify and propose improvements for the structural characterisation of MmpL3 and MmpL7. Molecular analysis and the MmpL7 homology model facilitated the identification of residues in the transmembrane and periplasmic domain that were verified by genetics and lipid analysis as critical for PDIM synthesis and transport. Even though MmpL7 is an RND transporter, there was no evidence of conserved PMF sites or a network forming proton translocation channel. Conveniently within the same genetic context is *drrC*, part of the *drrABC* cluster, that has a co-dependent relationship with *mmpL7* in PDIM transport. Interestingly the overexpression of

only *drrAB* genes function as a multi-drug ATP-binding cassette (ABC) pump. Structural modelling and molecular analysis revealed that *drrABC* encodes a heterodimeric ABC transporter where *drrB* and *drrC* encode the transmembrane spanning domains that create a pore or channel for substrate entry/exit, while *drrA* encodes the nucleotide binding domain for ATP binding and hydrolysis mediated transport suggesting a potential mechanism for PDIM/PGL transport. Genetics and biochemical analyses verified that all *drrABC* genes were required for PDIM transport across the membrane. Indeed, this work provides evidence that MmpL7 does not operate as an independent transporter but instead serves as a scaffold linking lipid synthesis and transport. The knowledge gained from such investigations related to MmpL proteins endeavours to aid in better understanding of anti-Tb drug development.

Declaration

The work in this thesis was carried out in the School of Biosciences at the University of Birmingham, UK, B15 2TT during the period of September 2015 to September 2019. The work in this thesis is original except where acknowledged by references.

No portion of the work is being, or has been submitted for a degree, diploma or any other qualification at any other University.

Acknowledgements

I want to express thanks and gratitude to my supervisor Dr. Apoorva Bhatt for giving the opportunity to pursue my PhD and for his wisdom, guidance, patience and understanding throughout my PhD. Also, to Prof. Gurdyal Besra, Dr. Luke Alderwick and Prof. David Minnikin, thank you for your innovative ideas and support towards my PhD.

Thank you to all past and present colleagues with whom I have shared this experience and developed strong friendships. You all have made this journey colourful.

I want to express my deepest gratitude to the Darwin trust of Edinburgh for the financial support that has made this PhD possible and for their incredible efficiency and support.

I want to extend a big thank you to the following people for their invaluable contribution to my PhD:

Dr. Robert Marshall (University of Birmingham) and Dr. Vassily Bavro (University of Essex) for help with molecular modelling.

Prateek Sharma, for all your help with the bacterial two-hybrid assays.

Pooja Sridhar for your expertise, technical help and pieces of advice on protein purification. I will always remember your kindness.

Katherine, Patrick and Ian, for help and support with protein purification.

Albel, Sid, Parisa and Natacha for technical assistance, support and personal advice.

From the University of Leeds, Dr. Vincent Postis for the *acrb* CD41(DE3) mutant strain and Dr Stephen Muench your continuous support and input has motivated me in trying times for which I am truly grateful and honoured.

Prof. Geoffrey Candy (University of the Witwatersrand) thank you for your support, faith (in me) and for pushing me beyond my fears and limitations.

I give the greatest thanks to Almighty, to my Family for their support and love that carried me through tough times and for motivating and reminding me of who I am, my Friends for your never-ending help and laughs, I am humbled and blessed.

Dedication

I dedicate this work to my family.

“Allah! There is no God but Him, the Alive, the Eternal. Neither slumber nor sleep overtaketh Him. Unto Him belongeth whatsoever is in the heavens and whatsoever is in the earth. Who is he that intercedeth with Him but by His leave? He knoweth that which is in front of them and that which is behind them, while they encompass nothing of His knowledge but what He will. His throne includeth the heavens and the earth, and He is never weary of preserving them. He is the Sublime, the Tremendous.” Holy Qur'an 2:255

Table of contents

List of figures

List of tables

List of abbreviations

aph	Gene encoding kanamycin resistance
BCIP/NBT	5-Bromo-4-chloro-3-indolyl phosphate/Nitro blue tetrazolium
AES	Allelic exchange substrate
Amp	Ampicillin
TA	Annealing temperature
bp/s	Base pair/s
°C	degrees Celsius
DNA	Deoxyribonucleic acid
dNTPs	Deoxyribonucleotide triphosphates
ESAT-6 or esxA	Early secreted Ag of 6 kDa
EB	Elution buffer
E.coli	*Escherichia coli*
EDTA	Ethylenediaminetetra acetic acid
sacB	Gene encoding levansucrase
lacZ	Gene encoding β galactosidase activity
GC	Guanosine Cytosine
HME	Heavy Metal Efflux
hr	hour
HCl	Hydrochloric acid
HAE	hydrophobe/amphiphile efflux
Hyg	Hygromycin
IgG	Immunoglobulin G

IPTG	Isopropyl β-D-1 thiolgalatcopyranoside
J	Joules
Kan^R	Kanamycin resistance
Kbp	Kilobase pairs
KDa	Kilodalton
KEGG	Kyoto Encyclopedia of Genes and Genomes
L	Ladder
λ	Lamda
TM	Melting temperature
mA	Milliampere
min	minutes
M	Molar
MP	Mycobacteriophage
BCG	*Mycobacterium bovis* BCG
Mtb	*Mycobacterium tuberculosis*
DDM	n-Dodecyl-β-D-Maltoside (DDM)
NC	negative control
NEB	New England Bioloabs
OADC	Oleic acid Albumin Dextrose Catalase
Overnight	ON
1D	one-dimensional
Ori	Origin of replication
PBS	Phosphate buffered saline

PCR	Polymerase Chain Reaction
Tween	Polyoxyethylene sorbitan monooleate
psi	pound per square inch
PDB	protein data bank
rpm	Revolutions per minute
RNase	Ribonuclease
RT	Room temperature
s	seconds
NaCl	Sodium chloride
SDS	Sodium dodecyl sulfate
SMA	Styrene-co- maleic acid polymer
T	Temperature
2D	Two-dimensional
UV	Ultraviolet
V	Voltage
v/v	Volume/volume
w/v	Weight/ volume
WHO	World Health Organization

Chapter 1: General introduction

Chapter 1: General introduction

1.1. *Mycobacterium tuberculosis* (Mtb)

Mycobacteria is a class of Actinobacteria, and relatives include *Corynebacterium*, *Nocardia*, *Gordonia*, and *Rhodococcus*. These bacteria are classified as Gram-positive peptidoglycan containing bacteria, but cannot be detected with the traditional Gram stain method using crystal violet due to their hydrophobic outer layer containing mycolic acids and diverse glycolipids (1,2). Instead Mycobacteria are detected by lipid soluble dyes that penetrate the waxy layer and avoid acid-alcohol decolouration, referred to as acid fastness (2). Several pathogens belong to the mycobacterial group. These include *Mycobacterium leprae* causing leprosy, *Mycobacterium ulcerans* responsible for Buruli ulcer disease, *Mycobacterium bovis* responsible for bovine tuberculous in cattle and *Mycobacterium tuberculosis* (Mtb) the causative agent for human tuberculosis (3).

At present the origin of Mtb is unknown. It was initially thought that *M. bovis* was the ancestral causative agent for tuberculosis (4). Instead, data from whole genome sequencing and lipid analysis of well-preserved ancient skeletons and bison revealed that Mtb was an animal disease (5,6) and *M. bovis* and Mtb come from a common mycobacterial ancestor (5–7) and have co-evolved independently in their respective hosts (7).

However, it was only in 1882 that Robert Koch identified the bacillus *Mycobacterium tuberculosis* (Mtb) as the causal agent of tuberculosis (Tb) leading to death in the human host (8). Before the characterisation of Tb, works carried out by Benjamin Marten (1722) and Jean-Antoine Villemin (1865) demonstrated the contagious nature of Tb, while the description of the tubercle was made as early as 1819 by René Laennec (9). Moreover, it was Albert Calmette and Camille Guérin that in 1905 produced the bacilli Calmette-Guérin (BCG) vaccine (9). At

present this century old vaccine remains the only preventative measure of Tb. All of these early studies laid the foundation of present-day understanding of the Tb bacilli, infection and disease.

Today Tb remains a global problem that continues to plague human survival, as it remains one of the highest global health threats as declared by the World Health Organization (WHO) (10). In 2017 about 10 million people developed Tb, predominantly in Africa, Asia and Middle Eastern countries. Of this population, approximately 9% were also HIV positive, while 20.6% (new incidences and previously treated cases) had multidrug-resistant (MDR) Tb of which 8.5% were extensively drug-resistant (XDR) (10). These alarming statistics are attributed to numerous factors (discussed below) such the emergence of MDR and XDR strains, no effective preventative therapy, current chemotherapeutic regimen ineffective against drug-resistant strains, various anti-Tb drugs that are either currently in clinical trials, or their mode of action is unknown or lack efficacy required for shortened treatment, and the lethal synergy between Tb and HIV (10).

1.2. *Mycobacterium tuberculosis* (Mtb) infection in the human host

Predominantly, the site of Tb infection is the lungs causing intra-pulmonary Tb, but Tb can infect the lymphatic system, bones, the nervous system, and organs causing extra-pulmonary Tb (11). Intra-pulmonary infection is initiated by the inhalation of infectious aerosols coughed or sneezed into the environment by an individual with active Tb (11,12). Alveolar macrophages engulf the bacilli and stimulate the production and chemotaxis of antigen-presenting dendritic cells and macrophages via cytokines and chemokines (11,12). In turn, these immune cells exhibit the bacilli as an antigen which induces a pro-inflammatory response promoting T cells amongst an array of immune cells to migrate to the site of infection (11,12). The variety of immune cells aggregate and form an organised structure containing the bacilli, known as a granuloma, a hallmark of Mtb infection (11,12).

T cells release interferon-gamma (INFγ) that activates macrophages fusing the phagosome and lysosome (13,14), resulting in the killing of the resident bacilli by acidification and reactive nitrogen and oxygen species (RNS and ROS) (13,14). Mtb bacilli prevent acidification by inhibiting phagosome- lysosome fusion via the synthesis of ammonia, presence of cell wall lipids and isoprenoid molecules and interference of the increase in hydrogen ions (H^+) by the host proton-ATPase pump (13,14). Also, Mtb bacilli within the granuloma are not killed by the various stresses such as hypoxia, low pH, starvation, RNI and ROS (11,12). Ironically, these stresses induce a metabolic shift via the DosR/S/T regulon which consists of about 47 genes regulating fatty acid metabolism (15–17). The metabolic shift assists bacilli in entering into a non-replicating state defined as dormancy (15,17). This transition ensures the prolonged survival of Mtb within the host despite its harsh environment (11,12,17). This state represents 95% of latent individuals with Tb that present no disease symptoms (11,12,14,15).

Intra-phagosomal bacilli use the granuloma as a protective niche and can persist within the host until the granuloma is destroyed (11,12,14,15). As the innate immunity develops, intra-phagosomal bacilli are killed, causing necrosis at the centre of the granuloma (11,12,14). Continuous decay leads to the liquefication of the granuloma (11,12,14). Also, when the host immune system is compromised due to ageing, or exposed to another infection or developing a disease, it can no longer maintain the granuloma structure (11,12,14,15) . This results in free bacilli disseminated systemically and into the lung airways, which represents the 5% of individuals that have active Tb (11,12,14,15).

1.3. Available Tb treatment

1.3.1 Tb control

Tb was kept under control in the 1950's due to the discovery of antibiotics: isoniazid (1952), pyrazinamide (1954), ethambutol (1962) and rifampicin (1963) which is still presently used in

the Tb regimen known as Directly Observed Treatment, Short-course (DOTS) (18). The drugs used in DOTS are termed first-line drugs (Table 1-1) as they remain the most effective against active Tb with a short treatment period (18).

Briefly, DOTS is a six-month-long continuous drug treatment that includes two months of ethambutol, pyrazinamide, isoniazid and rifampicin followed by four months of isoniazid and rifampicin (18). Isoniazid requires activation by KatG, a catalase-peroxidase enzyme and reacts with nicotinamide dinucleotide (NAD) to form an isoniazid-NAD adduct that inhibits InhA, an enoyl acyl carrier protein reductase involved in the synthesis of mycolic acids (demonstrated *in vivo*) and dihydrofolate reductase required for nucleic acid biosynthesis (19). These adducts have also been reported to have effects on other key fatty acid synthase enzymes *in vitro* namely: KasA, a β-ketoacyl acyl carrier protein synthase and MabA, a β-ketoacyl acyl carrier protein reductase involved in mycolic acid biosynthesis (19). This drug remains the most efficient bactericidal agent against replicating bailli (20). Mutations to *katG* and *inhA* genes confer isoniazid resistance as these genes encode the activation enzyme KatG and the direct target of isoniazid, InhA, respectively (19). From the analysis of isoniazid resistant strains, mutations in *katG* and *inhA* genes occur more frequently than any other mutation/s associated with isoniazid resistance (21).

Ethambutol is activated by EthA, a monooxygenase and the active form of this drug targets EmbCAB, arabinofuranosyltransferases that play a critical role in arabinogalactan synthesis (20). Arabinogalactan is a cell wall component and is required in the formation of the mycolyl-arabinogalactan-peptidoglycan core (mAGP) and lipoarabinomannan (LAM) (20). Therefore, the abrogation of arabinogalactan causes a major disruption in the organisation of the cell wall and increases the permeability of the mycobacterial cell wall (20). This drug is bacteriostatic against intra- and extracellular, replicating bacilli and resistance can be mapped to *embCAB*

and *embR* genes that encode EmbCAB, arabinofuranosyltransferases and its transcription regulator, EmbR respectively (21).

Rifampicin abolishes gene transcription by targeting the β-subunit of DNA-dependent RNA polymerase and as such is bactericidal against replicating and non-replicating bacilli (20). Rifampicin resistance is due to mutations in the *rpoB* gene that encodes the DNA-dependent RNA polymerase (21). Whereas, pyrazinamide is another prodrug that requires activation by pyrazinamidase and the exact mode of action has not yet been determined (20). However, it has been reported to create a highly acidic environment that interferes with the function of proteins, membrane potential and to some extent has been reported to inhibit fatty acid synthase enzymes in mycolic acid synthesis (20). This agent is bactericidal and bacteriostatic against non-replicating bacilli and resistance to pyrazinamide is due to mutations in the *pncA* gene that encodes pyrazinamidase (21).

DOTS aims to improve patient adherence to the chemotherapy, prevent relapse and avoid resistance to these first-line drugs by supervision (18). However, due to numerous reasons including poor implementation, the length of the program and restricted access to the treatment, have led to patient noncompliance, which in turn resulted in acquired drug resistance (18)

The emergence of drug-resistant strains such as MDR, XDR and totally drug-resistant (TDR) threatens the possibility of Tb control, as drug-resistant Tb can be transmitted to healthy individuals developing primary drug-resistant disease (18). MDR is described as resistance to isoniazid and rifampicin, which are front line drugs, while XDR is defined as bacilli resistant to front line (isoniazid and rifampicin), and to any of these second-line drugs: any fluoroquinolone and amikacin, or capreomycin, or kanamycin (Table 1-1) (18). MDR and XDR resulted in TDR, which are resistant Mtb bacilli to any combination of first-line and second-line drugs (18). DOTS plus program was implemented to combat drug resistance by combining

first-line and an array of second-line drugs (22). This strategy was not effective in treating drug resistance as second line drugs are more toxic but with reduced efficacy and hence required prolonged and expensive treatment (22).

A further complication to the current Tb dilemma is the lethal synergy of Tb and the Human Immuno-virus (HIV) co-infection (10). Areas burdened with high rates of HIV are also areas with increased rates of new Tb incidences (10). HIV reduces host immune cells required for the containment of Tb infection while, Mtb bacilli provide replication sites for HIV infection (23,24). Besides, another concern is the drug-drug interactions between treatments for Tb (rifampicin) and HIV (anti-retroviral drugs) that could potentially pose as threats to patients (25).

These alarming factors motivate for new drugs to be generated to control Tb effectively and its drug-resistant variants without nullifying anti-retroviral therapy. Third line drugs (Table 1-1) are already being evaluated in clinical trials to treat MDR and potentially XDR, that aim to provide effective treatment of active and latent Tb in a shortened period (18,26). Recently, Bedaquiline and Delamanid have been approved to treat drug-resistant Tb as in Table 1-1 (27).

Intriguingly, like Delamanid, a few promising drug candidates in phase two clinical trials (Table 1-1) are also aimed at inhibiting the synthesis of the characteristic mycobacterial cell wall (26,27). Pretomanid and Delamanid are both from the same class of nitroimidazoles and are prodrugs that require bio-reductive enzymatic activation for efficacy (26,27). Both inhibit mycolic acid synthesis making treatment specific to mycobacteria. While a few targets are suspected none have been determined (26,27). These anti-drug Tb drugs are bactericidal in replicating and non-replicating Mtb strains, while Delamanid is also effective against drug-sensitive and drug-resistant Mtb (26,27).

To improve the efficacy of ethambutol, new ethylenediamine analogues were generated and tested for low cytotoxicity and inhibition of Mtb growth *in vivo* (28). Of the thousands of analogues screened, SQ109 was discovered to be more potent than ethambutol with low cytotoxicity (28). Interestingly SQ109 and ethambutol, both ethylenediamine analogues, have different chemical structures, efficacy and modes of action (29). SQ109 has been shown to inhibit MmpL3 responsible for the export of trehalose monomycolates (TMM) required for the formation of the mAGP core and trehalose dimycolates (TDM) (30–32). SQ109 resulting in defective TMM export is bactericidal, and its activity is increased together with isoniazid, rifampicin, ethambutol, streptomycin and bedaquiline against MDR- and XDR- Tb strains and has low mutation rate *in vivo* (29).

Arabinogalactan is another vital constituent of the mycobacterial cell wall that is inhibited by benzothiazinone (BTZ) drugs such as Piperazinobenzothiazone (PBTZ)-169, BTZ043 and TCA1 via inactivation of DprE1 and are bactericidal activity against MDR-TB strains (26,27). Pathways contributing to the mycobacterial cell wall are attractive drug candidates that promise to treat drug-sensitive/resistant and active/latent Tb and shorten chemotherapy with fewer side effects.

Table 1-1: Anti-Tb drugs used to control Tb. [Adapted: (18,20,26,27,33)]

Class of drugs	Cell wall synthesis			Protein synthesis	RNA synthesis or transcription	DNA replication	Metabolism	Transport
	Mycolic acid	Arabino-galactan	Peptido-glycan					
First-line	Isoniazid	Ethambutol			Rifampicin, Rifapentine Rifabutin		Pyrazinamide	
Second-line	Thioamides		Terizidone	Aminoglyco-sides Polypeptides Linezolid	Fluoroquinolones	Fluoroquino-lones	Cycloserine Para-amino salicylic acid	
Third-line			Meropenem Clavulanate Amoxicillin Imipenem Cilastatin	Clarithromycin				Clofazimine
Drugs in clinical trials	Pretomanid	PBTZ169 BTZ043 TCA1			Sutezolid Delpazolid		Pretomanid Q203	SQ109
Approved drugs	Delamanid						Bedaquiline	

1.3.2 Prevention

The only preventative measure against Tb is the Bacille Calmette-Guerin (BCG) vaccine derived from an attenuated *Mycobacterium bovis* strain. The BCG vaccine is an inexpensive, safe and the most administered human vaccine in the world but it only protects infants from Tb meningitis (34). To date, the mechanism of protective immunity of the BCG vaccine is unknown despite it being a century old and successfully administered globally. This vaccine displays highly variable efficacy in adults but does not protect adults against Tb infection (35,36).

The failure of BCG is because BCG does not fully represent Mtb in the host (37). As such, 23% of the known T cell epitopes evolutionarily conserved in the Mtb complex were not found in BCG (37). Thus, BCG is not fully equipped with all the Mtb virulence factors, despite the high genetic similarities between *M. bovis* and Mtb as they are thought to have a common evolutionary precursor (37). Further deletion of several genes associated with virulence, contained in loci designated as regions of differences (RD), was as a result of the attenuation process of *M. bovis* (37). RD1 was one of these deleted regions, encoding a protein secretion system Esx1 that is responsible for ESAT6 secretion, a known virulence factor that modulates the host innate and adaptive immune responses (37). The inability of BCG to mount an immune response similar to Mtb infection leads to failure in promoting protection against Mtb (37).

MTBVAC is the first live attenuated safe Mtb vaccine in history that successfully passed phase one in clinical trials (38). This vaccine was engineered by deleting *phoP* and *fadD26* in Mtb. *phoP* is part of the PhoPR two-component system that regulates two transport systems such as Esx1 and twin-arginine translocation export pathway in the secretion of ESAT6 and components of the Ag85 complex respectively, the biosynthesis of acyltrehaloses glycolipids of the outer mycobacterial membrane and induces Whib6 expression (37,38). While, *fadD26*

is involved with phthiocerol dimycocerosates (PDIM) biosynthesis another antigenic glycolipid from the outer membrane of Mtb (39–41). This Mtb based vaccine offers enhanced protection against Tb better than BCG as it expresses its native antigenic factors required for host recognition and eliciting cell-mediated immune responses but is not pathogenic (37,38).

Alternatively, in the last ten years, many attempts have been made to strengthen the BCG vaccine by a two-step enhancement strategy (42). This strategy serves uses BCG and another vaccine known as a booster, to achieve protection against Tb (42). Potential candidates of booster vaccines include the expression of virulence factors namely: the Esx family of proteins, the Antigen 85 complex (Ag85), and proline-proline-glutamate (PPE) family (43–46). Andersen and Kaufmann (42) were the first to produce vaccines that consist of a mixture of Esx, Ag85 and PPE proteins that are packaged in an empty (no DNA) viral vector, that are currently being assessed in clinical trials. MVA85A was the first vaccine expressing the A subunit of Ag85 that passed the clinical trial phase one but failed to prevent BCG vaccinated infants from Tb infection or disease (47). Another combination strategy was shown to be a promising potent booster vaccine known as BM, which consists of five Esx fused proteins (displaying a high sequence identity to EsxB) and was shown to provide enhanced protection than Ag85A, PPE18, and EsxB that are being evaluated in clinical trials (48).

1.4. Mycobacterial cell wall

The mycobacterial cell wall is a natural defence mechanism that resists a diversity of damages from drugs and the host due to its complex architecture (49,50). The cell wall, as in Figure 1-1 consists of the capsule, myco-membrane and plasma membrane (51,52). The mycobacterial capsule layer is heterogeneously species-specific and mainly consists of polysaccharides, proteins and a small proportion of lipids making it hydrophilic (51,52). The myco-membrane can be further divided into the outer- and inner- membrane and consists of a large variety of

complex lipids, polysaccharides and some proteins that are non-covalently and covalently bound, respectively (51,52). The plasma membrane is the inner compartment of the cell wall and comprises of a phospholipid bilayer consisting of lipids on the outer side (hydrophobic layer) and polysaccharides on the inside (hydrophilic layer) which have yet to be identified (53).

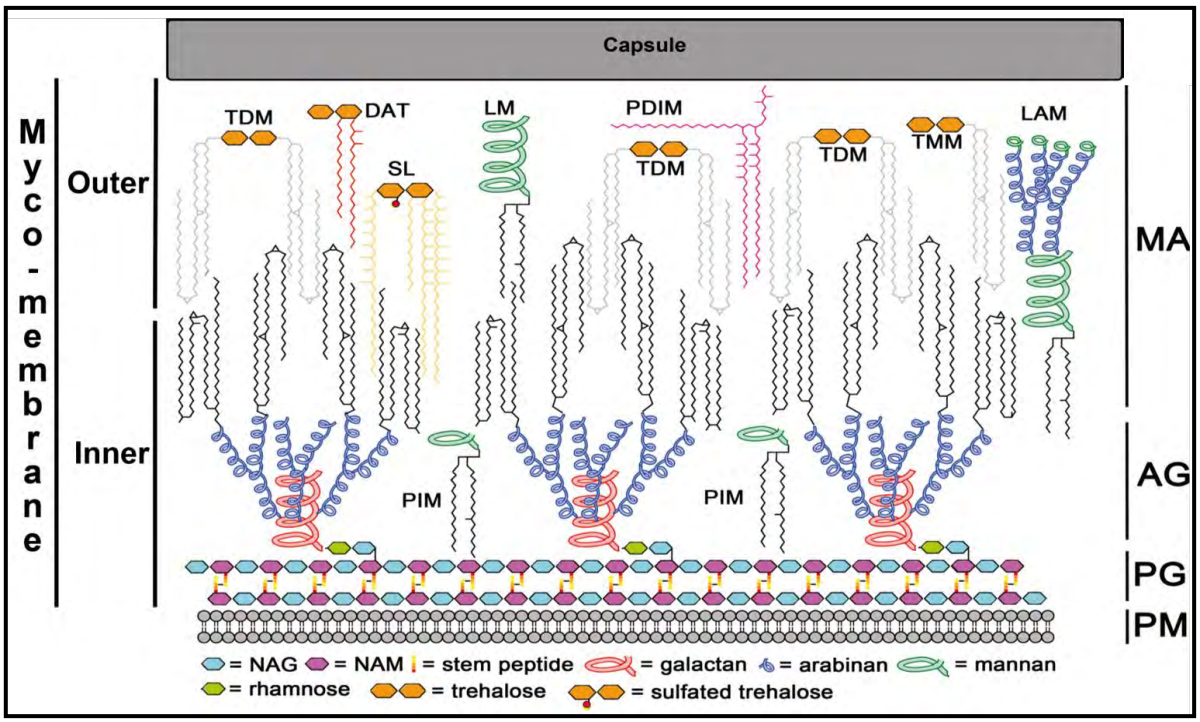

Figure 1-1: The mycobacterial cell wall. The myco-membrane is divided into outer and inner membranes that consist of unbound lipids and bound mycolic acids (MA)- arabinogalactan (AG)- peptidoglycan (PG) respectively, while the phospholipid bilayer represents the plasma membrane (PM) (retrieved and adapted with permission from Dr. Luke Alderwick, University of Birmingham).

Much of the mycobacterial genome is dedicated to lipid production and degradation (54), which explains why a large proportion (up to 60%) of the dry weight of Mtb consists of lipids (53,55,56). In particular, mycolic acids are the main constituents of the myco-membrane giving the cell wall its impeccable hydrophobicity and rigidity, unique to mycobacteria (Figure 1-1) (49–52,57,58). The inner membrane is a covalently linked complex comprising of mycolic acids bound to arabinogalactan, which is in turn anchored to peptidoglycan (Figure 1-1) (49–

52,57,58). Peptidoglycan is an organised layer of chains alternating in N-acetylglucosamine residues (NAG) and N-acetyl muramic acids (NAM), including to some extent N-glycolyl muramic acids (NGM), which are cross-linked with stem peptides (51–53,55,59). The coiled galactan domains of mycolates bound to arabinogalactan at the non-reducing end link with the coiled glycan domains of peptidoglycan by rhamnose-N- acetylglucosamine-phosphodiester linker units (59). This mesh-like structure is termed as the mAGP core and forms a hydrophobic complex for surface-exposed lipids of the outer membrane (59).

1.5. Constituents of the outer membrane lipids

Surface exposed lipids are non-covalently bound glycolipids (Figure 1-1) that are easily extractable (53,55). They are diverse and abundant in mycobacteria, but collectively they have antigenic and physiological properties that make mycobacteria pathogenic and resistant to attack, amongst other factors (52,53,55,57). These lipids are complex with long fatty acid branched chains, representative of successive cycles of extension and modification catalysed by numerous enzymes such as (but not limited to) polyketide synthase (Pks), fatty acyl amp-ligase (FadD), acyltransferase (Pap), and methyltransferases (52,53,55,57,60). The information presented in this section is based on several excellent reviews from (52,53,55–58,60). Only a few outer membrane lipids will be introduced as these are the lipids relevant in this study and have been divided into four groups, namely: mycolyl glycolipids, trehalose esters, phthiocerol family and other lipids.

1.5.1 Mycolyl glycolipids

Mycolic acids are long-chain α-branched β-hydroxy fatty acid chains made from acetyl- and malonyl- CoA generated by the tricarboxylic acid cycle (TCA) (56,57,60,61). These substrates processed by enzymes of fatty acid synthase system (FAS) I form straight fatty acids (C_{18-26}) used as building blocks for other glycolipids of the cell wall (62). Also, these fatty acids are

extended by repetitive cycles of elongation carried out by FASII into meromycolate chains (C_{60-90}) (63). Further modification of meromycolate fatty acids include the condensation of straight fatty acids and meromycolate chains by Pks13 generating oxo-mycolic acids that are reduced by a reductase (Rv2509) to create mature hydroxy- mycolic acids (57,58,61,64,65).

In Mtb, there are three classes of mycolic acids, namely α-mycolates that represent non-oxygenated mycolates and methoxy and keto-mycolates that are both oxygenated mycolates (Figure 1-2A). Various modifications to these oxygenated and non-oxygenated mycolates are species-specific, and hence identification of mycolic acids contributes to taxonomic identification (57,60). These mycolates are integral for the inner myco-membrane mAGP (mycolyl-arabinogalactan–peptidoglycan) core while esterified forms constitute the outer membrane (57,60).

The simplest mycolate in mycobacteria is glucose monomycolate (GMM) that is glucose bound to mycolic acids that occur in various proportions (56–58,60). Mycolates can be esterified to trehalose, forming trehalose monomycolates (TMM) and trehalose dimycolate (TDM) as in Figure 1-2B. TMM and TDM are found in all mycobacterium species, unlike the other acylated trehaloses (described below) that are species-specific, as they are a critical component of the outer membrane (56–58,60). TMM components, trehalose and mycolic acids, are synthesised and assembled in the cytoplasm from where TMM is transported to the periplasm by a dedicated transporter *mmpL3* (30,66–68). TMM, the precursor of TDM, provides a source of mycolic acids that are bound to arabinogalactan to form the cell wall core (56–58,60).

The Antigen (Ag) 85 ABC mycolyltransferase complex (also known as FbpABC) is involved in the synthesis of TDM and GMM and arabinogalactan mycolation using TMM as a mycolyl donor (69–73). The specific activity of Ag85A involves the transfer of the mycolyl group from TMM to glucose forming GMM when glucose is readily available (73). Alternatively, TMM

is broken down into trehalose and mycolic acids that are covalently attached to the reducing end of arabinogalactan (73). While, Ag85C is responsible for transferring a mycolyl group from one TMM to another, producing TDM (72), and no activity has been assigned to Ag85B (53,55). Individual deletion of each of the genes encoding the Antigen 85 ABC mycolyltransferase complex indicates that each gene is dispensable for Mtb growth, but deletion of all genes is lethal (53,55,74). This enzymatic complex maintains the proportions of TDM, TMM and GMM for successful host immune modulation and evasion (53,55–58).

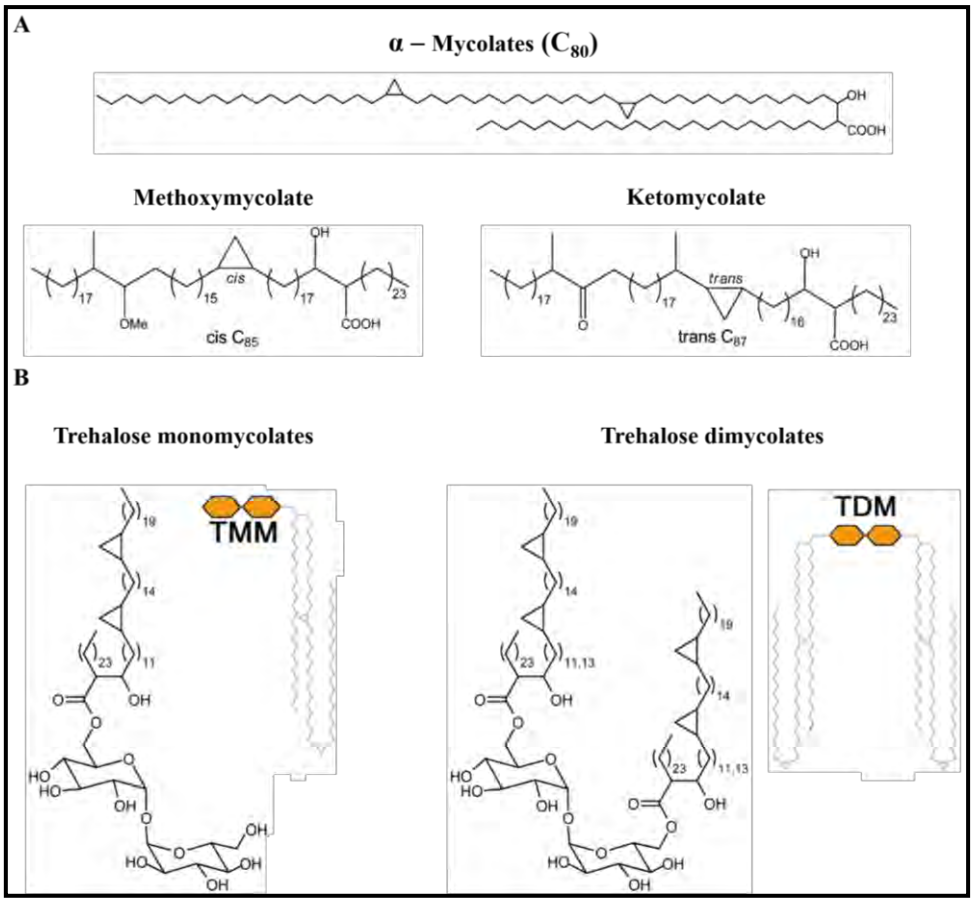

Figure 1-2: Mycolyl glycolipids. A) Mycolic acids and B) Mycolic esters trehalose monomycolates (TMM) and trehalose dimycolate (TDM). [Adapted: (60)].

1.5.2 Trehalose esters

This classification includes di-, tri-, and penta-acyltrehaloses (DAT, TAT and PAT), sulfolipids (SL) and lipooligosaccharides (LOS) as in Figure 1-3 (53,55). These lipids have

been clustered together because they are synthesised, regulated and transported in very similar ways, as discussed below (53,55,60). These lipids are all trehalose esterified to straight fatty acid chains (minor constituents) and then extended by different types and combinations of poly-methyl branched fatty acid units which represent major constituents of these glycolipids (53,55,60,75).

DAT, TAT and PAT can be separated by the number of their acyl groups and mycobacterial species can be distinguished by the composition of their acyl groups (53,55,60,75). DAT refers to two acyl groups, TAT has three acyl groups and PAT has five groups (53,55,75,76). As DAT is the precursor of TAT and PAT, it can be found in the pathogenic Mtb complex [Mtb, *Mycobacterium africanum* (*M. africanum*), *Mycobacterium bovis* (*M. bovis*)] (77) and non-pathogenic *Mycobacterium fortuitum* (*M. fortuitum*) species (78). However, acyltrehaloses from pathogenic Mtb strains differ structurally from *M. fortuitum* as the acyl groups consist of mycosanoic and mycolipenic (phthienoic) acids, types of multi-methyl branched fatty acid (79,80). Besides, there are several variations of TAT only associated with *M. fortuitum* (81).

DAT is synthesised in the cytoplasm and serves as precursor to PAT (Figure 1-3), generated in the periplasm (53,55,60,75,82). First, activated fatty acyl adenlyates supplied by FadD21 (82) are extended with multi-methyl branched fatty acids by Pks3/4 to produce mycosanoic and mycolipenic fatty acid chains (83). After that, PapA3 esterifies a palmitoyl group to the trehalose core creating trehalose 2-palmitate (T2P), and following this performs another esterification between the mycosanoic and mycolipenic fatty acid products and T2P (82,84) generating DAT. Lastly, an acyltransferase, (cutinase-like hydrolase protein 2) Chp2 is responsible for modifying DAT into TAT and PAT (82,85). Conflicting evidence exists as to whether PAT and to some extent TAT is generated in the periplasm (82) or cytoplasm (85) which remains to be determined.

SL are lipids with a sulfated trehalose core with four acyl groups, one contains a saturated fatty acid (palmitic or stearic acid) while the other three consists of multi methyl-branched phthioceranic and hydroxyphthioceranic acids (Figure 1-3) (53,55,60,86). These glycolipids are exclusively found in Mtb (86). The sulfotransferase (Stf0) initialises SL biosynthesis (87) by adding sulphate to trehalose (T2S) that is acylated with a straight fatty acid chain to form a monoacyl intermediate (SL_{659}) by PapA2 (88,89). In parallel, an activated substrate from FadD23 (90) is extended with multi methyl-branched fatty acids by Pks2 (91). SL_{659} and the multi methyl-branched phthioceranic and hydroxyphthioceranic product are esterified to form SL_{1278} by PapA1 (88,89). To complete the structure of $SL_{1278,}$ this precursor undergoes two rounds of sequential acylation by another type of acyltransferase, (cutinase-like hydrolase protein 1) Chp1 to produce SL (92).

As with all trehalose esters, the core of LOS is trehalose but with many groups consisting of oligosaccharides and multi-methyl branched fatty acids making these lipids highly polar (Figure 1-3) (53,55,60). They are produced by pathogenic mycobacteria namely, *Mycobacterium kansasii* (*M. kansasii*) (93,94), *Mycobacterium canetti* (*M. canetti)* (95), *Mycobacterium malmoense* (*M. malmoense*) (96), *Mycobacterium marinum* (*M. marinum*) (97) and non-pathogenic mycobacteria including *Mycobacterium smegmatis* (98,99) and *Mycobacterium gastri* (*M. gastri*) (100). Common to all species in mycobacteria is the polyacylated trehalose core of LOS, but the composition and length of the oligosaccharides display considerable variation between mycobacterial species (53,55,60). For instance, the presence of N-acylkansosamine a long chain sugar was restricted to *M. kansasii* (60,97,101), two monosaccharides were unique identifiers in *M. marinum* and only one novel monosaccharide was exclusive to *M. gastri* (100).

Similar to the poly-methyl branched lipids in this category, this class of lipids also uses several enzymes to produce the backbone of LOS identified in *M. smegmatis* and *M. marinum* (53,55). The genetic organisation of the LOS biosynthetic cluster in *M. smegmatis* is conserved in *M. marinum*. Mtb H37Rv is deficient in LOS as it only contains a third of the genes in the LOS biosynthetic cluster of *M. marinum* (102). FadD25 is required to provide activated acyl-adenylates for the further extension with methylmalonyl- CoA by Pks5 resulting in a polymethyl-branched fatty acid product (103–106). PapA4 esterifies the polymethyl-branched fatty acid on to a sugar group creating the glycan backbone of LOS production (106), which is further extended and modified by several methyltransferases and glycosyltransferases to produce classes of LOS (53,55).

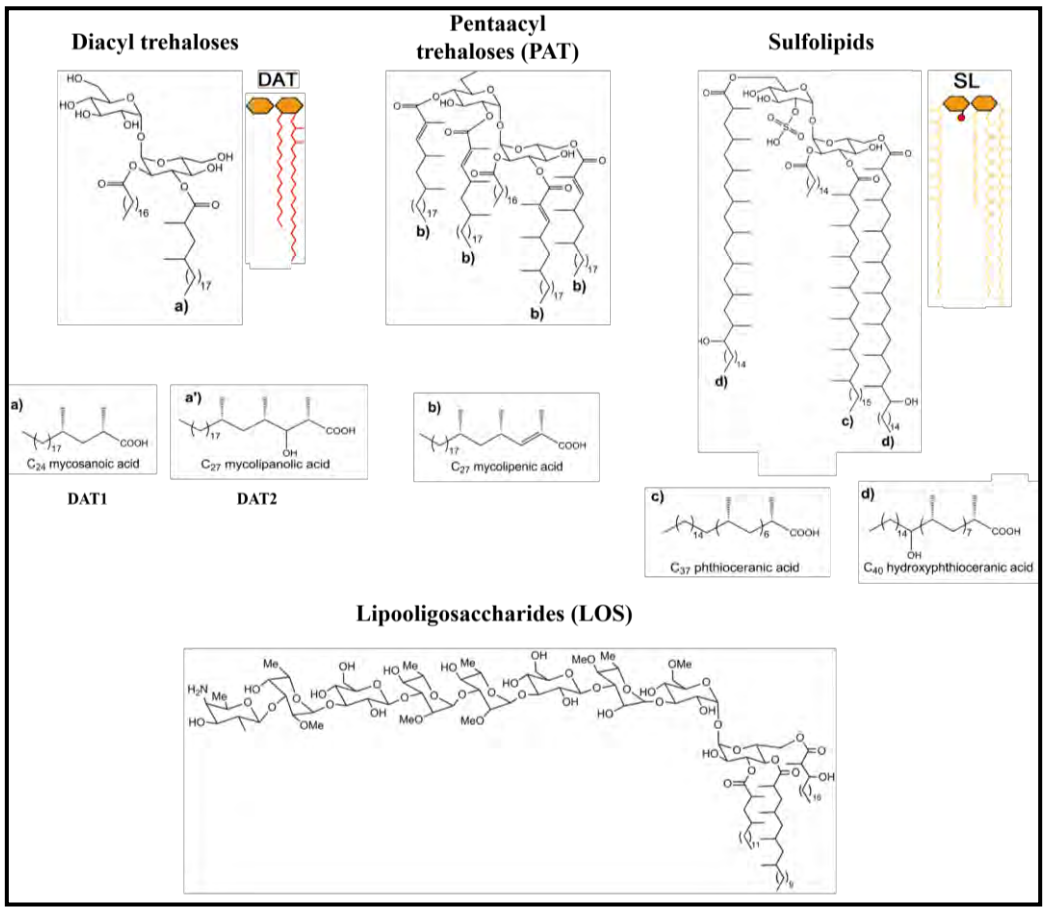

Figure 1-3: Acyl trehalose esters. Di- and penta-acyltrehaloses (DAT/PAT), sulfolipids (SL) and lipooligosaccharides (LOS). [Adapted: (60)].

1.5.3 Phthiocerol family

Phthiocerol dimycocerosates (PDIM), phthiocerol diphthioceranates (PDIP) and phenolphthiocerol dimycocerosates or phenolic glycolipids (PGL) are constituents of this family of lipids with a highly hydrophobic core of β-diols or phthiocerol as in Figure 1-4 (53,55,60,107). Phthiocerol is elongated with two units of long-chain multi-methyl fatty acids that exist in two forms, dimycocerosates (PDIM) or diphthioceranates (PDIP). PDIM is associated with strains in the Mtb complex, while PDIP is only in *M. ulcerans* and *M. marinum* (53,55,60,107).

The PDIM locus spanning over ~73 Kbp, encodes genes dedicated to PDIM and PGL biosynthesis and translocation to the outer membrane (39,40). In this locus, biosynthetic enzymes include Pks enzymes (PpsA, PpsB, PpsC, PpsD, PpsE, Mas, Pks15/1), reductases (Rv2951, Rv2953), methyltransferases (Rv2952), Amp ligases (FadD26, FadD28, FadD22 and FadD29), an acyltransferase (PapA5) and a thioesterase (TesA). Briefly, for PDIM synthesis, FadD26 and FadD28 activate short, or monomethyl branched fatty acid chains as acyl adenylates (103) added onto Pks enzymes, PpsA-E (108) and Mas (109,110) for phthiodiolone and mycocerosic acid production. Phthiodiolone is further processed by a keto-reductase (Rv2951) and a methyltransferase (Rv2952) to form phthiotriol and phthiocerol that are esterified to dimycocerosates by PapA5 to generate phthiodiolone dimycocerosates (DIM B), phthiotriol dimycocerosates and phthiocerol dimycocerosates (PDIM or DIM A) (111–116).

PGL is only present in certain strains of Mtb/ Mtb complex, like ‘canettii’ and a few of the Beijing strains, also in *M. bovis*, *M. bovis* BCG, *M. microti*, *Mycobacterium pinnipeddii* (*M. pinnipeddii*) and *M. africanum*, *M. kansasii* and *M. gastri*, *M. marinum* and *M. ulcerans* (117,118). The precursor of the phenolic moiety of PGL is *p*-hydroxybenzoic (*p*-HBAD) acid produced from chorismate by a lyase (Rv2949c) (119) that is activated by FadD22 and, for

strains with an intact *pks15/1*, extended to form a glycosylated long fatty acid chain with methylmalonyl CoA (120,121). FadD29 then activates this chain and loads it onto PpsA (120–124).

The extension of the glycosylated long fatty acid chain by PpsA-E and downstream processes to form PGL carried out exactly as described for PDIM synthesis and as such these lipids share a common lipidic core (120–124). In both processes, TesA (125) is required to cleave off PDIM and PGL from PpsE where PapA5 (112) is needed to complete the last step of PDIM and PGL production. Since Mtb has a 7 bp deletion in *pks15/1*, resulting in a frame-shift mutation (117,126), extension of *p*-HBAD critical for PGL biosynthesis does not occur (120–124). Instead, saccharide units can be added to *p*-HBAD by glycosyltransferases and methyltransferases and *p*-HBAD and its glycosylated forms can be found in the culture filtrate (127,128). The number of saccharide units in *p*-HBAD is species-specific with *M. kansasii* containing four saccharides, '*M. canettii'*/Mtb Beijing has three saccharides, and *M. bovis* has only one saccharide unit (Figure 1-4) (60).

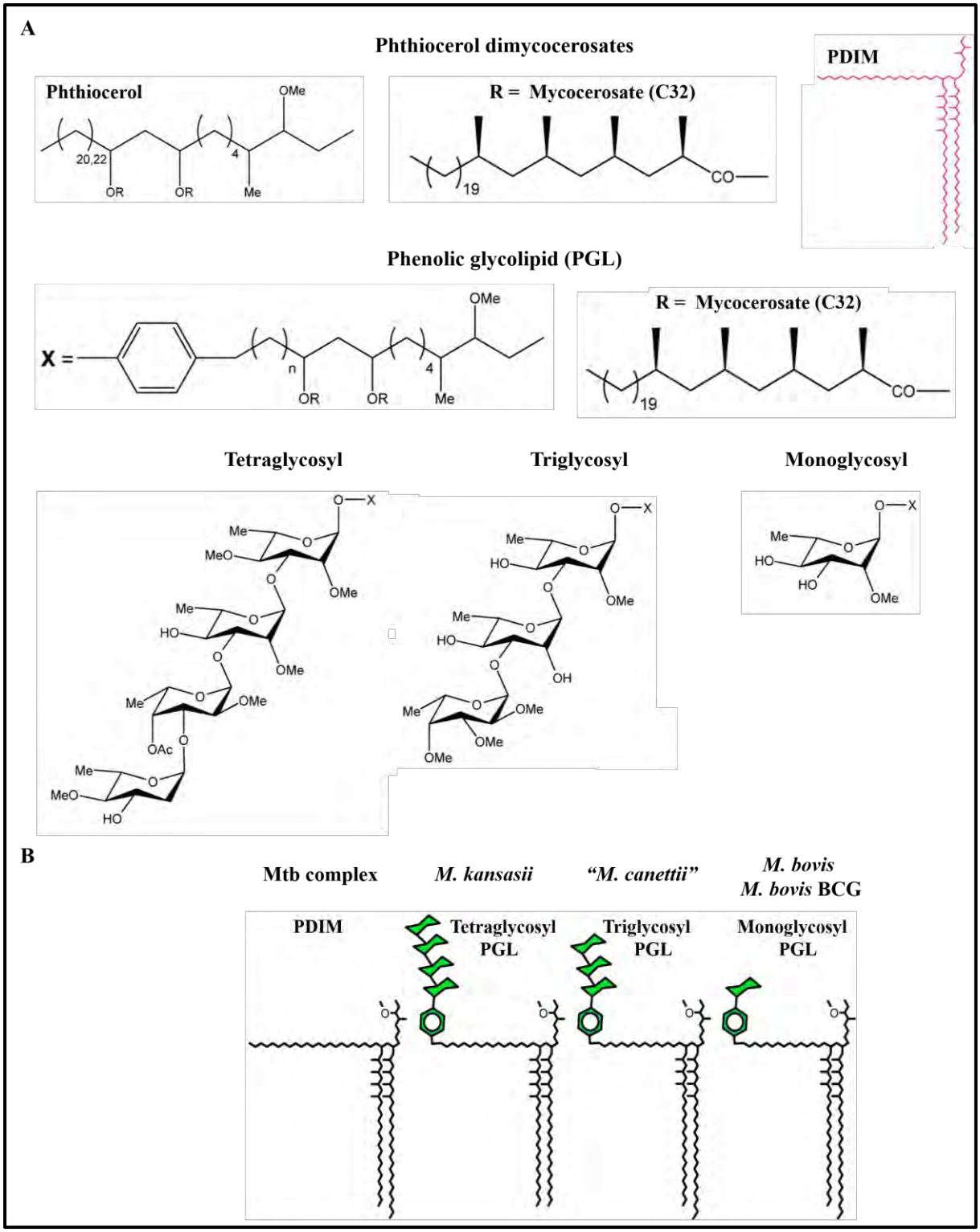

Figure 1-4: Phthiocerol derived lipids. A) PDIM and PGL showing differences in glycosyl units B) Basic representation of the shared lipid core between PDIM/PGL. [Adapted: (60)].

1.5.4 Phosphatidylinositol-derived lipoglycans (PI)

This group of phospholipids are conserved in all mycobacteria and have a common structural core consisting of phosphatidylinositol (PI) as in Figure 1-5 that is integral for generating mannosyl- phosphatidyl-myo-inositol (PIM) (55,129). PIM can accommodate up to four acyl chains, and the consecutive addition of two mannosyl units results in PIM_2, a precursor of PIM_4 (with four mannosyl units) and PIM_6 (with six mannosyl units), of which only PIM_2 and PIM_6 are predominant (53,55). The successive addition of mannosyl units to PIM_6 produces more complex structures known as lipomannan (LM) and with an added arabinan group, lipoarabinomannan (LAM) that can be mannosylated (ManLAM) at the non-reducing ends of arabinan (60,130). Variations of ManLAM represent species-specific heterogeneity among mycobacterial species (53,55,60,130). Specifically for the Mtb complex, ManLAM can exhibit one, or two or three mannoside caps with novel sugars such as xylose (53,55,60,130).

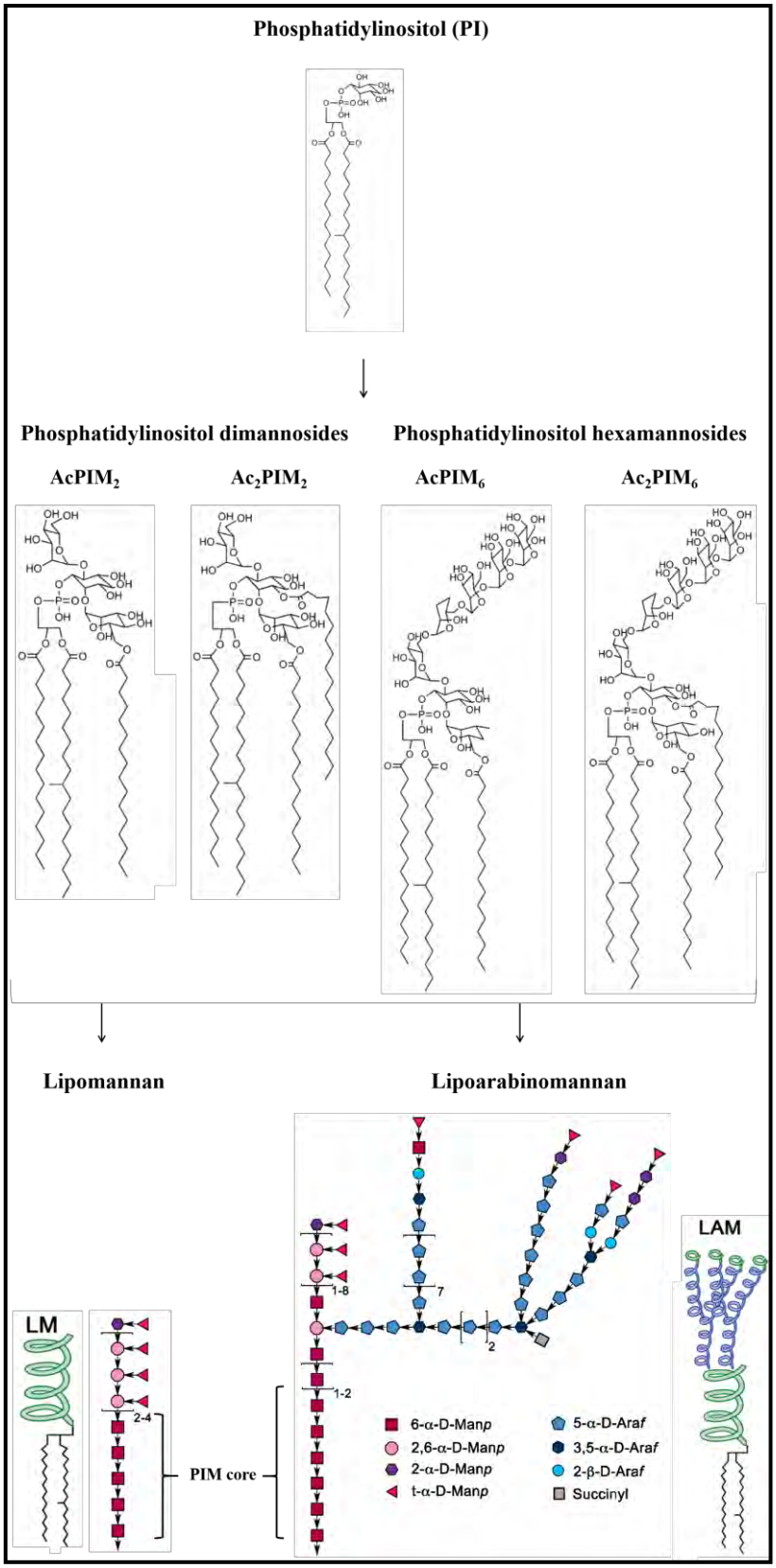

Figure 1-5: Phosphatidylinositol mannosides (PIM) derived lipids. [Adapted: (60)].

1.6. Role of outer membrane lipids

It is no coincidence that PDIM, SL, polyacylated trehalose glycolipids are restricted to pathogenic mycobacteria (108,126). As surface extractable lipids, they play multiple roles in cell wall permeability, pathogenesis and cell survival as shown in reviews from (53,55,60,131). Collectively, these multi-methyl branched glycolipids are significant virulence factors that contribute to Mtb survival and pathogenesis (132).

1.6.1 Maintaining cell wall permeability

TMM, TDM and GMM preserve the integrity of the cell wall (49,50,56–58,60). Specifically, TDM causes the cording of mycobacteria which is a characteristic virulence phenotype and therefore termed, cord factor (56,57,60). TDM produced in all mycobacteria, but more abundantly in virulent mycobacteria (49,50,56–58,60). In the absence of agitation and cell surfactants, mycobacteria can spontaneously form monolayers either attached to cell surfaces known as biofilms or not attached at all (133,134). In this case, mycobacteria grow between the air and water/media interface known as pellicles (50,58,133,134). Nonetheless, both formations require TDM to form extremely rigid, hydrophobic, insoluble and stable structures in the long term (133,134).

DAT and PAT act as intermediaries between the layers of the myco-membrane, able to interact with the hydrophobic cell wall and the hydrophilic capsule due to their amphiphilic nature (135). As such, they play an essential role in protecting the innermost and outermost layers of the tubercle (135). A deficiency of PDIM leads to increased cell wall permeability and susceptibility to damage from exposure to drugs, host immune cells and other potential threats (40,121,136). The absence of PDIM, SL, acyl trehaloses (DAT/TAT/PAT) diminishes the hydrophobic layer, exposing a fluid cell wall that can be quickly saturated with neutral red dye (137). Also, the total loss of these apolar lipid species contributes to a decline in Mtb virulence

(132). Therefore, modern-day Mtb is equipped with these lipid species (higher apolar content) than less evolved mycobacterial species (138).

1.6.2 Virulence

TMM, GMM and TDM are considered highly toxic to macrophages and have been implicated as a driving force in initiating dormancy, formation of the and caseation of the granuloma and modulation of immune cells (50,58,133,134). Explicitly, TDM and GMM are recognised by T cells as antigens by CD1 presentation (139–142) and stimulate T cell chemotaxis and pro-inflammatory responses that in turn activate granuloma formation (130,143,144).

TDM and the hypoxic conditions of the human granuloma induce host TAG accumulation as lipid droplets in macrophages termed foamy macrophages (145,146). Kim et al. (145) also showed that TDM induces foam cell formation and recruits these lipid loaded macrophages to the centre of the granuloma, by amplifying the pro-inflammatory response. This, in turn, results in the death of the foamy macrophages that release their lipid loads into the granuloma (145,146). The Mtb bacilli use host TAG to synthesise and accumulate their TAG, as an energy source in a non- replicating state (146–148). Mtb enter into dormancy, where they are drug-tolerant, as indicated by an up-regulation of lipid metabolism and dormancy related genes (145–147). Besides, TDM was also associated with inducing a group of zinc metalloendopeptidases in caseating and liquefying the tuberculous granuloma (149).

Phosphatidylinositol-derived glycolipids such as PIM and LAM, aid granuloma formation by triggering a pro-inflammatory response, as they are also recognised antigens of the CD1 pathway (141,150). Alternatively, ManLAM triggers an anti-inflammatory response, mediated by a C-type lectin receptor on dendritic cells to control the downstream mechanism of acute infection, apoptosis and bacillus detection (151).

Each of the following antigenic lipids: SL, ManLAM, PDIM, PGL, TDM, block phagosome-lysosome fusion and phagosome acidification (131,144,152). Purified SL lipids block monocyte and macrophage activation and inhibit INFγ mediated RNI killing (153–155). The virulence properties of SL are not reflected in mouse models (87,156–158), but only demonstrated in human immune cells (159). Other trehalose esters (DAT, TAT, PAT) are pro-inflammatory mediators that inhibit cytokines responsible for the proliferation of T cells and pro-inflammatory responses to avoid killing by RNI (84,159–162).

PDIM is a potent virulence factor, like TDM. "PDIM-less" Mtb strains are not able to survive in the mouse model (40,41,121,163,164). PDIM interferes with the normal functioning of an infected macrophage by disrupting its maturation, activation, acidification, killing by nitric oxide and more recently was found to facilitate autophagy for phagosomal escape (165,166). As an added advantage, PGL is associated with the modulation of infected macrophages to resist nitric oxide killing (167) and acts as an antioxidant, scavenging oxygen radicals due to its sugar phenol group (168). Even though Mtb cannot produce PGL, *p*-HBAD and its glycosylated derivates, mimic PGL immunological responses that suppress the innate immune response (169). Both, PDIM and PGL can avoid microbicidal macrophage killing by different strategies. PDIM can mask pathogen-associated molecular patterns (PAMPs) involved in activating the Toll-like receptor pathway that stimulates microbicidal macrophages while PGL activates the chemokine receptor 2 pathway that induces the recruitment of permissive macrophages at the site of infection (136).

LOS biosynthesis and virulence have been most studied in *M. marinum* where the deficiency thereof, is significant (106,170,171). LOS aids in sliding motility, colony morphology, biofilm formation, and invasion of host macrophages (106,170,171). LOS is a virulence factor that has not been fully characterised yet (53,55).

1.6.3 Lipid Metabolism in the context of infection

Upon entry into dormancy, Mtb lipid metabolic genes are up-regulated to utilise and break down host-derived fatty acids as an energy source (53,55,146,147). As a consequence, an increased concentration of propionyl-CoA is generated, which if further processed results in toxic metabolites (172,173). However, propionyl-CoA is a significant substrate in the production of Pks derived poly-methylmalonyl CoA lipids, relieving propionate-mediated stress (53,55,172,173).

1.7. Mycobacterial membrane protein Large (MmpL) transporter family

The building of the complex and hydrophobic outer membrane of mycobacteria, which give it intrinsic drug resistance, relies on an extensive repertoire of genes involved in biosynthesis and transport (54). A class of lipid transporters in Mtb designated MmpL, have been identified and associated with outer membrane lipid biosynthesis and translocation, conserved across mycobacteria (174–178). The number of MmpL transporters drastically varies between slow and fast-growing mycobacterial species, indicating that these proteins could potentially be transporters required for mycobacterial survival during infection (176). In the genomic context genes involved in lipid production are organised with lipid transport genes (175).

Mtb encodes 13 MmpL proteins, of which only *mmpL3* is essential and only the functions of *mmpL3*, *mmpL4*, *mmpL5*, *mmpL7*, *mmpL8*, *mmpL10*, and *mmpL11* have been discovered (174–177,179,180). As these genes encoding MmpL proteins (MmpL3, MmpL4, MmpL5, MmpL7, MmpL8, MmpL10, and MmpL11) have demonstrated lipid substrate specificity (Figure 1-6) their primary role is mainly in lipid transport, a function essential in cell wall physiology and virulence (174,181). There are still many MmpL proteins that have no function (175,177–179). According to the Chalut (175) and Viljoen et al. (176) MmpL proteins not operonic or clustered with biosynthetic enzymes are not considered as lipid transporters. Surprisingly, *mmpL3* and

mmpL11 are in the same genetic cluster and are lipid transporters but do not share the same genetic organisation of biosynthesis coupled to transport as seen with *mmpL4*, *mmpL5*, *mmpL7*, *mmpL8*, *mmpL10* (175–178). There is much confusion as to the exact role/s of MmpL proteins as mechanisms of action are yet to be determined. In this section, the roles of MmpL proteins characterised are discussed below with the use of several reviews from (175–177,179,180,182).

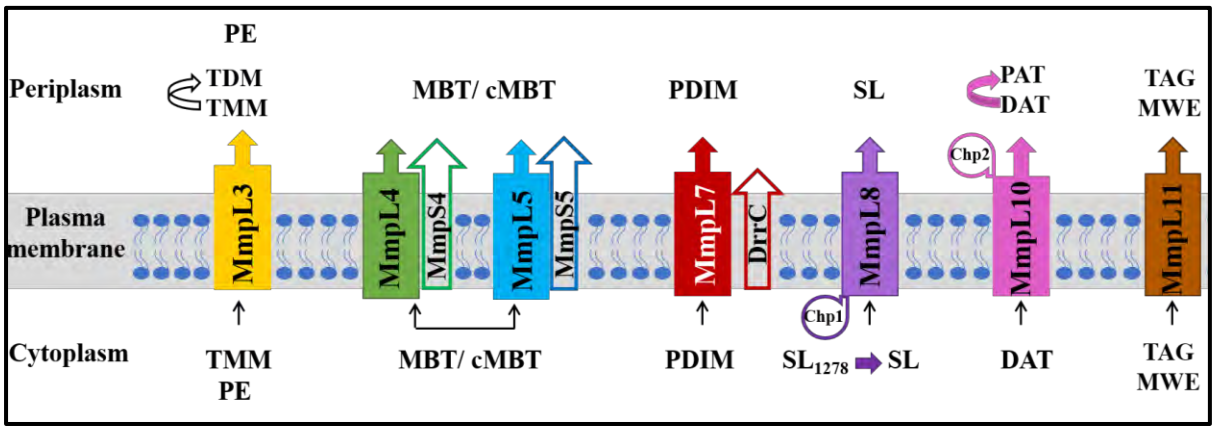

Figure 1-6: MmpL proteins with known roles in lipid transport and iron acquisition with biosynthetic/transport partners in Mtb (H37Rv). TMM - trehalose monomycolate, TDM - trehalose dimycolate, PE – phosphatidylethanolamine, (c)MBT - (carboxy)mycobactin, PDIM - phthiocerol dimycocerosate, SL- sulfolipid, SL_{1278} - sulfolipid intermediate, DAT/PAT - di/poly- acyl trehalose, MWE - mycolate wax ester, TAG – triacylglycerol [Adapted from (175,177,179)].

1.7.1 MmpL proteins and lipid transport

Since mycolyl glycolipids TDM and TMM are essential cell wall components and conserved across all mycobacteria; their transporters are equally as important (66–68). *mmpL3* is an essential requirement for the translocation of TMM and recently discovered polar phosphatidylethanolamine (PE) to the outer membrane (66–68,183). *M. smegmatis* tolerates the conditional loss of *mmpL3* better than in Mtb, where the bacilli are severely comprised (67,68).

Coryneybacterium glutamicum (*C. glutamicum*) was used to demonstrate a crucial step in TMM transport (184). *C. glutamicum* equipped with two homologs of *mmpL3* termed, CmpL1

and CmpL4, which are both required for the transport of coryne-trehalose-monomycolate (cTMM) (184). Before cTMM transport by CmpL1 and CmpL4 proteins, TMM had to undergo acetylation by an acetyltransferase (TmaT) (184). This fundamental step was also established in *M. smegmatis* (185). After that, TMM is converted to TDM and mycolates for the cell wall core, by mycolyltransferases encoded by proteins of the Ag85 complex as seen in Figure 1-6 (69–73). Besides the pre- and post *mmpL3* transport not much is known about the mechanism of transport.

Loss of *mmpL7* resulted in decreased survival and virulence *in vivo* and the accumulation of both PDIM and PGL in the cytoplasm, providing a clear role for *mmpL7* in the translocation of phthiocerol lipids to the outer membrane as in Figure 1-6 (39,41,121,126). Similarly, the loss of *drrC* also showed the same virulence phenotype due to failure in localising PDIM to the outer membrane (Figure 1-6) (40). In addition, a lipoprotein LppX has also been shown to be involved with transporting PDIM to the outermost layer of the cell wall. LppX, like other members of the lipoprotein family, are secreted proteins and not membrane-bound (186,187). Therefore, they have been isolated from the upper parts of the cell wall and found in culture filtrate, but not found in the cytoplasm (186,187). The X-ray crystallographic structure of LppX has been shown to have a hydrophobic pocket that could fit PDIM or PGL lipids (186). Since this molecule is not anchored to the membrane but free in the layers of the cell wall, it suggests that LppX could translocate PDIM to the outer membrane from the periplasm (179,186).

Lipoproteins, can also regulate their substrates such as LprG, that regulates LAM synthesis (188). It has not yet established whether LppX could regulate PDIM or PGL synthesis. Several serine/threonine kinase proteins such as PknB (189), PknH (190) and PknD (191) were proposed to coordinate PDIM synthesis and transport via phosphorylation respectively. As seen

with PapA5, it is not known whether phosphorylation occurs directly or indirectly with the aid of signalling mediating proteins (189).

Acylated trehalose such as SL and PAT are synthesised and transported in very similar ways (175,177). Unlike *mmpL7* that transports PDIM with no modifications before or after transport, *mmpL8* and *mmpL10* transport is reliant on acyltransferases (Chp1 and Chp2) for the translocation of SL and PAT to the outer membrane respectively as indicated by Figure 1-6 (82,85,92). Abrogation of *mmpL8* and *mmpL10* results in the accumulation of cytosolic SL_{1278} (156,157) and DAT intermediates (82). Similarly, loss of Chp1 and Chp2 result in the accumulation of SL_{1278} and DAT intermediates (82,85,92). Therefore, transport of SL and PAT by *mmpL8* and *mmpL10* are dependent on Chp1 and Chp2 and *vice-versa* (82,85,92). Both Chp1 and Chp2 are membrane-bound proteins with highly similar structure and function, but their catalytic domains may be organised differently from one another (82,85,92). Seeliger et al. (92) and Touchette et al. (116) agreed that the catalytic domains of Chp1 and Chp2 oriented towards the cytoplasm (92,116). However Belardinelli et al. (82) argued that although the catalytic domain of Chp1 was in the cytoplasm, the catalytic domain of Chp2 was in the periplasm.

Besides, Chp1 and Chp2, an accessory protein designated SL associated protein (Sap) was found to aid *mmpL8* in SL transport (92). Deficiency in Sap leads to reduced SL levels with higher SL_{1278} intermediates accumulated inside the cell (92). This result suggests that although *mmpL8* with Chp1 activity is capable of transporting SL to the outer cell compartment independently, Sap is required for enhanced transport (92). Similarities displayed in synthesis and transport between acyltrehaloses ends here, as no accessory protein can be found in Mtb to aid *mmpL10* in PAT transport (175,177). However, in other mycobacterial strains, a

homologous Sap protein termed glycopeptidolipid associated protein (Gap) was found to assist in glycopeptidolipid (GPL) and LOS translocation (102,192,193).

Genes encoding MmpL3 and MmpL11 are in the same genetic cluster and assumed to have a similar function (175,177). *mmpL3* has shown to be involved in TMM transport (30,66,67,194) while the loss of *mmpL11* in *M. smegmatis* led to defective biofilm formation and an accumulation of mycolic acid wax ester, TAG and monomeromycolyl diacylglycerol (MMDAG) (195). Recently, abrogation of *mmpL11* in Mtb displayed a more significant phenotype than in *M. smegmatis*, as this mutant had impaired survival *in vitro* and *in vivo*, shortened cell length, hypersensitivity to damage due to increased cell permeability, loss of biofilm formation, and the accumulation of mycolic acid wax ester and long-chain TAG (depicted in Figure 1-6) in the form of inclusion bodies (196). The authors associated the accumulation of mycolic acid wax ester and long-chain TAG to a phenotype related to dormancy, long term survival and drug tolerance (196).

1.7.2 MmpL proteins and iron acquisition

The roles of MmpL3 and MmpL11 are primarily in lipid transport; however, both proteins with Rv0203, have also been implicated in host iron acquisition (197,198). The X-ray crystallographic structure of Rv0203, indicated that this protein is a secreted heme-binding protein capable of acquiring exogenous heme and heme derived from haemoglobin, a primary source of exogenous iron in humans (197,199). However, this protein did not exhibit a high affinity to heme suggesting that it acquires heme and haemoglobin through another mechanism that has not yet been identified (199).

Double deletion mutants in Mtb of either *mmpL11* or *Rv0203* with *mbtB* (gene required for the mycobactin iron acquisition pathway described below) resulted in severely reduced growth in media with heme or haemoglobin (197). Since *mmpL3* and *mmpL11* are structurally similar

and organised with genes in the same genomic context, this cluster has been termed the heme uptake region (197). As such, the entire cluster was deleted in *M. smegmatis*, and each gene of the cluster complemented to test whether all of the genes in this region were involved with heme uptake (197). It was noted that every gene in the *mmpL3* and *mmpL11* cluster could restore growth in this mutant and could potentially contribute to heme uptake (197). Also, heme-binding motifs were located on non-transmembrane domains of MmpL3 and MmpL11 oriented towards the periplasm, enabling heme-binding (198). Heterologous expression of one of the periplasmic domains of Mtb MmpL3 and MmpL11 were shown to bind heme from Rv0203, proving that MmpL3 and MmpL11 are indeed involved in transferring heme into the cell (198). The mechanism of heme transfer from one protein to another was postulated to occur by an energy-driven protein-protein interaction, due to the fast transfer rate rather than transfer across a concentration gradient by passive diffusion or heme affinity (198).

Once heme has been transported into the inner cell by membrane transporters, MmpL3 and MmpL11, a mycobacterial heme utilisation degrader (MhuD) is used to degrade heme and release the iron therein (200,201). X-ray crystallographic structure of MhuD reveals that it is unlike any known heme degrading enzyme (201). Its unique properties include the formation of a unique mycobactin product without the release of carbon monoxide (CO), a signal used to trigger dormancy related genes to induce a non-replicating state, and it can hold up to two heme molecules (200,201). The number of heme molecules that MhuD accommodates (either one or two) not only changes the physical state of the protein from monomeric to dimeric but also switches its activity, from active to inactive (201). Unfortunately, no other genes in this cluster have roles associated with iron uptake (175).

Another pair of MmpL proteins that work together to acquire iron in Mtb are *mmpL4* and *mmpL5*, which are involved in by mycobactin and carboxymycobactin (MBT and cMBT)

siderophore recycling as described in Figure 1-6 (202,203). MBT and cMBT are siderophores that are produced and assembled by two Mtb loci termed *mbt1* and *mbt2*, which are induced by iron limitation (204–209). These molecules have a high affinity for host heme in the form of transferrin and lactoferrin, which represents a minority of exogenous heme available (210). MBT and cMBT have a common structure consisting of a core phenyloxazolidine ring derived from salicylate and a hydroxylated lysine with alkyl side chains (204–208). A main distinguishing feature between MBT and cMBT, is the chain length of the alkyl side chains which determine its localisation (211,212). MBT alkyl side chains are more extended and hydrophobic allowing it to be associated with the cell membrane (211,212). cMBT has shorter alkyl side chains that are carboxylated at the ends, making this molecule hydrophilic and efficiently secreted in the extracellular space to access exogenous transferrin and lactoferrin (211,212).

Briefly, once cMBT binds tightly to transferrin and lactoferrin in the extracellular space it can enter the cell via diffusion through mycobacterial family of porins (Msp), where it is loaded either directly or indirectly using MBT to IrtA and IrtB, an ABC iron transporter complex (211,212). The IrtA and IrtB complex has two roles, one as an importer of heme bound MBT and cMBT and the other as a reductase to dissociate heme from its captive siderophores (211,212). It has not been determined why both MBT and cMBT are produced if both can directly interact with the IrtA and IrtB complex (211,212). However, Jones et al. (203) suggests that since MBT and cMBT is hydrophobic and hydrophilic, respectively, each of these molecules are adept at sequestering iron from different environments. Unbound MBT and cMBT are exported from the cytoplasm by two transmembrane proteins, MmpL4 and MmpL5, with the help of small proteins designated as mycobacterial membrane protein small (MmpS) as listed in Table 1-2 that exclusively aid their respective MmpL protein (175,177). Once these

siderophores, MBT and cMBT, are extruded into the extracellular compartment ready for heme uptake, there is no need for Mtb to synthesis additional siderophores (202,203,211,212). The efficient recycling of siderophores provides an energy independent and inexpensive pathway, invaluable during nutrient starvation (202,203,211,212).

Table 1-2: *mmpS* genes of Mtb (H37Rv). [Adapted from (175,177,179,182)].

Gene	**Locus Number**	**Aids:**
mmpS1	Rv0403c	*mmpL1*
mmpS2	Rv0506	*mmpL2*
mmpS3	Rv2198c	Unknown
mmpS4	Rv0451c	*mmpL4* Siderophore mediated iron uptake
mmpS5	Rv0677c	*mmpL5* Siderophore mediated iron uptake

The genetic organisation of *mmpL4* and *mmpL5* with their respective *mmpS* genes (*mmpS4* and *mmpS5*) are surprisingly two separate loci and not operonic, suggesting that MmpL4/MmpS4 and MmpL5/MmpS5 represent two independent transport systems (175,212). However, the disruption of either *mmpL4* or *mmpL5* showed that both *mmpL4* and *mmpL5* have redundant roles in siderophore mediated recycling (202). Siderophore export was also inhibited due to the loss of either *mmpS4* or *mmpS5* and double deletions of *mmpL4*/*mmpS4* or *mmpL5*/*mmpS5* demonstrated that *mmpL4* and *mmpL5* were dependent on *mmpS4* and *mmpS5* respectively and *mmpL4*/*mmpS4* and *mmpL5*/*mmpS5* were not two independent transport systems (202,203). The intracellular accumulation of siderophores is toxic and thus, double deletion mutants of *mmpL4*/*mmpS4* or *mmpL5*/*mmpS5* display a significant attenuation phenotype *in vivo*, establishing *mmpL4*/*mmpS4* and *mmpL5*/*mmpS5* as virulence factors (181,202,203).

1.7.3 MmpL proteins and drug resistance

Mycobacteria do not only rely on their impenetrable cell wall as a barrier for intrinsic drug resistance but also efflux pumps (213,214). Efflux pumps are energy driven and comprise of membrane embedded proteins that actively transport a broad spectrum of compounds across the bacterial membrane (213,214). In Gram-negative bacteria, mycobacterial efflux pumps can be categorised into five super-families namely: ATP-binding cassette (ABC), resistance nodulation division (RND), major facilitator superfamily (MFS), small multidrug resistance (SMR) and multidrug and toxic-compound extrusion (MATE) families (213–217). These families of efflux pumps are differentiated by the energy source used to drive transport across the membrane (213–217). Since the energy used by ABC is derived from ATP, they are classified as primary transporters (213,214). Although, MFS, RND, SMR and MATE are classed as secondary transporters because their energy source is derived by hydrogen or sodium protons (213,214).

In mycobacteria these five super-families exist except there are not many orthologues of RND exporters; instead MmpL proteins represent a subclass of the RND superfamily (174,213,214). The overexpression of both MmpL7 (218,219) and MmpL5 (220–222) resulted in the extrusion of Isoniazid and Bedaquiline, Clofazimine and Azoles. Even though these proteins have primary roles in lipid (40,41,121) and siderophore transport (202,203) respectively, these results suggest MmpL proteins can serve drug extrusion efflux pumps, although mechanisms of extrusion are yet to be determined.

1.7.4 MmpL proteins and bacterial sensitivity

Amongst membrane proteins involved in stress detoxification such as NarI and NarK2 interestingly MmpL7 and MmpL10 were shown to interact with KdpF via bacterial two-hybrid *in vitro* assay (223,224). KdpF is in the same genetic context with genes encoding an ABC

transporter complex, KdpABC that is regulated by a two-component system, KdpDE involved with potassium transport and required for mycobacterial pathogenesis. However, KdpF does not facilitate transport driven by KdpABC or regulate KdpDE (224). Instead, when overexpressed, KdpF was shown to modulate MmpL7 activity by inducing MmpL7 degradation through interaction (223). Under nitrosative stress, the *mmpL7* gene together with genes responsible for PDIM synthesis were sharply down-regulated or repressed (223,225). PDIM offers resistance to the nitric oxide (136,163) and structural integrity of the myco-membrane (40,132,137,163). Therefore, KdpF-MmpL7 interaction results in increased bacterial sensitivity to nitrosative stress *in vitro* (223).

1.8. Overall study and aim

The aim was to study lipid transport pathways in Mtb, in particular, the MmpL proteins. I used the attenuated *M. bovis* strain Bacille Calmette-Guérin Pasteur strain (BCG) as a surrogate to investigate three transporters in Mtb, as the genome of *M. bovis* only displays about 3% difference to Mtb and it has a doubling time similar to Mtb (226). More specific to this study is the diversity of lipids present in this strain (108,126). Mycolates are conserved across all mycobacteria (50,58,133,134) however, non-mycolate lipids are species-specific (108,126). A common feature in the genetic context of outer membrane non-mycolate lipids is the coupling of synthesis and transport mechanisms that allows one to study the lipid with its respective transporter (175,177). Unlike Mtb (H37Rv), BCG additionally produces PGL and provides the opportunity to study PDIM/PGL transport (126).

Two decades of genetic, biochemical and immunological studies investigating MmpL proteins have revealed that these proteins are associated with the export of outer membrane surface-exposed glycolipids that are integral to virulence, mycobacterial cell wall maintenance and survival in the host. The large size of these transmembrane proteins has made it complicated

to gain much structural information. Hence, very little information regarding the structure and mechanism of action of MmpL proteins is known as compared to their RND counterparts in Gram-negative bacteria. Information regarding the structure, mechanism, co-ordination and regulation of MmpL proteins is not yet known. In an attempt to address these questions and understand the mechanisms of MmpL proteins, this study focusses on three transport systems MmpL3, MmpL7 and DrrABC in the following manner:

Chapter 2: Characterise the structure of MmpL3 and MmpL7 using styrene-maleic acid (SMA) co-polymer that directly extracts membrane proteins in their native membrane environment and compatible with single-particle electron microscopy, eliminating the need for detergent based methods that replace the native membrane and traditional X-ray crystallography methods that require large amounts of protein.

Chapter 3: Probe the mechanism of *mmpL7* (encoding MmpL7) in PDIM/PGL synthesis/transport by generating an *in-silico* model to identify residues for modification and assess the effects of these single mutations on synthesis/transport of PDIM/PGL using structural modelling, genetics and biochemical studies.

Chapter 4: Determine the individual and collective roles of *drrA*, *drrB* and *drrC* in PDIM/PGL transport by generating a mutant deficient in all *drrA/B/C* genes in *M. bovis* BCG and characterising all and individual *drr* genes by complementation.

Chapter 2: Structural characterisation of MmpL3 and MmpL7

Chapter 2: Structural characterisation of MmpL3 and MmpL7

2.1. Introduction

Phylogenetic and topological analyses revealed a class of thirteen putative glycolipid transporters in Mtb known as mycobacterial membrane protein large (MmpL) proteins which, represent a subclass of the RND superfamily (174,227,228). MmpL proteins are key players in maintaining the mycobacterial cell wall, virulence and survival of the pathogen (discussed in detail in Chapter 1) by transporting cell wall lipids and iron across the plasma membrane (Figure 2-1). These proteins are exclusively group within the hydrophobe/amphiphile efflux (HAE) sub-family (Figure 2-1) responsible for the transport of lipids, fatty acids and drug molecules (229) but also share broader similarity with different RND sub-families as they contain several transporter domains conserved in AcrB, actinorhodin, sterol sensing and hopanoid biosynthesis proteins (227). Additionally, MmpL proteins provide evidence of proton meditated substrate transport that is the underlying mechanism of function in the RND superfamily with conserved motifs in transmembrane (TM) helices 4 and 10 (TM4/10) (227).

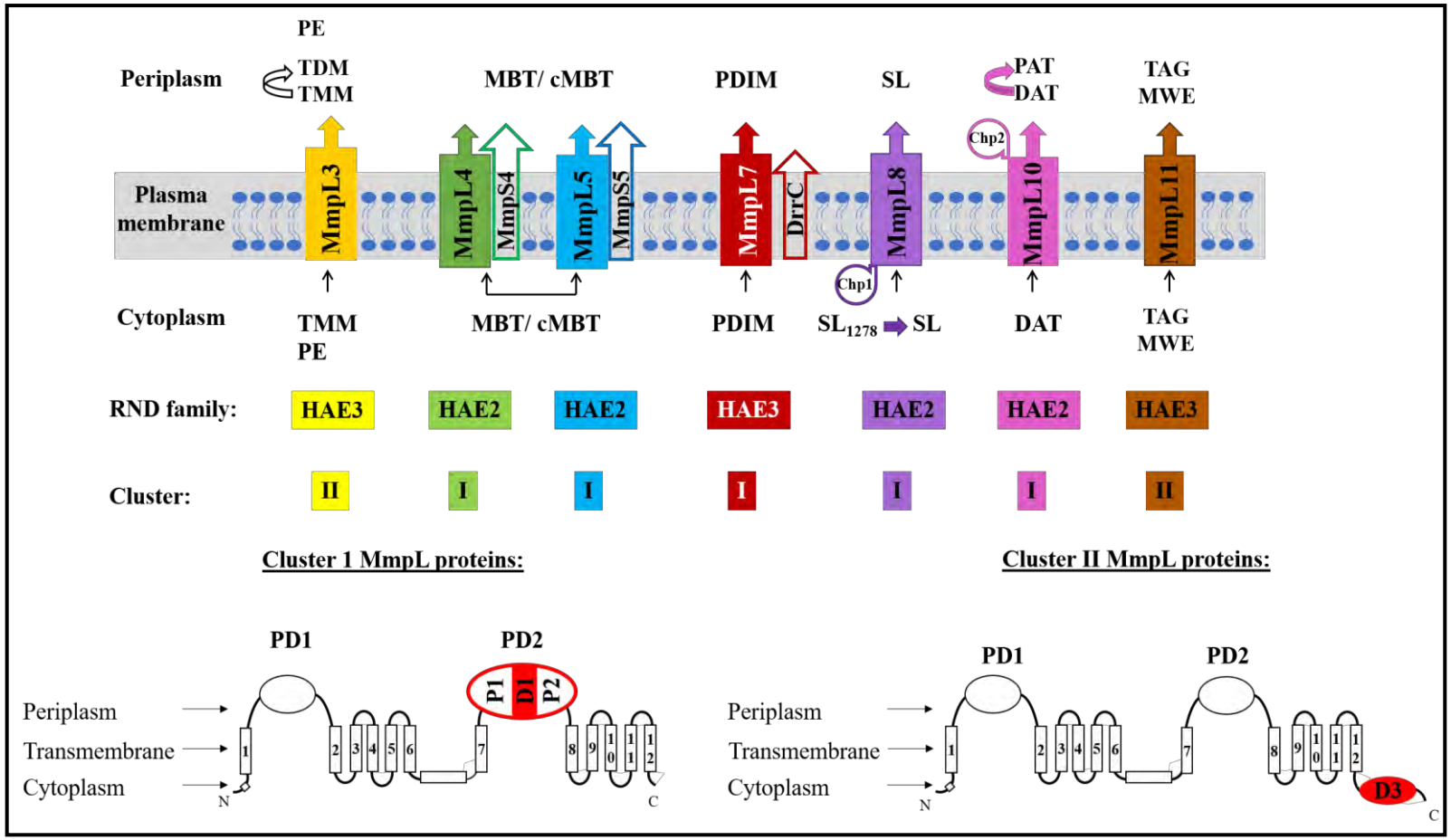

Figure 2-1: MmpL proteins with known functions and phylogenetic classifications. TMM - trehalose monomycolate, TDM - trehalose dimycolate, PE – phosphatidylethanolamine, (c)MBT - (carboxy)mycobactin, PDIM - phthiocerol dimycocerosate, SL- sulfolipid, SL_{1278} - sulfolipid intermediate, DAT/PAT - di/poly- acyl trehalose, MWE - mycolate wax ester, TAG – triacylglycerol, HAE - hydrophobe/amphiphile efflux, PD1/2 - periplasmic domain 1/2, D1 - docking domain 1, D3 - cytoplasmic soluble domain [Adapted from (175,228)].

RND transporters are characterised as large TM proteins consisting of about twelve TM helices and two soluble ectodomains located in the periplasm inserted between TM1/2 and TM7/8 based on crystal structures of RND transporters belonging to the HAE [AcrB (230), MexB (231) and MtrD (232)] and heavy metal efflux (HME) [CusA (233) and ZneA (234)] sub-families.

Previous topological analysis revealed that overall, MmpL proteins have eleven- twelve TM domains and two periplasmic domains (227). However, truncated MmpL proteins such as MmpL6 consists of five TM helices and MmpL13 split into MmpL13a, and MmpL13b contain four and seven TM helices respectively (227). Exceptions include MmpL10 predicted to only contain one periplasmic domain between TM6/7, where periplasmic domain 2 is inserted for MmpL3, MmpL4, MmpL5 and MmpL9 (227). MmpL proteins were further differentiated into two clusters according to the presence of additional motifs in periplasmic domain 2 and in the cytoplasm at the C terminal end as shown in Figure 2-1 (228). The molecular weight of most MmpL proteins is predicted to be about 100 kDa similar to their RND counterparts (174,227). Despite the predicted topological variations between MmpL proteins, structural information of these proteins depends on *in silico* modelling based on crystal structures of RND proteins (227,228). Determining the structure of membrane proteins presents major challenges as they are not abundant, can be problematic to purify and stabilise and are difficult to maintain in a stable environment for characterisation and functional assays.

In order to tackle these problems various technologies have been developed such as: amphipols, bicelles, nanodiscs and styrene-maleic acid (SMA) co-polymer that all encapsulate membrane proteins to enhance their stability and solubility in aqueous solution while retaining their native lipids from the membrane, unlike detergent that replaces the membrane as depicted in Appendix 6 (235–239). However, amphipols, bicelles and nanodiscs, attempt to create a natural

membrane environment but rely on extracting the membrane protein from the lipid bilayer using detergent and after the membrane protein is encapsulated the detergent is removed (235–239). The detergent presents a risk of disrupting protein-protein interaction and complex formation and decreases the native lipid composition maintaining membrane proteins (238,240). In terms of nanodiscs the proteinaceous belt can interfere with analytical UV based spectroscopy applications (237,238). Only SMA directly extracts the native bilayer and thus contains the natural biological membrane without the use of detergents (241–245).

SMA has broad application in numerous hosts such as: murine, insect, bacteria and yeast expression systems (243,246–250). SMA application improved the lipidic cubic phase (LCP) method by producing high-quality crystals at high-resolution (251) but importantly maintains protein function (247,248). SMA encapsulated proteins do not interfere with analytical techniques that allow for biophysical characterisation (243). SMA is compatible with single-particle electron microscopy [such as negative stain electron microscopy (NEM) and cryo-electron microscopy (CEM)] an alternate method for determining protein structures that do not rely on generating highly ordered crystals as with X-ray crystallography. In this approach, a homogeneous low protein concentration is required for visualisation (244,252).

Since members of the MmpL family bear structural and phylogenetic differences as they are evolutionary different, there is no fixed *in silico* model that can be assigned to any MmpL protein (174,227,228). Therefore, many structural aspects regarding MmpL proteins have yet to be determined. In our lab, already two colleagues attempted to achieve the structure of Mtb MmpL3 and generated the MmpL3 expressing construct and optimised the protein expression conditions. According to their results, the heterologous overexpression of MmpL3 was toxic, and hence the yield was not sufficient for X-ray crystallographic methods. Therefore, the use of SMA and single-particle electron microscopy presented a possible effective strategy which

was also readily accessible from the developer Prof. Timothy Dafforn (at the University of Birmingham).

The aim of this study was to determine the structure of MmpL3 and MmpL7 using SMA coupled with single-particle electron microscopy as described by Parmar et al. (252) and Postis et al. (244).

2.2. Material and methods

2.2.1 Generation of expression plasmids and strains

Briefly, MmpL7 was amplified by PCR using the primers in Table 2-1, where the resulting 2763 bp fragment was cloned into the His-tagged expression vector pET26b at the C terminus using *Nde*I and *Hind*III restriction enzymes. The MmpL3 expression construct was generated by a previous PhD student Vijayashankar Nataraj (65). Briefly, the *mmpL3* gene was codon optimised and synthesised by Genscript.Inc for the heterologous overexpression in *E. coli* and cloned in-frame with the C terminal His tag end of the pET28b vector (65). The recombinant vector (pET26b:MmpL7) was verified by DNA sequencing to be correct and together with pET28b:MmpL3 (65), was transformed into *E. coli* C41(DE3) and C41A^{-}(DE3) to produce the expression strains listed in Table 2-2. One colony was grown in 25 ml LB with 50 µg/ml kanamycin overnight (37 ºC, 180 rpm) as a preculture that was in turn used to inoculate small- and large-scale cultures.

Table 2-1: Primers used in this study (5'-3') for the construction of pET26b:MmpL7. All primer sequences are in the 5' to 3' direction, while F and R indicate the forward and reverse primers respectively. Underlined sequences indicate extra base pairs and italicised sequences denote the restriction sites, NdeI (CATATG) and HindIII (AAGCTT) used for cloning into pET26b.

MmpL7 CHIS				
F	GCG*CATATG* CCTAGTCCGGCTGGCCG	R	GAT*AAGCTT* ACGCCGCCCTGGCGTGG	2763 bp amplicon

Table 2-2: List of plasmids and bacterial strains used and generated in this study.

Plasmid, Mycobacteriophages and Bacterial strains	**Genetic characteristics**	**Origin**
Plasmids		
pET26b	*E. coli* expression vector with a six His tag	Novagen
pET26b:MmpL7	Full-length Mtb *mmpL7* (*Rv2942*) cloned into an expression vector pET26b in-frame with the C-terminal six His tag	This study
pET28b:MmpL3	Full-length Mtb *mmpL3* (*Rv0206c*) codon optimised for expression in *E. coli* cloned into an expression vector pET28b in-frame with the C-terminal six His tag	(65)
Bacterial strains		
E. coli C41(DE3)	F-ompT hsdsB (rb-mb)gal dcm (DE3)	Invitrogen™
MmpL7	C41(DE3) transformed with pET26b:MmpL7	This study
MmpL3	C41(DE3) transformed with pET28b:MmpL3	(65)
E. coli C41A^{-}(DE3)	*E. coli* Δ*acrB* C41(DE3)	The kind gift from Dr. Vincent Postis, University of Leeds

MmpL7- A^{-}	Δ*acrB* C41(DE3) transformed with pET26b:MmpL7	This study
MmpL3- A^{-}	Δ*acrB* C41(DE3) transformed with pET28b:MmpL3	This study
Control	C41(DE3) transformed with pET26b	This study

2.2.2 Protein expression

The protein expression of MmpL3 was optimised by a previous PhD student Vijayashankar Nataraj (65) and a postdoctoral researcher Dr. Cristian Varela and therefore, no small-scale expression tests were performed. MmpL3 expression in C41(DE3) and C41A^{-}(DE3) strains, involved inoculating 10 ml of the preculture into 1 L TB with 50 µg/ml kanamycin and allowed to grow until OD_{600} ~ 0.5 then induced with 1 mM isopropyl β-D-1 thiolgalatcopyranoside (IPTG) and allowed to produce protein for 8 hrs at 37 ºC, 180 rpm.

Whereas the protein expression of MmpL7 and MmpL7- A^{-} required small-scale protein expression tests to compare protein produced between these strains in TB and LB. About 50 ml of TB/LB with 50 µg/ml kanamycin were inoculated with 0.5 ml of preculture and grown to OD_{600} ~ 0.5 then induced with 1 mM IPTG and allowed to produce protein overnight (ON) at 16 ºC, 180 rpm. Thereafter, large-scale cultures in TB were tested for protein expression between MmpL7 and MmpL7- A^{-} under different post-induction conditions. Briefly, 10 ml of the preculture was inoculated into 1 L TB with 50 µg/ml kanamycin and allowed to grow until OD_{600} ~ 0.5 then induced with 1 mM IPTG and allowed to produce protein either overnight at 16 ºC, 180 rpm or for 3 hrs at 37 ºC, 180 rpm. Cultures of small- or large-scale were harvested by centrifugation at 4000 rpm, 20 min, at 4 ºC. The pellets were washed with 20 ml of 1x PBS and centrifuged at 4000 rpm, 20 min, at 4 ºC and were stored at -20 ºC for future use or processed for membrane preparation thereafter. For the control strain, 10 ml of preculture was inoculated into 1 L TB with 50 µg/ml kanamycin and allowed to grow until OD_{600} ~ 0.5 then

induced with 1 mM IPTG and allowed to grow overnight at 16 ºC, 180 rpm. The culture was harvested in the same manner as MmpL3 and MmpL7.

2.2.3 Membrane preparation

Pellets (referring to MmpL3, MmpL7 and the control) were resuspended in lysis buffer [20 mM Tris- HCl pH 7.9, 0.5 mM ethylenediaminetetraacetic acid (EDTA), 1 protease inhibitor cocktail tablet EDTA free (Roche) at a ratio of 4:1, buffer to pellet] and lysed using sonication (15 s on, 45 s off, 10 cycles) or high-pressure cell rupture (20,000 psi, 3 cycles) and centrifuged at 10000 rpm, 15 min, at 4 ºC. The pellet was discarded, and the supernatant was further centrifuged at high speed 40000 rpm, 1 hr, at 4 ºC to sediment the membrane that was resuspended with 20 ml of 20 mM Tris-HCl pH 7.9 (4 °C) and centrifuged at high speed 40000 rpm, 1 hr, at 4 ºC. This washing step was repeated, and the membrane was weighed and either stored at -80 ºC for future use or solubilised thereafter.

2.2.4 Solubilisation using Styrene-co- Maleic Acid (SMA) and n-Dodecyl-β-D-Maltoside (DDM)

Membranes (referring to MmpL3, MmpL7 and the control) were resuspended in buffer [50 mM Tris- HCl pH 7.9, 500 mM NaCl, 10% glycerol, 1 protease inhibitor cocktail tablet EDTA free (Roche)] to a final concentration of 40 mg/ml or in some cases 80 mg/ml, homogenised and either 2.5% (w/v) styrene-co- maleic acid polymer (SMA) or 1% (w/v) n-dodecyl-β-d-maltoside detergent (DDM, Thermo Scientific™). The SMA used in this work was SMA2000-P prepared at a ratio of 2:1 (styrene: maleic acid) by and obtained from members of Prof. Dafforn's group (University of Birmingham). For SMA solubilisation the mixture was allowed to roll for 2 hrs at RT, and in the case of solubilisation using DDM, the mixture was allowed to roll for 1.5 hr at 4 ºC. After solubilisation the mixtures were centrifuged at 40000 rpm, 1 hr, at 4 ºC, separating the supernatant containing encapsulated membrane proteins (soluble

fraction) with SMA from the pellet (insoluble fraction). The soluble fraction was filtered before adding to pre-washed and equilibrated nickel charged resin, while the insoluble fraction was mixed with 1 ml PBS to be used as a control before being discarded.

2.2.5 Protein purification

2.2.5.1 Immobilised metal affinity chromatography (IMAC)

IMAC is a commonly used method of protein isolation and purification, based on the affinity between the tag engineered to the protein of interest and the metal ion that has been chelated to an insoluble matrix. In this study, IMAC was always the first step to isolate MmpL3 and MmpL7 His tagged proteins by gravity flow using the nickel charged resin from Qiagen (Ni-NTA agarose). About 2 - 4 ml of Ni-NTA agarose were washed twice with 50 ml distilled water and then equilibrated with 50 ml buffer [50 mM Tris- HCl pH 7.9, 500 mM NaCl, 10% glycerol] and packed into empty columns designed for gravity-flow purifications (Thermo Scientific^{TM}). Briefly, the filtered solubilised supernatant was added to the column with washed and pre-equilibrated Ni-NTA agarose, and the resulting flow-through (FT) was collected. About 15 ml of buffer (50 mM Tris- HCl pH 7.9, 500 mM NaCl, 10% glycerol) was used to wash the column and this fraction was collected and recorded as wash (W). Then 5 ml of buffer (50 mM Tris-HCl pH 7.9, 500 mM NaCl, 10% glycerol) with imidazole concentrations (mM) from 10 - 300, and 100 mM EDTA solution to strip the column. The fractions were collected and analysed by SDS-PAGE/ Western blot. This procedure was used for SMA and DDM, but the buffers used for DDM purifications included 0.05% DDM (w/v) in the equilibration, elution and 100 mM EDTA solutions.

2.2.5.2 Dialysis and concentration

Fractions containing the protein of interest were pooled and dialysed to remove imidazole for further purification and concentration; against 50 mM Tris-HCl, 500 mM NaCl, 10% glycerol

(pH 7.9) for 3 - 4 hrs and replacing the buffer twice at 4 ºC. Thereafter the pooled sample was added to an Amicon® ultra 15 ml centrifugal filter concentrator (Merck Millipore) and concentrated to 1 mg/ml measured using the Nanodrop and analysed on SDS-PAGE/ Western blot. Both the dialysis tubing and the concentrator had a 10 kDa cut off.

2.2.5.3 Gel filtration chromatography

Gel filtration chromatography is another method used to separate proteins based on their size (preparative) and can be used to assess the different states a protein can form (analytical), e.g., monomer, dimer, trimer, oligomer etc. The Superdex-200 10/300GL (GE healthcare) column was equilibrated with 50 mM Tris-HCl pH 7.9, 500 mM NaCl, 10% glycerol and the concentrated protein sample/s were loaded after that and eluted 30 fractions with 1 ml each using buffer (50 mM Tris-HCl pH 7.9, 500 mM NaCl, 10% glycerol). Fractions of interest were analysed by SDS-PAGE/ Western blot.

2.2.6 Protein analysis

2.2.6.1 SDS-PAGE (Sodium Dodecyl Sulphate- Polyacrylamide Gel Electrophoresis)

Protein samples were mixed with loading dye (62.5 mM Tris-HCl pH 6.8, 0.002% bromophenol blue, 10% glycerol) and loaded on precast 4 - 20% PAGE (supplied from Biorad) and electrophoresed with 1 x Tris-Glycine-SDS buffer (10 x stock pH 8.0 from National Diagnostics) with an electric field of 200 V, 35- 45 mA, in vertical units (Bio-Rad). SDS is an ionic detergent that disrupts non-covalent bonds (hydrogen-bonding, hydrophobic and ionic bonds) resulting in linear proteins with a net uniform negative charge. Therefore, proteins are separated primarily on their molecular mass when the voltage is applied. Protein molecular weight marker (Thermo scientific) in Appendix 4 was used to assess fragment sizes of samples in kDa. Two SDS-PAGE gels were loaded with the same samples and electrophoresed simultaneously producing two identical gels, where one gel was stained with instant blue to

show the total protein, while the other identical gel was used for Western blotting analysis to detect specific His-tagged proteins only. The pair of gels were used together to identify targeted tagged protein and assess the purity of the sample/s containing the desired protein.

2.2.6.2 Non-denaturing or Native PAGE (Polyacrylamide Gel Electrophoresis)

Protein samples were mixed with loading dye (62.5 mM Tris-HCl pH 6.8, 0.002% bromophenol blue, 10% glycerol) and loaded on precast 4 - 20% PAGE (supplied from Biorad) and electrophoresed with native buffer (25 mM Tris-HCl pH 8.3, 192 mM glycine) with an electric field of 200 V, 35 - 45 mA, in vertical units (Bio-Rad). Since proteins are in their native conformation, this application is generally used to detect changes in conformation, degradation, aggregation and protein interactions. Thus, the mobility of native PAGE depends on the protein's innate charge, the pH of the buffer and its molecular mass when voltage is applied. Protein molecular weight marker (Thermo scientific) in Appendix 4 was used to assess fragment sizes of samples in kDa. Similar to the procedure in SDS-PAGE analysis, two native PAGE gels were loaded with the same samples and electrophoresed simultaneously producing two identical gels, where one gel was stained with instant blue to show the total protein, while the other identical gel was used for Western blotting analysis to detect specific His-tagged proteins only. The pair of gels were used together to identify targeted tagged protein and assess the purity of the sample/s containing the desired protein.

2.2.6.3 Western blot analysis

From the pair of either SDS-PAGE or native PAGE gels as explained above, one of the gels the was transferred onto a nitrocellulose membrane (Pierce, Thermo scientific) by packing the gel with the membrane closely together in a cassette, submerged in vertical units (Bio-Rad) with transfer buffer (25 mM Tris-HCl pH 8.3, 192 mM glycine and 20% methanol) at an electric field of 30 V, 300 mA for 3 hrs. The membrane was incubated in 5 % blocking solution

(milk powder) to prevent non-specific binding of antibodies to the membrane for 1 hr at RT then washed with TBST (20 mM Tris-HCl pH 7.6, 150 mM NaCl, 0.1% Tween 20) three times and incubated (ON, with gentle shaking, at 4℃) with 1:2000 primary antibody (mouse IgG anti-Penta-His from Qiagen. After the primary antibody incubation, the membrane was washed with TBST (20 mM Tris-HCl pH 7.6, 150 mM NaCl, 0.1% Tween 20) three times and incubated with 1:20000 secondary antibody Anti IgG conjugated to alkaline phosphatase, Sigma with for 1 hr, with gentle shaking at RT. Then washed twice with TBST (20 mM Tris-HCl pH 7.6, 150 mM NaCl, 0.1% Tween 20) and twice with TBS (20 mM Tris-HCl pH 7.6, 150 mM NaCl) before visualising the proteins using a chromogenic substrate SIGMA FAST™ NBT/BCIP (nitro-blue tetrazolium/ 5-bromo-4-chloro-3'-Indolyphosphate, Sigma Aldrich) dissolved in water.

2.3. Results

To avoid AcrB (~120 kDa) co-expression and co-purification with MmpL3 (~101 kDa) and MmpL7 (~95 kDa), the use of an *acrB* C41(DE3) mutant strain was used (Table 2-2). The protein expression of MmpL3 and MmpL7 was compared between *acrB* functional and deficient C41(DE3) strains.

2.3.1 MmpL3 expression in *acrB* functional and deficient C41(DE3) strains

The protein expression of MmpL3 (~ 101 kDa) was optimised by two previous colleagues and MmpL3 was abundantly expressed in the *acrB* functional strain in 1 L (Appendix 7A) and 3 L (Figure 2-2). Lower amounts of MmpL3 were observed in the *acrB* deficient strain as determined by Western blot (Figure 2-2) despite using three times the concentrated membrane material.

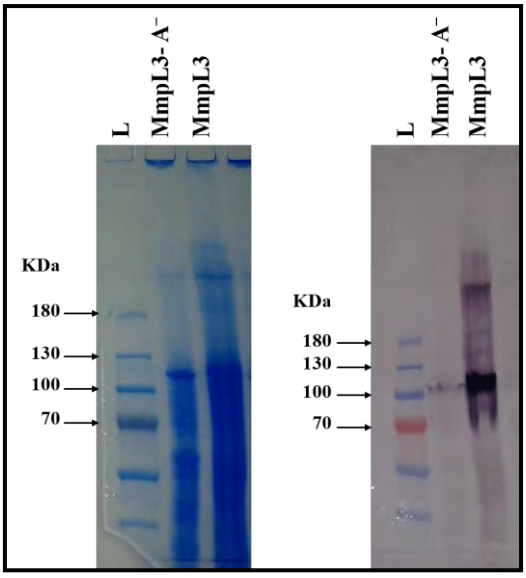

Figure 2-2: MmpL3 expression in membranes of C41(DE3) strains with and without the *acrB* gene. Membranes were prepared from 3 L cultures pooled. Left panel represents the total protein on SDS-PAGE while the right panel shows His-tagged proteins on the Western blot. L represents the protein ladder.

2.3.2 MmpL7 expression in *acrB* functional and deficient C41(DE3) strains

Small-scale protein expression testing of MmpL7 determined that terrific broth (TB) produced higher levels of MmpL7 (~95 kDa) observed in the Western blot (Figure 2-3) but no definitive band corresponding to MmpL7 in the *acrB* deficient strain. The same results were observed for assessing MmpL7 expression under two post-induction conditions in 1 L cultures of *acrB* deficient strains as compared to MmpL7 expressed in the *acrB* functional strain at one post-induction condition (Figure 2-4).

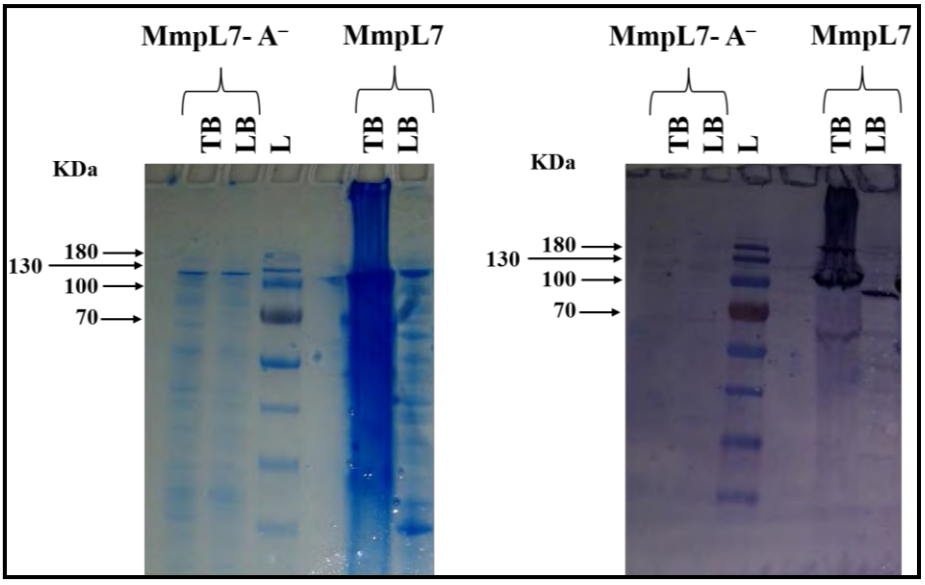

Figure 2-3: Small-scale testing MmpL7 expression comparing two different media in membranes of C41(DE3) strains with and without the *acrB* gene. Membranes were prepared from 50 ml cultures. Left panel represents the total protein on SDS-PAGE while the right panel shows His-tagged proteins on the Western blot. L represents the protein ladder; TB is terrific broth and LB is Luria-Bertani broth.

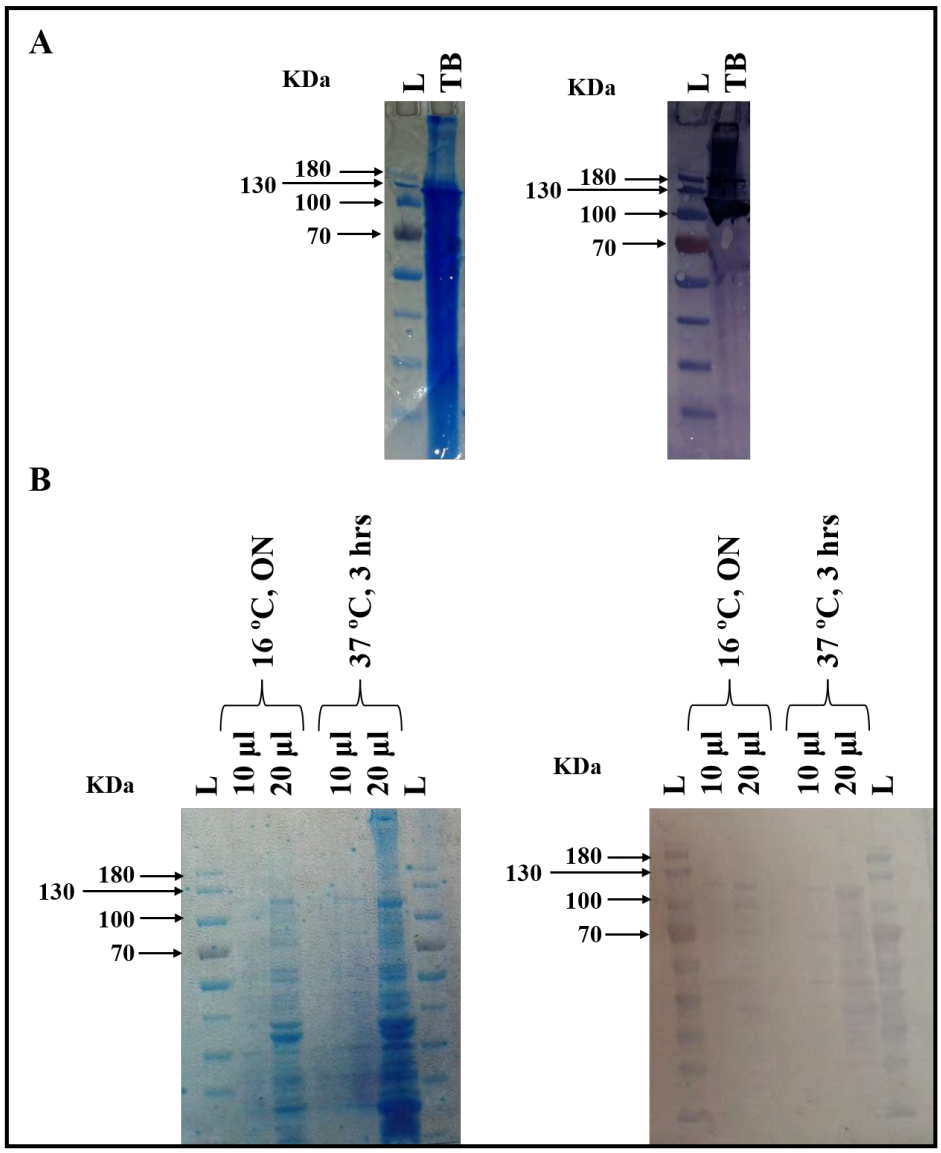

Figure 2-4: Testing MmpL7 expression in C41(DE3) and Δ*acrB* C41(DE3) strains in TB media. A) C41(DE3) strain with the *acrB* gene at 16 ºC, ON post-induction condition and B) C41(DE3) without the *acrB* gene at different post-induction conditions. Membranes were prepared from 1 L cultures. Left panels represents the total protein on SDS-PAGE while the right panels show His-tagged proteins on the Western blot. L represents the protein ladder and TB is terrific broth.

Unfortunately, both MmpL3 and MmpL7 protein expression were undetectable in the *acrB* C41(DE3) mutant strain regardless of the media or post-induction conditions. It has been noted previously that the *acrB* mutant affects the growth of Gram-negative bacteria that in turn resulted in low MmpL3 and MmpL7 production (from our collaborators at the University of

Leeds). Therefore, experiments were carried out in the C41(DE3) strain with the functional *acrB* gene, as MmpL3 and MmpL7 expression were abundant in 1 L cultures.

2.3.3 Purification of the Control using SMA

To overcome any concerns regarding contamination of RND proteins that possibly could be co-expressed and co-purified with MmpL3 and MmpL7, a vector only (i.e. no protein-expressing) C41(DE3) strain (Table 2-2) was included in this work. This control strain was induced, prepared, solubilised using SMA and purified alongside MmpL3 and MmpL7 strains to avoid technical error (Appendix 7). The membrane fraction of the control strain showed similar amounts of total protein as compared to membrane fractions of MmpL3 and MmpL7 on SDS-PAGE (Appendix 7). The absence of non-specific proteins in the Western blot analysis validated the specificity of this technique in detecting MmpL3 and MmpL7 (Appendix 7).

2.3.4 Purification of MmpL3 using SMA

Initially, for IMAC purifications, the membrane prepared from 1 L cultures were sufficient for NEM imaging as low protein concentrations were favoured. Very little to no total protein was observed in the purification of MmpL3 (Figure 2-5A) using SMA. Therefore, another attempt was made to analyse the samples by loading double the sample volume (Figure 2-5B). Surprisingly, no MmpL3 was detected in both the SDS-PAGE/ Western blot after a day of performing the IMAC purification (Figure 2-5B). After that, two low concentration imidazole eluates from purifications of MmpL3 and MmpL7 were concentrated from 5 ml to 200 µl and analysed on SDS-PAGE (Figure 2-6).

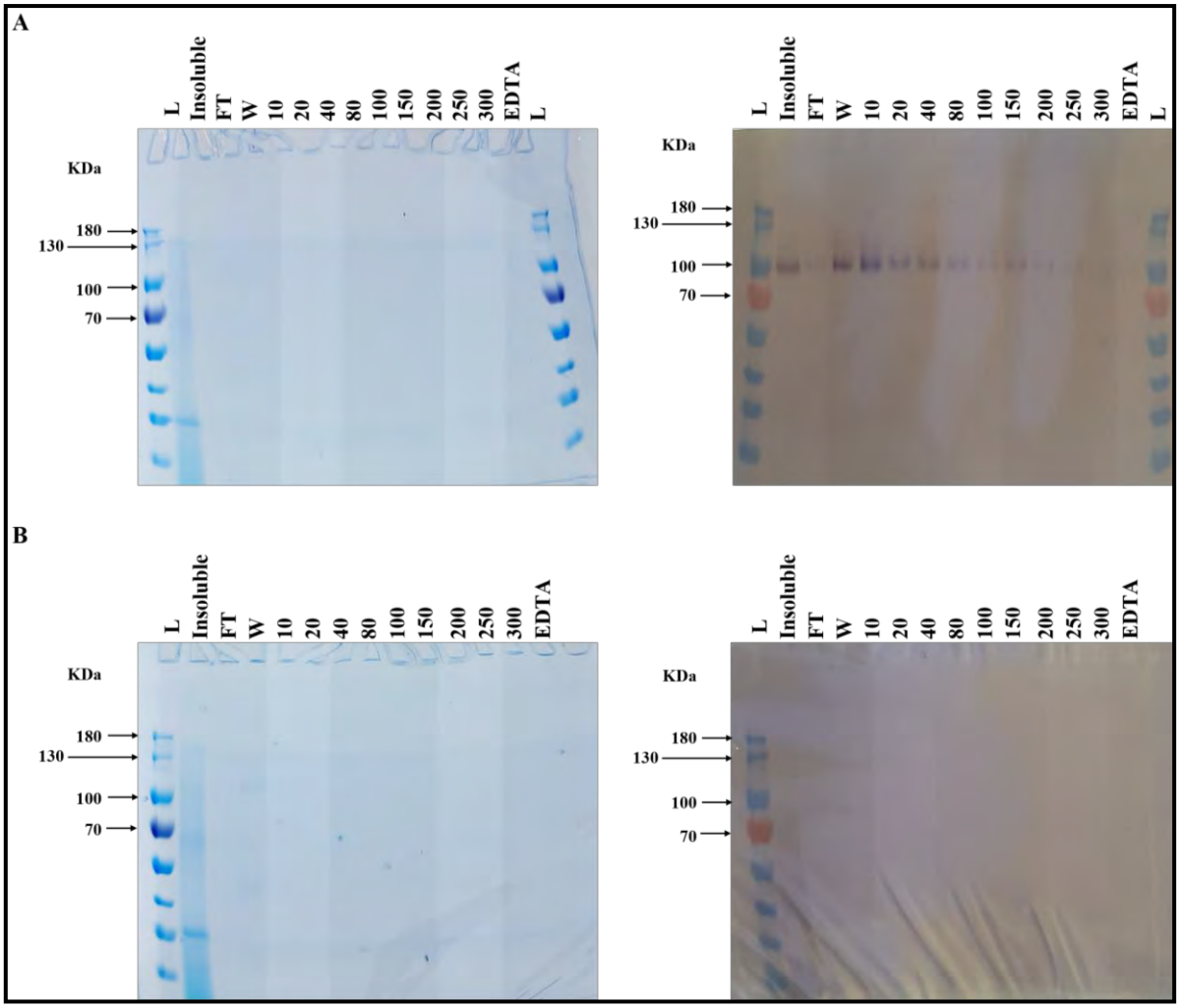

Figure 2-5: MmpL3 IMAC purification with varying imidazole concentrations showing protein degradation over 2 days. A) day 1, B) day 2. Membrane used was from 1 L culture. Left panels represents the total protein on SDS-PAGE while the right panels shows His-tagged proteins on the Western blot. Imidazole concentrations (mM) are shown as 10, 20, 40, 80, 100, 150, 200, 250 and 300. L represents the protein ladder; FT is the flow through; W is the wash and EDTA represents the 'strip' of the column.

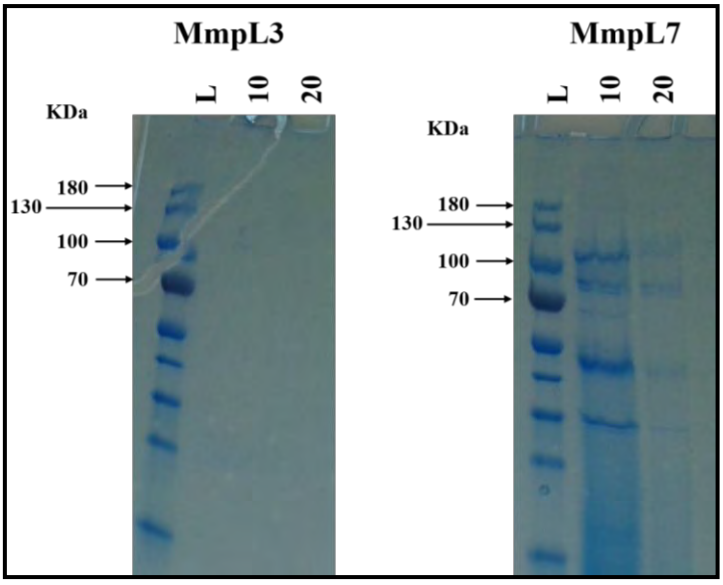

Figure 2-6: SDS-PAGE analysis comparing concentrated IMAC eluates of MmpL3 and MmpL7 at day 2. Membranes used were from 1 L cultures and eluates were concentrated to 200 µl of which 20 µl was loaded. Imidazole concentrations (mM) are shown as 10 and 20. L represents the protein ladder.

It was expected that by concentrating the eluates, total protein would be evident as seen in the MmpL7 purification, but this was not the case for the MmpL3 purification (Figure 2-6). While protein degradation is known to occur over time, it was strange that the eluates collected from the MmpL3 purification were completely degraded by day two. As SDS is a denaturing agent that could contribute to the degradation of MmpL3, this motivated analysis under non-denaturing conditions. Another purification was performed using the same conditions/ parameters as before but eluates collected were concentrated and analysed by native PAGE/ Western blot over three days (Appendix 8). Native PAGE/ Western blot analysis showed less protein at day 3 that indicated overall protein degradation at a slower rate (Appendix 8).

Since membrane prepared from 1 L cultures resulted in undetectable total protein analysed on both SDS- and native PAGE, it was expected that using three times more membrane material would improve the MmpL3 purification using SMA (Figure 2-7). Evidently MmpL3 was observed in the insoluble fraction, FT and in two eluates as confirmed by Western blot (Figure

2-7A). All IMAC eluates were concentrated and dialysed for further purification by gel filtration chromatography. The resulting chromatogram in Figure 2-7B only indicated a single peak at elutions 13 – 18 ml representing the absorbance 220 nm that were collected and analysed by SDS-PAGE/ Western blot. Unexpectedly, there were no traces of any protein, including MmpL3 in these fractions analysed by SDS-PAGE/ Western blot (Figure 2-7B).

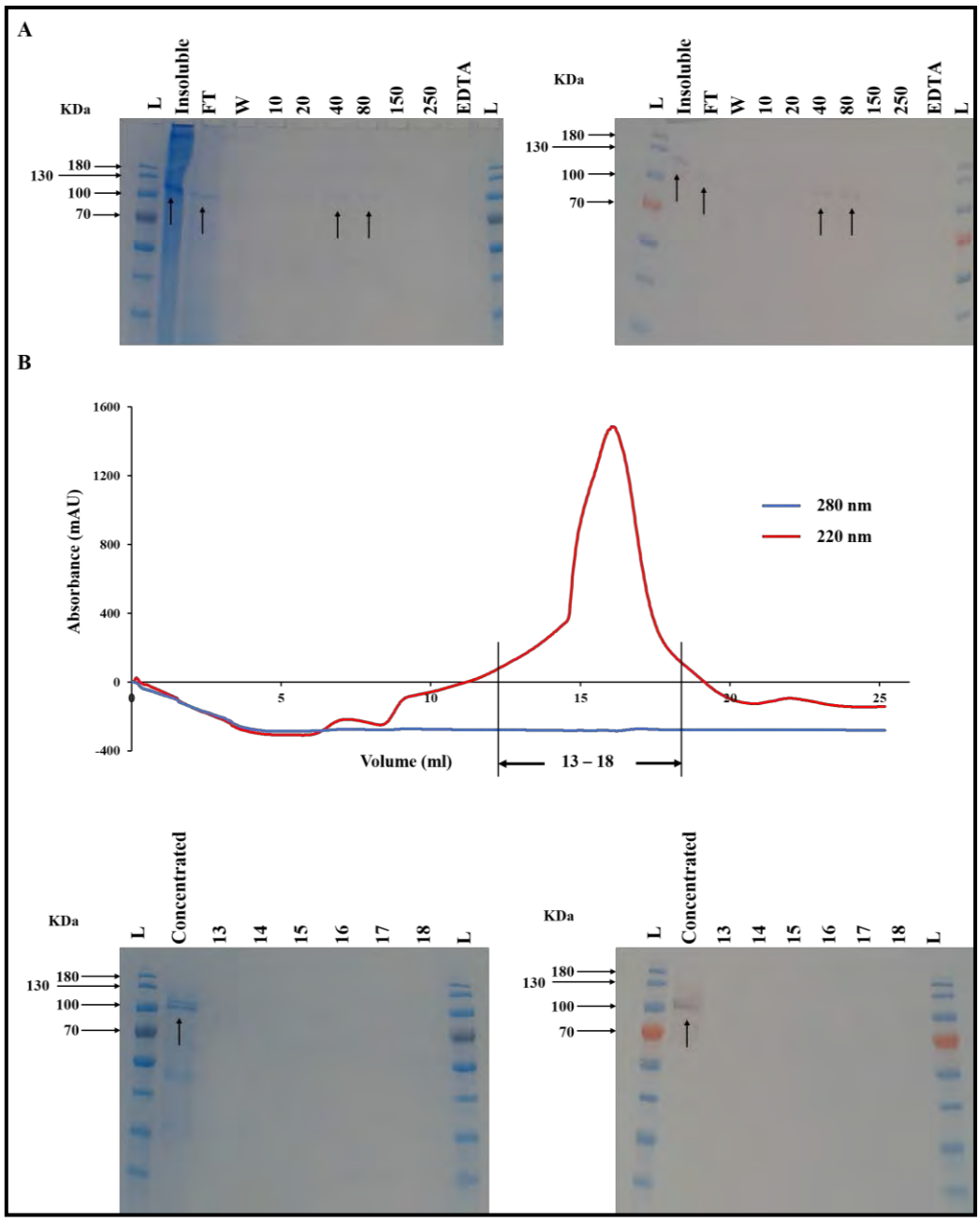

Figure 2-7: SDS-PAGE/ Western blot analysis of MmpL3 two-step purification. A) IMAC with varying imidazole concentrations (mM) are shown as 10, 20, 40, 80, 150, and 250. B) Gel filtration showing a single peak in red corresponding to the 13-18 ml eluates which were collected and analysed. Membrane used was from 3 L cultures. Black arrow indicates MmpL3. Left panels represents the total protein on SDS-PAGE while the right panels show His-tagged proteins on the Western blot. L represents the protein ladder; FT is the flow through; W is the wash and EDTA represents the 'strip' of the column.

Possibly during gel filtration, the low protein concentration was diluted to the point of no detection on a Western blot. Interestingly, a quarter of the insoluble sample was loaded as

compared to the other samples in Figure 2-7A yet higher yields of protein including MmpL3 were observed. This indicated that SMA did not effectively solubilise the membrane. Indeed, the FT was also another indicator that depicted poor SMA solubilisation as in this sample, there was very little to no protein background.

2.3.5 Purification of MmpL7 using SMA

Poor membrane solubilisation was also observed in the MmpL7 purification using SMA (Appendix 9). When three times more membrane was used for solubilisation with SMA there was more total protein in the FT including MmpL7 that was also detected in the wash step with no imidazole and eluates with low imidazole concentrations as verified by Western blot analysis (Figure 2-8). Analysing fractions before solubilisation (i.e. the membrane) and after solubilisation (i.e. soluble and insoluble) were included in determining the efficiency of SMA solubilisation (Figure 2-8). Notably, the insoluble fraction contained more MmpL7 than the soluble fraction as indicated by the Western blot.

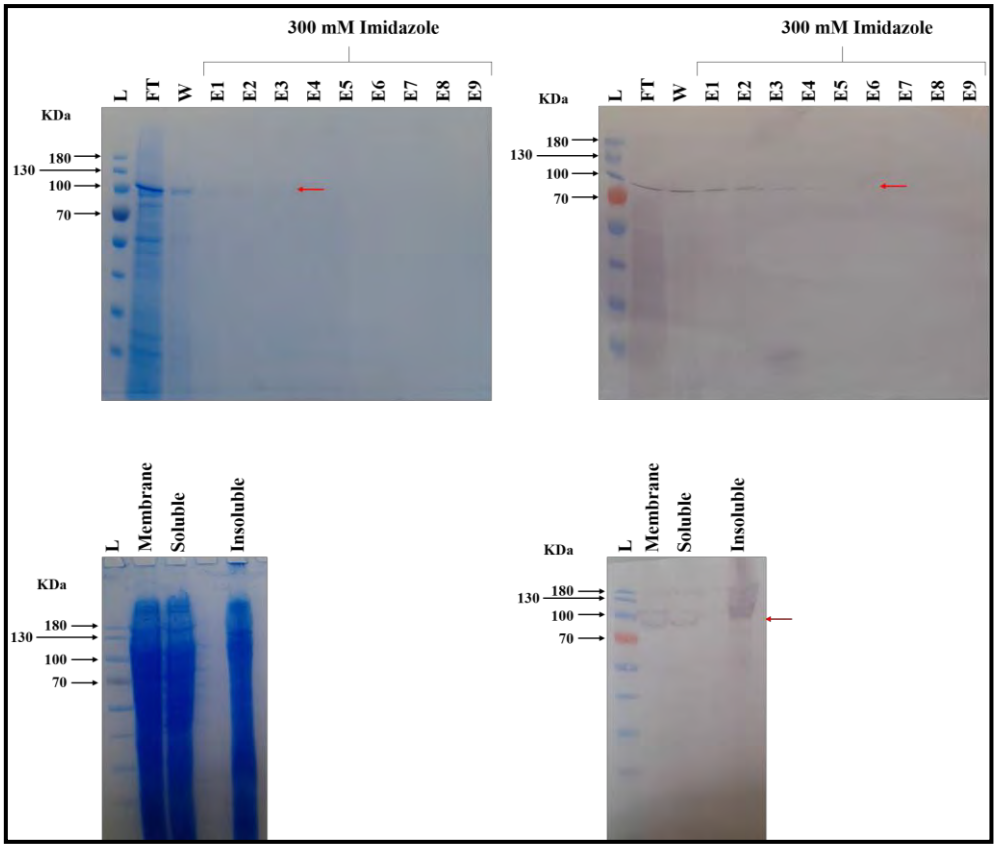

Figure 2-8: MmpL7 IMAC purification with one imidazole concentration using SMA including fractions before and after SMA solubilisation. The membrane represents the fraction before SMA solubilisation, while soluble and insoluble represent fractions after SMA solubilisation. Equal amounts of the membrane, soluble and insoluble fractions were loaded and were from 3 L cultures. Left panels represents the total protein on SDS-PAGE while the right panels show His-tagged proteins on the Western blot. L represents the protein ladder; FT is the flow through and W is the wash. Red arrow indicates MmpL7.

Collectively very little to no total protein was observed in purifications of the control strain (Appendix 7B), MmpL3 (Figure 2-5) and MmpL7 (Figure 2-8) using SMA resulting in unsuccessful purification attempts because the membranes were not being solubilised by SMA effectively. Besides, MmpL3 and MmpL7 were eluted in washes with no and low concentrations of imidazole (referred to as "leaky"), indicating weak affinity between the His-tag and the charged nickel resin (Ni-NTA agarose). One possible cause of weak interactions could be the SMA polymer blocking the tag from the nickel resin.

2.3.6 Purification of MmpL7 using DDM

To determine if solubilisation using SMA was ineffective and if SMA was hindering the affinity between His tagged MmpL3 and MmpL7 proteins and the charged nickel resin, solubilisation and downstream purifications were performed using n-dodecyl-β-d-maltoside (DDM) detergent. Undeniably, solubilisation of the membrane was markedly improved using DDM as indicated by the total protein in the FT in Figure 2-9. In Figure 2-9A, the majority of MmpL7 was eluted in the FT and continued to "leak" throughout the purification. However, in Figure 2-9B, MmpL7 was mainly detected in the FT and EDTA fraction suggesting that not all the protein passed through the column. Surprisingly these results indicated that the concentration of membrane material extracted with DDM was crucial and required further consideration. Although there was an improvement in membrane extraction using DDM, there was no enrichment for MmpL7, indicating that there was another reason for the weak affinity between tagged proteins and the nickel resin.

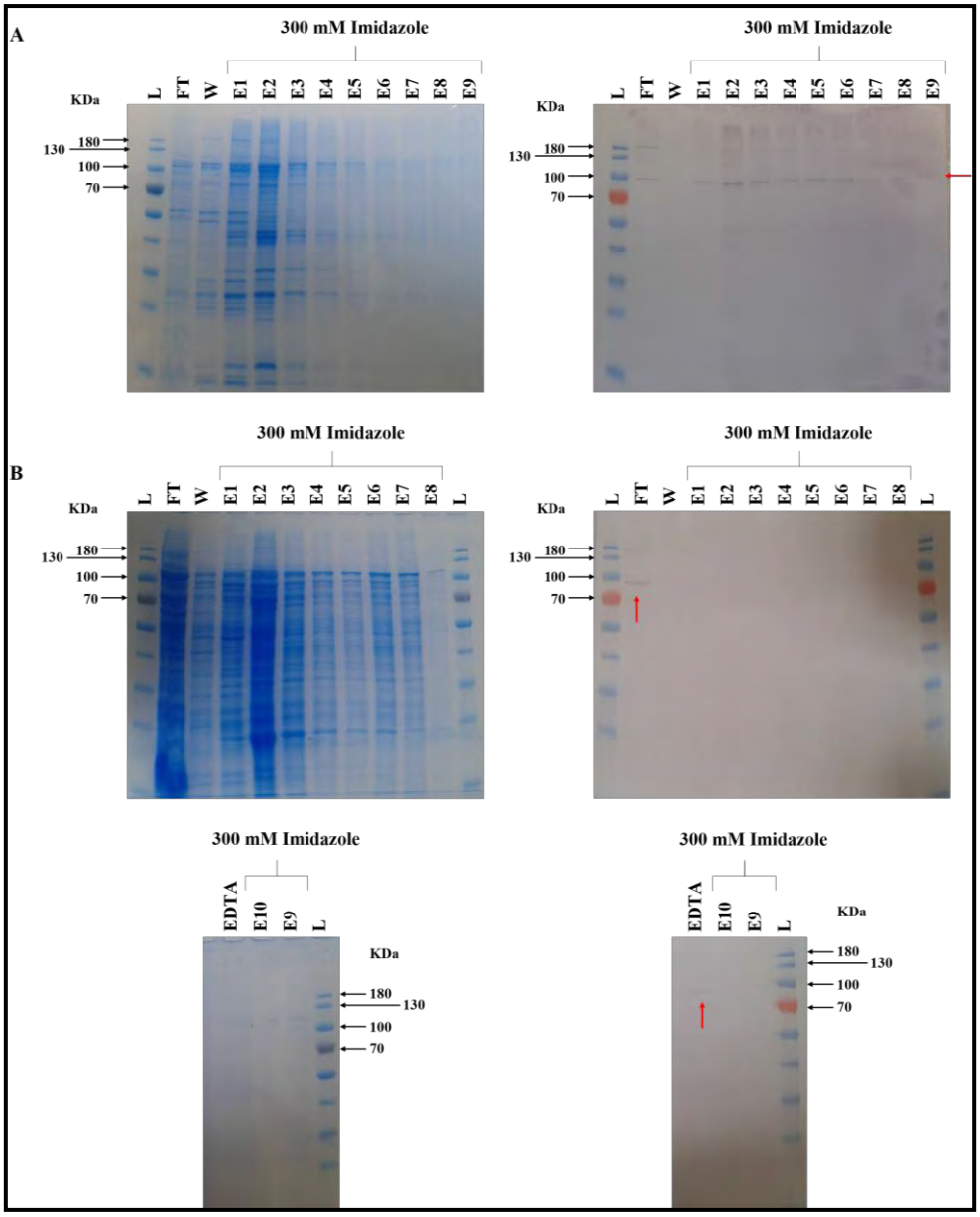

Figure 2-9: MmpL7 IMAC purification with one imidazole concentration using DDM. Membrane material of: A) 40 mg/ml and B) 80 mg/ml. Left panels represents the total protein on SDS-PAGE while the right panels show His-tagged proteins on the Western blot. L represents the protein ladder; FT is the flow through; W is the wash and EDTA represents the 'strip' of the column. Red arrow indicates MmpL7.

According to the predicted solvent accessibility calculated by the I-TASSER server (253) of MmpL3 and MmpL7 including their respective six His tag at the C terminal ends, revealed that five of six His residues in these proteins were buried explaining the weak interaction (Appendix 10). Therefore, primers to generate a longer C terminal His tag (up to twelve His) and a TEV

site (Tobacco Etch Virus sequence-specific protease) to cleave off the His-tag were created to improve MmpL7 IMAC purification (Appendix 11). However, due to time constraints, the improved version of the MmpL7 protein expression construct was not generated, and protein expression and purification experiments were not performed.

2.4. Discussion

MmpL proteins are significant contributors to Mtb survival and pathogenesis by building the cell wall with virulence-related lipids, acquiring iron acquisition through different methods and serving as drug efflux pumps when overexpressed. In an attempt to determine the structure of two MmpL proteins, MmpL3 and MmpL7, the objective was to use the styrene-maleic acid (SMA) co-polymer coupled with single-particle electron microscopy (NEM/CEM) over detergent-based and X-ray crystallography methods (244,252).

Indeed, the first hurdle of expressing proteins was overcome. MmpL3 and MmpL7 were produced in commonly used *E. coli* expressing vectors and strains observed in small- and large-scale cultures. The expression of MmpL3, together with the construction of the expression vector was the previous work of a PhD student (65) and postdoctoral colleague. They found the overexpression of MmpL3 produced a lethal effect and therefore, the post-induction period was restricted. The overexpression of MmpL7 was not toxic and hence, the post-induction period was longer and set to facilitate correct protein folding. To avoid AcrB contamination, an expressing strain without the *acrB* gene was used for the heterologous overexpression of MmpL3 and MmpL7. Both proteins were not confidently identified in the *acrB* deficient strain despite changing the growth media, post-induction conditions and volumes of cultures. To verify the presence of RND proteins after purification and NEM/CEM imaging a no protein control or negative control was included in membrane preparation and purification.

SMA membrane extraction or solubilisation was the chosen method as it has been shown to directly extract membrane proteins and keep them in their the native lipid bilayer that provides protein stability and preserves protein function, it is economical and straightforward to use, it is compatible with analytical techniques and single-particle electron microscopy that requires lower levels of protein for structural determination (243,244,247,248,252). For the solubilisation of MmpL3 and MmpL7, SMA was used but resulted in ineffective membrane extraction as higher levels of total protein including MmpL3 and MmpL7 were detected in the insoluble fraction after SMA solubilisation, regardless of the amount of membrane used. Also, the unsuccessful MmpL3 and MmpL7 purifications were a result of weak binding affinity.

However, SMA has limitations such as in the presence of divalent cations the SMA polymer precipitates (254) and is rendered insoluble at an acidic pH (255). Divalent cations could have been present as MmpL3/11 are known to acquire heme aside from lipid transport that is a divalent cation (197,198). As MmpL3 is a heme associated protein, it could also interact with other divalent cations to promote conformational changes and for its function (256). These reasons could be applied to MmpL7 explaining the equally poor solubilisation with SMA but has not been determined whether this protein interacts with divalent cations for its activity. Besides, the lysis buffer in this work included EDTA that chelates divalent cations. The EDTA containing buffer was only used at the lysis step and washed thereafter with Tris-based buffers containing no EDTA to avoid interference with the IMAC purification. The pH of the buffer was monitored before and after SMA solubilisation and before IMAC purification with and without imidazole. Thus, all buffers and mixtures were maintained at pH 7.9 - 8.0.

DDM was used to determine whether the SMA was blocking the His-tag and hindering affinity during purification and to compare the efficiency of SMA solubilisation. DDM significantly improved solubilisation of the membrane suggests that the high protein levels found in the

insoluble fraction were not due to protein contained in inclusion bodies (also referred to as insoluble) as detergents are ineffective in extracting protein from these structures. The improved membrane extraction with DDM did not improve the IMAC purification. With the use of I-TASSER the predicted solvent accessibility of the six His tag at the C terminal ends of MmpL3 and MmpL7 were found to be mostly buried explaining the weak affinity between the tag and the charged nickel resin resulting in poor IMAC purifications. The results of I-TASSER were surprising for MmpL3 as the C terminus follows the soluble cytoplasmic domain (D3) and was expected to be exposed. Collectively, these analyses revealed the most prominent problems impeding successful isolation and purification of MmpL3 and MmpL7 were at the solubilisation step using SMA and the almost buried His tag of MmpL3 and MmpL7 expression constructs.

Some unexpected findings were also presented in this work, such as protein degradation unique to MmpL3 evident in denaturing and non-denaturing analyses despite using protease inhibitors and autoclaving buffers (in addition to filtering). In 2019, two publications have determined the structure of MmpL3 (32,183), significant contributions to the understanding of MmpL proteins and achievement in membrane protein structural biology. Interestingly, these independent findings reported the cytoplasmic soluble D3 domain of MmpL3 caused interference in the structural determination process as it was subject to proteolytic cleavage resulting into truncated versions of MmpL3 all without D3, that validated our observations of protein degradation associated with MmpL3 (32,183).

Notably, DDM was used in the structural determination of MmpL3 and its homolog CmpL1 in *Corynebacterium glutamicum* (*C. glutamicum*) by conventional X-ray crystallography (32,183) and single-particle electron microscopy (185) indicating that detergents remain the method of choice despite the widespread use and success of SMA. In contrast to these studies,

difficulties in isolating MmpL7 were experienced when solubilising higher concentrations of membrane material using DDM suggesting that optimisation was required. Since the molecular weight of the DDM corona (65- 70 kDa) and MmpL3 and MmpL7 (~ 101/95 kDa) were similar another consideration of using DDM was effectively removing excess detergent without losing protein and drastically changing the critical micelle concentration (cmc) that could result in destabilization and denaturation (240). As single-particle electron microscopy was the route preferred in this study, NEM would have been performed first to verify the integrity of the protein sample then CEM. However, the presence of DDM micelles with/without protein would have been difficult to distinguish with NEM. Further considerations of DDM application in addition to the buffer used in this study composed of high concentrations of salt and glycerol, producing artefacts that can be misinterpreted in NEM (257).

Even though the structure of MmpL3 has now been solved (32,183), there remain twelve MmpL proteins that await structural determination. From our failed attempts in achieving the structure of MmpL3 and MmpL7 many lessons were learnt and could be used to improve experimental design and execution. Future work involves the modification of the MmpL7 expressing vector to enhance the IMAC purification, preparation of membrane from at least 6 L of culture and to optimise the use of DDM for extracting membrane proteins coupled with traditional X-ray crystallography methods as in (32,183). While SMA could be used for protein-lipid assays and protein-protein interactions that are of relevance in understanding the mechanisms of MmpL proteins.

Chapter 3: Determining the mechanism of MmpL7

Chapter 3: Determining the mechanism of MmpL7

3.1. Introduction

A class of lipid transporters termed mycobacterial membrane protein large (MmpL) have been identified and required for mycobacterial survival, as discussed in detail in Chapter 1. The genome of *Mycobacterium tuberculosis* (Mtb) encodes thirteen MmpL proteins (54) of which only seven have known functions as dedicated lipid transporters that contribute to cell wall permeability and virulence, but also involved in drug efflux and heme acquisition (175,177,179) as discussed in detail in Chapter 1. Except for *mmpL3*, the other *mmpL* genes are not required for the growth of Mtb *in vitro*, but disruption of several *mmpL* genes result in drastic consequences *in vivo* (156,174,181).

The *mmpL* gene, *mmpL7* is contained within a locus that spans over ~73 Kbp long, encodes genes dedicated to phthiocerol dimycocerosates (PDIM) and glycosylated phenolphthiocerol dimycocerosates (PGL) biosynthesis and translocation to the outer membrane (Figure 3-1) (39,40). PDIM constitutes a diol backbone (phthiocerol), esterified to two methyl-branched fatty acyl moieties (dimycocerosates) (Figure 3-1A) (258). Briefly, the PDIM cluster constitutes a set of five Type-I polyketide synthases, PpsA-E integral for the synthesis of phthiocerol while a Type-I fatty acid synthase termed mycocerosic acid synthase (Mas) produces mycocerosic acid (Figure 3-1B) (258). PGL shares this common lipidic core, but is further expanded by a phenolic group, and glycosylation, introduced by a polyketide synthase encoded by *pks1-15* and numerous glycosyltransferases (Figure 3-1) (117,127,258). Interestingly a biochemical interaction between MmpL7 and the last polyketide synthase PpsE in the production of phthiocerol was demonstrated, linking PDIM synthesis and transport (259). *mmpL7* transports PDIM and PGL but other transport genes are also required for PDIM transport to the outer membrane (40,126,186).

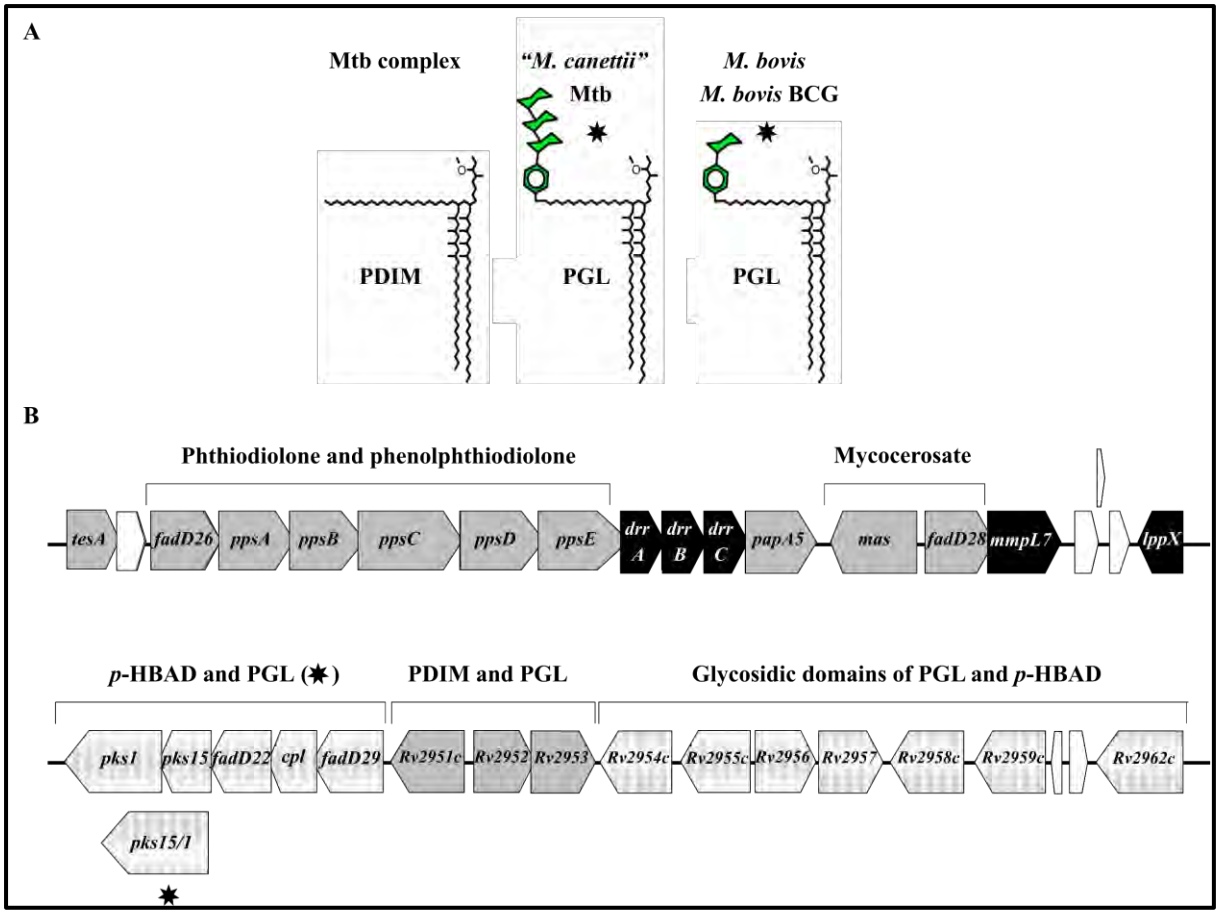

Figure 3-1: The structure and genetic context of PDIM/PGL. A) Simplified structure and B) the PDIM cluster. The * indicates an intact *pks15/1* gene is required for PGL production. [Adapted from (60,111)].

MmpL proteins are classified as part of the resistance-nodulation-cell division (RND) permease superfamily (174,227) based on phylogenetic analyses and structurally similarities (228). The principle mechanism of RND substrate translocation is based on the proton relay pathway and depends on critical residues that facilitate proton transfer and coordinate substrate translocation (230,260–262). In RND permeases these key residues are conserved and situated in transmembrane (TM) helices TM4 and TM10 (230,260–262). The characterised Gram-negative multidrug RND transporter AcrB forms a trimer for complete function, and protonmotive force (PMF) residues form salt bridges that maintain the structure of the protein (230,260–262). Upon protonation these salt bridges are disrupted leading to conformational

changes in the tripartite efflux pump and after deprotonation are re-formed or paired restoring the tertiary structure of the protein (230,260–262). RND mediated export is the result of consecutive cycles of protonation and deprotonation of the PMF network (230,260–262).

Recently the mechanism of PMF has also been described in MmpL proteins. In-depth analyses by Bernut et al. (263) has highlighted the role of conserved Asp/Tyr pairs in PMF amongst MmpL proteins situated in TM4/10 aligned with crucial residues of proton relay in AcrB. Single mutations to Asp residue in TM4 and Asp/Tyr pair in TM10 in MmpL3 were found to be essential for mycobacterial viability (263). Two protein structures of MmpL3, albeit without its cytoplasmic domain, corroborate the involvement of these Asp/Tyr pairs in proton translocation (32,183). Indeed four promising drugs (SQ109, AU1235, ICA38 and rimonabant) some of which were already recognised as PMF inhibitors (194) were shown to directly bind to the proton translocation channel defined by TM4/10 disrupting PMF (32).

Furthermore, Bernut and colleagues reported (175,179,180,263) that MmpL7 was the only member of the MmpL family that does not possess these conserved Asp/Tyr residues at TM4/10. However, *mmpL7* is classified as an RND member (174,227) and has a function in PDIM synthesis/transport (39–41,259). Thus, the aim of the study described in this chapter was to determine the mechanism of *mmpL7* (encoding MmpL7) in PDIM synthesis/transport by generating an *in-silico* model to identify residues for modification using site-directed mutagenesis (SDM) and assessing the effects of these single mutations on synthesis/transport of PDIM/PGL.

3.2. Methods and materials

3.2.1 MmpL7 homology model and identification of residues for investigation

I-TASSER (253) was used to generate an *in-silico* model of MmpL7 based on previously solved structures of AcrB (PDB: 4DX5) and MmpL3 (PDB: 6OR2) and viewed and edited

with Pymol (264). Using the MmpL7 homology model and the guidance of a postdoctoral researcher Dr. Robert Marshall at the University of Birmingham, we identified several residues that could possibly contribute to PDIM/PGL synthesis/transport as listed in Table 3-1 based on structural alignments with previously solved structures of AcrB (PDB: 4DX5) and MmpL3 (PDB: 6OR2), molecular analyses of the thirteen MmpL proteins and MmpL7 homologs and the extensive PMF network outlined by (185,194,228). All bioinformatics analyses in this study were performed using web-based tools listed in Chapter 6.

Table 3-1: Amino acid residues in MmpL7 targeted for site-directed mutagenesis with modifications to the nucleotide sequence.

Native amino acid	Amino acid position	Modification	Strain	Reasons
Ala- GCA	287	Ser- AGC	**A287S**	Aligned to MmpL3 TM4 PMF
Ala- GCC	288	Thr- ACC	**A288T**	Aligned to MmpL3 TM4 PMF
Ala- GCC	292	Gly- GGC	**A292G**	TM4 region
Asp- GAC	524	Leu- CTG	**D524L**	Conserved in MmpL7 homologs
Arg- CGC	610	Asp- GAC	**R610D**	Conserved in MmpL7 homologs
Iso- ATC	611	Arg- CGG	**I611R**	Conserved in MmpL7 homologs Required for PpsE binding to MmpL7 periplasmic domain 2 (PD2) (259)
Asp- GAT	670	Arg- CGG	**D670R**	Conserved amongst MmpL proteins and MmpL7 homologs Aligned to AcrB PD2
Asp- GAT	673	Ala- GCC	**D673A**	Aligned to AcrB PD2
Glu- GAG	676	Ala- GCC	**E676A**	Aligned to AcrB PD2
Pro- CCG	836	Asp- GAC	**P836D**	Aligned to AcrB TM10 PMF
Tyr- TAT	837	Phe- TTC	**Y837F**	Aligned to AcrB TM10 PMF Conserved in MmpL proteins and MmpL7 homologs
Arg- CGT	846	Ala- GCC	**R846A**	Conserved in MmpL proteins

3.2.2 Δ*mmpL7* mutant generation in BCG

Since the *mmpL7* genes of Mtb (H37Rv) and *M. bovis* are identical, genetic and phenotypic characterisation of *mmpL7* Mtb (H37Rv) could be performed in the biosafety level two microorganism, *M. bovis* BCG (BCG). Briefly 1 Kbp PCR fragments upstream and downstream using primers in Appendix 5A of the *mmpL7* gene from H37Rv genomic DNA was cloned into p0004S, flanking a hygromycin resistance cassette and verified by DNA sequencing. This construct was packaged into the temperature-sensitive mycobacteriophage required for transduction of wild type BCG with phΔ*mmpL7* as described in detail in Chapter 6. All hygromycin resistant transductants were selected and verified by Southern blot analysis that was used to identify a mutant; confirm that no re-arrangements have occurred and ascertain the integrity of the upstream and downstream regions of the *mmpL7* deletion. Only one transductant was selected and designated Δ*mmpL7* used for further studies.

3.2.3 Generation of twelve site-directed mutagenized strains in BCG

The complemented *mmpL7* construct was created by cloning full-length *mmpL7* (using primers indicated in Appendix 5B) into the replicating vector, pMV261 under the GroEL (Hsp) promoter (265) and verified by DNA sequencing. This vector was used as a template for constructing the twelve site-directed mutagenized strains of MmpL7 with the aid of the site-directed mutagenesis kit explained in Chapter 6. The NEB base changer website (http://nebasechanger.neb.com/) was used to design primers for site-specific modification (Appendix 5C), and details of the Q5 site-directed mutagenesis process were followed, as indicated in Chapter 6. The resulting mutagenized plasmids containing individual site-specific modifications were verified by DNA sequence analysis.

The native *mmpL7* complementation vector with the twelve mutagenized vectors were electroporated into the Δ*mmpL7* mutant, and after recovery and incubation, kanamycin and

hygromycin resistant transformants were selected and confirmed by PCR. The positive transformants were subject to another round of DNA sequencing analysis to verify the modifications made in the *mmpL7* gene. After that, all strains in Table 3-2 together with the wild type BCG strain were analysed for *mmpL7* expression by reverse transcriptase- PCR using primer pairs in Appendix 5E and by general and specific lipid analysis, as described in detail in Chapter 6.

3.2.4 Plasmids and strains

Table 3-2 below provides a list of the plasmids, bacterial strains and recombinant mycobacteriophages only generated in this study, while the reference plasmids, bacterial strains and recombinant mycobacteriophages described in Chapter 6, Table 6-1.

Table 3-2: A list of plasmids, mycobacteriophages and bacterial strains generated in this study.

	Genetic characteristics
Plasmids	
p∆*mmpL7*	Derivative of p0004s cosmid obtained by cloning upstream and downstream flanks of Mtb *mmpL7* (*Rv2942*)
pMV261:*mmpL7*	A copy of Mtb *mmpL7* (*Rv2942*) cloned into pMV261 *E. coli*/mycobacterial shuttle vector, in frame with the GroEL (Hsp) promoter
pMV261_A287S	*mmpL7* complement vector with a codon modification at residue 287
pMV261_A288T	*mmpL7* complement vector with a codon modification at residue 288
pMV261_A292G	*mmpL7* complement vector with a codon modification at residue 292
pMV261_D524L	*mmpL7* complement vector with a codon modification at residue 524
pMV261_R610D	*mmpL7* complement vector with a codon modification at residue 610
pMV261_I611R	*mmpL7* complement vector with a codon modification at residue 611
pMV261_D670R	*mmpL7* complement vector with a codon modification at residue 670

pMV261_D673A	*mmpL7* complement vector with a codon modification at residue 673
pMV261_E676A	*mmpL7* complement vector with a codon modification at residue 676
pMV261_P836D	*mmpL7* complement vector with a codon modification at residue 836
pMV261_Y837F	*mmpL7* complement vector with a codon modification at residue 837
pMV261_R846A	*mmpL7* complement vector with a codon modification at residue 846
pMV306::*mmpL7*	A copy of Mtb *mmpL7* (*Rv2942*) cloned into pMV306 *E. coli*/mycobacterial shuttle vector, in frame with 400bp upstream of the native promoter region and 200bp downstream of *mmpL7*
Mycobacteriophages	
phΔ*mmpL7*	Derivative of phAE159 obtained by cloning pΔ*mmpL7* at the *Pac*I site
Bacterial strains	
Δ*mmpL7*	BCG strain with Mtb *mmpL7* (*Rv2942*) replaced with *hyg-sacB* cassette
mmpL7-C	Δ*mmpL7* BCG strain that contains pMV261:*mmpL7*
A287S	Δ*mmpL7* BCG strain that contains pMV261_A287S
A288T	Δ*mmpL7* BCG strain that contains pMV261_A288T
A292G	Δ*mmpL7* BCG strain that contains pMV261_A292G
D524L	Δ*mmpL7* BCG strain that contains pMV261_D524L
R610D	Δ*mmpL7* BCG strain that contains pMV261_R610D
I611R	Δ*mmpL7* BCG strain that contains pMV261_I611R
D670R	Δ*mmpL7* BCG strain that contains pMV261_D670R
D673A	Δ*mmpL7* BCG strain that contains pMV261_D673A
E676A	Δ*mmpL7* BCG strain that contains pMV261_E676A
P836D	Δ*mmpL7* BCG strain that contains pMV261_P836D
Y837F	Δ*mmpL7* BCG strain that contains pMV261_Y837F
R846A	Δ*mmpL7* BCG strain that contains pMV261_R846A
mmpL7- NC	Δ*mmpL7* BCG strain that contains pMV306::*mmpL7*

3.3. Results

3.3.1 Identifying residues in transmembrane (TM) domain in MmpL7

A homology model of MmpL7 was generated using the I-TASSER server based on characterised RND transporters, AcrB in *E. coli* and MmpL3 in *M. smegmatis* (Figure 3-2). While the MmpL7 model shared all the structural features of RND transporters (Figure 3-2), superimpositions at conserved PMF sites revealed Ala residues at TM4 (positions 287/288) and at TM10, Pro836 and Tyr837 amino acids (Figure 3-2) in line with previous observations (175,179,263).

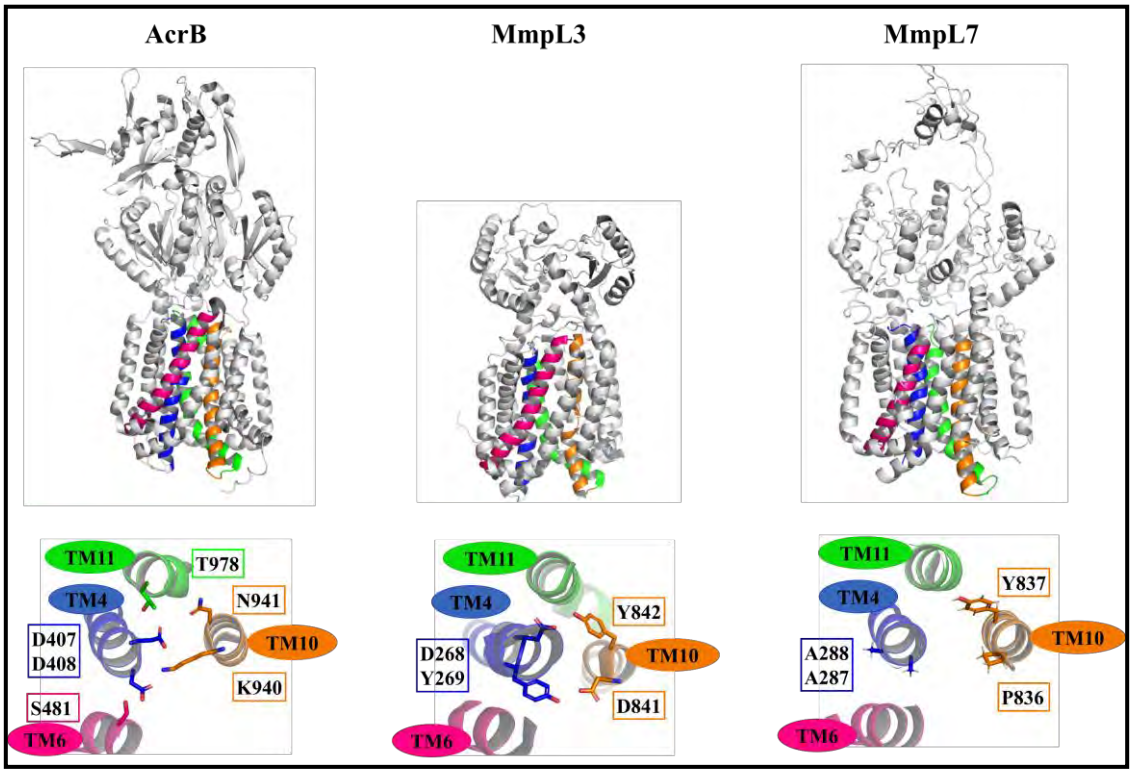

Figure 3-2: MmpL7 homology model highlighting the lack of PMF associated residues. The top panel indicates the overall protein topology of the MmpL7 model as compared with solved structures of AcrB (PDB: 4DX5) and MmpL3 (PDB: 6OR2). Transmembrane regions (TM) involved in proton relay are coloured in blue (TM4), magenta (TM6), orange (TM10) and green (TM11). The bottom panel highlights the known residues involved in PMF in AcrB and MmpL3 and the corresponding amino acids in MmpL7. [Presented as in (263)].

A proton translocation channel constitutes an extensive network of residues involved in proton relay distributed in the TM domain. In AcrB, residues located TM6/11 are also crucial for PMF as shown in Figure 3-2 (230,260,261,266). Thus, by examining the literature in AcrB, (230,260,261,266), SecDF (267), CusA (233) and MmpL3 (32,183,185,194,228) we found an extensive list of residues distributed in the TM domain required for PMF. This list was mapped onto the amino acid sequence of MmpL7 to see the potential corresponding residues (Figure 3A) and compared with the other MmpL members (Figure 3-3A) and the MmpL7 homologs amongst PDIM producing mycobacteria (Figure 3-3B) by multiple sequence alignments (MSA).

Strangely, upon inspection of the amino sequence of MmpL7 there were no Asp-Tyr pairs in the entire protein sequence in Mtb (data not shown). Even though MmpL13 and MmpL6 are truncated members of the MmpL family, one Asp- Tyr pair remains conserved (Figure 3-3A). Already, we have shown that MmpL7 is deficient in Asp-Tyr pairs in TM4/10 except for the widely conserved Tyr837 in TM10 amongst MmpL members and MmpL7 homologs (Figure 3-3). In the same TM unit, another conserved residue across MmpL proteins, Arg846 (Figure 3-3A) not mentioned in previous works, was found. Analysis of MmpL7 homologs of PDIM producing mycobacteria revealed conservation of Ala287 in TM4 and Pro836 in TM10 (Figure 3-3B). From these results, most residues outlined in the literature to form a proton relay network distributed throughout the TM domain in other RND members were not found in MmpL7. Nonetheless, residues in TM4/10 were selected to probe whether they contributed to MmpL7 activity (Figure 3-3).

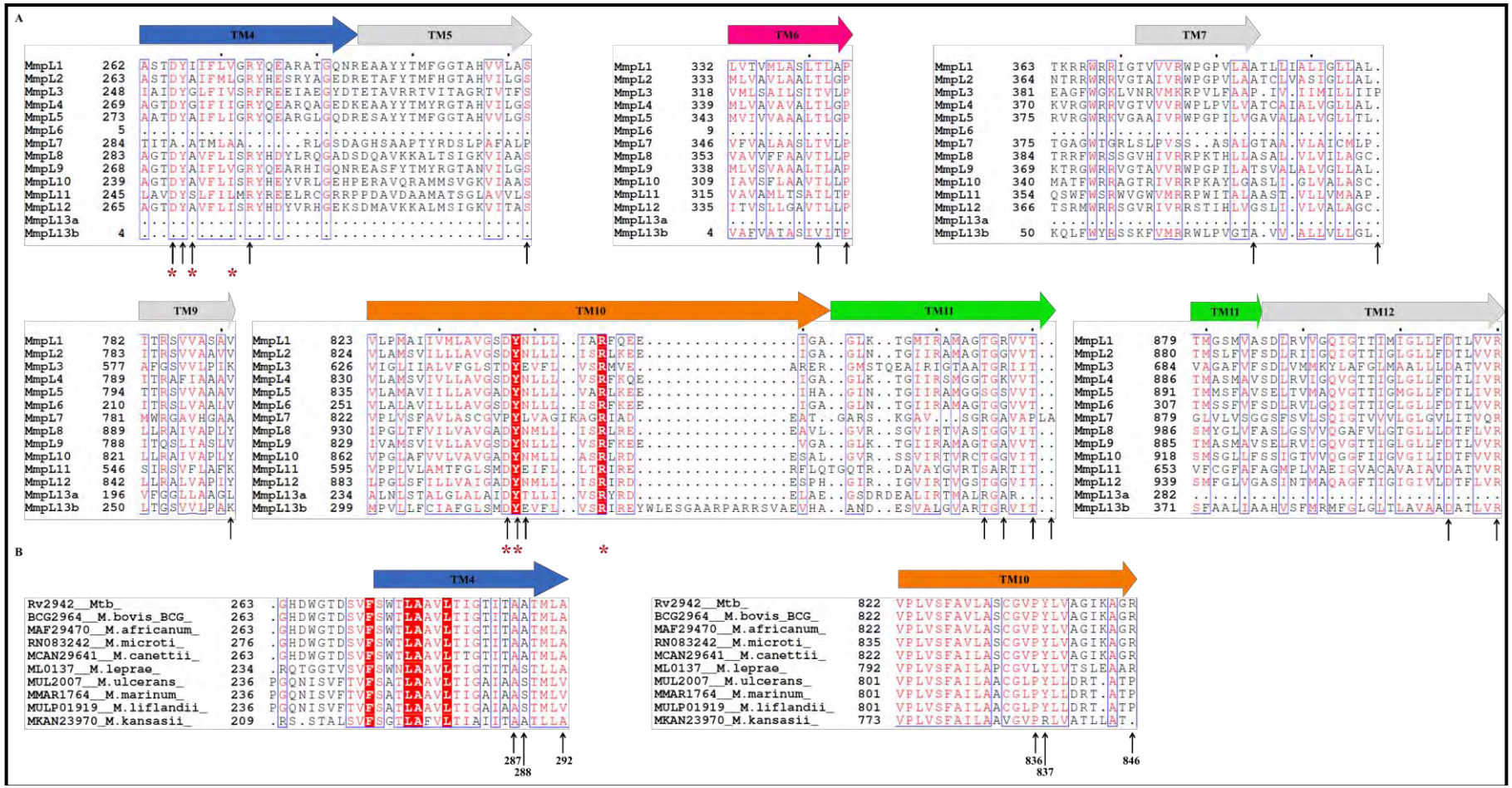

Figure 3-3: Multiple sequence alignment (MSA) emphasising residues involved in PMF. A) MmpL proteins in Mtb and B) MmpL7 homologs in PDIM producing mycobacteria.TM4, TM6, TM10 and TM11 are coloured in blue, magenta, orange and green respectively. A list of residues involved in PMF are indicated by arrows, while the red asterisks and arrows labelled with the corresponding MmpL7 residue position denotes amino acid residues investigated in this study.

3.3.2 Identifying residues in periplasmic domain 2 (PD2) MmpL7

The periplasmic domains of RND transporters are vital components of the protein that enable substrate binding and dictate specificity and with regards to AcrB, also interact with adaptor and outer membrane proteins to form functional multi efflux pumps (268,269). Interestingly, Jain and Cox (259) revealed a biochemical interaction between the PD2 region of MmpL7 with PpsE, the last polyketide synthase to produce phthiodiolone in PDIM.

The majority of MmpL proteins have an additional structural motif in PD2 that is similar to AcrB (228). Therefore, the MmpL7 model was superimposed with RND members AcrB and MmpL3 to examine the structural features of PD2 further. The alignment with MmpL3 highlighted the additional structural motif in PD2 (Figure 3-4A). Superimposition with AcrB revealed that while there was a similar organisation of the porter and docking domains, there were also significant structural differences between the docking domains of AcrB and MmpL7 (Figure 3-4A). This observation suggested that PD2 of MmpL7 and other MmpL proteins alike is unique to the MmpL family.

Molecular analysis revealed a list of conserved residues between MmpL7 homologs and AcrB. Interestingly, Asp524, Arg610 and Ile611 residues were highly conserved in PDIM producing mycobacteria, and two Asp residues at positions 670 and 673 were conserved with AcrB (Figure 3-4B). Only Asp670 was strictly conserved amongst MmpL7 homologs and found in other MmpL proteins (Appendix 12), but Asp673 and Glu676 were mainly found within MmpL7 homologs (Figure 3-4B). Both Ile611 and Asp673 resulted in the abrogation of MmpL7-PpsE binding (259). Since the PD2 region of MmpL7 is vast with the aid of the Jain and Cox (259) findings, structural and sequence analyses we were able to select several residues in the docking domain of PD2.

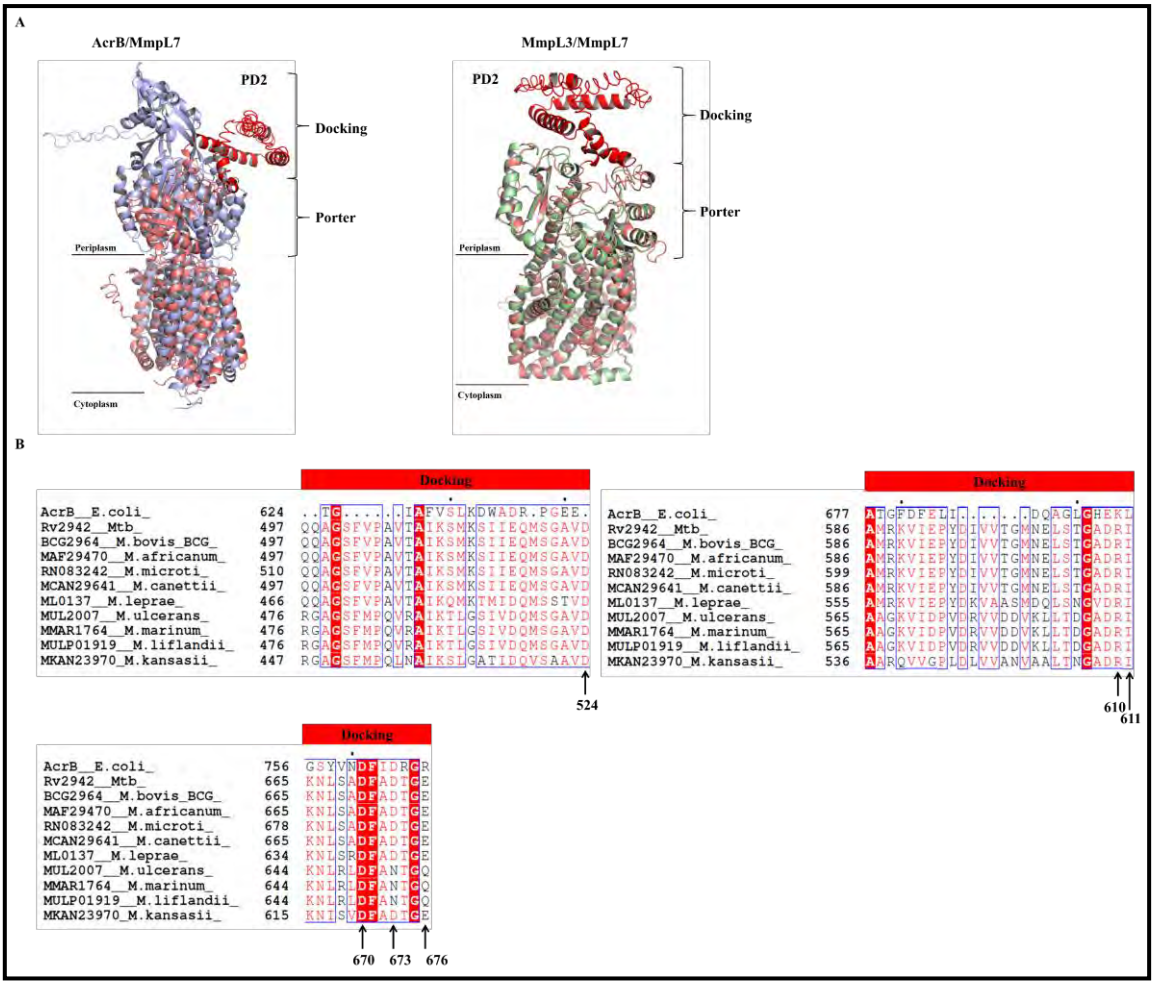

Figure 3-4: Structural and sequence analyses of MmpL7 periplasmic domain 2 (PD2). A) Superimposed structures of MmpL7 with AcrB and MmpL3 emphasising MmpL7 PD2 and B) MSA of MmpL7 homologs with AcrB focussing on the PD2 region. Alignments of MmpL7 indicated in deep salmon with solved structures of AcrB (PDB: 4DX5) depicted in light blue and MmpL3 (PDB: 6OR2) coloured in pale green, generated by I-TASSER specifically highlighting MmpL7 periplasmic domain 2 (PD2) in red. Amino acids investigated in this study were indicated by an arrow with the residue position.

3.3.3 Generation of the *mmpL7* mutant, *mmpL7* complemented and twelve *mmpL7* mutagenized strains

To investigate whether the residues identified in this study located in the TM domain and PD2 were involved in MmpL7 function, conservative modifications to these residues were made (as shown in Appendix 13), using the pMV261-7C vector as a template that resulted in twelve mutagenized vectors. Also, the *mmpL7* mutant was constructed and verified by Southern blot

in Figure 3-5 for complementation with the pMV261-7C vector and the twelve mutagenized vectors resulting in twelve mutagenized *mmpL7* strains and the *mmpL7*- C strain. Each of the strains was tested for *mmpL7* expression by reverse transcriptase- PCR (Appendix 14).

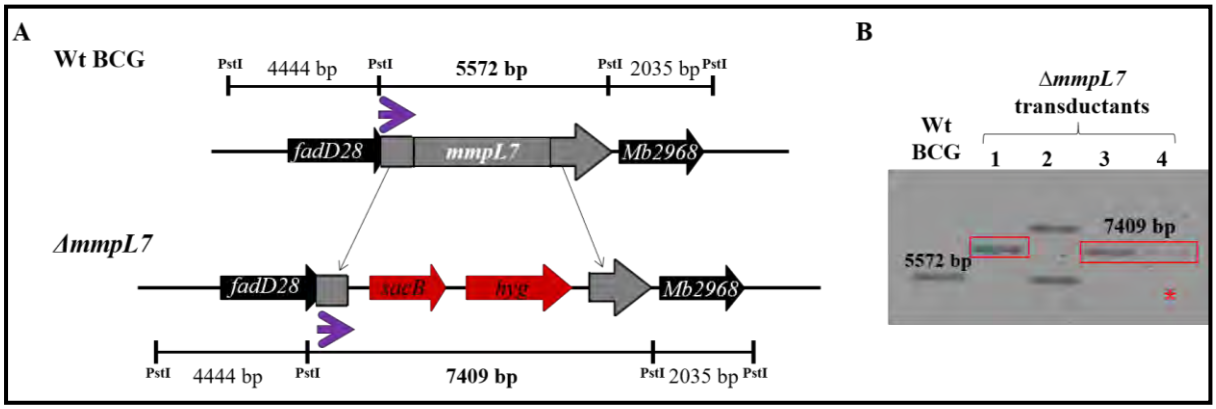

Figure 3-5: Southern blot verification of the Δ*mmpL7* mutant in BCG. A) Genetic context of *mmpL7* in wild type (Wt) BCG and the mutant. (B) Genomic DNA from the Wt BCG strain and four transductants were digested with *Pst*I and probed with the upstream PCR amplicon (941 bp). The expected fragment sizes for Wt BCG was 5572 bp and for the *ΔmmpL7* mutant was 7409 bp outlined by the red box evident for transductants 1, 3 and 4. Only transductant 4 was used for further experiments indicated by the red asterisk and designated *ΔmmpL7*. The probe is indicated as the purple arrow and where *hyg*, hygromycin resistance gene from *Streptomyces hygroscopicus*; *sacB*, sucrose counter selectable gene from *Bacillus subtilis*.

3.3.4 Lipid analysis

For selectively detecting PDIM/PGL, [^{14}C]-propionate a radioactive metabolic label was used as in previous reports (39–41,120). Apolar lipids were extracted from the culture filtrate that represented the outside apolar lipids and from the bacterial cells that represented the inside apolar lipids, respectively. Outside and inside apolar lipids were separated by one-dimensional/ two-dimensional thin-layer chromatography (1D/2D TLC) to resolve PDIM/PGL.

In addition, all the strains were labelled with [^{14}C]-acetate a radioactive metabolic label incorporated in all lipids to verify that the deletion/restoration of the *mmpL7* gene was specific to PDIM/PGL. Total apolar and polar lipids were extracted from bacterial cells (as described in Chapter 6) and separated on 1D/2D TLC to generate a general lipid profile (Appendix 15).

The extractable total apolar and polar lipids of the mycobacterial cell wall were not affected by the genetic manipulations of *mmpL7* (Appendix 15C/D). Only PDIM/PGL transport was affected by the deletion of *mmpL7* (Appendix 15A/B) as expected.

3.3.5 PDIM analysis

PDIM was present in both the outside and inside fractions of the wild type strain, indicating that PDIM is synthesised and transported as expected (Figure 3-6). The *mmpL7* mutant demonstrates that PDIM was only present in the inside fraction, whereas, the complemented strain *mmpL7*- C mimics the wild type and restores PDIM transport (Figure 3-6). Evidently substitutions to the triad of Ala residues in TM4 or the Pro836 at TM10 did not result in failed PDIM production or transport (Figure 3-6). Similarly, mutations to D524 and I611 did not affect MmpL7 activity as PDIM was observed both inside and outside of cells (Figure 3-6). However, an accumulation of PDIM inside the cells was observed with single mutations to R846 at TM10 and D673 in PD2 (Figure 3-6). Both I611 and D673 were reported to abrogate the MmpL7 PD2 and PpsE interaction (259), and yet PDIM synthesis was unaffected in both mutant plasmid transformed strains (Figure 3-6). Consistent with the findings of Jain and Cox (259), a mutation to I611 did not affect MmpL7 activity (Figure 3-6). Unexpectedly, modification to the highly conserved Tyr837 residue and substitution of charged residues Asp670 and Glu676 at PD2 resulted in a loss of PDIM synthesis and transport (Figure 3-6).

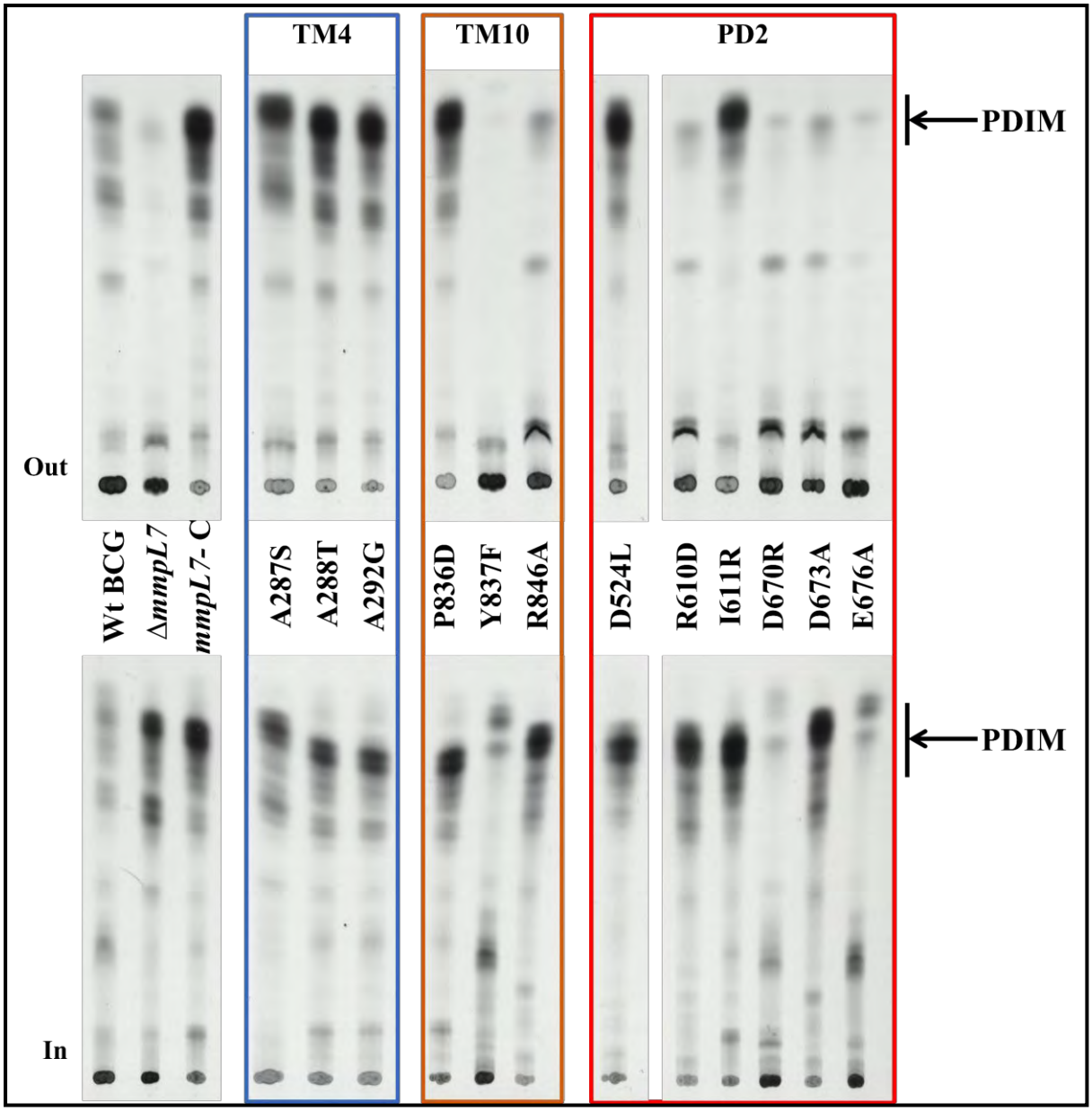

Figure 3-6: PDIM analysis of *mmpL7* SDM mutants. TLC autoradiography of [^{14}C]-propionate labelled lipids from Wild type (Wt), Δ*mmpL7* mutant and thirteen *mmpL7* complemented strains. Apolar lipid extracts from the culture filtrate (Out) and intracellular lipids (In) were separated using petroleum ether: diethyl ether (9:1 v/v). An arrow shows the PDIM species.

To rule out the possibility that these results occurred due to random mutations in the PDIM cluster (164,270), genomic DNA of Tyr837, Asp670 and Glu676 mutagenized strains were analysed by whole-genome sequencing. The whole-genome sequencing analysis revealed that there were no mutations in the PDIM cluster (data not shown). Also, from the reverse

transcriptase- PCR data, the *mmpL7* gene was expressed in all strains except the *mmpL7* mutant as expected (Appendix 14).

3.3.6 PGL analysis

Since PDIM and PGL share a common lipidic core and are transported by *mmpL7* (126), it was expected that PGL would also reflect the same results seen in Figure 3-6. PGL was evident in wild type BCG and inside cells for the *mmpL7* mutant as expected (Figure 3-7). However, PGL was not observed in the complemented strain or any of the mutagenized strains (Figure 3-7). The same results were observed when using a different metabolic label [^{14}C]-acetate (Appendix 15B).

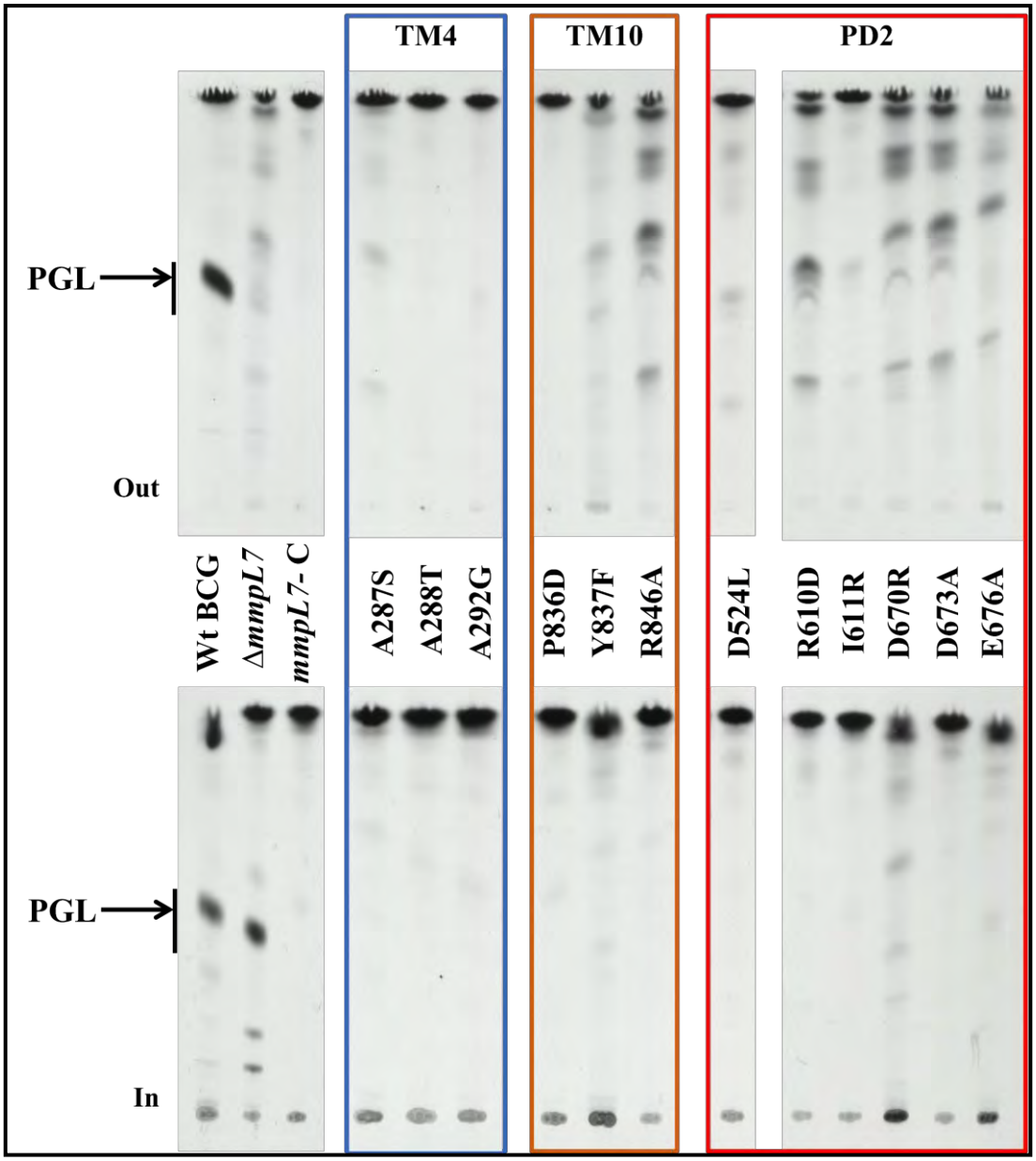

Figure 3-7: PGL analysis of *mmpL7* SDM mutants. TLC autoradiography of [^{14}C]-propionate labelled lipids from Wild type (Wt), Δ*mmpL7* mutant and thirteen *mmpL7* complemented strains. Apolar lipid extracts from the culture filtrate (Out) and intracellular lipids (In) were separated using chloroform: methanol (19:1 v/v). The arrow points to PGL.

To account for the possibility that the overexpression of *mmpL7* abrogated PGL synthesis or transport, *mmpL7* was cloned into an integrative vector (pMV306) under its native promoter and introduced into the *mmpL7* mutant to generate the *mmpL7*- NC strain. This strain together with wild type, the *mmpL7* mutant and *mmpL7*- C strains were labelled with [^{14}C]-propionate,

extracted and resolved by 2D TLC in the same manner as described earlier. PDIM/PGL were synthesised/transported in wild type, but PDIM/PGL was only synthesised and accumulated in the *mmpL7* mutant as expected (Figure 3-8). In both the over- and constitutively expressing *mmpL7* strains, only PDIM was present inside and outside of cells indicating the function of *mmpL7* was restored. Whereas, PGL was not detectable in either *mmpL7* expressing strains (Figure 3-8). Therefore, whole genome sequencing analysis was performed on the genomic DNA of the *mmpL7*-C strain and *fadD22* gene mutations were found (data not shown).

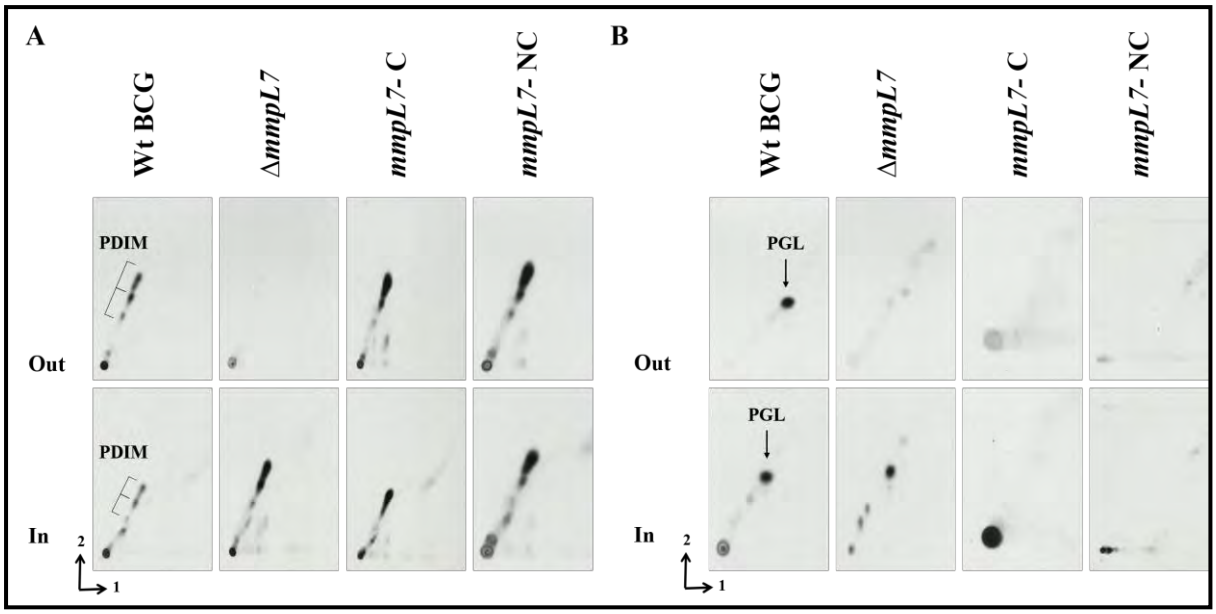

Figure 3-8: Functional analysis of over-and constitutively expressed *mmpL7*. A) PDIM and B) PGL. 2D TLC autoradiography of [^{14}C]-propionate labelled lipids from Wild type (Wt), Δ*mmpL7* mutant and two *mmpL7* complemented strains. Apolar lipid extracts from the culture filtrate (Out) and intracellular lipids (In) were separated using System A/C. The three-pointed bracket shows the PDIM species, while the arrow depicts PGL.

3.4. Discussion

MmpL proteins are responsible for transporting mycobacterial lipids and depositing these into the outer membrane for the protection, viability and pathogenesis of Mtb (175–177,179). MmpL proteins are a subclass of the RND superfamily that depends on protonmotive force (PMF) for substrate extrusion. Known residues responsible for proton relay in transmembrane

(TM) helices TM4 /10 create a proton translocation channel observed in characterised RND transporters such as AcrB (230), CusA (233), SecDF (267) and MexB (231). Similarly, in MmpL proteins the Asp-Tyr pairs residues at TM4/10 were found to play a key role in PMF (32,183,185,194,228,263). These PMF residues are conserved amongst MmpL proteins except for MmpL7, that has a role in PDIM/PGL transport (39–41,126), linked to PDIM synthesis (259) and in isoniazid efflux when the *mmpL7* gene is overexpressed (218,219). In this chapter, we attempted to understand how mmpL7 executes these activities in mycobacteria by using *in-silico* analysis, genetics, *in vivo* complementation and biochemical studies.

Besides molecular analysis in select TM helices, there are no pieces of evidence demonstrating whether PMF mediates MmpL7 transport or not. The mechanism of PMF relies on a network of residues distributed throughout the TM domain creating a proton translocation channel that guides the substrate via proton transfer. Therefore, compiling a list of residues involved in PMF from previous works in other RND members allowed for a broader search of PMF residues in the TM domain of MmpL7, structural and sequence analysis and comparisons. From these results, a shorter list of residues was selected for genetic modification and PDIM/PGL assessment. Altogether these results demonstrated that MmpL7 does not support the mechanism of PMF mediated transport as i) from structural modelling the Ala/Pro residues in TM4/10 do not form ion pairs, ii) PMF residues distributed in other TM helices were not spatially conserved and not found, iii) genetic modifications to the Ala/Pro residues in TM4/10 did not have any effect on PDIM synthesis/transport, representative of MmpL7 function.

In support of our findings, it is known that *mmpL7* is not solely responsible for the transport of PDIM to the periplasm as it is dependent on *drrC* (encodes a subunit in an ATP-binding cassette transporter) to carry out this function (40). Pasca et al. (219) demonstrated the existence of an energetics-based mechanism driving *mmpL7* function. However, several reports hypothesise

the energy is derived from *drrC* and not *mmpL7* (175,179,263) as this gene is operonic with *drrA/B* genes known to operate as an ATP-binding cassette (ABC) multi-drug exporter in mycobacteria (271). The role of *drrA/B/C* genes in PDIM/PGL transport has been investigated in Chapter 4.

However, MmpL7 did contain the widely conserved Tyr837 PMF residue in TM10, and from our analysis, we found another conserved residue amongst MmpL members in the same region, Arg846. Interestingly, genetic modification of Arg846 to Ala846, resulted in defective PDIM transport yet PDIM synthesis was unaffected. While the subtle change of Tyr837 to Phe837 lead to the disruption in PDIM synthesis in our work, the same single mutation was synonymous with defective glycopeptidolipid (GPL) synthesis reported by Bernut et al. (263). This result was surprising as PDIM and GPL are unrelated lipids that are synthesized and transported by independent enzymes encoded by genes clustered on different chromosomal contexts (39–41,192).

MmpL periplasmic domains were shown to facilitate heme uptake (197,198) and more recently by structural advances in MmpL3 involved in substrate binding, specificity and extrusion (32,183). Considering the importance of these domains in MmpL function and the majority of MmpL members including MmpL7 that contain an additional structural motif in periplasmic domain 2 (PD2) classified as cluster I proteins (228), very little information regarding the structure/function of PD2 in cluster I MmpL proteins is available.

Indeed Jain and Cox (259) demonstrated a direct interaction between PD2 of MmpL7 with PpsE, the last enzyme required for phthiodiolone/phenolphthiodiolone synthesis (a significant component of PDIM/PGL). This domain was also the preferred phosphorylation site by serine/threonine kinase protein PknD that potentially could regulate PDIM/PGL transport if exact mechanisms of phosphorylation events were known (191). To further understand the

contribution of PD2 in MmpL7 function, structural and molecular methods were used as described before to identify select residues for genetic and biochemical assessment.

Structural analysis of the MmpL7 homology model highlighted that PD2 is distinct from the AcrB periplasmic domains, that made it challenging to identify residues for investigation. Nonetheless, charged residues in the docking domain of PD2 were identified using the homology model, and from molecular analysis these select residues were not conserved with other MmpL members, suggesting that this sub-domain in cluster I MmpL proteins may perform specific activities. Except for residue Asp670 conserved across cluster I MmpL members and Asp673 conserved in AcrB.

Unexpectedly, complementation analysis showed that substitutions to residues Asp670 and Glu676 produced a severe phenotype that abrogated PDIM synthesis while modifications to Arg610 and Asp673 resulted in defective PDIM transport alone. Coherent with the results of Jain and Cox (259), regardless of the alterations to Ile611 no inhibition of MmpL7 activity was observed. Strangely, Ile611 and Asp673 were identified by Jain and Cox (259) to be involved with the MmpL7-PpsE interaction. However, modifications to these residues did not abrogate PDIM synthesis. Collectively, it is clear that PD2 in cluster I proteins is unique to the MmpL family and its residues are integral to MmpL7 function.

Independent studies have shown that PDIM/PGL synthesis is not dependent on *mmpL7* as the null *mmpL7* mutant does not perturb PDIM/PGL synthesis (40,41,126), in agreement with our results. It was unexpected that single mutations to Tyr837, Asp670 and Glu676 resulted in a phenotype more severe than displayed by the *mmpL7* mutant. The *mmpL7* gene was expressed in all mutagenized strains as verified by reverse transcriptase- PCR and whole-genome sequencing results confirmed that no mutations existed in PDIM and PGL synthesis genes in

Tyr837, Asp670 and Glu676 strains. Therefore, the phenotype associated with these strains is not due to disruptions in the backbone of MmpL7 but are valid indicators of MmpL7 function.

These three residues in the TM domain and PD2 could be crucial in facilitating the MmpL7-PpsE interaction explaining the significant phenotype when modified. Indeed MmpL7 was modulated by the MmpL7-KdpF interaction during nitrosative stress (223) suggesting protein modulation of MmpL7 or PpsE or both proteins, due to the MmpL7-PpsE interaction. The finding that the MmpL7-KdpF interaction occurred at the TM domain (224) supports the conclusions of this chapter and emphasises that the TM domain is potentially involved in protein-protein interaction whereas, previously it was assumed that only the soluble periplasmic domains were suited for protein-protein interactions.

Despite our attempts to study the effect of these single mutations on PGL synthesis/transport, we were not successful as it was difficult to ascertain whether PGL was produced in the complemented strains. In order to investigate the confusing PGL results only the overexpressing *mmpL7* (*mmpL7*- C) strain was sent for whole-genome sequencing analysis that revealed mutations in the *fadD22* gene, which is exclusively required for PGL synthesis but does not affect PDIM synthesis (124). Due to time constraints the *mmpL7*- NC and the nine-remaining site-directed mutagenized strains were not analysed by whole-genome sequencing to identify any mutations inhibiting PGL biosynthesis. Therefore, the reason/s for impaired PGL synthesis remains unknown for the *mmpL7*- NC and the nine-remaining site-directed mutagenized strains. Future work involves generating more transformants of all fourteen strains and screening for PDIM/PGL synthesis and whole-genome sequencing analysis.

The overall analysis of MmpL7 has provided a unique challenge as we identified only a few conserved residues present in TM and PD2 domains across characterised RND transporters, AcrB and MmpL3 already suggesting that MmpL7 operates differently. In support of this,

bioinformatics analysis revealed that the network of residues in the TM domain required for the formation of a proton translocation channel or pore present in RND transporters was not found in MmpL7 strongly suggesting that MmpL7 is not capable of promoting PMF also verified by genetics and biochemical analysis. Structural analysis of MmpL7 *in silico* model revealed that PD2 was distinct from other RND transporters.

Previously, the TM and PD2 domains were studied separately where the TM domain was associated with PMF mediated transport only while PD2 was related to protein-protein interactions. Instead, the work in this chapter has demonstrated that residues in the TM domain and PD2 were involved in both PDIM synthesis and transport. As MmpL7 does not independently export PDIM across the membrane, the entire protein likely serves as a scaffold in facilitating interactions between lipid synthesis and transport proteins. This study was a small step into understanding the mechanism of MmpL7 activity as MmpL proteins have adept mechanisms for their function that we are only beginning to understand.

Future work involves investigating the other conserved residues amongst the MmpL family that we identified in this study and assessing whether there are other protein partners of MmpL7 besides PpsE (259) using protein-protein interaction *in vitro* assays as such findings aid in our understanding of the mode of action of MmpL proteins.

Chapter 4: The role of *drrABC* genes in PDIM/PGL transport

Chapter 4: The role of *drrABC* genes in PDIM/PGL transport

4.1. Introduction

ATP binding cassette (ABC) transporters are integral membrane proteins that constitute four functional units with two nucleotide-binding domains (NBD) and two transmembrane domains (TMD) assembled in various combinations (272). The characteristic feature of ABC transporters in eukaryotes is the single polypeptide that contains all four functional units. Exceptions in some members include a polypeptide that contains only two functional units organised as either identical (homo-) or different (hetero-) dimers (272).

Prokaryotic ABC transporters display more flexibility in their assemblies with combinations of individual functional units or two functional units generating either homo- or hetero-dimers (272). The NBD subunit/s represents the hallmark of the ABC transporter family recognised by conserved motifs within the ATP-binding cassette. Unsurprisingly the tertiary structure and mechanism of coupling ATP-binding/hydrolysis to transport are strictly conserved. The NBD uses energy to drive conformational changes in the TMD subunits required for transport (272). The transmembrane (TM) units of the TMD are organised in a manner that they create the transmembrane pore either facing inwards or outwards and the substrate-binding site/pocket/cavity lined with either definitive residues for binding specific substrates or overlapping drug-binding residues for multiple binding substrates simultaneously (272).

In Mtb ABC transporters represent one of the largest transmembrane protein families that play a critical role in maintaining Mtb survival and pathogenesis (273). ABC transporters have been identified in extruding antigenic-related lipids of the outer membrane namely: phthiocerol dimycocerosates (PDIM), galactans, lipoarabinomannan (LAM) and (phosphatidyl-myo-inositol mannosides) PIMs (273–276). In particular PDIM and its phenolic-glycosylated

derivative phenolphthiocerol dimycocerosates (PGL) are well characterised virulence factors that promote long term survival in the host (121,126,136,163–167,277).

Genes encoding biosynthetic and transport machinery of PDIM/PGL are clustered on the mycobacterial chromosome and referred to as the PDIM cluster. Both PDIM and structurally related PGL are complex lipids containing long methyl-branched fatty acids produced as a consequence of repeated cycles of extension and modification catalysed by numerous enzymes, as described in Figure 4-1. The PDIM cluster also reveals genes (*mmpL7*, *lppX* and *drrC*) encoding proteins belonging to different transporter families (Figure 4-1). Indeed *mmpL7*, encodes a member of the RND superfamily and mutants of this gene showed an accumulation of PDIM and PGL in the cytoplasm indicating that both glycolipids were made in the cytoplasm, and *mmpL7* was integral for PDIM/PGL transport across the membrane (39–41,126). The null mutant of *lppX*, encoding a lipoprotein, displayed an accumulation of PDIM in the periplasm representing that this gene was responsible for PDIM export to the outer membrane surface (186). Further inspection of the PDIM cluster proved that *mmpL7* was not solely responsible for PDIM transport across the membrane as transposon insertions in *drrC* also resulted in the accumulation of PDIM in the cytoplasm (40). The intracellular PDIM accumulation by mutants of *mmpL7*, *lppX* and *drrC* were attenuated in animal models of infection indicating the requirement of extracellular PDIM for virulence (39–41,174,186,258). These findings suggest that the transport of PDIM may be a complicated process that involves at least *mmpL7*, *lppX* and *drrC* (Figure 4-1C).

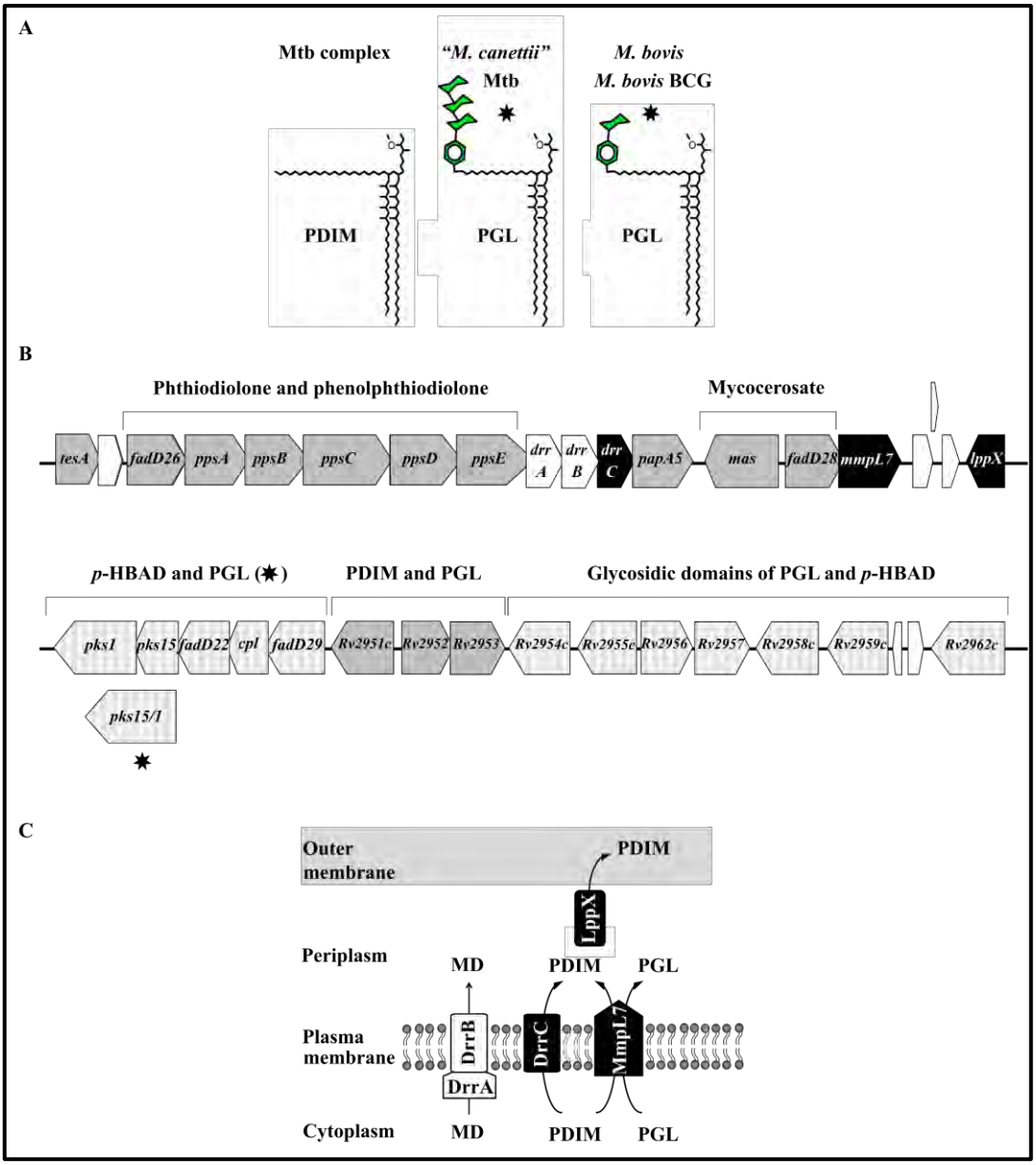

Figure 4-1: The structure, genetic context and transport of PDIM/PGL. A) Simplified structure, B) the PDIM cluster and C) transport. MD represents multiple drugs. The * indicates an intact *pks15/1* gene for PGL production. [Adapted from (60,111,175)].

Intriguingly, the *drr* genes in the PDIM cluster are similar to the cluster of genes responsible for daunorubicin/ doxorubicin (dnr/dox) biosynthesis/resistance annotated as '*drr'* in *Streptomyces peucetius* (Sp) (278). Sp has developed several self-defence mechanisms to protect itself from the toxic effects of its products, dnr/dox. One such mechanism involves the active extrusion of drugs by the $DrrA_2B_2$ pump encoded by *drrA/B* genes (279).

Correspondingly, biochemical characterisation of DrrA/B encoded by *drrA/B* genes in Mtb also resulted in the formation of a similar complex for multi-drug extrusion (271). Genetic arrangement of the PDIM cluster clearly shows that *drrA/B* genes are operonic with *drrC*, in addition to polyketide synthase genes.

Consequently, it has been assumed that *drrA/B/C* genes function together in either antibiotic transport or PDIM transport. However, genetic and biochemical analyses have investigated these *drr* genes separately and thus have assigned separate functions to *drrA/B* and *drrC* (40,271). Therefore, it remains unclear whether *drrA* and *drrB* play a critical role in PDIM transport and whether these *drrA/B/C* genes form a complex or operate individually to carry out this function. Furthermore, as PGL shares a common lipidic core with PDIM, it still unknown whether the two lipids also share a common transport pathway.

In this study we investigated the individual roles of *drrA*, *drrB* and *drrC* in PDIM and PGL transport, to explore any redundant functions therein, by generating a mutant in *Mycobacterium bovis* BCG (BCG) deficient in all *drrA/B/C* genes and characterising all and individual *drr* genes by complementation.

4.2. Methods and materials

4.2.1 Plasmids and strains

Table 4-1 provides a list of the plasmids, bacterial strains and recombinant mycobacteriophages only generated in this study, while the reference plasmids, bacterial strains and recombinant mycobacteriophages described in Chapter 6 (Table 6-1). This study involves the analysis of two positive transformants designated as C/C2 referring to two bacterial strains in Table 4-1.

Table 4-1: A list of plasmids, mycobacteriophages and bacterial strains generated in this study.

	Genetic characteristics
Plasmids	
p∆*drrABC*	Derivative of p0004s cosmid obtained by cloning upstream and downstream flanks of Mtb *drrA* and *drrC* (*Rv2936* and *Rv2938*)
pMV306::*drrABC*	A copy of Mtb *drrA*, *drrB* and *drrC* (*Rv2936*, *Rv2937* and *Rv2938*) cloned into pMV306 *E. coli*/mycobacterial shuttle vector in frame with 400bp upstream of the native promoter region of *Rv2936* and 200bp downstream of *Rv2938*
pMV306::*drrAB*	A copy of Mtb *drrA* and *drrB* (*Rv2936* and *Rv2937*) cloned into pMV306 *E. coli*/mycobacterial shuttle vector in frame with 400bp upstream of the native promoter region of *Rv2936* and 200bp downstream of *Rv2938*
pMV306::*drrBC*	A copy of Mtb *drrB* and *drrC* (*Rv2937* and *Rv2938*) cloned into pMV306 *E. coli*/mycobacterial shuttle vector in frame with 400bp upstream of the native promoter region of *Rv2936* and 200bp downstream of *Rv2938*
pMV306::*drrAC*	A copy of Mtb *drrA* and *drrC* (*Rv2936* and *Rv2938*) cloned into pMV306 *E. coli*/mycobacterial shuttle vector in frame with 400bp upstream of the native promoter region of *Rv2936* and 200bp downstream of *Rv2938*
Mycobacteriophages	
ph∆*drrABC*	Derivative of phAE159 obtained by cloning p∆*drrABC* at the *Pac*I site
Bacterial strains	
∆*drrABC*	BCG strain with Mtb *drrA*, *drrB* and *drrC* (*Rv2936*, *Rv2937* and *Rv2938*) replaced with *hyg-sacB* cassette
drrABC- C/C2	∆*drrABC* strain transformed with pMV306::*drrABC*
drrBC- C/C2	∆*drrABC* strain transformed with pMV306::*drrBC*
drrAC- C/C2	∆*drrABC* strain transformed with pMV306::*drrAC*
drrAB- C/C2	∆*drrABC* strain transformed with pMV306::*drrAB*

4.2.2 Δ*drrABC* mutant generation in BCG

The *drr* operon of *Mycobacterium bovis* BCG (BCG) containing genes *drrA*, *drrB* and *drrC* was disrupted by replacing these genes with a hygromycin resistance gene using specialised transduction by (280,281) as described in Chapter 6. Briefly, an allelic exchange substrate (AES) construct was created by cloning in-frame 0.8- 1 Kbp PCR fragments upstream of *drrA* and downstream of *drrC* using primers in Appendix 5A from H37Rv genomic DNA, into p0004S, flanking a hygromycin resistance cassette and verified by DNA sequencing. The AES construct was packaged into the temperature-sensitive mycobacteriophage phAE159 resulting in phΔ*drrABC*, which was used to transduce wild type BCG. Hygromycin resistant transductants were selected and screened by PCR, but only one transductant was verified by whole genome sequencing to be correct and was designated Δ*drrABC* mutant used for all further studies (Appendix 16).

4.2.3 Functional complementation

The Δ*drrABC* mutant was complemented with wild type genes *drrABC* amplified from H37Rv genomic DNA using the *drrABC*- C primer pair (Appendix 5B). This fragment was cloned into pMV306 using *Xba*I and *Hind*III to create pMV306::*drrABC* which was then verified by DNA sequencing. The recombinant plasmid pMV306::*drrABC* was introduced to the *drrABC* mutant by electroporation, and then kanamycin and hygromycin resistant transformants were selected and screened by PCR. Two positive transformants were used for further analyses termed *drrABC*- C/C2 (Table 4-1). The *drrABC* mutant was also used to generate strains by complementation that had a loss of individual genes (*drrA*, *drrB* and *drrC* as in Appendix 17) in two ways: three-way cloning and site-directed mutagenesis (SDM).

Three-way cloning was only successful in generating the pMV306::*drrAB* plasmid. Two fragments were amplified using the primer pairs, as stated in Appendix 5B and simultaneously

cloned into pMV306. The SDM kit from NEB was used to construct pMV306::*drrBC* and pMV306::*drrAC* where the sequence-verified recombinant plasmid pMV306::*drrABC* served as a template for selective amplification using primer pairs in Appendix 5D (designed using the website: http://nebasechanger.neb.com/). All the complementation plasmids- pMV306::*drrBC*, pMV306::*drrAC* and pMV306::*drrAB*, were sequence-verified and electroporated into the Δ*drrABC* mutant strain and then kanamycin and hygromycin resistant transformants were selected and screened by PCR. Two positive transformants of each strain were used in this work and designated as *drrBC*- C/C2, *drrAC*- C/C2 *drrAB*- C/C2 (Table 4-1).

After that, all strains in Table 4-1 together with the wild type BCG strain were analysed for expression of each *drr* gene by reverse transcriptase- PCR using primer pairs in Appendix 5E and by general and specific lipid analysis, as described in detail in Chapter 6.

4.3. Results

4.3.1 Bioinformatics analyses

The *drrA/B/C* genes of Mtb (H37Rv) is part of the PDIM cluster encompassing polyketide PDIM synthase and transport genes such as *mmpL7* and *lppX* (Figure 4-2). Interestingly, with the use of SyntTax (282) and KEGG servers (283) all three *drrA/B/C* genes occur in the same genetic milieu as other mycobacterial PDIM producing species together with *mmpL7* and *lppX* including *Mycobacterium leprae* (*M. leprae*) an efficient pathogen with a minimal genome (Figure 4-2).

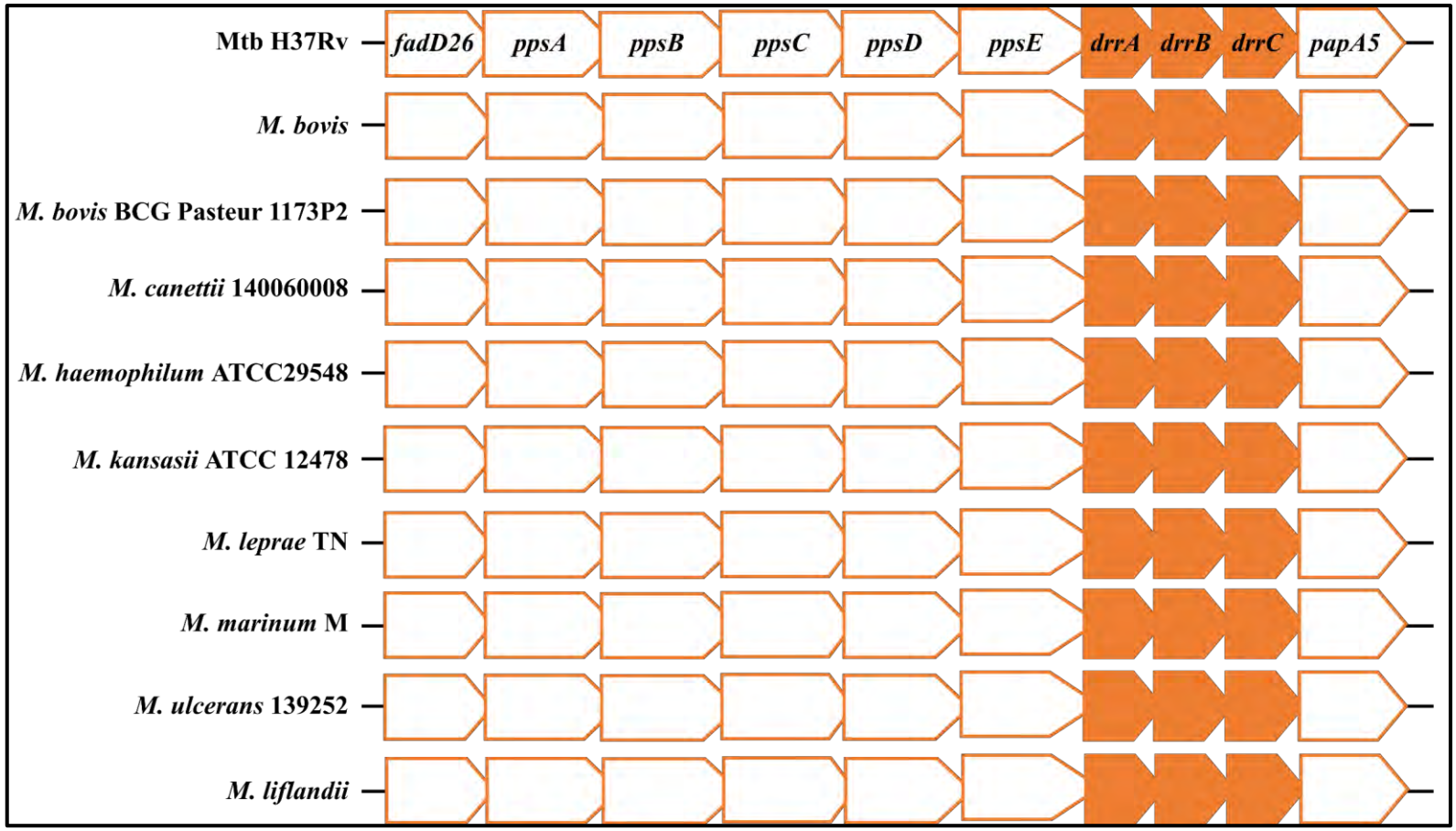

Figure 4-2: Conservation of *drrA/B/C* genes in PDIM producing Mycobacteria.

Since the *drr* genes in Sp are orthologous to those in Mtb, we compared the genetic contexts of *drr* genes from these micro-organisms that are both from the same taxonomic order Actinomycetales using the KEGG server (283) and findings from Madduri and Hutchinson (284) (Figure 4-3). The results revealed that they both contain large genetic clusters of numerous genes dedicated to the biosynthesis/transport of PDIM and dnr/dox and *drrA/B* remain operonic (Figure 4-3). Exceptions include that *drrC* is operonic with Mtb *drrA/B,* but *drrD* is operonic with *drrA/B* in Sp, and additional transport genes such *mmpL7* and *lppX* are required for PDIM translocation to the outer membrane in Mtb, but Sp solely relies on *drrA/B* for drug extrusion (Figure 4-3). Despite these differences, the Drr cluster in Sp has been well characterised as compared to the little information regarding the Mtb *drr* genes. Thus, in this study, the genetic and biochemical findings of Drr proteins in Sp were used as a reference.

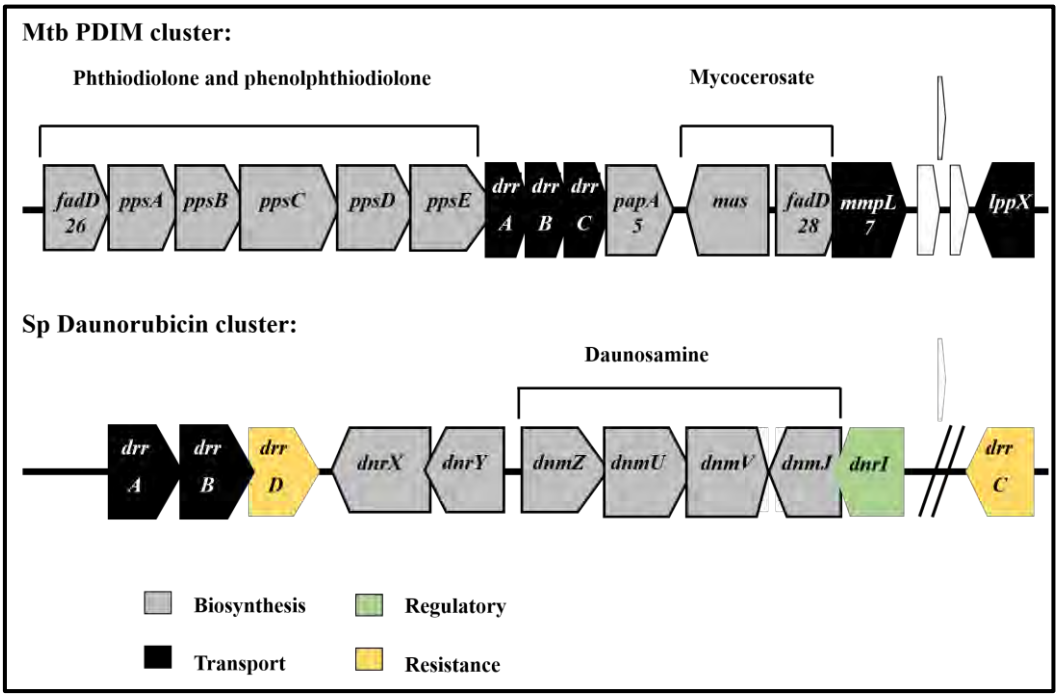

Figure 4-3: Genomic comparisons between Mtb and Sp showing part of their respective PDIM and daunorubicin clusters. [Adapted from (284)].

In Mtb Braibant et al. (273) has identified that DrrA contained the ATP or nucleotide-binding domain (NBD) and both DrrB/C each represented the transmembrane domain (TMD). To highlight the ATP binding region that contains motifs essential for ATP dependent transport, a multiple sequence alignment was performed with close and distantly related homologs of DrrA Mtb (Figure 4-4). The motifs in the N terminal domain (NTD) region outlined in Figure 4-4 show sequence conservation among the homologs of Mtb DrrA but with varying degrees of sequence similarity in the C terminal domain (CTD) except between DrrA of Mtb and Sp. Interestingly, other sequences in the CTD were found in ModC and Wzt. Overall the sequences of DrrA Mtb and Sp share a 45.65% sequence similarity (Figure 4-4). Surprisingly the sequence similarity between DrrB Sp and mycobacterial DrrB and DrrC was less than 30% (Appendix 18). The only known motif characterised in DrrB Sp is the EAA motif (285) that was not evident in mycobacterial DrrB/C also reported by Braibant et al. (273) (Appendix 18).

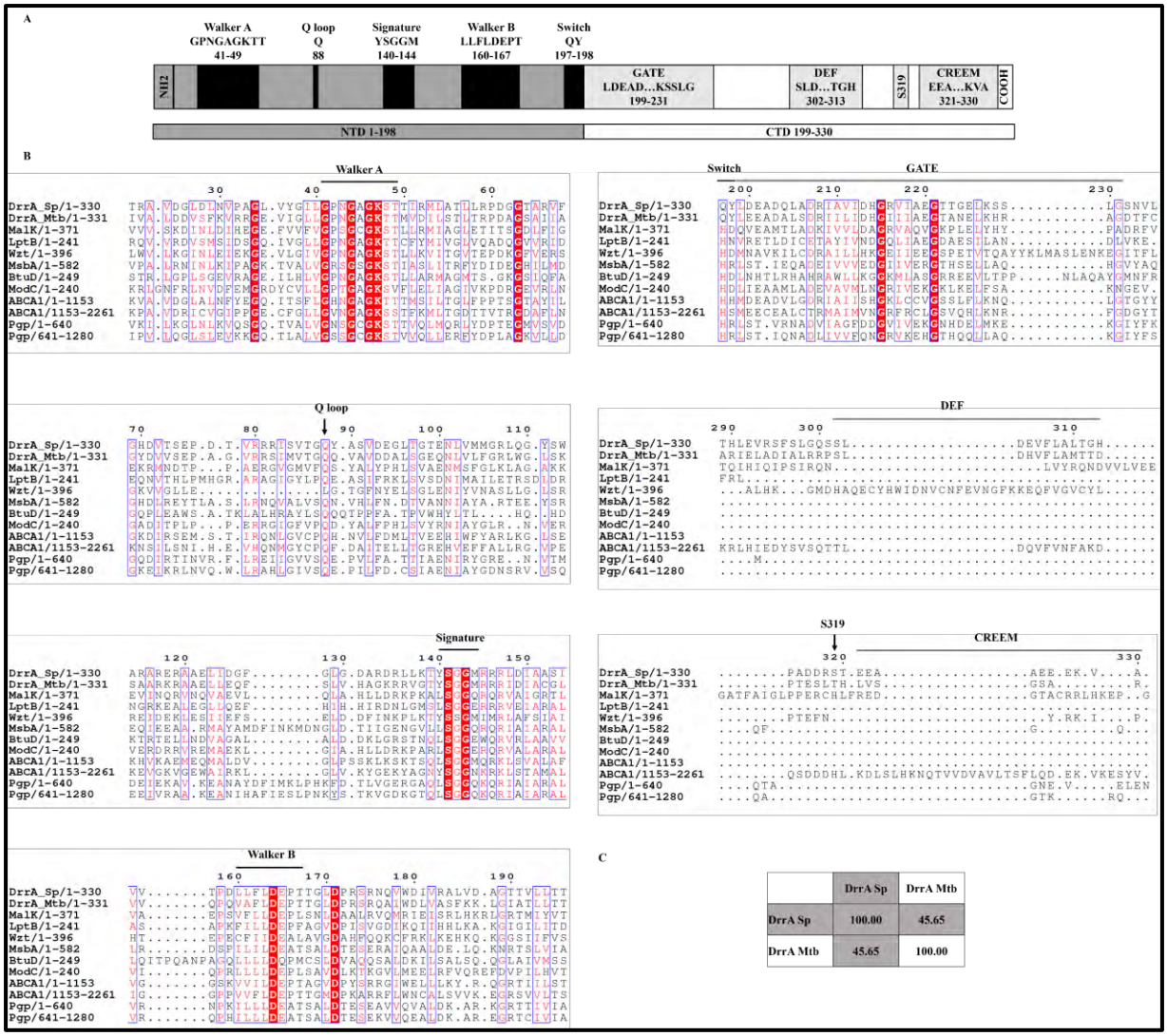

Figure 4-4: DrrA Mtb sequence analysis using Drr Sp as a reference. A) A schematic representation of the ABC transporter motifs of DrrA at N/C terminal domains (NTD/CTD) adapted from (286). B) Multiple amino acid sequence alignment of DrrA with close and distant homologs of DrrA Mtb. C) Percent identity matrix between DrrA from Mtb and Sp. Uniprot accession number of each protein is: DrrA_Mtb (P9WQL9), DrrA_Sp (P32010), *Escherichia coli* (*E. coli*) Maltose/maltodextrin importer MalK (P68187), *Pseudomonas aeruginosa* lipopolysaccharide transporter LptB (Q9HVV6), *Aquifex aeolicus* Wzt O-antigen polysaccharide ABC-transporter (O67181), *Salmonella typhimurium* MsbA Lipid A exporter (P63359), *E. coli* Vitamin B12 importer BtuD (P06611), *Archaeoglobus fulgidus* ModC Molybdate/tungstate transporter (O30144), Homo sapiens ABCA1 cholesterol transporter (O95477) and P-glycoprotein multidrug exporter (P08183).

To gain insight into the mycobacterial DrrB/C that both represent the TMD, homology models using I-TASSER (253) were generated as there are no established structures of DrrA, DrrB or

DrrC at present (Figure 4-5). Interestingly, both models of DrrB/C look identical as they each contained seven large and three smaller helices organised similarly (Figure 4-5). Besides, both had a distinct N terminus tail, or extension also highlighted in a previous *in silico* model of DrrB in Sp (287).

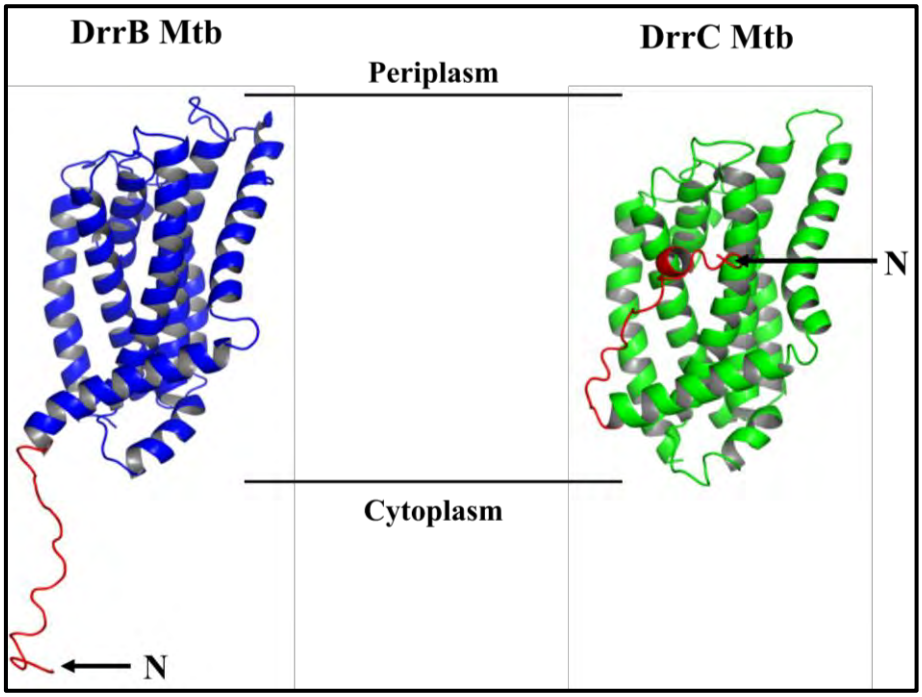

Figure 4-5: Homology models of Mtb DrrB (blue) and DrrC (green) generated by I-TASSER. The N terminals tails highlighted in red in both modelled proteins.

Additionally, structural information obtained from I-TASSER indicated that 7 threading programs of 10 had a significant alignment between DrrB and DrrC from Mtb with the O-antigen polysaccharide ABC-transporter also referred to as Wzm (PDB: 6OIH) as seen in Figure 4-6. All the defining features and functional characteristics of Wzm were aligned with the DrrB model (Figure 4-6B). The same result was observed between Wzm and the DrrC model (Figure 4-6C). This information gives valuable insight into the overall topology of mycobacterial DrrB and DrrC and provides a possible mechanism of complex lipid export.

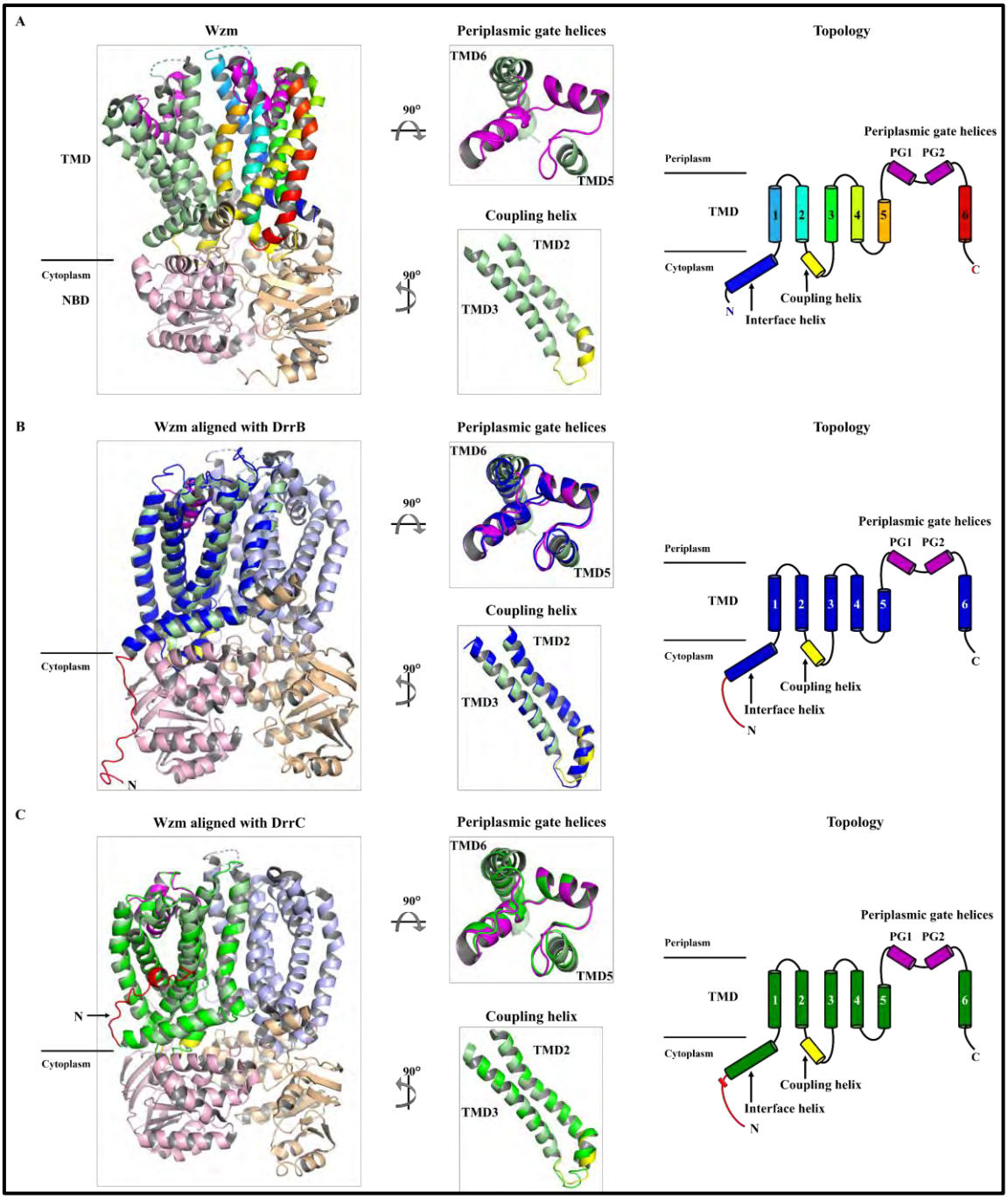

Figure 4-6: Superimposition of the O-antigen polysaccharide ABC-transporter Wzm with mycobacterial DrrB/C. A) Structural features and architecture of Wzm (PDB: 6OIH) superimposed with models of mycobacterial B) DrrB and C) DrrC. The Wzm structure with one monomer coloured in pale green, while the other monomer is coloured a rainbow spectrum starting from the N terminus (blue) to the C terminus (red) corresponding to its architecture. For the alignments with DrrB/C, the monomers coloured pale green and light blue, and for all structures, the Wzt (NBD) coloured wheat and light pink. The periplasmic gate helices and coupling helix are coloured in magenta and yellow domains. Mycobacterial DrrB and DrrC are coloured blue and green respectively, and both the N terminals tails highlighted in red.

Other alignments included eukaryotic lipids/multidrug exporters such as the ATP-binding cassette sub-family A member 1 (ABCA1) and members of the ATP-binding cassette sub-family G (ABCG2, ABCG5 and ABCG8) and $LptB_2FG$ a lipopolysaccharide (LPS) exporter in prokaryotes. Superimpositions of ABCG2 multidrug exporter (PDB: 5NJ3) and $LptB_2FG$ (PDB: 5X5Y) with homology models of mycobacterial DrrB/C were included to compare with the alignments between Wzm and models of DrrB/C (Appendix 19). Collectively, all alignments with Wzm, ABCG2 and $LptB_2FG$ revealed that *in silico* models of mycobacterial DrrB and DrrC had six TM helices each and an interface or connecting helix (Figure 4-6; Appendix 19) parallel to the membrane extending into the cytoplasm. The second similarity was that there were no extracellular loops like EL3 of ABCG2 or periplasmic β-jellyroll-like domains of $LptB_2FG$ present in the homology models of mycobacterial DrrB/C (Appendix 19). Thirdly, none of the solved structures had N terminus tail-like structures extending into the cytoplasm as found in DrrB/C models (Figure 4-6; Appendix 19). The sequence similarity of mycobacterial DrrB and DrrC are low and yet models of DrrB and DrrC aligned to the same monomer but not with $LptB_2FG$. $LptB_2FG$ is the only transporter where the TMD is not formed by dimerisation and contains two TMDs represented by LptF and LptG. Models of DrrB and DrrC aligned to LptG and LptF respectively providing insight into the potential domain organisation of DrrB and DrrC (Appendix 19).

4.3.2 Generation of the Δ*drrABC* mutant and complemented strains in BCG

It has been presumed that mycobacterial *drrA/B/C* genes are all required for PDIM transport but to date, only *drrC* has been reported to contribute to PDIM transport together with *mmpL7* (40). To determine if the *drr* genes were required for PDIM transport, the mycobacterial *drrA/B/C* genes were all deleted using specialised transduction explained in Chapter 6. These three genes were replaced with a hygromycin resistance cassette (*hyg*) to generate the triple

mutant strain Δ*drrABC* in BCG (Appendix 16). This strain was transformed with an integrative plasmid containing *drrABC* with the associated native promoter, or with versions of this plasmid containing combinations of *drrA*, *drrB* or *drrC* as depicted in Appendix 17. These complementing plasmids were introduced into the Δ*drrABC* mutant producing BCG strains with all *drrA/B/C* genes and strains with inactive *drrA*, *drrB* or *drrC* (Appendix 17). The expression of individual *drrA/B/C* genes of the recombinant strains were confirmed by reverse transcriptase- PCR (Appendix 20).

4.3.3 Lipid analysis

In this study two metabolic labels, namely [^{14}C]-acetate and [^{14}C]-propionate were used to assesses all synthesised lipids and specific methyl branched fatty acid lipids such as PDIM and PGL. The BCG strains listed in Table 4-1 including the wild type BCG strain, were labelled with the [^{14}C] metabolic labels and apolar lipids associated with the culture supernatant and cells were extracted from the culture filtrate that represented outside and inside apolar lipids respectively, that were resolved by one-dimensional/ two-dimensional thin-layer chromatography (1D/2D TLC). Also, to verify that outer membrane lipids were not affected by the genetic modifications of the *drrABC* genes total apolar and polar lipids labelled with [^{14}C]-acetate were extracted and resolved by TLC (Appendix 21). All other mycobacterial lipids were present in all strains comparable with wild type BCG and as expected, only PDIM/PGL were affected (Appendix 21).

4.3.4 PDIM analysis

As expected PDIM was observed in both the inside and outside fractions of the wild type and the complemented strain containing all *drrA/B/C* genes indicating PDIM synthesis/transport, while PDIM was absent only in the outside fraction of the null mutant denoting failed PDIM transport (Figure 4-7). All strains with a loss of *drrA*, *drrB* or *drrC* resembled the mutant strain

indicating no PDIM restoration (Figure 4-7). Importantly, PDIM was present intracellularly for all strains verifying a defect in transport instead of a loss in biosynthesis (Figure 4-7). There were no differences in lipids labelled with [^{14}C]-acetate and [^{14}C]-propionate observed (Appendix 21A; Figure 4-7) and therefore, we could make a confident assessment that all *drrA/B/C* genes are required for PDIM export.

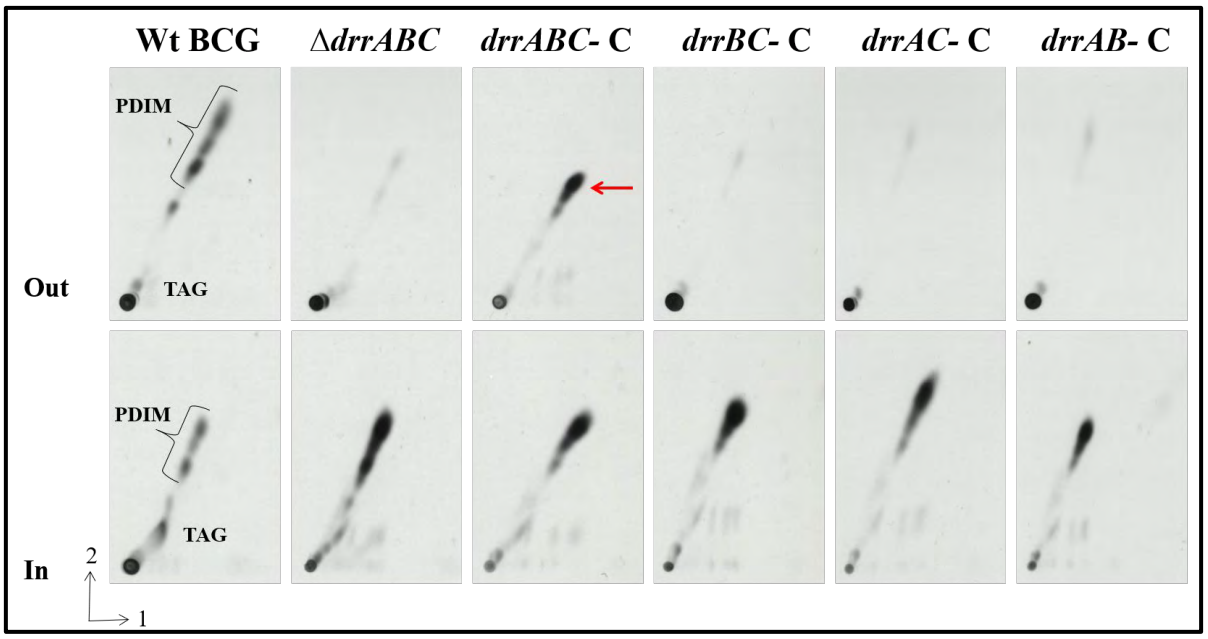

Figure 4-7: PDIM analysis of the *drr* complemented strains. 2D TLC autoradiography of [14C]-propionate labelled lipids from Wild type (Wt), Δ*drrABC* mutant and four *drr* complemented strains. Apolar lipid extracts from the culture filtrate (Out) and intracellular lipids (In) were separated using System A. The three-pointed bracket shows the PDIM species, while the arrow depicts the presence of PDIM.

4.3.5 PGL analysis

Unlike the Mtb H37Rv strain that has a *pks1* frameshift mutation, *M. bovis* BCG (BCG) has a functional *pks1* gene that synthesises PGL, and thus, PGL transport could be assessed (117). Additionally, there is a co-dependency between *drrC* and *mmpL7* in executing PDIM transport (40) and *mmpL7* has also been implicated in PGL transport (126). Thus, we evaluated the potential role of the *drrABC* genes in PGL transport in the same manner as performed for PDIM

analysis. PGL was evident in the outside fraction of all strains except the mutant, that showed an accumulation of PGL inside as expected (Figure 4-8). Some of the various complemented strains did not show detectable levels of PGL for the inside fraction (Figure 4-8). From Appendix 21B depicting [^{14}C]-acetate incorporated lipids, PGL was synthesised in the wild type and mutant strains but not in the various complemented strains.

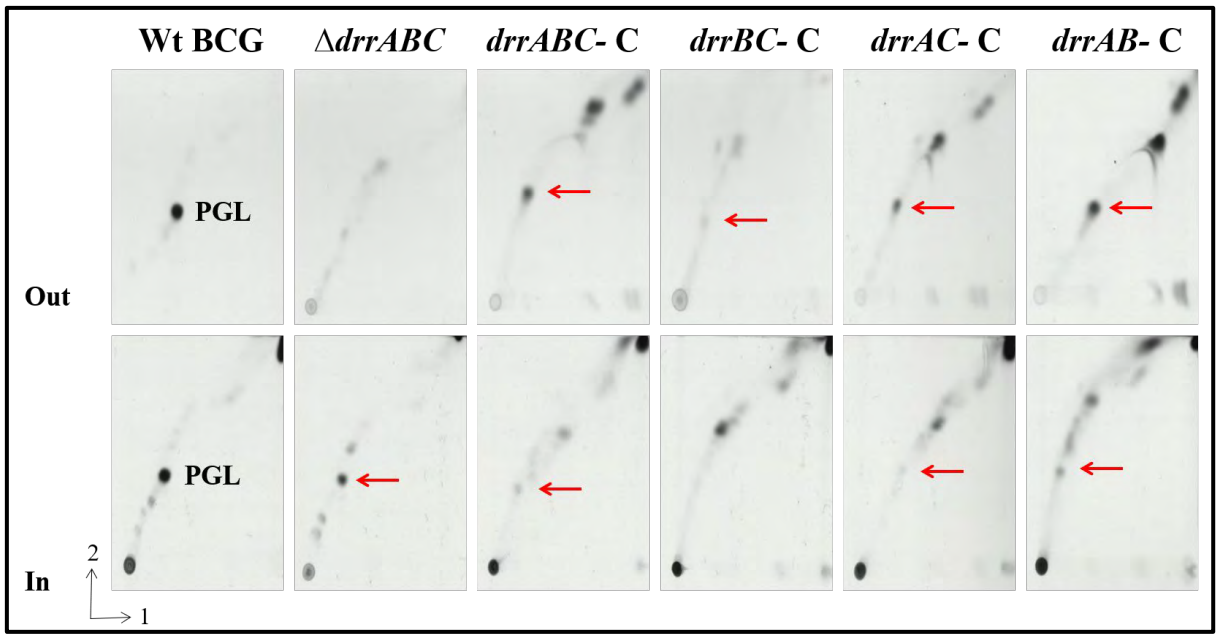

Figure 4-8: PGL analysis of the *drr* complemented strains. 2D TLC autoradiography of [^{14}C]-propionate labelled lipids from Wild type (Wt), Δ*drrABC* mutant and four *drr* complemented strains. Apolar lipid extracts from the culture filtrate (Out) and intracellular lipids (In) were separated using System C. The arrow depicts the presence of PGL.

Therefore, to verify these findings, another set of complemented strains were labelled with [^{14}C]-propionate and the PDIM/PGL analysis repeated (Appendix 22). The same results were observed that displayed PDIM production but defective PDIM transport in strains with a loss in *drrA*, *drrB* or *drrC* (Appendix 22A). Unfortunately, the second set of transformants did not demonstrate PGL synthesis either but did show more PGL in the outside fraction, including the mutant strain (Appendix 22B). Therefore, it was not clear whether strains with a loss in *drrA*, *drrB* or *drrC* were defective in PGL synthesis/transport. Altogether these results indicated that

the *drrA/B/C* genes were all required for PGL transport as evident by the PGL accumulation in the mutant strain. The fully complemented strains presented clearly PGL synthesis/transport but only in [^{14}C]-propionate (Figure 4-8/Appendix 21B). Unexpectedly, only strains inactive in *drrA/B/C* exhibited either undetectable levels of or no PGL synthesis as compared to the wild type and mutant for reasons undetermined due to time restrictions.

4.4. Discussion:

Strict conservation of the PDIM cluster in PDIM producing mycobacteria emphasises that all the genes contained in the cluster are critical for PDIM synthesis/transport. Indeed, the PDIM cluster was also conserved in *Mycobacterium leprae* (*M. leprae*) with all three *drr* genes in a transcriptional unit with polyketide PDIM synthase genes that highlight the significance of these genes in an efficient pathogen with a minimal genome, contributing to survival and pathogenesis.

The designation *drr* was first assigned to the daunorubicin and doxorubicin (dnr/dox) cluster in *Streptomyces peucetius* (Sp) that produces and transports two well-known antitumor antibiotics dnr/dox as a self-protective mechanism (278). To gain a clearer understanding of the *drr* genes many similarities/differences were drawn from comparing genetic clusters containing *drr* genes of Sp and Mtb. Intriguingly, common to both Actinomycetales were the large chromosomal clusters with genes dedicated to the biosynthesis/transport of PDIM and dnr/dox respectively, of which were operonic *drrA/B* genes. Genes in the *drr* cluster of Sp have been well characterised, and only *drrA*/*B* encode and DrrAB proteins that form the ATP dependent multi-drug resistant pump (288). Even though *drrD* is operonic with *drrA*/*B* it is not involved with any DrrAB transport activities as it encodes a protein that inactivates dnr/dxr to a non-toxic form (289). While the *drrC* genes of Sp in a different locus encodes a protein that

scans DNA intercalated with DNR/DXR like a UvrA protein of the excision repair system that also depends on ATP for its function and releases the antibiotics from the DNA (290–292).

However, the analysis of Braibant et al. (273) revealed that all *drrA/B/C* encode ABC transport proteins as DrrA contained the ATP or nucleotide-binding domain (NBD) and both DrrB/C each represented the transmembrane domain (TMD). As expected, the ATP binding region of DrrA contained all the characteristic motifs essential for ATP dependent transport conserved across close and distantly related homologs of DrrA particularly in the N terminal domain (NTD) region. The C terminal domain (CTD) was highly variable between homologs due to recent discoveries that is an independent domain that includes additional sequences associated with specialised functions (286,293). Particularly other sequences were observed in the CTDs of molybdate/tungstate transporter ModC (of ModBC), and the O-antigen polysaccharide transporter Wzt (of Wzt/Wzm) as these sites are integral for substrate binding (294,295). Both DrrA orthologs in Mtb and Sp lacked additional residues in their CTD required for specialised functions. Nevertheless, these orthologs displayed high sequence similarity and contained all characteristic ABC transport motifs emphasising a conserved mechanism of energy coupling. Therefore, this work has shown evidence that DrrA in mycobacteria is an ATP binding protein equipped for ATP binding and hydrolysis and functions in the same manner as its ortholog in Sp.

At present there are no solved DrrA, DrrB or DrrC structures available to gain structural insight thus, I-TASSER homology models of mycobacterial DrrB/C were generated and depicted an identical structure in DrrB/C despite the low sequence similarity shared. Typically TMD proteins display no significant sequence conservation but share a similar topology (272). Unique to models of DrrB and DrrC were the long N terminal tails extending into the cytoplasm that was previously discovered by Gandlur et al. (287) that suggested this structure was

involved in interacting with DrrA. Indeed, three motifs [LDEVFL (DEF) and C-terminal regulatory Glu (E)-rich motif (CREEM), Glycine-loop And Transducer Element (GATE)] contained in the CTD of DrrA were found to interact with this N terminal tail structure to facilitate assembly and interaction of DrrA and DrrB crucial for catalytic function of the DrrAB complex in Sp (286,293). Furthermore, a novel motif previously restricted to ABC importers termed as the EAA motif was exposed in the cytoplasmic N tail of DrrB in Sp to interact with DrrA for the function of the DrrAB pump (285). However, in the sequence analyses of mycobacterial DrrB and DrrC, the EAA motif was not found, and Braibant et al. (273) supported these results. This cytoplasmic N tail may have more interaction interfaces other than the EAA motif that suggests there are more contact points to be discovered in this unique structure (285).

All the defining features and functional characteristics of Wzm were aligned with both models of DrrB and DrrC, providing valuable insight into the overall topology of mycobacterial DrrB/C. Wzm is the TMD component of the ABC transporter Wzt/Wzm where Wzt is the NBD (296). This transporter is formed by dimerisation and exports the O-antigen polysaccharide produced in the cytoplasm as an undecaprenyl diphosphate (UND- PP)-linked intermediate to the periplasm (296). It was found that the cytoplasmic and periplasmic helices were necessary for substrate binding, the coupling of TMD (Wzm) with NBD (Wzt) and facilitated substrate entry and exit (296). While TM1/5 were involved in forming the channel spanning the entire membrane required for substrate extrusion (296). The Wzt/Wzm transporter has suggested a mechanism of exporting complex lipids such as PDIM/PGL that are also synthesised in the cytoplasm and in the case of PGL that has a phenolic-sugar moiety attached to a PDIM lipid core.

The O-antigen polysaccharide exported via Wzt/Wzm is a crucial component for lipopolysaccharide (LPS) formation that is transported by $LptB_2FG$ that was also considered as a template for the DrrB/C homology models but to a lesser extent. The $LptB_2FG$ plays a crucial role in survival, pathogenesis and drug resistance in LPS abundant Gram-negative bacteria (297). This LPS ABC exporter is a three-component system equipped with two NBDs, LptB and two different TMDs, LptF and LptG (297). This transporter does not export across the inner membrane; instead, it adopted a mechanism for LPS extraction from the inner membrane (297). Critical features of $LptB_2FG$ were not aligned with models of DrrB or DrrC suggesting that DrrA/B/C does not function in the same manner. Importantly the superimposition provided understanding into the organisation of DrrA/B/C that could not be achieved with the Wzt/Wzm dimer.

Interestingly mycobacterial DrrB/C were also similar to eukaryotic lipid transporters belonging to ABCA and ABCG families exporting various lipophilic molecules and anti-tumour drugs from cells (298–302). Braibant et al. (273) reported that mycobacterial DrrA/B/C proteins were categorised as antibiotic transporters and Choudhuri et al. (271) corroborated those findings by showing that DrrAB of Mtb served as a multi-drug pump as in Sp. These findings suggest that DrrABC serves as a poly-substrate transporter. Indeed, multi-drug binding pockets are equipped to accommodate multiple substrates with bulky hydrophobic and aromatic residues as described in ABCG2 and DrrB Sp respectively (302,303).

Given that the *drrA/B/C* genes are in the PDIM cluster operonic with polyketide synthase genes and *drrC* has already been linked to PDIM export (40), it has been assumed these genes are involved in PDIM transport but not established as contributors to PDIM and PGL export. This study determined the contribution of *drrA/B/C* in PDIM/PGL transport using two metabolic radioactive labels to verify the presence of mycobacterial lipids, particularly, PDIM/PGL. With

certainty, all *drrA/B/C* genes were required in PDIM transport as a loss in all or any one *drr* gene abrogated export indicating a non-redundant role for these *drr* genes in PDIM export. These results contradicted the findings of Choudhuri et al. (271) that showed that only proteins encoding *drrA/B* were required for drug extrusion. In this study *drr* genes were not overexpressed as in Choudhuri et al. (271) but each of the strains were tested for expression of individual *drr* genes. Presumably overexpressed *drrA/B* or *drrA/C* generates two subunits of each protein required for a functional ABC transporter.

From the PGL analysis of the wild type and mutant strain deficient in all *drrA/B/C* genes, it was evident that *drrA/B/C* genes were all critical for PGL transport as seen with PDIM transport. Therefore, we expected that PGL transport would be defective as a result of the loss of individual *drr* genes as observed with PDIM transport. However, assessing PGL transport in the complemented strains to confirm this expectation was difficult as it was challenging to identify PGL synthesis/ transport confidently.

Two sets of complemented strains were analysed, and both displayed undetectable levels of PGL synthesis while PGL appeared on the outside, suggesting transport only when [^{14}C]-propionate was used. As explained in the previous chapter, propionate is a toxic metabolite in mycobacteria (172,173) resulting in bacterial cell lysis that leads to an over-representation of radioactively labelled methyl-branched lipids in the outside fraction. Additionally, we could not verify if PGL was synthesised/transported or not as PGL was not identified for complemented strains when labelled with the non-toxic [^{14}C]-acetate. All other critical mycobacterial apolar and polar lipids were synthesised in all strains proving that genetic manipulations of *drrA/B/C* genes only had a specific effect on PDIM/PGL as expected. If time permitted the issue regarding PGL synthesis in the complemented strains could have been further investigated by whole genome sequencing that would allow identification of mutations

in PGL synthesis genes. Also, larger volumes of cultures could be labelled with [^{14}C]-acetate and [^{14}C]-propionate and the experiment repeated with concentrated labelled lipids to detect the presence of PGL and confirmed by mass spectroscopy.

The work in this chapter provided evidence that all *drrABC* genes are required for PDIM transport, highlighted how each of the subunits is equipped to form a functional ABC transporter and proposed a potential mechanism of complex lipid transport. Future work involves investigating if all the *drrABC* genes are required for multidrug efflux as observed when *drrAB* genes are overexpressed (271). It is well known that *mmpL7* and *drrABC* have redundant roles in PDIM transport and from previous reports in agreement with our findings it has been suggested that the DrrABC transporter is the driving force mediating lipid or drug efflux but the mechanism between MmpL7 and DrrABC has not been identified. With the use of protein-protein interaction assays we can determine whether DrrABC can interact with MmpL7 or *vice versa*, expanding to our understanding of lipid transport.

Chapter 5: General discussion

Chapter 5: General discussion

The mycobacterial membrane protein large (MmpL) proteins of Mtb are significant contributors in the physiology of the mycobacterial cell wall as well as the survival of the pathogen (discussed in detail in Chapter 1). Mtb (specifically the H37Rv strain) encodes thirteen MmpL proteins primarily involved in transporting virulent cell wall lipids and iron across the plasma membrane (Chapter 2). *mmpL3* is the only essential gene (66,174,197) encoding MmpL3 responsible for the translocation of trehalose monomycolate (TMM) (30,66,304). While *mmpL7* and *mmpL8* (encodes MmpL7 and MmpL8) transport methyl branched fatty acid-derived lipids such as phthiocerol dimycocerosate (PDIM) and sulfolipid-1 (SL), respectively (39–41,92,156), *mmpL11* (encodes MmpL11) exports mycolate ester wax (MWE) and long-chain triacylglycerol (TAG) (195,196). Both *mmpL4* and *mmpL5* (encodes MmpL4 and MmpL5) display redundant roles in iron acquisition via siderophore mycobactin/ carboxymycobactin (MBT/cMBT) recycling (202). Additionally, MmpL3 and MmpL11 can acquire iron via interaction with a heme carrier protein (197,305). Indeed, MmpL proteins are potent virulence factors as MmpL4, MmpL5, MmpL7, MmpL8 and MmpL11 enable long term survival in the host while MmpL4 and MmpL7 are also required for pathogenesis (174,181). Potential other roles of MmpL proteins in drug efflux (218–220) and nitrosative stress adaptation (223,224).

How MmpL proteins function as dedicated lipid transporters remains mostly unknown. Since they are phylogenetically and structurally classified as RND members in Gram-negative bacteria, MmpL proteins are also thought to adopt dimer/trimer formation and a three-component system involving interactions with periplasmic adaptor and outer membrane proteins for complete function (269,306). This discussion focuses on the strategies used to determine the structure of MmpL3 and MmpL7, the molecular modelling and analyses of

MmpL7 highlighting critical residues and regions integral for protein activity, and lastly the contribution of *drr* genes in PDIM export.

The structures of membrane proteins are notoriously difficult to characterise as these large proteins are embedded in the membrane requiring extraction, are not produced in large quantities and overexpression can be fatal, leading to lower protein yields. Before working on this project, two preceding colleagues attempted to achieve the structure of MmpL3 and generated the MmpL3 expressing construct and optimised the protein expression conditions. According to their results, the overexpression of MmpL3 was toxic, and hence the yield was not sufficient for crystallography. As SMA with single-particle electron microscopy offered a fast and straightforward way of achieving membrane protein structures while requiring microliter quantities of protein (244), these methods were adopted. Indeed, SMA has been widely used to characterise the structure of numerous membrane proteins as it offers many advantages over detergents such as n-dodecyl-β-d-maltoside (DDM) and other lipid mimetics discussed in detail in Chapter 2 and was also readily accessible from Prof. Timothy Dafforn the developer of this technology situated at the University of Birmingham. Therefore, this work was aimed at generating structures of MmpL3 and MmpL7 using these novel techniques to gain insight into the mechanism of these proteins.

As no attempts were made previously for MmpL7 similar strategies developed for MmpL3 were followed. One of the main hurdles in the structural determination of proteins is protein expression. Both proteins were expressed in the C41 DE3 expressing strain (*E. coli*) but not in the same strain deficient in *acrB,* which was used to avoid AcrB contamination throughout the preparative process. MmpL7 was expressed regardless of media, post-induction conditions or volume of cultures used as its overexpression was not lethal, unlike MmpL3. Nonetheless, the quantities of protein produced from 1 L cultures were enough for structural determination using

single-particle electron microscopy. Then a vector with no protein was constructed to serve as a negative control to provide insight into the homogeneity of the sample after purification and any artefacts that could lead to misinterpretation of results using single-particle electron microscopy.

With the use of two solubilisation agents, SMA and DDM, and analyses of fractions before and after solubilisation revealed that SMA solubilisation was ineffective at membrane extraction even though EDTA was used to chelate divalent cations and pH 7.9 was maintained throughout the experimental procedures. Despite DDM resulting in better membrane extraction, it was not able to improve the binding affinity between the His-tag on the C terminal of MmpL3 and MmpL7 and the charged nickel resin. Structural analyses of MmpL3 and MmpL7 presented that the C terminal His-tag was mostly buried explaining the weak interaction. Since we chose to image proteins using single-particle electron microscopy specific concerns with using DDM arose such as problems in distinguishing DDM [DDM corona (65- 70 kDa) from MmpL3 and MmpL7 (~ 101/95 kDa)] and artefacts produced from DDM and high concentrations of salt and glycerol that can be misinterpreted (257). Strangely, we noticed that MmpL3 was subject to degradation even though efforts to minimise this were followed. Recently two groups reported the solved structure of MmpL3 by removing the cytoplasmic C terminal domain as it was responsible for proteolysis (32,183) and not required for function (185). These research groups used detergent-based and crystallographic methods (32,183) indicating that SMA with single-particle electron microscopy offers a novel approach but future work to optimise the expression constructs and solubilisation is required to make any advancement in structural biology and the field of MmpL proteins.

With the aid of structural modelling the homology model of Mtb MmpL7 based on solved structures AcrB (*E. coli*) and MmpL3 of *Mycobacterium smegmatis* (*M. smegmatis*) was

generated, an alternate approach to understanding the mechanism of MmpL proteins. The MmpL7 model denoted all the characteristic features of RND transporters depicting the twelve transmembrane (TM) helices with two soluble ectodomains located in the periplasm (referred to as periplasmic domains) between TM 1/2 and TM7/8 as shown in Chapter 2/3. Superimpositions with MmpL3 and AcrB emphasised the large periplasmic domain 2 (PD2) of the MmpL7 model is a structural motif distinct to MmpL proteins (Chapter 2/3). Recently discovered the structure of MmpL3 periplasmic domains are not similar to Gram-negative RND transporters and are thought to be unique to the MmpL family (32,183). These domains are integral for substrate specificity, binding and extrusion (32,183) and were also found to play a role in heme uptake (197,305). MmpL7 serves as a scaffold in facilitating interactions between lipid synthesis and transport proteins (259), similar to the periplasmic domains in AcrB that are integral for establishing interactions with AcrA (adaptor protein) and TolC (channel protein) to form a three-component transporter for multidrug extrusion (268,269). Considering that the majority of MmpL members contain a structural motif similar to PD2 domain (228) and the importance of these domains in MmpL activity/ies, it is surprising that very little information regarding them is available.

While Jain and Cox (259) were the first to discover that the PD2 in MmpL7 directly interacted with PpsE, the result of single mutations to select residues in PD2 did not abrogate PDIM synthesis as expected. Therefore, this motivated further investigation into MmpL7 PD2. The MmpL7 homology model outlined six charged residues lining the docking domain within PD2, of which two residues were previously investigated (259). Surprisingly, of the six residues, only one was conserved between MmpL members bearing the PD2 motif, indicating that PD2 may be an exclusive feature used to perform specific activity/ies. Unexpectedly, single modifications to four of these residues resulted in defective PDIM synthesis/ transport,

corroborating the link between MmpL7 and PpsE and emphasising the importance of this domain in MmpL7 activity.

Previous analysis showed that MmpL7 was the only member of the MmpL group that did not consist of conserved Asp/Tyr pairs in TM4/10 required for protonmotive force (PMF) mediated transport (263). Further genetic and biochemical studies performed in our work revealed that MmpL7 is not equipped to drive substrates across the membrane via PMF. In fact, did not only the entire MmpL7 amino acid sequence lack these paired PMF residues but also residues identified by Chim et al. (228), Belardinelli et al. (185) and Li et al. (194) via structural modelling of MmpL3 were not found in MmpL7. Except, MmpL7 had the conserved PMF residue Tyr837 in transmembrane (TM) 10 and in the same region, Arg846 conserved amongst all MmpL members. Single mutations to Tyr837 and Arg846 resulted in defective PDIM synthesis/ transport respectively. This was synonymous with the results of Bernut et al. (263) that showed an abrogation of glycopeptidolipid (GPL) synthesis/transport due to the subtle modification of the conserved Tyr residue in TM10. These results were unexpected as PDIM and GPL are unrelated lipids that are independently synthesised/transported (39–41,192). Altogether these results emphasised that MmpL7 is not equipped with a network of residues that form the proton translocation channel required for substrate translocation mediated by proton transfer. Residues in the TM domain and PD2 were involved in both PDIM synthesis/transport suggesting that the entire MmpL7 protein acts as a scaffold linking lipid production and transport instead of an independent transporter. Structural differences between the periplasmic domains of AcrB and MmpL7 have highlighted that PD2 of MmpL7 is unique, a feature present in the majority of MmpL proteins classified as cluster one proteins that warrant further investigation.

Despite MmpL7 being characterised as an RND member, its transport is not mediated via PMF, and it is not solely responsible for the transport of PDIM across the membrane either. Camacho et al. (40) displayed that the co-dependent relationship between *mmpL7* (encodes MmpL7) and *drrC* (encodes DrrC) in PDIM transport. It has been suggested that MmpL7 uses another energy mechanism presumably from DrrC, a component of an ATP-binding cassette (ABC) transporter. Commonly found genetically and functionally associated with MmpL proteins are smaller membrane proteins that aid transport across the membrane such as the Mycobacteria Membrane Protein Small (MmpS) and the Gap/Sap family (175,182). Similarly, *drrA/B/C* genes are genetically associated with genes encoding PDIM synthesis/transport and as shown in this work are strictly conserved amongst PDIM producing mycobacteria. However, only *drrC* is functionally related to *mmpL7* (40). Whereas, the overexpression of *drrAB* acts as a multidrug efflux pump (271) synonymous to *drrAB* orthologs in *Streptomyces peucetius* (Sp). The roles of these *drr* genes have been investigated individually; however, it is presumed that they form an ABC transporter (due to their genetic organisation) to drive PDIM transport together with MmpL7, which was the next question we addressed.

Generally, a functional ABC transporter constitutes two subunits of the nucleotide-binding domain (NBD) and two subunits of the transmembrane domain (TMD) where the organisation/assembly of these domains in prokaryotes are highly variable (272). In our work, we showed that the Mtb DrrA represented the NBD as it consisted of all the characteristic ATP binding/hydrolysis motifs and was highly similar to its ortholog in Sp supporting a common mechanism. In Mtb there were two TMD represented by DrrB and DrrC forming a three-component system, unlike in Sp where there was only DrrB. As there are no solved structures for DrrA/B/C, so two homology models, each of DrrB/C were generated and were found to resemble each other. As such both models were matched/threaded with the O-antigen

polysaccharide ABC transporter that plays a crucial role in transporting a core constituent in lipopolysaccharide (LPS) that is essential for survival and pathogenesis in Gram-negative bacteria. This transporter operates in an unusual manner where the TMD protomers create a channel spanning the entire membrane to allow substrate entry and extrusion; however the openings on either end are controlled by the NBD subunits (297).

Since MmpL7 cannot form a proton translocation channel as presented in our work, the potential mechanism of the DrrABC transporter based on the channel forming O-antigen polysaccharide ABC transporter may explain how complex lipids such as PDIM and PGL (has a phenolic-sugar moiety attached to a PDIM lipid core) traverses the membrane. Interestingly, templates with lesser matches were lipid/multi-drug transporters, and superimpositions revealed that the Mtb DrrABC transporter is a three-component system forming a heterodimer. Corroborating the structural data, biochemical analyses proved that all three *drrABC* genes are required for PDIM transport and are non-redundant verified by two radioactive metabolic labels.

Based on phylogenetic and structural predictions, MmpL proteins are highly comparable to members of the RND superfamily (174,227,228). Together with our work and recent structural advances in the field are beginning to distinguish MmpL proteins from their RND counterparts in Gram-negative bacteria. Novel approaches in preserving protein integrity were preferred, to determine the structures of MmpL3 and MmpL7 that required further optimisation, providing the opportunity also to probe function and protein-protein interaction. From our structural modelling, we have shown that MmpL7 consists of distinct structural features with emphasis on the PD2. Genetics and biochemical studies revealed that conserved residues in the transmembrane region and residues in PD2 directly affected MmpL7 activity in PDIM transport and synthesis. Additionally, all *drrA/B/C* genes form a heterologous DrrABC

transporter for PDIM translocation across the membrane. While evidence in this work proves MmpL7 does not act as an independent PMF mediated transporter, it may serve as a scaffold connecting proteins in lipid synthesis and transport providing and efficient service in Mtb.

The emergence and incidence of drug-resistant Tb strains and co-infected HIV-Tb individuals renders the current chemotherapy ineffective. Already anti-Tb drugs approved and in late stages of clinical trials are aimed at inhibiting the synthesis of mycolic acids (i.e. the hallmark of the mycobacterial cell wall) and the transport of mycolate esters by MmpL3, essential for mycobacterial survival. Collectively we have demonstrated the importance of MmpL proteins in mycobacterial survival and pathogenesis and attempted to understand the mechanism of MmpL7. For the future, determining the structure of MmpL7 and the remaining eleven MmpL proteins and identifying interacting protein partners of MmpL7 using protein-protein interaction *in vitro* assays and possibly SMA pull down assays will greatly contribute to our understanding of the mechanism of MmpL proteins, as this knowledge is vital for the development of effective new anti-Tb drugs.

Chapter 6: General methods and materials

Chapter 6: General methods and materials

6.1. Bioinformatics analyses

Routine DNA or protein sequence analyses were performed using the nucleotide or protein Basic Local Alignment Tool (https://blast.ncbi.nlm.nih.gov/Blast.cgi). In this study, all genetic and proteomic information in Mtb H37Rv was retrieved from the Mycobrowser database (https://mycobrowser.epfl.ch/)(307). I-TASSER (http://zhanglab.ccmb.med.umich.edu/I-TASSER/) was used to generate homology models and alignments (253) while Pymol (264) was used to view and edit these models as well as solved protein structures retrieved from the protein data bank (PDB). The SyntTax (https://archaea.i2bc.paris-saclay.fr/synttax/) (307) and Kyoto Encyclopaedia of Genes and Genomes (KEGG) servers (https://www.genome.jp/kegg/) were used to visualise the genomic context of mycobacterial genes and identify orthologs (283). The T-coffee web tool (https://www.ebi.ac.uk/Tools/services/web_tcoffee/toolform.ebi) with default parameters (308) was used to perform standard multiple sequence alignments (MSA) and the percentage identity matrix followed by the Espript server (http://espript.ibcp.fr/ESPript/cgi-bin/ESPript.cgi) that was used to achieve high-resolution output with added protein structural information (309).

6.2. Maintenance of bacterial strains

The media used for the routine culturing of bacteria in this study described in Appendix 1. Briefly, all *E. coli* strains were cultured in Luria-Bertani broth (LB) overnight, at 37 °C shaking (at 180 rpm) and where necessary, supplemented with antibiotics as listed in Appendix 2. Liquid cultures of *E. coli* were spread on Luria-Bertani agar plates (LA) for isolation of single colonies and were appropriate, contained antibiotics (listed in Appendix 2) and incubated at 37 °C. *M. smegmatis* and *Mycobacterium bovis* BCG (BCG) strains were cultured on Middlebrook 7H10 agar (with 10% OADC) for the isolation of single colonies at 37 °C and in liquid culture

using 7H9 broth with 10% OADC at 37 °C shaking at 180 rpm. For mycobacterial strains, antibiotics were added to the media according to Appendix 2, where required.

All bacterial strains and plasmids used in this study were stored at -80 °C and -20 °C, respectively. All *E. coli* strains were stored in 25% glycerol (v/v), while all mycobacterial strains were stored in 12.5% glycerol (v/v).

6.3. General plasmid, mycobacteriophages and bacterial strains used in this study

Table 6-1: A list of commonly used plasmid, mycobacteriophages and bacterial strains used in this work.

Plasmid, Mycobacteriophages and Bacterial strains	**Genetic characteristics**	**Origin**
Plasmids		
p0004S	Cosmid vector containing Hyg-sacB cassette	(280)
pMV261	Kan^R, *E.coli*-mycobacterial shuttle vector with the GroEL (Hsp) promoter of Mtb	(265)
pMV306	Kan^R; *E.coli*-mycobacterial shuttle vector that integrates a single copy at the *attB* site of mycobacterial chromosomes	(265)
Mycobacteriophages		
phAE159	Temperature sensitive, conditionally replicating shuttle phasmid derived from lytic mycobacteriophage TM4	(280)
Bacterial strains		
E. coli Top10	F^- *mcr*A Δ(*mrr-hsd*RMS-*mcr*BC) Φ80*lac*ZΔM15 Δ*lac*X74 *rec*A1 *ara*D139 Δ(*ara leu*) 7697 *gal*U *gal*K *rps*L (*Str*R) *end*A1 *nup*G For general cloning	Invitrogen™
E. coli HB101	*E.coli* K-12 F^- *mcr*B *mrr-hsd*S20(r_B^- m_B^-) *rec*A13 *leu*B6 *ara*-14 *pro*A2 *lac*Y1 *gal*K2 *xyl*-5 *mtl*-1 *rps*L20(SmR) *gln*V44 λ-	Stratagene

	For generating phasmids	
M. smegmatis	mc^2155, Wild type strain (*ept-1* mutant of *M. smegmatis* strain mc^26)	(310)
BCG	Wild type strain of *Mycobacterium bovis BCG* var Pasteur	

6.4. DNA extraction

6.4.1 Mycobacterial genomic DNA extraction

The following method was modified from the DNA extraction protocol described by (311). 10-20 ml of mycobacterial fully-grown cultures were centrifuged at 4000 rpm for 15 min and the pellet was resuspended in 1.8 ml TE buffer (50 mM Tris-HCl pH 8.0, 10 mM EDTA) and lysed with 50 µl lysozyme (10 mg/ml) overnight (ON) at 37 °C. After that, the suspension was further treated with 50 µl of proteinase K (20mg/ml) and 100 µl SDS (10%) for 30 min at 55 °C. Then, 100 µl of NaCl (5M) was added to the mixture and allowed to incubate for 15 min at 65 °C and 400 µl of chloroform was added and vortexed until the mixture turned white. Thereafter, the mixture was centrifuged at 13000 rpm for 10 min and the upper layer was transferred to a clean Eppendorf tube. To precipitate the DNA, 0.7 volumes of isopropanol was added, mixed gently and stored at -20 °C for 20 min. Thereafter, the mixture was centrifuged at 13000 rpm for 10 min and discarded. The pellet was washed with 500 µl of ice-cold 70% ethanol and left at room temperature to evaporate. Finally, the dried pellet was resuspended in 45 µl of EB buffer (10 mM Tris-HCl, pH 8.5) with 5 µl of RNase (10 mg/ml) and incubated at 37 °C for 1 hr.

6.4.2 *E.* coli plasmid extraction

1- 3 ml of *E. coli* cultures were grown overnight and were harvested by centrifugation at 13000 rpm for 10 min, RT. DNA was extracted using QIAprep spin miniprep kit (Qiagen) per manufacturer's instructions.

6.5. DNA manipulation

In the construction of all the plasmids/constructs/vectors generated in this study, DNA manipulations, such as enzymatic reactions used for DNA- amplification, cloning and analysis, were performed according to the molecular protocols of Sambrook and Russell (312) and Parish and Brown (313). Besides, *E. coli* Top10 was the host strain used for the cloning and propagation of all plasmids in this study.

6.5.1 DNA amplification using Polymerase Chain Reaction (PCR)

6.5.1.1 Oligonucleotide or Primer preparation:

All primers were ordered and received as lyophilised pellets from Eurofinn, Germany, and resuspended in EB buffer (10 mM Tris-HCl, pH 8.5) to 10 µM for the reaction.

6.5.1.2 PCR reagents and program:

The Q5® High-Fidelity DNA Polymerase kit was used for PCR and reactions were prepared according to the manufacturer's instructions. A no-template control or negative control (NC) that lacks DNA in the PCR reaction was included in every reaction to exclude the possibility of DNA contamination in the reagents. The reactions were then put into a thermocycler and programmed according to Table 6-2, as per manufacturer's instructions. The annealing temperature of all primers in this study were calculated using the following website: http://tmcalculator.neb.com/#!/. Once the programme was completed the PCR products or fragments were analysed by agarose electrophoresis.

Table 6-2: Thermocycler programme

Number of cycles:	Stages:	Temperature (°C)	Time (Minutes : Seconds)
1	Initial Denaturation	98	10:00
35	Denaturation	98	00:40
	Annealing	Depends on primers	00:40
	Elongation	72	00:45 (30-40s/1 Kbp)
1	Final elongation	72	10:00

1	Hold	16	Infinity

6.6. Cloning

To obtain single fragments free from chemicals that may hinder or alter the cloning process, all fragments were purified before and after every enzymatic reaction.

6.6.1 DNA purification

6.6.1.1 DNA purification from agarose gel

After DNA fragments required for cloning were verified to be correct by DNA analysis, the fragments were excised from the gel and put into clean Eppendorf tubes. The QIAquick® gel extraction kit (Qiagen) was used to purify the DNA fragment as per the manufacturer's instructions. Briefly, the excised gel slices were melted and solubilised at 55 °C with the QG buffer (5.5 M guanidine thiocyanate, 20 mM Tris-HCl pH 6.6) and the suspensions were loaded onto DNA binding columns. The columns were then washed with PE buffer (20 mM Tris-HCl pH 7.5, 80% ethanol) before the DNA fragment was eluted with 30 µl of EB buffer (10 mM Tris-HCl, pH 8.5).

6.6.1.2 DNA purification of PCR products

QIAquick® PCR purification kit (Qiagen) was used to purify the PCR fragments after restriction endonuclease reactions as per the manufacturer's instructions. In summary, PB binding buffer (5.0 M guanidine thiocyanate, 30% isopropanol) was added to PCR fragments and loaded onto DNA binding columns, which were then washed with PE buffer (20 mM Tris-HCl pH 7.5, 80% ethanol) and eluted with 30 µl of EB buffer (10 mM Tris-HCl, pH 8.5).

6.6.2 Restriction endonuclease digestion

Restriction endonuclease digestion was used to digest genomic DNA in the Southern blot technique (also described in this section), to verify plasmids by restriction mapping and

generate compatible ends of DNA fragments for cloning purposes. Restriction endonucleases or enzymes were supplied with the specified buffers from Thermo scientific or NEB. All enzymatic reactions were performed as per manufacturers' instructions in a total volume of 20 µl (unless otherwise stated). Generally, for plasmid restriction mapping, DNA was digested for 1 hr at 37 °C, but PCR fragments (required for cloning) were digested up to 4 hrs at 37 °C, while genomic DNA (required for Southern blot analysis) was digested overnight at 37 °C. Where two restriction endonucleases were needed, they were added consecutively for full efficiency with the compatible buffer and before the addition of the second enzyme, the first reaction was heat-inactivated.

6.6.3 DNA ligation

Purified plasmid and DNA fragments with compatible ends were ligated with T4 DNA ligase (NEB) according to the manufacturer's instructions. The reaction was incubated ON at room temperature (RT) and then heat denatured at 65 °C for 5-10 min. To optimise cloning events, 50 ng of plasmid was used for all ligation reactions and plasmid to DNA fragment ratios of 1:1, 1:2 or 1:3 were calculated as follows:

For 50 (ng) of plasmid:

The mass of DNA fragment = [50 ng x DNA fragment (bp)] ÷ plasmid size (bp)
= X (ng) of DNA fragment
The volume (µl) of DNA fragment = X (ng) of DNA fragment ÷ concentration of DNA fragment (ng/µl)
= Y (µl) of DNA fragment

The ligation reactions were transformed into chemically competent *E. coli* Top10 cells.

6.7. DNA/RNA analysis

6.7.1 Agarose gel electrophoresis

DNA/RNA/PCR/Restriction digested products were analysed by separation using agarose gel electrophoresis. Agarose gels were made by dissolving and melting molecular biology grade

agarose (Bioline) in 1x- Tris-acetate EDTA (TAE) buffer and 5 µl of Midori Green, UV fluorescent dye, added per 100 ml agarose. The percentage of agarose varied from 0.8 to 2.0% depending on the molecular weight of the DNA/RNA fragments analysed. 1% agarose gels were prepared for low molecular weight DNA fragments of less than 1 Kbp, while 0.8% agarose gels were used for DNA fragments more than 1 Kbp. DNA/RNA fragments were separated with an electric field of 100-140 V, 400 mA in horizontal submarine units (Bio-Rad). Gels were visualised by a UV-light imaging system (Bio-Rad Gel Doc systems); with image acquisition software. Lambda DNA molecular weight markers (NEB) in Appendix 3 was used to assess fragment sizes of samples.

6.7.2 Spectrophotometry

The integrity of extracted or purified, DNA/RNA and plasmids were evaluated using NanoDrop ND-1000 Spectrophotometer (NanoDrop Technologies) used in conjunction with software (Coleman Technologies) the with a UV absorbance at 260 nm. The measures determined from the NanoDrop were used to estimate the approximate concentrations of DNA and plasmids required for cloning.

6.7.3 DNA Sequencing

Plasmids generated in this study were sent to Eurofinns, Germany, for sequencing to verify the integrity of the cloned fragment/s. Sequencing primers were designed using Clone manager and SnapGene software, and the sequencing data was analysed using SnapGene software.

6.8. RNA extraction, cDNA synthesis and Reverse transcriptase- PCR

RNA was extracted from pellets of 50 ml liquid cultures at mid logarithmic phase (OD_{600nm} 0.8-1.0) as described by (314,315). The pellets were resuspended in 600 µl of lysozyme solution [5 mg/ml prepared in Tris (pH 8.0)] and 7 µl/ml β-mercaptoethanol was added to the mixture that was kept on ice and subjected to mechanical lysis by homogenisation for 1 min

(at 400 speed). Then, to the mixture 60 µl of 10% sodium dodecyl sulfate (SDS) was added and homogenised for 2 min (kept on ice). To this, 60 µl of 3M sodium acetate pH 5.2 was added together with 726 µl of acid phenol pH 4.2 (i.e. phenol solution saturated with 0.1 M citrate buffer, Sigma) and tubes were mixed well by inversion and incubated at 65 °C for 5 min (mixing every 30 s by inversion). Samples were centrifuged at 13000 rpm for 5 min, and the upper aqueous phase was transferred to a new tube. An equal volume of acid phenol pH 4.2 was added, vortexed and incubated at 65 °C for 2 min (mixing every 30 s by inversion). Again, the mixtures were centrifuged at 13000 rpm for 5 min and the upper aqueous phase was transferred to a new tube. To this 550 µl of chloroform: isoamyl alcohol (24:1) mix was added, and the mixture was inverted several times and centrifuged at 13000 rpm for 5 min. The upper aqueous phase was transferred to a new tube, and 1/10 volume of 3M sodium acetate pH 5.2 and 3 volumes of 100% ethanol were added, incubated at -20 °C for one hr and centrifuged at 13000 rpm for 10 min. The ethanol was discarded, and the pellet was washed with 500 µl of 70% ethanol, centrifuged at 13000 rpm for 10 min, the ethanol removed, the pellet left to air dry and resuspended in 50 µl of water (free from DNA/RNA). The integrity of RNA extracted was verified on a 2% agarose gel and evaluated using NanoDrop ND-1000 Spectrophotometer.

About 10 µg of RNA was treated with DNase (using Turbo DNA free kit, Invitrogen™) to remove any traces of residual DNA that was confirmed by a 2% agarose gel and by NanoDrop. Then, 2 ug of treated/purified RNA was converted to cDNA using random hexamers (Invitrogen™) and reverse transcriptase (contained in the SuperScript™ III Reverse Transcriptase kit from Invitrogen™) as indicated by the manufacturer's protocol. To ensure that the RNA post-DNase treatment was, in fact, free of DNA, a set of no reverse transcriptase reactions were used as controls. Primers were designed to target specific genes in this study (Appendix 5E) and *sigA* a housekeeping gene constitutively expressed served as a positive

control. The cDNA synthesised from reactions with RT and RNA from reactions without RT were used as templates in a standard PCR reaction amplified by the specific primer pairs to assess if particular genes were expressed in the strains under investigation using the reagents in the Q5 polymerase kit (NEB). PCR cycling conditions were set at 35 cycles and transcripts (20 µl each) were analysed on a 2% agarose gel.

6.9. Transformation of chemically competent *E. coli* Top10 cells

6.9.1 Preparation of chemically competent cells

An overnight culture of *E. coli* Top10 cells were prepared from inoculating 5 ml of LB with a single colony, which was used to inoculate 100 ml of LB supplemented with 20 mM magnesium sulphate. This culture was allowed to grow to mid-log phase (an OD600nm to approximately 0.40- 0.60), and then the culture was placed in ice for 15- 30 min before harvesting the cells by centrifugation at 3500 rpm for 10 min, at 4 °C. The bacterial pellet was resuspended in 0.4 volume of TFBI (15% v/v glycerol, 30 mM potassium acetate, 100 mM rubidium chloride, 10 mM calcium chloride, 50 mM manganese chloride) and kept on ice for 15 min. The cells were pelleted again by centrifugation at 3500 rpm for 10 min, at 4 °C and the pellet was re-suspended in 0.04 volume TFBII (10 mM 3-(N-morpholino) propanesulfonic acid [MOPS], 75 mM calcium chloride) and chilled in ice for 60- 90 min. 200 µl aliquots were flash-frozen and stored at -80 °C for future use.

6.9.2 Transformation of chemically competent cells

Chemically competent cells were thawed on ice and 100-200 µl of cells were gently mixed with each ligation reaction and kept on ice for 15 min. No DNA or negative control (NC) was included to verify that the competent cells were not contaminated. The mixture was heat-shocked at 42 °C for 90 s to allow for DNA uptake and placed on ice for a further 10-15 min. 900 µl of LB was added and incubated at 37 °C for 1 hr, for recovery of the cells. After that,

for the selection of transformants, the cells were spread on LA plates containing the appropriate antibiotics and incubated overnight to allow for colony growth.

6.10. Electroporation of electro-competent mycobacterial cells

The following procedures were adapted from the protocol described by (316).

6.10.1 Preparation of electro-competent mycobacterial cells

A fully-grown culture of mycobacterial BCG cells was prepared from inoculating 10 ml of 7H9 with a single colony. This preculture was used to inoculate 100 ml of 7H9 broth (with the appropriate antibiotics and supplements where required) and allowed to grow to mid-log phase (OD_{600nm} 0.40- 0.70). Thereafter, the culture was centrifuged at 4000 rpm for 15 min, at RT or at 37 °C. The pellet was resuspended in 40 ml prewarmed 10% glycerol and centrifuged as above. Then, the pellet was resuspended in 20 ml prewarmed 10% glycerol, centrifuged again as above and finally resuspended in 2 ml prewarmed 10% glycerol. The cell suspension was kept at RT or at 37 °C and used immediately.

6.10.2 Electroporation

200 µl of electro-competent mycobacterial cells were distributed into 2 mm electroporation cuvettes (Gene pulser; Bio-Rad) at RT, and gently mixed with 1-2 µg of plasmid DNA. No DNA or negative control (NC) was included to verify that the electro-competent cells were not contaminated. Then, the cuvettes were placed in the shock pod of the Eppendorf Electroporator (model No. 2510) and electroporated at 2500 V. Immediately after electroporation, 900 µl 7H9 for BCG was added for recovery and replication and incubated overnight at 37 °C. For the selection of transformants, cells were spread on 7H10 agar (supplemented with 10% OADC) containing appropriate antibiotics and incubated at 37 °C for 3- 4 weeks.

6.11. Generation of null mutants by specialised phage transduction

The generation of knockout mutants using specialised transduction involves the following processes: construction of knockout phage's, amplification of phage to high titres and transduction of BCG, all explained by (280,281).

6.11.1 Construction of knockout phage

For the construction of all allelic exchange substrate plasmids, 0.8- 1 Kbp each of homologous upstream and downstream regions of the genes (including about 100 bp of the genes) were cloned into the plasmid, p0004S. The upstream and downstream regions on either side of (i.e. flanking) the hyg cassette of p0004S were sequence verified. Then, all allelic exchange substrate plasmids were ligated into phAE159 at the *Pac*I site and packaged into temperature-sensitive mycobacteriophages (λ-phage heads), resulting in phasmids, which were transduced into *E. coli* HB101 cells. The phasmids were extracted from the transformants and electroporated into *M. smegmatis* (mc^2155) and allowed to recover with 1 ml of TSB at 30 °C, overnight. After that, the cells were divided into 200 µl and 800 µl and diluted with 100 µl each of log phase (actively growing) *M. smegmatis*. Each of the dilutions were mixed with 4 ml of 7H9 top agar (pre-warmed to 55 °C) and overlaid on 7H9 basal plates and incubated at 30°C for 2-3 days for plaques to be formed. The plates were soaked in 4 ml of mycobacteriophage (MP) buffer (50 mM Tris pH 7.5, 150 mM NaCl, 10mM $MgSO_4$, 2mM $CaCl_2$) for 3-4 hrs, which was recovered and filtered and stored at 4 °C.

6.11.2 High titre phage

Briefly, the titre of the phage lysate recovered from the plaques is estimated by serial dilutions of phage lysate that are spotted onto 7H9 basal plates overlaid with 400 µl of log phase (actively growing) *M. smegmatis* and incubated at 30 °C. After that, 100 µl of the dilution of phage lysate required to generate 1000 plaques was mixed with 100 µl of log phase (actively growing) *M.*

smegmatis and 4 ml of 7H9 top agar (pre-warmed to 55 °C) and overlaid on 7H9 basal plates, incubated at 30°C for 2-3 days. The plates were soaked in 4 ml of MP buffer for 3-4 hrs, which was recovered, filtered and stored at 4 °C. The titre of this phage lysate was determined as explained above and the entire procedure was repeated until the phage titre was 10^8 – 10^{10}.

6.11.3 Specialised transduction of BCG

BCG was grown to an OD_{600nm} of 0.60 and harvested by centrifugation at 4000 rpm, 15 min, RT. The pellet was washed with 50 ml of MP buffer, pelleted by centrifugation as above and washed again with 50 ml of MP buffer and then centrifuged again. Finally, the pellet was resuspended in 5 ml of MP buffer and 1 ml of the cell suspension was mixed with 1 ml of high titre (10^8-10^{10}) phage lysate. A negative control (NC) containing 1 ml of MP buffer mixed with 1 ml of cells was included to verify that the cells were not contaminated. The transductions were incubated at 37 °C overnight, harvested by centrifugation at 4000 rpm, 15 min, RT and recovered in 7H9 and incubated at 37 °C, overnight. Thereafter, the cells were centrifuged at 4000 rpm, 15 min, RT and resuspended in 400 µl of 7H9 of which, aliquots of 100 µl were plated on 7H10 agar with 100 µg/ml hygromycin and incubated at 37 °C. After, 3-4 weeks of incubation, hygromycin resistant colonies are selected and inoculated into 10 ml of 7H9 for genomic DNA extraction. The exchange of each full-length gene with the allelic exchange substrate (i.e. the 1 Kbp upstream and downstream regions of the target gene flanking the hygromycin cassette of p0004S) was either verified by PCR or Southern blot analysis.

6.12. Southern blot analysis

Southern blot analysis is used to genetically verify that a targeted gene has been successfully disrupted as compared to the full-length gene in the wild type. This technique involves-restriction mapping and digests of genomic DNA of wild type and potential mutants or transductants, blotting, probe labelling and hybridisation and detection. Firstly, genomic DNA

was digested with restriction enzyme/s that distinctly differentiates the mutant from the wild type, and fragments of the digest are separated by gel electrophoresis on 0.7% agarose gel. An image of the gel was captured alongside a ruler using the GelDoc viewing system to verify the sizes of the fragments later. For the transfer of DNA, the double-stranded DNA on the gel needs to be denatured into single strands, accomplished by washing the gel with the following buffers: depurination (0.25 M HCl), denaturation (1.5 M NaCl, 0.5 M NaOH) and neutralising (0.5 M Tris-HCl pH 7.2, 1 M NaCl).

Blotting uses a high salt solution (20X SSC, 3 M NaCl, 0.3 M sodium citrate, pH 7.0) to transfer denatured DNA fragments from the gel onto a positively charged nylon membrane (No. 11209299001, Roche) by capillary action. The blot was fixed by cross linking the DNA bound to the nylon membrane under UV light. The labelling of probes, hybridisation and immunological chemiluminescence detection uses a digoxygenin based system as described by protocols of the DIG High Prime Labelling and Detection Starter Kit II, (No.11555614910, Roche). A random-priming method was used to incorporate the Digoxigenin-11-dUTP into the probe sequence. After hybridisation with DIG labelled probes, the membrane was visualised using an antibody against digoxigenin with an alkaline phosphatase label by adding a chemiluminescent alkaline phosphatase substrate (CSPD). The enzymatic reaction of the alkaline phosphatase with the CSPD results in luminescence that was visualised by exposing the membrane to an X-ray film.

6.13. Site-Directed Mutagenesis (SDM)

The Q5 SDM kit and protocol from NEB was used generate amino acid substitutions as described in Chapter 3 and complementation strains with a loss of individual *drrA/B/C* genes as explained in Chapter 4. The fundamental step of SDM is the design of custom primers to generate the specific modification. As previously mentioned, custom primers were designed

using the NEB base changer website (http://nebasechanger.neb.com/) and were used in a standard PCR with the DNA template and PCR reagents provided in the kit. As per manufacturer's instructions the PCR amplicon was treated with the Kinase-Ligase-Dpn1 (KLD) mixture, to rapidly circularise and enrich the modified plasmid by digesting the template DNA. Thereafter, the modified product was transformed in *E. coli* Top10 competent cells and, plated on selection media. Then single colonies were cultured for plasmid extraction to verify the modification by DNA sequencing analysis.

6.14. Biochemical lipid analysis

The biochemical analysis of lipids includes radiolabelling of lipids, lipid extraction and analysis by separation on TLC silica gel plates using various solvent systems.

6.14.1 Radioactive labelling of lipids using carbon 14 [^{14}C]-acetate

Log phase cultures of Mycobacteria were used to inoculate 10 ml of 7H9 (with 10% OADC and 0.05% tween) at an OD_{600nm} of 0.03 and then labelled with 1 µCi/ml of [^{14}C]-acetate Perkin Elmer, 45-60 mCi). The labelled culture was allowed to grow to log phase. After that, the cultures were allotted into glass tubes for lipid extraction labelled Tube 1 and centrifuged at 3500 rpm for 10 min at RT to separate the spent culture from pellets. The spent culture was passed through a 0.22µm filter to exclude debris into an empty tube (labelled Tube 2) while the pellets (Tube 1) were washed with 1x PBS before freeze-drying.

6.14.2 Radioactive labelling of lipids using carbon 14 [^{14}C]-propionate

Log phase cultures of Mycobacteria were used to inoculate 10 ml of 7H9 (with 10% OADC and 0.05% tween) at an OD_{600nm} of 0.70- 0.80 and then labelled with 0.2 µCi/ml of [^{14}C]-acetate American Radiolabelled Chemicals, specific activity 50-60 mCi. The labelled culture was allowed to grow to overnight. Thereafter, the cultures were allotted into glass tubes for lipid extraction labelled Tube 1 and centrifuged at 3500 rpm for 10 min at RT to separate the spent

culture from pellets. The spent culture was passed through a 0.22 µm filter to exclude debris into an empty tube (labelled Tube 2) while the pellets (Tube 1) were washed with 1x PBS before freeze-drying.

6.14.3 Lipid extraction

Generally, methods describing lipid extraction were followed according to Besra (317). To account for all the surface extractable apolar lipids we analysed apolar lipids from the spent media as well the pellets. As a consequence of using the detergent Tween-80 in the media and shaking the cultures, surface extractable lipids such as PDIM are sloughed off from the outer membrane and found in the spent culture (40,41). Lipids from the spent culture were extracted by adding equal amounts of petroleum ether (60- 80 °C) in Tube 2 and mixing on a rotator for 30 min, then centrifuged at 4000 rpm for 10 min. The upper layer was transferred to another tube (labelled Tube 3) and the process repeated. The accumulated lipid extracts in Tube 3 were dried on a heating block (at 50 ºC) under nitrogen and represented the outside fraction.

Total apolar lipids were extracted from the pellets in Tube 1 with 2 ml methanolic saline [methanol: 0.3% NaCl (10:1, v/v)] and 2 ml petroleum ether (60- 80 °C) mixed on a rotator for 15 min and centrifuged at 3500 rpm for 5 min. The upper layer was transferred to another tube (labelled Tube 4). To extract the remaining total apolar lipids, another 2 ml of petroleum ether (60- 80 °C) was added to Tube 1, allowed to mix on a rotator for 15 min, and centrifuged at 3500 rpm for 5 min. The upper layer was transferred to Tube 4, and the accumulated extracts were dried on a heating block (at 50 ºC) under nitrogen that represented the total apolar lipids associated with the cells (i.e. inside fraction).

Tube 1 was further processed to extract polar lipids, by adding 2.3 ml of chloroform: methanol: 0.3% NaCl (9:10:3, v/v/v) and allowing this to mix for 60 min on a rotator, then centrifuged at 3500 rpm for 15 min. The supernatant was removed to another tube (labelled Tube 5). The

pellet in Tube 1 was resuspended with 0.75 ml of chloroform: methanol: 0.3% NaCl (5:10:4, v/v/v) and mixed for 30 min, centrifuged at 3500 rpm for 15 min, and the supernatant was transferred to Tube 5 and the process repeated. 1.3 ml of chloroform and 1.3 ml of 0.3% NaCl was added to the pooled extracts in Tube 5, mixed for 10 min on a rotator, centrifuged at 3500 rpm for 5 min. This time, the lower layer was transferred to another tube (labelled Tube 6) and dried on a heating block (at 50 ^{o}C) under nitrogen.

All dried lipid extracts in Tube 3, Tube 4 and Tube 6 were resuspended in 200 µl of chloroform: methanol (2:1) and stored at RT for thin-layer chromatography (TLC) analysis. To load equal amounts of [^{14}C] radioactively labelled samples, the amount of radioactivity was quantified by spotting 5 µl of each radioactively labelled extract in a scintillation vial and allowing it to dry before mixing with 10 ml scintillation fluid where the measurements were in counts per minute.

6.14.4 Thin-layer Chromatography (TLC) analysis of lipids

In general, equivalent amounts of radioactively labelled samples about 15, 000- 20, 000 counts per minute (cpm) were spotted on TLC plates (5554 silica gel 60F524; Merck) and resolved using the systems described below. [^{14}C]-acetate and [^{14}C]-propionate labelled lipids were visualised after 72 and 24 hrs exposure to Kodak X-Omat AR film respectively and developed by autoradiography.

6.14.4.1 Solvent systems for TLC analysis of apolar and polar lipids

Both one- and two-dimensional TLC (1D/2D TLC) were used to separate apolar and polar lipids. For the separation of PDIM and its species on TLC, petroleum ether: diethyl ether (9:1) was used (40,120) and on a 2D TLC system A as described by Besra (317) in Table 6-3. Similarly, to analyse PGL on TLC, chloroform: methanol (19:1) was used and on a 2D TLC, system C (as described in Table 6-3) was used (317). TLC was used to resolve other relevant apolar and polar lipids using chloroform: methanol: distilled water (80:20:2) and chloroform:

methanol: ammonium hydroxide: distilled water (65:25:3.6:0.5). In all cases, TLC plates were well dried before loading of the samples and after every solvent system.

Table 6-3: Solvent systems used to separate apolar and polar lipids for 2D TLC analysis. [Adapted from (317)].

Solvent systems	**Direction 1**	**Direction 2**
A	Petroleum ether (60- 80 °C): ethyl acetate 95:2 (v/v) Repeat 3 times	Petroleum ether (60- 80 °C): acetone 92:8 (v/v) Once
C	Chloroform: methanol 96:4 (v/v) Once	Toluene: acetone 80:20 (v/v) Once

References

1. Stackebrandt E, Rainey FA, Ward-Rainey NL. Proposal for a new hierarchic classification system, Actinobacteria classis nov. Int J Syst Bacteriol [Internet]. 1997 Apr 1;47(2):479–91. Available from: https://www.microbiologyresearch.org/content/journal/ijsem/10.1099/00207713-47-2-479

2. Trifiro S, Bourgault AM, Lebel F, René P. Ghost Mycobacteria on Gram stain. J Clin Microbiol [Internet]. 1990 Jan;28(1):146–7. Available from: http://www.ncbi.nlm.nih.gov/pubmed/1688872

3. Leão SC, Romano MI, Jesus M. Tuberculosis, leprosy, and other mycobacterioses. In: Gruber A, Durham AM, Huynh C et al., editor. Bioinformatics in Tropical Disease Research: A Practical and Case-Study Approach [Internet]. Bethesda (MD): National Center for Biotechnology Information (US); 2008. Available from: https://www.ncbi.nlm.nih.gov/books/NBK6820/

4. Smith I. *Mycobacterium tuberculosis* pathogenesis and molecular determinants of virulence. Clin Microbiol Rev [Internet]. 2003 Jul 1;16(3):463–96. Available from: http://cmr.asm.org/cgi/doi/10.1128/CMR.16.3.463-496.2003

5. Lee OYC, Wu HHT, Donoghue HD, Spigelman M, Greenblatt CL, Bull ID, et al. *Mycobacterium tuberculosis* complex lipid virulence factors preserved in the 17,000-year-old skeleton of an extinct bison, bison antiquus. PLoS One. 2012;7(7):1–10.

6. Minnikin DE, Lee OY-C, Wu HHT, Besra GS, Bhatt A, Nataraj V, et al. Ancient mycobacterial lipids: Key reference biomarkers in charting the evolution of tuberculosis. Tuberculosis [Internet]. 2015 Jun;95:S133–9. Available from: http://www.sciencedirect.com/science/article/pii/S1472979215000104

7. Nerlich AG, Lösch S. Paleopathology of human tuberculosis and the potential role of climate. Interdiscip Perspect Infect Dis [Internet]. 2009 Jan 6;2009(2):1–9. Available from: http://www.hindawi.com/journals/ipid/2009/437187/

8. Kaufmann SHE. Robert Koch, the Nobel Prize, and the ongoing threat of tuberculosis. N Engl J Med. 2005;353(23):2423–6.

9. Bloom BR, Murray CJL. Tuberculosis: Commentary on a reemergent killer. Science (80-) [Internet]. 1992;257(5073):1055–64. Available from: http://www.sciencemag.org/cgi/doi/10.1126/science.257.5073.1055

10. World Health Organization. Global Report Tuberculosis 2018. 2018;(September):12. Available from: https://www.who.int/tb/publications/global_report/GraphicExecutiveSummary.pdf?ua=1

11. Theodor Z. The immune response to *Mycobacterium tuberculosis* infection in humans. in: Tuberculosis - current issues in diagnosis and management [Internet]. InTech; 2013. Available from: http://www.intechopen.com/books/tuberculosis-current-issues-in-diagnosis-and-management/the-immune-response-to-mycobacterium-tuberculosis-infection-in-humans

12. Ramakrishnan L. Revisiting the role of the granuloma in tuberculosis. Nat Rev Immunol [Internet]. 2012;12(5):352–66. Available from: http://www.nature.com/doifinder/10.1038/nri3211

13. Meena LS, Rajni T. Survival mechanisms of pathogenic *Mycobacterium tuberculosis* H37Rv. FEBS J. 2010;277(11):2416–27.

14. Sakamoto K. The pathology of *Mycobacterium tuberculosis* infection. Vet Pathol [Internet]. 2012 May 18;49(3):423–39. Available from: http://journals.sagepub.com/doi/10.1177/0300985811429313

15. Andersen P. Vaccine strategies against latent tuberculosis infection. Trends Microbiol. 2007;15(1):7–13.

16. Ashwani Kumar, Jose C. Toledo, Rakesh P. Patel, Jack R. Lancaster Jr. and AJCS. *Mycobacterium tuberculosis* DosS is a redox sensor and DosT is a hypoxia sensor. Proc Natl Acad Sci [Internet]. 2007;104(28):11568–73. Available from: http://www.pnas.org/cgi/doi/10.1073/pnas.0705054104

17. Leistikow RL, Morton RA, Bartek IL, Frimpong I, Wagner K, Voskuil MI. The *Mycobacterium tuberculosis* DosR regulon assists in metabolic homeostasis and enables rapid recovery from nonrespiring dormancy. J Bacteriol. 2010;192(6):1662–70.

18. Zumla A, Nahid P, Cole ST. Advances in the development of new tuberculosis drugs and treatment regimens. Nat Rev Drug Discov [Internet]. 2013;12(5):388–404. Available from: http://www.nature.com/doifinder/10.1038/nrd4001

19. Timmins GS, Deretic V. Mechanisms of action of isoniazid. Mol Microbiol [Internet]. 2006 Dec;62(5):1220–7. Available from: http://doi.wiley.com/10.1111/j.1365-2958.2006.05467.x

20. Du Preez I, Loots DT. Novel insights into the pharmacometabonomics of first-line tuberculosis drugs relating to metabolism, mechanism of action and drug-resistance. Drug Metab Rev [Internet]. 2018;50(4):466–81. Available from: http://www.ncbi.nlm.nih.gov/pubmed/30558443

21. Singh R, Dwivedi SP, Gaharwar US, Meena R, Rajamani P, Prasad T. Recent updates on drug resistance in *Mycobacterium tuberculosis*. J Appl Microbiol [Internet]. 2019 Oct 29;(Who 2018):jam.14478. Available from: https://onlinelibrary.wiley.com/doi/abs/10.1111/jam.14478

22. Kibret KT, Moges Y, Memiah P, Biadgilign S. Treatment outcomes for multidrug-resistant tuberculosis under DOTS-Plus: a systematic review and meta-analysis of published studies. Infect Dis Poverty [Internet]. 2017;6(1):7. Available from: http://idpjournal.biomedcentral.com/articles/10.1186/s40249-016-0214-x

23. Tornheim JA, Dooley KE. Tuberculosis associated with HIV infection. Microbiol Spectr [Internet]. 2017 Jan 1;5(1):473–7. Available from: http://www.ncbi.nlm.nih.gov/pubmed/28233512

24. Diedrich CR, Flynn JL. HIV-1/*Mycobacterium tuberculosis* coinfection immunology: How does HIV-1 exacerbate tuberculosis? Infect Immun. 2011;79(4):1407–17.

25. McIlleron H, Meintjes G, Burman WJ, Maartens G. Complications of antiretroviral therapy in patients with tuberculosis: Drug interactions, toxicity, and immune reconstitution inflammatory syndrome. J Infect Dis [Internet]. 2007;196(s1):S63–75. Available from: https://academic.oup.com/jid/article-lookup/doi/10.1086/518655

26. Mishra SK, Tripathi G, Kishore N, Singh RK, Singh A, Tiwari VK. Drug development against tuberculosis: Impact of alkaloids. Eur J Med Chem [Internet]. 2017; Available from: http://linkinghub.elsevier.com/retrieve/pii/S022352341730449X

27. Bahuguna A, Rawat DS. An overview of new antitubercular drugs, drug candidates, and their targets. Med Res Rev. 2019;(May).

28. Protopopova M, Hanrahan C, Nikonenko B, Samala R, Chen P, Gearhart J, et al. Identification of a new antitubercular drug candidate, SQ109, from a combinatorial library of 1,2-ethylenediamines. J Antimicrob Chemother. 2005;56(5):968–74.

29. Sacksteder KA, Protopopova M, Barry CE, Andries K, Nacy CA. Discovery and development of SQ109: a new antitubercular drug with a novel mechanism of action. Future Microbiol [Internet]. 2012 Jul;7(7):823–37. Available from: https://www.futuremedicine.com/doi/10.2217/fmb.12.56

30. Grzegorzewicz AE, Pham H, Gundi VAKB, Scherman MS, North EJ, Hess T, et al. Inhibition of mycolic acid transport across the *Mycobacterium tuberculosis* plasma membrane. Nat Chem Biol. 2012 Feb 19;8(4):334–41.

31. Tahlan K, Wilson R, Kastrinsky DB, Arora K, Nair V, Fischer E, et al. SQ109 targets MmpL3, a membrane transporter of trehalose monomycolate involved in mycolic acid donation to the cell wall core of *Mycobacterium tuberculosis*. Antimicrob Agents Chemother. 2012;56(4):1797–809.

32. Zhang B, Li J, Yang X, Wu L, Zhang J, Yang Y, et al. Crystal structures of membrane transporter MmpL3, an anti-tb drug target. Cell [Internet]. 2019 Jan;176(3):636-648.e13. Available from: https://linkinghub.elsevier.com/retrieve/pii/S0092867419300364

33. http://www.newtbdrugs.org/pipeline/clinical. http://www.newtbdrugs.org/pipeline/clinical. :1–9. Available from: http://www.newtbdrugs.org/pipeline/clinical

34. Colditz GA, Brewer TF, Berkey CS, Wilson ME, Burdick E, Fineberg H V, et al. Efficacy of BCG vaccine in the prevention of tuberculosis. Meta-analysis of the published literature. JAMA [Internet]. 1994 Mar 2;271(9):698–702. Available from: http://www.ncbi.nlm.nih.gov/pubmed/8309034

35. Abubakar I, Pimpin L, Ariti C, Beynon R, Mangtani P, Sterne J, et al. Systematic review and meta-analysis of the current evidence on the duration of protection by Bacillus Calmette–Guérin vaccination against tuberculosis. Heal Technol Assess [Internet]. 2013 Sep;17(37):1–4. Available from: https://www.journalslibrary.nihr.ac.uk/hta/hta17370/

36. Brewer TF. Preventing tuberculosis with Bacillus Calmette-Guerin vaccine: A meta-analysis of the literature. Clin Infect Dis [Internet]. 2000;31(Supplement 3):S64–7. Available from: https://academic.oup.com/cid/article-lookup/doi/10.1086/314072

37. Marinova D, Gonzalo-Asensio J, Aguilo N, Martin C. MTBVAC from discovery to clinical trials in tuberculosis-endemic countries. Expert Rev Vaccines [Internet]. 2017;16(6):14760584.2017.1324303. Available from: https://www.tandfonline.com/doi/full/10.1080/14760584.2017.1324303

38. Broset E, Martín C, Gonzalo-Asensio J. Evolutionary landscape of the *Mycobacterium tuberculosis* complex from the viewpoint of PhoPR: implications for virulence regulation and application to vaccine development. MBio [Internet]. 2015 Oct 20;6(5):e01289-15. Available from: http://www.ncbi.nlm.nih.gov/pubmed/26489860

39. Camacho LR, Ensergueix D, Perez E, Gicquel B, Guilhot C. Identification of a virulence gene cluster of *Mycobacterium tuberculosis* by signature-tagged transposon mutagenesis. Mol Microbiol [Internet]. 1999 Oct;34(2):257–67. Available from: http://www.ncbi.nlm.nih.gov/pubmed/10564470

40. Camacho LR, Constant P, Raynaud C, Lanéelle M-A, Triccas JA, Gicquel B, et al. Analysis of the phthiocerol dimycocerosate locus of *Mycobacterium tuberculosis*. J Biol Chem [Internet]. 2001 Jun 8;276(23):19845–54. Available from: http://www.jbc.org/lookup/doi/10.1074/jbc.M100662200

41. Cox JS, Chen B, McNeil M, Jacobs WR. Complex lipid determines tissue-specific replication of *Mycobacterium tuberculosis* in mice. Nature. 1999 Nov 4;402(6757):79–83.

42. Andersen P, Kaufmann SHE. Novel vaccination strategies against tuberculosis. Cold Spring Harb Perspect Med. 2014 Jun 1;4(6):a018523–a018523.

43. Borremans M, de Wit L, Volckaert G, Ooms J, de Bruyn J, Huygen K, et al. Cloning, sequence determination, and expression of a 32-kilodalton-protein gene of *Mycobacterium tuberculosis.* Infect Immun [Internet]. 1989 Oct;57(10):3123–30. Available from: http://www.ncbi.nlm.nih.gov/pubmed/2506131

44. Bassey EOE, Life PF, Catty D, Gaston JSH, Kumararatne DS. T-cell response to mycobacterial proteins: A comparative study of tuberculous and control immunoblots of *Mycobacterium tuberculosis* and *M. bovis* BCG. Tuber Lung Dis. 1996;77(2):146–53.

45. Coler RN, Skeiky Y a, Vedvick T, Bement T, Ovendale P, Campos-Neto A, et al. Molecular cloning and immunologic reactivity of a novel low molecular mass antigen of *Mycobacterium tuberculosis*. J Immunol [Internet]. 1998 Sep 1;161(5):2356–64. Available from: http://www.ncbi.nlm.nih.gov/pubmed/9725231

46. Dietrich J, Aagaard C, Leah R, Olsen AW, Stryhn A, Doherty TM, et al. Exchanging ESAT6 with TB10.4 in an Ag85B fusion molecule-based tuberculosis subunit vaccine: Efficient protection and ESAT6-based sensitive monitoring of vaccine efficacy. J Immunol [Internet]. 2005;174(10):6332–9. Available from: http://www.jimmunol.org/cgi/doi/10.4049/jimmunol.174.10.6332

47. Tameris MD, Hatherill M, Landry BS, Scriba TJ, Snowden MA, Lockhart S, et al. Safety and efficacy of MVA85A, a new tuberculosis vaccine, in infants previously vaccinated with BCG: A randomised, placebo-controlled phase 2b trial. Lancet [Internet]. 2013;381(9871):1021–8. Available from: http://dx.doi.org/10.1016/S0140-6736(13)60177-4

48. Ji Y, Sun J, Zhang L, Liu J, Z-h X, R-f S, et al. Immunogenicity and protective efficacy of a fusion protein tuberculosis vaccine combining five Esx family proteins. Artic Front Cell Infect Microbiol. 2017;7(7):2263389–226.

49. Jarlier V, Nikaido H. Mycobacterial cell wall: structure and role in natural resistance to antibiotics. FEMS Microbiol Lett. 1994;123:11–8.

50. Brennan PJ, Nikaido H. The envelope of mycobacteria. Annu Rev Biochem [Internet]. 1995;64(1):29–63. Available from: http://www.annualreviews.org/doi/10.1146/annurev.bi.64.070195.000333

51. Minnikin DE. Chemical principles in the organization of lipid components in the mycobacterial cell envelope. Res Microbiol [Internet]. 1991 Jan;142(4):423–7. Available from: http://linkinghub.elsevier.com/retrieve/pii/092325089190114P

52. Brennan PJ. Structure, function, and biogenesis of the cell wall of *Mycobacterium tuberculosis*. Tuberculosis. 2003;83(1–3):91–7.

53. Crick DC, Jackson M, Daffé M. Genetics of capsular polysaccharides and cell envelope (glyco)lipids. Microbiol Spectr. 2014 Aug 22;2(4):1–78.

54. Cole ST, Brosch R, Parkhill J, Garnier T, Churcher C, Harris D, et al. Deciphering the biology of *Mycobacterium tuberculosis* from the complete genome sequence. Nature. 1998;393(6685):537–44.

55. Jackson M. The mycobacterial cell envelope-lipids. Cold Spring Harb Perspect Med [Internet]. 2014 Aug 7;4(10):317–317. Available from: http://www.ncbi.nlm.nih.gov/pubmed/25104772

56. Nataraj V, Varela C, Javid A, Singh A, Besra GS, Bhatt A. Mycolic acids: deciphering and targeting the Achilles' heel of the tubercle bacillus. Mol Microbiol [Internet]. 2015;98(1):7–16. Available from: http://doi.wiley.com/10.1111/mmi.13101

57. Marrakchi H, Lanéelle MA, Daffé M. Mycolic acids: Structures, biosynthesis, and beyond. Chem Biol. 2014;21(1):67–85.

58. Barry CE, Lee RE, Mdluli K, Sampson AE, Schroeder BG, Slayden RA, et al. Mycolic acids: structure, biosynthesis and physiological functions. Prog Lipid Res [Internet]. 1998;37(2–3):143–79. Available from: http://www.ncbi.nlm.nih.gov/pubmed/9829124

59. Alderwick LJ, Harrison J, Lloyd GS, Birch HL. The mycobacterial cell wall—

Peptidoglycan and arabinogalactan. Cold Spring Harb Perspect Med [Internet]. 2015 Aug;5(8):a021113. Available from: http://perspectivesinmedicine.cshlp.org/lookup/doi/10.1101/cshperspect.a021113

60. Minnikin DE, Lee OY, Wu HHT, Nataraj V, Donoghue HD, Ridell M, et al. Pathophysiological implications of cell envelope structure in *Mycobacterium tuberculosis* and related taxa. In: Tuberculosis - Expanding Knowledge [Internet]. InTech; 2015. p. 145–75. Available from: http://www.intechopen.com/books/tuberculosis-expanding-knowledge/pathophysiological-implications-of-cell-envelope-structure-in-mycobacterium-tuberculosis-and-related%5Cnhttp://dx.doi.org/10.5772/59585

61. Takayama K, Wang C, Besra GS. Pathway to synthesis and processing of mycolic acids in *Mycobacterium tuberculosis* genetic analysis of synthesis and processing of mycolic acid. Society [Internet]. 2005;18(1):81–101. Available from: http://www.pubmedcentral.nih.gov/articlerender.fcgi?artid=544180&tool=pmcentrez&rendertype=abstract

62. Kruh NA, Borgaro JG, Ruzsicska BP, Xu H, Tonge PJ. A novel interaction linking the FAS-II and phthiocerol dimycocerosate (PDIM) biosynthetic pathways. J Biol Chem. 2008;283(46):31719–25.

63. Bhatt A, Molle V, Besra GS, Jacobs WR, Kremer L. The *Mycobacterium tuberculosis* FAS-II condensing enzymes: Their role in mycolic acid biosynthesis, acid-fastness, pathogenesis and in future drug development. Mol Microbiol [Internet]. 2007;64(6):1442–54. Available from: http://doi.wiley.com/10.1111/j.1365-2958.2007.05761.x

64. Bhatt A, Brown AK, Singh A, Minnikin DE, Besra GS. Loss of a mycobacterial gene encoding a reductase leads to an altered cell wall containing beta-oxo- mycolic acid analogs and accumulation of ketones. Chem Biol [Internet]. 2008;15(9):930–9. Available from: http://linkinghub.elsevier.com/retrieve/pii/S1074552108002731

65. Nataraj V. Identification and biochemical characterisation of genes involved in mycobacterial cell wall assembly. PhD thesis. 2014;

66. Varela C, Rittmann D, Singh A, Krumbach K, Bhatt K, Eggeling L, et al. *mmpL* genes are associated with mycolic acid metabolism in Mycobacteria and Corynebacteria. Chem Biol [Internet]. 2012 Apr;19(4):498–506. Available from: https://linkinghub.elsevier.com/retrieve/pii/S1074552112001056

67. Degiacomi G, Benjak A, Madacki J, Boldrin F, Provvedi R, Palù G, et al. Essentiality of *mmpL3* and impact of its silencing on *Mycobacterium tuberculosis* gene expression.

Sci Rep [Internet]. 2017;7(January):43495. Available from: http://www.nature.com/articles/srep43495

68. Li W, Obregon-Henao A, Wallach JB, North EJ, Lee RE, Gonzalez-Juarrero M, et al. Therapeutic potential of the *Mycobacterium tuberculosis* mycolic acid transporter, MmpL3. Antimicrob Agents Chemother. 2016;60(9):5198–207.

69. Belisle JT. Role of the Major antigen of *Mycobacterium tuberculosis* in cell wall biogenesis. Science (80-). 1997 May 30;276(5317):1420–2.

70. Jackson M, Raynaud C, Lanéelle MA, Guilhot C, Laurent-Winter C, Ensergueix D, et al. Inactivation of the *antigen 85C* gene profoundly affects the mycolate content and alters the permeability of the *Mycobacterium tuberculosis* cell envelope. Mol Microbiol. 1999;31(5):1573–87.

71. Puech V, Bayan N, Salim K, Leblon G, Daffé M. Characterization of the *in vivo* accepters of the mycoloyl residues transferred by the corynebacterial PS1 and the related mycobacterial Antigens 85. Mol Microbiol. 2000;35(5):1026–41.

72. Sathyamoorthy N, Takayama K. Purification and characterization of a novel mycolic acid exchange enzyme from *Mycobacterium smegmatis*. J Biol Chem [Internet]. 1987 Oct 5;262(28):13417–23. Available from: http://www.ncbi.nlm.nih.gov/pubmed/3654621

73. Matsunaga I, Naka T, Talekar RS, Mcconnell MJ, Katoh K, Nakao H, et al. Mycolyltransferase-mediated glycolipid exchange in Mycobacteria *. 2008;283(43):28835–41.

74. Harth G, Horwitz MA, Tabatadze D, Zamecnik PC. Targeting the *Mycobacterium tuberculosis* 30/32-kDa mycolyl transferase complex as a therapeutic strategy against tuberculosis: Proof of principle by using antisense technology. Proc Natl Acad Sci U S A [Internet]. 2002;99(24):15614–9. Available from: http://www.ncbi.nlm.nih.gov/pubmed/12427974%5Cnhttp://www.pubmedcentral.nih.gov/articlerender.fcgi?artid=PMC137765

75. Dubey VS, Sirakova TD, Cynamon MH, Kolattukudy PE. Biochemical function of *msl5* (*pks8* plus *pks17*) in *Mycobacterium tuberculosis* H37Rv: Biosynthesis of monomethyl branched unsaturated fatty acids. J Bacteriol. 2003 Aug 1;185(15):4620–5.

76. Nataraj V, Pang P, Haslam SM, Veerapen N, Minnikin DE, Dell A, et al. MKAN27435 is required for the biosynthesis of higher subclasses of lipooligosaccharides in *Mycobacterium kansasii*. PLoS One [Internet]. 2015;10(4):e0122804. Available from:

http://dx.plos.org/10.1371/journal.pone.0122804

77. Daffé M, Lacave C, Lanéelle MA, Gillois M, Lanéelle G. Polyphthienoyl trehalose, glycolipids specific for virulent strains of the tubercle bacillus. Eur J Biochem [Internet]. 1988 Mar 15;172(3):579–84. Available from: http://www.ncbi.nlm.nih.gov/pubmed/3127210

78. Ariza MA, Martin-Luengo F, Valero-Guillen PL. A family of diacyltrehaloses isolated from *Mycobacterium fortuitum*. Microbiology. 1994 Aug 1;140(8):1989–94.

79. Muñoz M, Lanéelle MA, Luquin M, Torrelles J, Julián E, Ausina V, et al. Occurrence of an antigenic triacyl trehalose in clinical isolates and reference strains of *Mycobacterium tuberculosis*. FEMS Microbiol Lett [Internet]. 1997 Dec 15;157(2):251–9. Available from: http://doi.wiley.com/10.1016/S0378-1097(97)00483-7

80. Minnikin DE, Kremer L, Dover LG, Besra GS. The methyl-branched fortifications of *Mycobacterium tuberculosis*. Chem Biol [Internet]. 2002 May;9(5):545–53. Available from: https://linkinghub.elsevier.com/retrieve/pii/S1074552102001424

81. Gautier N, López Marín LM, Lanéelle M a, Daffé M. Structure of mycoside F, a family of trehalose-containing glycolipids of *Mycobacterium fortuitum*. FEMS Microbiol Lett [Internet]. 1992 Nov 1;77(1–3):81–7. Available from: http://www.ncbi.nlm.nih.gov/pubmed/1459422

82. Belardinelli JM, Larrouy-Maumus G, Jones V, Sorio de Carvalho LP, McNeil MR, Jackson M. Biosynthesis and translocation of unsulfated acyltrehaloses in *Mycobacterium tuberculosis*. J Biol Chem [Internet]. 2014 Oct 3;289(40):27952–65. Available from: http://www.jbc.org/lookup/doi/10.1074/jbc.M114.581199

83. Dubey VS, Sirakova TD, Kolattukudy PE. Disruption of *msl3* abolishes the synthesis of mycolipanoic and mycolipenic acids required for polyacyltrehalose synthesis in *Mycobacterium tuberculosis* H37Rv and causes cell aggregation. Mol Microbiol. 2002;45(5):1451–9.

84. Hatzios SK, Schelle MW, Holsclaw CM, Behrens CR, Botyanszki Z, Lin F, et al. PapA3 is an acyltransferase required for polyacyltrehalose biosynthesis in *Mycobacterium tuberculosis*. J Biol Chem. 2009;284(19):12745–51.

85. Touchette MH, Holsclaw CM, Previti ML, Solomon VC, Leary JA, Bertozzi CR, et al. The *rv1184c* locus encodes Chp2, an acyltransferase in *Mycobacterium tuberculosis* polyacyltrehalose lipid biosynthesis. J Bacteriol. 2015;197(1):201–10.

86. Goren MB. Mycobacterial fatty acid esters of sugars and sulfosugars. In: Kates M, editor. Glycolipids, Phosphoglycolipids, and Sulfoglycolipids [Internet]. Boston, MA: Springer US; 1990. p. 363–461. Available from: https://doi.org/10.1007/978-1-4899-2516-9_5

87. Mougous JD, Petzold CJ, Senaratne RH, Lee DH, Akey DL, Lin FL, et al. Identification, function and structure of the mycobacterial sulfotransferase that initiates sulfolipid-1 biosynthesis. Nat Struct Mol Biol [Internet]. 2004;11(8):721–9. Available from: http://www.nature.com/doifinder/10.1038/nsmb802

88. Bhatt K, Gurcha SS, Bhatt A, Besra GS, Jacobs WR. Two polyketide-synthase-associated acyltransferases are required for sulfolipid biosynthesis in *Mycobacterium tuberculosis*. Microbiology. 2007;153(2):513–20.

89. Kumar P, Schelle MW, Jain M, Lin FL, Petzold CJ, Leavell MD, et al. PapA1 and PapA2 are acyltransferases essential for the biosynthesis of the *Mycobacterium tuberculosis* virulence factor sulfolipid-1. Proc Natl Acad Sci U S A [Internet]. 2007 Jul 3 [cited 2017 May 25];104(27):11221–6. Available from: http://www.ncbi.nlm.nih.gov/pubmed/17592143

90. Lynett J, Stokes RW. Selection of transposon mutants of *Mycobacterium tuberculosis* with increased macrophage infectivity identifies *fadD23* to be involved in sulfolipid production and association with macrophages. Microbiology. 2007;153(9):3133–40.

91. Sirakova TD, Thirumala AK, Dubey VS, Sprecher H, Kolattukudy PE. The *Mycobacterium tuberculosis pks2* gene encodes the synthase for the hepta- and octa-methyl-branched fatty acids required for sulfolipid synthesis. J Biol Chem [Internet]. 2001;276(20):16833–9. Available from: http://www.ncbi.nlm.nih.gov/pubmed/11278910

92. Seeliger JC, Holsclaw CM, Schelle MW, Botyanszki Z, Gilmore S a., Tully SE, et al. Elucidation and chemical modulation of sulfolipid-1 biosynthesis in *Mycobacterium tuberculosis*. J Biol Chem. 2012;287(11):7990–8000.

93. Hunter SW, Murphy RC, Clay K, Goren MB, Brennan PJ. Trehalose-containing lipooligosaccharides. A new class of species-specific antigens from *Mycobacterium*. J Biol Chem [Internet]. 1983 Sep 10;258(17):10481–7. Available from: http://www.ncbi.nlm.nih.gov/pubmed/6411715

94. Hunter SW, Jardine I, Yanagihara DL, Brennan PJ. Trehalose-containing lipooligosaccharides from Mycobacteria: Structures of the oligosaccharide segments and recognition of a unique N-acylkanosamine-containing epitope. Biochemistry. 1985;24(11):2798–805.

95. Daffe M, McNeil M, Brennan PJ. Novel type-specific lipooligosaccharides from *Mycobacterium tuberculosis*. Biochemistry [Internet]. 1991 Jan 15;30(2):378–88. Available from: http://www.ncbi.nlm.nih.gov/pubmed/1899023

96. McNeil M, Tsang AY, McClatchy JK, Stewart C, Jardine I, Brennan PJ. Definition of the surface antigens of *Mycobacterium malmoense* and use in studying the etiology of a form of mycobacteriosis. J Bacteriol [Internet]. 1987 Jul;169(7):3312–20. Available from: http://www.ncbi.nlm.nih.gov/pubmed/3597323

97. Minnikin DE, Ridell M, Wallerström G, Besra GS, Parlett JH, Bolton RC, et al. Comparative studies of antigenic glycolipids of Mycobacteria related to the leprosy bacillus. Acta Leprol [Internet]. 1989;7 Suppl 1:51–4. Available from: http://www.ncbi.nlm.nih.gov/pubmed/2504005

98. Saadat S, Ballou CE. Pyruvylated glycolipids from *Mycobacterium smegmatis*. Structures of two oligosaccharide components. J Biol Chem [Internet]. 1983 Feb 10;258(3):1813–8. Available from: http://www.ncbi.nlm.nih.gov/pubmed/6822534

99. Kamisango K, Saadat S, Dell A, Ballou CE. Pyruvylated glycolipids from *Mycobacterium smegmatis*. Nature and location of the lipid components. J Biol Chem [Internet]. 1985 Apr 10;260(7):4117–21. Available from: http://www.ncbi.nlm.nih.gov/pubmed/3980471

100. Gilleron M, Vercauteren J, Puzo G. Lipooligosaccharidic antigen containing a novel C4-branched 3,6-dideoxy-alpha-hexopyranose typifies *Mycobacterium gastri*. J Biol Chem [Internet]. 1993 Feb 15;268(5):3168–79. Available from: http://www.ncbi.nlm.nih.gov/pubmed/8428994

101. Hunter SW, Fujiwara T, Murphy RC, Brennan PJ. N-acylkansosamine. A novel N-acylamino sugar from the trehalose-containing lipooligosaccharide antigens of *Mycobacterium kansasii*. J Biol Chem [Internet]. 1984 Aug 10;259(15):9729–34. Available from: http://www.ncbi.nlm.nih.gov/pubmed/6547719

102. Ren H, Dover LG, Islam ST, Alexander DC, Chen JM, Besra GS, et al. Identification of the lipooligosaccharide biosynthetic gene cluster from *Mycobacterium marinum*. Mol Microbiol. 2007;63(5):1345–59.

103. Trivedi OA, Arora P, Sridharan V, Tickoo R, Mohanty D, Gokhale RS. Enzymic activation and transfer of fatty acids as acyl-adenylates in Mycobacteria. Nature [Internet]. 2004 Mar 25;428(6981):441–5. Available from: http://www.ncbi.nlm.nih.gov/entrez/query.fcgi?cmd=Retrieve&db=PubMed&dopt=Citation&list_uids=15042094%5Cnhttp://www.nature.com/nature/journal/v428/n6981/pdf/nature02384.pdf

104. Gokhale RS, Saxena P, Chopra T, Mohanty D. Versatile polyketide enzymatic machinery for the biosynthesis of complex mycobacterial lipids. Nat Prod Rep [Internet]. 2007 Apr;24(2):267–77. Available from: http://www.ncbi.nlm.nih.gov/pubmed/17389997

105. Etienne G, Malaga W, Laval F, Lemassu A, Guilhot C, Daffe M. Identification of the polyketide synthase involved in the biosynthesis of the surface-exposed lipooligosaccharides in Mycobacteria. J Bacteriol [Internet]. 2009 Apr 15;191(8):2613–21. Available from: http://jb.asm.org/cgi/doi/10.1128/JB.01235-08

106. Rombouts Y, Alibaud L, Carrère-Kremer S, Maes E, Tokarski C, Elass E, et al. Fatty acyl chains of *Mycobacterium marinum* lipooligosaccharides: Structure, localization and acylation by PapA4 (MMAR-2343) protein. J Biol Chem. 2011;286(38):33678–88.

107. Daffé M, Laneelle M a. Distribution of phthiocerol diester, phenolic mycosides and related compounds in Mycobacteria. J Gen Microbiol [Internet]. 1988 Jul;134(7):2049–55. Available from: http://www.ncbi.nlm.nih.gov/pubmed/3149973

108. Azad AK, Sirakova TD, Fernandes ND, Kolattukudy PE. Gene knockout reveals a novel gene cluster for the synthesis of a class of cell wall lipids unique to pathogenic Mycobacteria. J Biol Chem [Internet]. 1997 Jul 4;272(27):16741–5. Available from: http://www.jbc.org/lookup/doi/10.1074/jbc.272.27.16741

109. Mathur M, Kolattukudy PE. Molecular cloning and sequencing of the gene for mycocerosic acid synthase, a novel fatty acid elongating multifunctional enzyme, from *Mycobacterium tuberculosis var. bovis* Bacillus Calmette-Guerin. J Biol Chem [Internet]. 1992 Sep 25;267(27):19388–95. Available from: http://www.ncbi.nlm.nih.gov/pubmed/1527058

110. Rainwater DL, Kolattukudy PE. Fatty acid biosynthesis in *Mycobacterium tuberculosis var. bovis* Bacillus Calmette-Guérin. Purification and characterization of a novel fatty acid synthase, mycocerosic acid synthase, which elongates n-fatty acyl-CoA with methylmalonyl-CoA. J Biol Chem [Internet]. 1985 Jan 10;260(1):616–23. Available from: http://www.ncbi.nlm.nih.gov/pubmed/3880746

111. Pérez E, Constant P, Laval F, Lemassu A, Lanéelle M-A, Daffé M, et al. Molecular dissection of the role of two methyltransferases in the biosynthesis of phenolglycolipids and phthiocerol dimycoserosate in the *Mycobacterium tuberculosis* complex. J Biol Chem [Internet]. 2004 Oct 8;279(41):42584–92. Available from: http://www.jbc.org/lookup/doi/10.1074/jbc.M406134200

112. Onwueme KC, Ferreras JA, Buglino J, Lima CD, Quadri LEN. Mycobacterial polyketide-associated proteins are acyltransferases: Proof of principle with

Mycobacterium tuberculosis PapA5. Proc Natl Acad Sci [Internet]. 2004 Mar 30;101(13):4608–13. Available from: http://www.pnas.org/cgi/doi/10.1073/pnas.0306928101

113. Onwueme KC, Vos CJ, Zurita J, Soll CE, Quadri LEN. Identification of phthiodiolone ketoreductase, an enzyme required for production of mycobacterial diacyl phthiocerol virulence factors. J Bacteriol [Internet]. 2005 Jul 15;187(14):4760–6. Available from: http://jb.asm.org/cgi/doi/10.1128/JB.187.14.4760-4766.2005

114. Siméone R, Constant P, Malaga W, Guilhot C, Daffé M, Chalut C. Molecular dissection of the biosynthetic relationship between phthiocerol and phthiodiolone dimycocerosates and their critical role in the virulence and permeability of *Mycobacterium tuberculosis*. FEBS J [Internet]. 2007 Apr;274(8):1957–69. Available from: http://doi.wiley.com/10.1111/j.1742-4658.2007.05740.x

115. Purwantini E, Daniels L, Mukhopadhyay B. F420H2 is required for phthiocerol dimycocerosate synthesis in Mycobacteria. Henkin TM, editor. J Bacteriol. 2016 Aug 1;198(15):2020–8.

116. Touchette MH, Bommineni GR, Delle Bovi RJ, Gadbery JE, Nicora CD, Shukla AK, et al. Diacyltransferase activity and chain length specificity of *Mycobacterium tuberculosis* PapA5 in the synthesis of alkyl beta-diol lipids. Biochemistry. 2015;54(35):5457–68.

117. Constant P, Perez E, Malaga W, Lanéelle M-A, Saurel O, Daffé M, et al. Role of the *pks15/1* gene in the biosynthesis of phenolglycolipids in the *Mycobacterium tuberculosis* complex. J Biol Chem [Internet]. 2002 Oct 11;277(41):38148–58. Available from: http://www.jbc.org/lookup/doi/10.1074/jbc.M206538200

118. Huet G, Constant P, Malaga W, Lane M, Kremer K, Soolingen D Van, et al. A lipid profile typifies the beijing strains of *Mycobacterium tuberculosis*. 2009;284(40):27101–13.

119. Stadthagen G, Korduláková J, Griffin R, Constant P, Bottová I, Barilone N, et al. p - Hydroxybenzoic acid synthesis in *Mycobacterium tuberculosis*. J Biol Chem [Internet]. 2005 Dec 9;280(49):40699–706. Available from: http://www.jbc.org/lookup/doi/10.1074/jbc.M508332200

120. Vergnolle O, Chavadi SS, Edupuganti UR, Mohandas P, Chan C, Zeng J, et al. Biosynthesis of cell envelope-associated phenolic glycolipids in *Mycobacterium marinum*. O'Toole GA, editor. J Bacteriol [Internet]. 2015 Mar 15;197(6):1040–50. Available from: http://jb.asm.org/lookup/doi/10.1128/JB.02546-14

121. Yu J, Tran V, Li M, Huang X, Niu C, Wang D, et al. Both phthiocerol dimycocerosates and phenolic glycolipids are required for virulence of *Mycobacterium marinum*. Flynn JL, editor. Infect Immun [Internet]. 2012 Apr;80(4):1381–9. Available from: http://iai.asm.org/lookup/doi/10.1128/IAI.06370-11

122. Ferreras JA, Stirrett KL, Lu X, Ryu J-S, Soll CE, Tan DS, et al. Mycobacterial phenolic glycolipid virulence factor biosynthesis: mechanism and small-molecule inhibition of polyketide chain initiation. Chem Biol [Internet]. 2008 Jan;15(1):51–61. Available from: http://linkinghub.elsevier.com/retrieve/pii/S0167945708000213

123. He W, Soll CE, Chavadi SS, Zhang G, Warren JD, Quadri LEN. Cooperation between a coenzyme A-independent stand-alone initiation module and an iterative type I polyketide synthase during synthesis of mycobacterial phenolic glycolipids. J Am Chem Soc. 2009;131(46):16744–50.

124. Siméone R, Léger M, Constant P, Malaga W, Marrakchi H, Daffé M, et al. Delineation of the roles of FadD22, FadD26 and FadD29 in the biosynthesis of phthiocerol dimycocerosates and related compounds in *Mycobacterium tuberculosis*. FEBS J. 2010;277(12):2715–25.

125. Alibaud L, Rombouts Y, Trivelli X, Burguière A, Cirillo SLG, Cirillo JD, et al. A *Mycobacterium marinum tesA* mutant defective for major cell wall-associated lipids is highly attenuated in *Dictyostelium discoideum* and zebrafish embryos. Mol Microbiol. 2011;80(4):919–34.

126. Reed MB, Domenech P, Manca C, Su H, Barczak AK, Kreiswirth BN, et al. A glycolipid of hypervirulent tuberculosis strains that inhibits the innate immune response. Nature. 2004;431(7004):84–7.

127. Pérez E, Constant P, Lemassu A, Laval F, Daffé M, Guilhot C. Characterization of three glycosyltransferases involved in the biosynthesis of the phenolic glycolipid antigens from the *Mycobacterium tuberculosis* complex. J Biol Chem [Internet]. 2004 Oct 8;279(41):42574–83. Available from: http://www.jbc.org/lookup/doi/10.1074/jbc.M406246200

128. Simeone R, Huet G, Constant P, Malaga W, Lemassu A, Laval F, et al. Functional characterisation of three O-methyltransferases involved in the biosynthesis of phenolglycolipids in *Mycobacterium tuberculosis*. Skurnik M, editor. PLoS One [Internet]. 2013 Mar 11;8(3):e58954. Available from: http://dx.plos.org/10.1371/journal.pone.0058954

129. Jackson M, Crick DC, Brennan PJ. Phosphatidylinositol is an essential phospholipid of Mycobacteria. J Biol Chem. 2000;275(39):30092–9.

130. Chatterjee D, Khoo K-H. Mycobacterial lipoarabinomannan: An extraordinary lipoheteroglycan with profound physiological effects. Glycobiology [Internet]. 1998 Feb 1;8(2):113–20. Available from: https://academic.oup.com/glycob/article-lookup/doi/10.1093/glycob/8.2.113

131. Astarie-Dequeker C, Nigou J, Passemar C, Guilhot C. The role of mycobacterial lipids in host pathogenesis. Drug Discov Today Dis Mech [Internet]. 2010;7(1):e33–41. Available from: http://linkinghub.elsevier.com/retrieve/pii/S1740676510000246

132. Passemar C, Arbués A, Malaga W, Mercier I, Moreau F, Lepourry L, et al. Multiple deletions in the polyketide synthase gene repertoire of *Mycobacterium tuberculosis* reveal functional overlap of cell envelope lipids in host-pathogen interactions. Cell Microbiol. 2014;16(2):195–213.

133. Hunter RL, Armitige L, Jagannath C, Actor JK. TB research at UT-Houston--a review of cord factor: new approaches to drugs, vaccines and the pathogenesis of tuberculosis. Tuberculosis (Edinb) [Internet]. 2009;89 Suppl 1(0 1):S18-25. Available from: http://www.pubmedcentral.nih.gov/articlerender.fcgi?artid=3682682&tool=pmcentrez&rendertype=abstract

134. Ojha AK, Trivelli X, Guerardel Y, Kremer L, Hatfull GF. Enzymatic hydrolysis of trehalose dimycolate releases free mycolic acids during mycobacterial growth in biofilms. J Biol Chem. 2010;285(23):17380–9.

135. Rousseau C, Neyrolles O, Bordat Y, Giroux S, Sirakova TD, Prevost MC, et al. Deficiency in mycolipenate- and mycosanoate-derived acyltrehaloses enhances early interactions of *Mycobacterium tuberculosis* with host cells. Cell Microbiol. 2003;5(6):405–15.

136. Cambier CJ, Takaki KK, Larson RP, Hernandez RE, Tobin DM, Urdahl KB, et al. Mycobacteria manipulate macrophage recruitment through coordinated use of membrane lipids. Nature [Internet]. 2014 Jan 15;505(7482):218–22. Available from: http://www.nature.com/articles/nature12799

137. Cardona PJ, Soto CY, Martín C, Giquel B, Agustí G, Guirado E, et al. Neutral-red reaction is related to virulence and cell wall methyl-branched lipids in *Mycobacterium tuberculosis*. Microbes Infect. 2006;8(1):183–90.

138. Jankute M, Nataraj V, Lee OY-C, Wu HHT, Ridell M, Garton NJ, et al. The role of hydrophobicity in tuberculosis evolution and pathogenicity. Sci Rep [Internet]. 2017 Dec 2;7(1):1315. Available from: http://www.nature.com/articles/s41598-017-01501-0

139. Ryll R, Kumazawa Y, Yano I. Immunological properties of trehalose dimycolate (cord factor) and other mycolic acid-containing glycolipids--a review. Microbiol Immunol [Internet]. 2001;45(12):801–11. Available from: http://www.ncbi.nlm.nih.gov/pubmed/11838897

140. Moody DB, Guy MR, Grant E, Cheng T-Y, Brenner MB, Besra GS, et al. Cd1b-Mediated T cell recognition of a glycolipid antigen generated from mycobacterial lipid and host carbohydrate during infection. J Exp Med [Internet]. 2000;192(7):965–76. Available from: http://www.jem.org/lookup/doi/10.1084/jem.192.7.965

141. Moody DB, Porcelli SA. Intracellular pathways of CD1 antigen presentation. Nat Rev Immunol [Internet]. 2003;3(1):11–22. Available from: http://www.nature.com/doifinder/10.1038/nri979

142. Moody DB, Reinhold BB, Guy MR, Beckman EM, Frederique DE, Furlong ST, et al. Structural requirements for glycolipid antigen recognition by CD1b-restricted T cells. Science [Internet]. 1997 Oct 10;278(5336):283–6. Available from: http://www.ncbi.nlm.nih.gov/pubmed/9323206

143. Fischer K, Scotet E, Niemeyer M, Koebernick H, Zerrahn J, Maillet S, et al. Mycobacterial phosphatidylinositol mannoside is a natural antigen for CD1d-restricted T cells. Proc Natl Acad Sci U S A. 2004;101(29):10685–90.

144. Neyrolles O, Guilhot C. Recent advances in deciphering the contribution of *Mycobacterium tuberculosis* lipids to pathogenesis. Tuberculosis [Internet]. 2011 May;91(3):187–95. Available from: http://linkinghub.elsevier.com/retrieve/pii/S1472979211000163

145. Kim MJ, Wainwright HC, Locketz M, Bekker LG, Walther GB, Dittrich C, et al. Caseation of human tuberculosis granulomas correlates with elevated host lipid metabolism. EMBO Mol Med. 2010;2(7):258–74.

146. Daniel J, Maamar H, Deb C, Sirakova TD, Kolattukudy PE. *Mycobacterium tuberculosis* uses host triacylglycerol to accumulate lipid droplets and acquires a dormancy-like phenotype in lipid-loaded macrophages. PLoS Pathog. 2011;7(6).

147. Daniel J, Sirakova T, Kolattukudy P. An Acyl-CoA synthetase in *Mycobacterium tuberculosis* involved in triacylglycerol accumulation during dormancy. PLoS One. 2014;9(12):1–21.

148. Garton NJ, Adegbola RA, Minnikin DE, Barer MR, Christensen H. Intracellular lipophilic inclusions of Mycobacteria *in vitro* and in sputum. Microbiology [Internet].

2002 Oct 1;148(10):2951–8. Available from: https://www.microbiologyresearch.org/content/journal/micro/10.1099/00221287-148-10-2951

149. Sakamoto K, Kim MJ, Rhoades ER, Allavena RE, Ehrt S, Wainwright HC, et al. Mycobacterial trehalose dimycolate reprograms macrophage global gene expression and activates matrix metalloproteinases. Infect Immun. 2013;81(3):764–76.

150. Krishna S, Ray A, Dubey SK, Larrouy-Maumus G, Chalut C, Castanier R, et al. Lipoglycans contribute to innate immune detection of Mycobacteria. PLoS One. 2011;6(12).

151. Schaefer M, Reiling N, Fessler C, Stephani J, Taniuchi I, Hatam F, et al. Decreased pathology and prolonged survival of human DC-SIGN transgenic mice during mycobacterial infection. J Immunol. 2008;180(10):6836–45.

152. Astarie-Dequeker C, Le Guyader L, Malaga W, Seaphanh F-K, Chalut C, Lopez A, et al. Phthiocerol dimycocerosates of *M. tuberculosis* participate in macrophage invasion by inducing changes in the organization of plasma membrane lipids. Flynn JL, editor. PLoS Pathog. 2009 Feb 6;5(2):e1000289.

153. Goren MB, Hart PD, Young MR, Armstrong JA. Prevention of phagosome-lysosome fusion in cultured macrophages by sulfatides of *Mycobacterium tuberculosis*. Proc Natl Acad Sci U S A [Internet]. 1976;73(7):2510–4. Available from: http://www.jstor.org/stable/65803

154. Pabst MJ, Gross JM, Brozna JP, Goren MB. Inhibition of macrophage priming by sulfatide from *Mycobacterium tuberculosis*. J Immunol [Internet]. 1988 Jan 15;140(2):634–40. Available from: http://www.ncbi.nlm.nih.gov/pubmed/2826597

155. Zhang L, Goren MB, Holzer TJ, Andersen BR. Effect of *Mycobacterium tuberculosis*-derived sulfolipid I on human phagocytic cells. Infect Immun. 1988;56(11):2876–83.

156. Converse SE, Mougous JD, Leavell MD, Leary J a, Bertozzi CR, Cox JS. MmpL8 is required for sulfolipid-1 biosynthesis and *Mycobacterium tuberculosis* virulence. Proc Natl Acad Sci U S A [Internet]. 2003 May 13;100(10):6121–6. Available from: http://www.ncbi.nlm.nih.gov/pubmed/12724526

157. Domenech P, Reed MB, Dowd CS, Manca C, Kaplan G, Barry CE. The role of MmpL8 in sulfatide biogenesis and virulence of *Mycobacterium tuberculosis*. J Biol Chem. 2004;279(20):21257–65.

158. Rousseau C, Turner OC, Rush E, Bordat Y, Sirakova TD, Kolattukudy PE, et al. Sulfolipid deficiency does not affect the virulence of *Mycobacterium tuberculosis* H37Rv in mice and guinea pigs sulfolipid deficiency does not affect the virulence of *Mycobacterium tuberculosis* H37Rv in Mice and Guinea Pigs. Infect Immun. 2003;71(8):4684.

159. Gilmore SA, Schelle MW, Holsclaw CM, Leigh CD, Jain M, Cox JS, et al. Sulfolipid-1 biosynthesis restricts *Mycobacterium tuberculosis* growth in human macrophages. ACS Chem Biol. 2012;7(5):863–70.

160. Saavedra R, Segura E, Leyva R, LA. Mycobacterial di-O-acyl-trehalose inhibits mitogen-and antigen-induced proliferation of murine T cells *in vitro*. Clin Vaccine [Internet]. 2001;8(6):1081–8. Available from: http://cvi.asm.org/cgi/content/abstract/8/6/1081

161. Lee K-S, Dubey VS, Kolattukudy PE, Song C-H, Shin A-R, Jung S-B, et al. Diacyltrehalose of *Mycobacterium tuberculosis* inhibits lipopolysaccharide- and mycobacteria-induced proinflammatory cytokine production in human monocytic cells. FEMS Microbiol Lett [Internet]. 2007 Feb;267(1):121–8. Available from: http://www.ncbi.nlm.nih.gov/pubmed/17156119

162. Espinosa-Cueto P, Escalera-Zamudio M, Magallanes-Puebla A, López-Marín LM, Segura-Salinas E, Mancilla R. Mycobacterial glycolipids di-O-acylated trehalose and tri-O-acylated trehalose downregulate inducible nitric oxide synthase and nitric oxide production in macrophages. BMC Immunol [Internet]. 2015;16(1):38. Available from: http://www.biomedcentral.com/1471-2172/16/38

163. Rousseau C, Winter N, Privert E, Bordat Y, Neyrolles O, Avé P, et al. Production of phthiocerol dimycocerosates protects *Mycobacterium tuberculosis* from the cidal activity of reactive nitrogen intermediates produced by macrophages and modulates the early immune response to infection. Cell Microbiol. 2004;6(3):277–87.

164. Kirksey MA, Tischler AD, Siméone R, Hisert KB, Uplekar S, Guilhot C, et al. Spontaneous phthiocerol dimycocerosate-deficient variants of *Mycobacterium tuberculosis* are susceptible to gamma interferon-mediated immunity. Infect Immun. 2011;79(7):2829–38.

165. Augenstreich J, Arbues A, Simeone R, Haanappel E, Wegener A, Sayes F, et al. ESX-1 and phthiocerol dimycocerosates of *Mycobacterium tuberculosis* act in concert to cause phagosomal rupture and host cell apoptosis. Cell Microbiol [Internet]. 2017 Jul;19(7):e12726. Available from: http://doi.wiley.com/10.1111/cmi.12726

166. Hughitt JQ, Keith V, Velikovsky CA, Mariuzza RA, C, Najib M. El-Sayed VB. The cell

wall lipid PDIM contributes to phagosomal escape and host cell exit of *Mycobacterium tuberculosis*. MBio. 2017;8(2):1–12.

167. Oldenburg R, Mayau V, Prandi J, Arbues A, Astarie-Dequeker C, Guilhot C, et al. Mycobacterial phenolic glycolipids selectively disable TRIF-dependent TLR4 signaling in macrophages. Front Immunol. 2018;9(JAN):1–12.

168. Chan J, Fujiwara T, Brennan P, McNeil M, Turco SJ, Sibille JC, et al. Microbial glycolipids: possible virulence factors that scavenge oxygen radicals. Proc Natl Acad Sci U S A. 1989;86(7):2453–7.

169. Stadthagen G, Jackson M, Charles P, Boudou F, Barilone N, Huerre M, et al. Comparative investigation of the pathogenicity of three *Mycobacterium tuberculosis* mutants defective in the synthesis of p-hydroxybenzoic acid derivatives. Microbes Infect [Internet]. 2006 Jul;8(8):2245–53. Available from: http://www.ncbi.nlm.nih.gov/pubmed/16782391

170. van der Woude AD, Sarkar D, Bhatt A, Sparrius M, Raadsen SA, Boon L, et al. Unexpected link between lipooligosaccharide biosynthesis and surface protein release in *Mycobacterium marinum*. J Biol Chem [Internet]. 2012 Jun 8;287(24):20417–29. Available from: http://www.jbc.org/lookup/doi/10.1074/jbc.M111.336461

171. Alibaud L, Pawelczyk J, Gannoun-Zaki L, Singh VK, Rombouts Y, Drancourt M, et al. Increased phagocytosis of *Mycobacterium marinum* mutants defective in lipooligosaccharide production a structure-activity relationship study. J Biol Chem. 2014;289(1):215–28.

172. Singh A, Crossman DK, Mai D, Guidry L, Voskuil MI, Renfrow MB, et al. *Mycobacterium tuberculosis* WhiB3 maintains redox homeostasis by regulating virulence lipid anabolism to modulate macrophage response. PLoS Pathog. 2009;5(8).

173. Lee W, VanderVen BC, Fahey RJ, Russell DG. Intracellular *Mycobacterium tuberculosis* exploits host-derived fatty acids to limit metabolic stress. J Biol Chem. 2013;288(10):6788–800.

174. Domenech P, Reed MB, Barry CE. Contribution of the *Mycobacterium tuberculosis* MmpL protein family to virulence and drug resistance. Infect Immun [Internet]. 2005 Jun;73(6):3492–501. Available from: http://www.ncbi.nlm.nih.gov/pubmed/15908378

175. Chalut C. MmpL transporter-mediated export of cell-wall associated lipids and siderophores in Mycobacteria. Tuberculosis (Edinb) [Internet]. 2016;100:32–45. Available from: http://www.ncbi.nlm.nih.gov/pubmed/27553408

176. Viljoen A, Dubois V, Girard-Misguich F, Blaise M, Herrmann J-L, Kremer L. The diverse family of MmpL transporters in Mycobacteria: from regulation to antimicrobial developments. Mol Microbiol [Internet]. 2017 Jun;104(6):889–904. Available from: http://www.ncbi.nlm.nih.gov/pubmed/28340510

177. Bailo R, Bhatt A, Aínsa J a. Lipid transport in *Mycobacterium tuberculosis* and its implications in virulence and drug development. Biochem Pharmacol [Internet]. 2015;96(3):159–67. Available from: http://linkinghub.elsevier.com/retrieve/pii/S0006295215002476

178. Cole ST. Micro Commentary Mechanistic insight into mycobacterial MmpL protein function. 2016;99(January):831–4.

179. Melly G, Purdy G. MmpL Proteins in Physiology and Pathogenesis of *M. tuberculosis*. Microorganisms [Internet]. 2019;7(3):70. Available from: https://www.mdpi.com/2076-2607/7/3/70

180. Székely R, Cole ST. Mechanistic insight into mycobacterial MmpL protein function. Mol Microbiol [Internet]. 2016 Mar;99(5):831–4. Available from: http://doi.wiley.com/10.1111/mmi.13306

181. Lamichhane G, Tyagi S, Bishai WR. Designer arrays for defined mutant analysis to detect genes essential for survival of *Mycobacterium tuberculosis* in mouse lungs. Society. 2005;73(4):2533–40.

182. Touchette MH, Seeliger JC. Transport of outer membrane lipids in Mycobacteria. Biochim Biophys Acta - Mol Cell Biol Lipids [Internet]. 2017 Jan [cited 2017 Jun 5]; Available from: http://linkinghub.elsevier.com/retrieve/pii/S1388198117300112

183. Su C-C, Klenotic PA, Bolla JR, Purdy GE, Robinson C V., Yu EW. MmpL3 is a lipid transporter that binds trehalose monomycolate and phosphatidylethanolamine. Proc Natl Acad Sci [Internet]. 2019;116(23):201901346. Available from: http://www.pnas.org/lookup/doi/10.1073/pnas.1901346116

184. Yamaryo-Botte Y, Rainczuk AK, Lea-Smith DJ, Brammananth R, van der Peet PL, Meikle P, et al. Acetylation of trehalose mycolates is required for efficient MmpL-mediated membrane transport in *Corynebacterineae*. ACS Chem Biol [Internet]. 2015 Mar 20;10(3):734–46. Available from: https://pubs.acs.org/doi/10.1021/cb5007689

185. Belardinelli JM, Yazidi A, Yang L, Fabre L, Li W, Jacques B, et al. Structure–function profile of MmpL3, the essential mycolic acid transporter from *Mycobacterium tuberculosis*. ACS Infect Dis [Internet]. 2016 Oct 14;2(10):702–13. Available from:

http://pubs.acs.org/doi/10.1021/acsinfecdis.6b00095

186. Sulzenbacher G, Canaan S, Bordat Y, Neyrolles O, Stadthagen G, Roig-Zamboni V, et al. LppX is a lipoprotein required for the translocation of phthiocerol dimycocerosates to the surface of *Mycobacterium tuberculosis.* EMBO J [Internet]. 2006 Apr 5;25(7):1436–44. Available from: http://emboj.embopress.org/cgi/doi/10.1038/sj.emboj.7601048

187. Lefèvre P, Denis O, De Wit L, Tanghe A, Vandenbussche P, Content J, et al. Cloning of the gene encoding a 22-kilodalton cell surface antigen of *Mycobacterium bovis* BCG and analysis of its potential for DNA vaccination against tuberculosis. Infect Immun [Internet]. 2000 Mar;68(3):1040–7. Available from: http://www.ncbi.nlm.nih.gov/pubmed/10678905

188. Gaur RL, Ren K, Blumenthal A, Bhamidi S, Gibbs S, Jackson M, et al. LprG-mediated surface expression of lipoarabinomannan is essential for virulence of *Mycobacterium tuberculosis*. PLoS Pathog. 2014;10(9).

189. Gupta M, Sajid A, Arora G, Tandon V, Singh Y. Forkhead-associated domain-containing protein Rv0019c and polyketide-associated protein PapA5, from substrates of serine/threonine protein kinase PknB to interacting proteins of *Mycobacterium tuberculosis*. J Biol Chem. 2009;284(50):34723–34.

190. Gomez-Velasco A, Bach H, Rana AK, Cox LR, Bhatt A, Besra GS, et al. Disruption of the serine/threonine protein kinase H affects phthiocerol dimycocerosates synthesis in *Mycobacterium tuberculosis*. Microbiology [Internet]. 2013 Apr 1;159(Pt_4):726–36. Available from: https://www.microbiologyresearch.org/content/journal/micro/10.1099/mic.0.062067-0

191. Pérez J, Garcia R, Bach H, de Waard JH, Jacobs WR, Av-Gay Y, et al. *Mycobacterium tuberculosis* transporter MmpL7 is a potential substrate for kinase PknD. Biochem Biophys Res Commun. 2006;348(1):6–12.

192. Ripoll F, Deshayes C, Pasek S, Laval F, Beretti J-L, Biet F, et al. Genomics of glycopeptidolipid biosynthesis in *Mycobacterium abscessus* and *M. chelonae*. BMC Genomics [Internet]. 2007;8(8):114. Available from: http://www.biomedcentral.com/1471-2164/8/114

193. Sondén B, Kocíncová D, Deshayes C, Euphrasie D, Rhayat L, Laval F, et al. Gap, a mycobacterial specific integral membrane protein, is required for glycolipid transport to the cell surface. Mol Microbiol. 2005;58(2):426–40.

194. Li W, Upadhyay A, Fontes FL, North EJ, Wang Y, Crans DC, et al. Novel insights into the mechanism of inhibition of MmpL3, a target of multiple pharmacophores in *Mycobacterium tuberculosis*. Antimicrob Agents Chemother. 2014;58(11):6413–23.

195. Pacheco SA, Hsu FF, Powers KM, Purdy GE. MmpL11 protein transports mycolic acid-containing lipids to the mycobacterial cell wall and contributes to biofilm formation in *Mycobacterium smegmatis*. J Biol Chem. 2013;288(33):24213–22.

196. Wright CC, Hsu FF, Arnett E, Dunaj JL, Davidson PM, Pacheco SA, et al. The *Mycobacterium tuberculosis* MmpL11 cell wall lipid transporter is important for biofilm formation, intracellular growth and non-replicating persistence. Infect Immun. 2017 May 15;(May):1–42.

197. Tullius M V, Harmston CA, Owens CP, Chim N, Morse RP, McMath LM, et al. Discovery and characterization of a unique mycobacterial heme acquisition system. Proc Natl Acad Sci U S A. 2011;108(12):5051–6.

198. Owens CP, Chim N, Graves AB, Harmston CA, Iniguez A, Contreras H, et al. The *Mycobacterium tuberculosis* secreted protein Rv0203 transfers heme to membrane proteins MmpL3 and MmpL11. J Biol Chem. 2013;288(30):21714–28.

199. Owens CP, Du J, Dawson JH, Goulding CW. Characterization of heme ligation properties of Rv0203, a secreted heme binding protein involved in *Mycobacterium tuberculosis* heme uptake. Biochemistry [Internet]. 2012 Feb 21;51(7):1518–31. Available from: http://pubs.acs.org/doi/abs/10.1021/bi2018305

200. Nambu S, Matsui T, Goulding CW, Takahashi S, Ikeda-Saito M. A new way to degrade heme: The *Mycobacterium tuberculosis* enzyme MhuD catalyzes heme degradation without generating CO. J Biol Chem. 2013;288(14):10101–9.

201. Chim N, Iniguez A, Nguyen TQ, Goulding CW. Unusual diheme conformation of the heme-degrading protein from *Mycobacterium tuberculosis*. J Mol Biol [Internet]. 2010 Jan;395(3):595–608. Available from: http://linkinghub.elsevier.com/retrieve/pii/S0022283609014028

202. Wells RM, Jones CM, Xi Z, Speer A, Danilchanka O, Doornbos KS, et al. Discovery of a siderophore export system essential for virulence of *Mycobacterium tuberculosis*. PLoS Pathog. 2013;9(1).

203. Jones CM, Wells RM, Madduri AVR, Renfrow MB, Ratledge C, Moody DB, et al. Self-poisoning of *Mycobacterium tuberculosis* by interrupting siderophore recycling. Proc Natl Acad Sci U S A [Internet]. 2014;111(5):1945–50. Available from:

http://www.pubmedcentral.nih.gov/articlerender.fcgi?artid=3918798&tool=pmcentrez&rendertype=abstract

204. LaMarca BBD, Zhu W, Arceneaux JEL, Byers BR, Lundrigan MD. Participation of *fad* and *mbt* genes in synthesis of mycobactin in *Mycobacterium smegmatis*. J Bacteriol. 2004;186(2):374–82.

205. Chavadi SS, Stirrett KL, Edupuganti UR, Vergnolle O, Sadhanandan G, Marchiano E, et al. Mutational and phylogenetic analyses of the mycobacterial *mbt* gene cluster. J Bacteriol. 2011;193(21):5905–13.

206. McMahon MD, Rush JS, Thomas MG. Analyses of MbtB, MbtE, and MbtF suggest revisions to the mycobactin biosynthesis pathway in *Mycobacterium tuberculosis*. J Bacteriol. 2012;194(11):2809–18.

207. Krithika R, Marathe U, Saxena P, Ansari MZ, Mohanty D, Gokhale RS. A genetic locus required for iron acquisition in *Mycobacterium tuberculosis*. Proc Natl Acad Sci U S A [Internet]. 2006;103(7):2069–74. Available from: http://www.pubmedcentral.nih.gov/articlerender.fcgi?artid=1413701&tool=pmcentrez&rendertype=abstract

208. Reddy PV, Puri RV, Chauhan P, Kar R, Rohilla A, Khera A, et al. Disruption of mycobactin biosynthesis leads to attenuation of *Mycobacterium tuberculosis* for growth and virulence. J Infect Dis. 2013;208(8):1255–65.

209. Quadri LE, Sello J, Keating TA, Weinreb PH, Walsh CT. Identification of a *Mycobacterium tuberculosis* gene cluster encoding the biosynthetic enzymes for assembly of the virulence-conferring siderophore mycobactin. Chem Biol. 1998;5(11):631–45.

210. Contreras H, Chim N, Credali A, Goulding CW. Heme uptake in bacterial pathogens. Curr Opin Chem Biol. 2014;19(1):34–41.

211. Voss JJ De, Rutter K, Schroeder BG, Iii CEB, Voss JJDE. Iron Acquisition and Metabolism by Iron Acquisition and Metabolism by Mycobacteria. J Bacteriol. 1999;181(15):4443–51.

212. Fang Z, Sampson SL, Warren RM, Gey Van Pittius NC, Newton-Foot M. Iron acquisition strategies in Mycobacteria. Tuberculosis [Internet]. 2015;95(2):123–30. Available from: http://dx.doi.org/10.1016/j.tube.2015.01.004

213. Li X-Z, Nikaido H. Efflux-mediated drug resistance in bacteria. Drugs [Internet].

2004;64(2):159–204. Available from: http://link.springer.com/article/10.2165/00003495-200464020-00004

214. Anes J, McCusker MP, Fanning S, Martins M. The ins and outs of RND efflux pumps in *Escherichia coli*. Front Microbiol [Internet]. 2015;6(June):587. Available from: http://journal.frontiersin.org/article/10.3389/fmicb.2015.00587

215. Louw GE, Warren RM, Gey Van Pittius NC, McEvoy CRE, Van Helden PD, Victor TC. A balancing act: Efflux/influx in mycobacterial drug resistance. Antimicrob Agents Chemother [Internet]. 2009;53(8):3181–9. Available from: http://aac.asm.org/cgi/doi/10.1128/AAC.01577-08

216. Viveiros M, Leandro C, Amaral L. Mycobacterial efflux pumps and chemotherapeutic implications. Int J Antimicrob Agents. 2003;22(3):274–8.

217. De Rossi E, Aínsa JA, Riccardi G. Role of mycobacterial efflux transporters in drug resistance: an unresolved question. FEMS Microbiol Rev [Internet]. 2006 Jan;30(1):36–52. Available from: http://www.ncbi.nlm.nih.gov/pubmed/16438679

218. Rodrigues L, Machado D, Couto I, Amaral L, Viveiros M. Contribution of efflux activity to isoniazid resistance in the *Mycobacterium tuberculosis* complex. Infect Genet Evol [Internet]. 2012;12(4):695–700. Available from: http://dx.doi.org/10.1016/j.meegid.2011.08.009

219. Pasca MR, Guglierame P, De Rossi E, Zara F, Riccardi G. *mmpL7* gene of *Mycobacterium tuberculosis* is responsible for isoniazid efflux in *Mycobacterium smegmatis*. Antimicrob Agents Chemother [Internet]. 2005 Nov 1;49(11):4775–7. Available from: http://aac.asm.org/cgi/doi/10.1128/AAC.49.11.4775-4777.2005

220. Hartkoorn RC, Uplekar S, Cole ST. Cross-resistance between clofazimine and bedaquiline through upregulation of *mmpL5* in *Mycobacterium tuberculosis*. Antimicrob Agents Chemother. 2014;58(5):2979–81.

221. Andries K, Villellas C, Coeck N, Thys K, Gevers T, Vranckx L, et al. Acquired resistance of *Mycobacterium tuberculosis* to bedaquiline. PLoS One. 2014;9(7):1–11.

222. Milano A, Pasca MR, Provvedi R, Lucarelli AP, Manina G, Luisa de Jesus Lopes Ribeiro A, et al. Azole resistance in *Mycobacterium tuberculosis* is mediated by the MmpS5-MmpL5 efflux system. Tuberculosis [Internet]. 2009;89(1):84–90. Available from: http://dx.doi.org/10.1016/j.tube.2008.08.003

223. Olvera MR, Vivès E, Molle V. Endogenous and Exogenous KdpF Peptide Increases

Susceptibility of *Mycobacterium bovis* BCG to Nitrosative Stress and Reduces Intramacrophage Replication. Front Cell Infect Microbiol Cell Infect Microbiol. 2017;7(April):1–12.

224. Gannoun-Zaki L, Alibaud L, Carrère-Kremer S, Kremer L, Blanc-Potard A-B. Overexpression of the KdpF membrane peptide in *Mycobacterium bovis* BCG results in reduced intramacrophage growth and altered cording morphology. Nigou J, editor. PLoS One [Internet]. 2013 Apr 5;8(4):e60379. Available from: http://dx.plos.org/10.1371/journal.pone.0060379

225. Cossu A, Sechi LA, Bandino E, Zanetti S, Rosu V. Expression profiling of *Mycobacterium tuberculosis* H37Rv and *Mycobacterium smegmatis* in acid-nitrosative multi-stress displays defined regulatory networks. Microb Pathog [Internet]. 2013;65:89–96. Available from: http://dx.doi.org/10.1016/j.micpath.2013.10.004

226. Altaf M, Miller CH, Bellows DS, O'Toole R. Evaluation of the *Mycobacterium smegmatis* and BCG models for the discovery of *Mycobacterium tuberculosis* inhibitors. Tuberculosis [Internet]. 2010;90(6):333–7. Available from: http://dx.doi.org/10.1016/j.tube.2010.09.002

227. Sandhu P, Akhter Y. The internal gene duplication and interrupted coding sequences in the *mmpL* genes of *Mycobacterium tuberculosis*: Towards understanding the multidrug transport in an evolutionary perspective. Int J Med Microbiol. 2015;305(3):413–23.

228. Chim N, Torres R, Liu Y, Capri J, Batot G, Whitelegge JP, et al. The structure and interactions of periplasmic domains of crucial MmpL membrane proteins from *Mycobacterium tuberculosis*. Chem Biol [Internet]. 2015 Aug;22(8):1098–107. Available from: https://linkinghub.elsevier.com/retrieve/pii/S1074552115002872

229. Tseng TT, Gratwick KS, Kollman J, Park D, Nies DH, Goffeau A, et al. The RND permease superfamily: an ancient, ubiquitous and diverse family that includes human disease and development proteins. J Mol Microbiol Biotechnol [Internet]. 1999;1(1):107–25. Available from: http://www.ncbi.nlm.nih.gov/pubmed/10941792

230. Murakami S, Nakashima R, Yamashita E, Yamaguchi A. Crystal structure of bacterial multidrug efflux transporter AcrB. Nature [Internet]. 2002 Oct;419(6907):587–93. Available from: http://www.nature.com/articles/nature01050

231. Sennhauser G, Bukowska MA, Briand C, Grütter MG. Crystal structure of the multidrug exporter MexB from *Pseudomonas aeruginosa*. J Mol Biol. 2009;389(1):134–45.

232. Bolla JR, Su C, Do S V, Radhakrishnan A, Kumar N, Long F, et al. Crystal structure of

the *Neisseria gonorrhoeae* MtrD inner membrane multidrug efflux pump. 2014;9(6):1–8.

233. Long F, Su CC, Zimmermann MT, Boyken SE, Rajashankar KR, Jernigan RL, et al. Crystal structures of the CusA efflux pump suggest methionine-mediated metal transport. Nature [Internet]. 2010 Sep;467(7314):484–8. Available from: http://dx.doi.org/10.1038/nature09395

234. Pak JE, Ekende EN, Kifle EG, O'Connell JD, De Angelis F, Tessema MB, et al. Structures of intermediate transport states of ZneA, a Zn(II)/proton antiporter. Proc Natl Acad Sci. 2013;110(46):18484–9.

235. Zoonens M, Popot JL. Amphipols for each season. J Membr Biol. 2014;247(9–10):759–96.

236. Whiles JA, Deems R, Vold RR, Dennis EA. Bicelles in structure-function studies of membrane-associated proteins. Bioorg Chem. 2002;30(6):431–42.

237. Denisov IG, Sligar SG. Nanodiscs in membrane biochemistry and biophysics. Chem Rev [Internet]. 2017 Mar 22;117(6):4669–713. Available from: http://pubs.acs.org/doi/10.1021/acs.chemrev.6b00690

238. Simon KS, Pollock NL, Lee SC. Membrane protein nanoparticles: the shape of things to come. Biochem Soc Trans. 2018;46(6):1495–504.

239. Mio K, Sato C. Lipid environment of membrane proteins in cryo-EM based structural analysis. Biophys Rev. 2018;10(2):307–16.

240. Birch J, Axford D, Foadi J, Meyer A, Eckhardt A, Thielmann Y, et al. The fine art of integral membrane protein crystallisation. Methods. 2018;147(May):150–62.

241. Knowles TJ, Finka R, Smith C, Lin Y-P, Dafforn T, Overduin M. Membrane proteins solubilized intact in lipid containing nanoparticles bounded by styrene maleic acid copolymer. J Am Chem Soc [Internet]. 2009 Jun 10;131(22):7484–5. Available from: https://pubs.acs.org/doi/10.1021/ja810046q

242. Morrison KA, Akram A, Mathews A, Khan ZA, Patel JH, Zhou C, et al. Membrane protein extraction and purification using styrene-maleic acid (SMA) copolymer: effect of variations in polymer structure. Biochem J. 2016;473(23):4349–60.

243. Gulati S, Jamshad M, Knowles TJ, Morrison KA, Downing R, Cant N, et al. Detergent-

free purification of ABC (ATP-binding-cassette) transporters. Biochem J [Internet]. 2014;461(2):269–78. Available from: http://biochemj.org/lookup/doi/10.1042/BJ20131477

244. Postis V, Rawson S, Mitchell JK, Lee SC, Parslow RA, Dafforn TR, et al. The use of SMALPs as a novel membrane protein scaffold for structure study by negative stain electron microscopy. Biochim Biophys Acta - Biomembr [Internet]. 2015;1848(2):496–501. Available from: http://dx.doi.org/10.1016/j.bbamem.2014.10.018

245. Lee SC, Khalid S, Pollock NL, Knowles TJ, Edler K, Rothnie AJ, et al. Encapsulated membrane proteins: A simplified system for molecular simulation. Biochim Biophys Acta - Biomembr [Internet]. 2016;1858(10):2549–57. Available from: http://dx.doi.org/10.1016/j.bbamem.2016.02.039

246. Dörr JM, Koorengevel MC, Schäfer M, Prokofyev A V., Scheidelaar S, van der Cruijsen EAW, et al. Detergent-free isolation, characterization, and functional reconstitution of a tetrameric K + channel: The power of native nanodiscs . Proc Natl Acad Sci. 2014;111(52):18607–12.

247. Jamshad M, Charlton J, Lin Y, Routledge SJ, Bawa Z, Knowles TJ, et al. G-protein coupled receptor solubilization and purification for biophysical analysis and functional studies, in the total absence of detergent. Biosci Rep. 2015;35(2):1–10.

248. Logez C, Damian M, Legros C, Dupré C, Guéry M, Mary S, et al. Detergent-free isolation of functional g protein-coupled receptors into nanometric lipid particles. Biochemistry. 2016;55(1):38–48.

249. Paulin S, Jamshad M, Dafforn TR, Garcia-Lara J, Foster SJ, Galley NF, et al. Surfactant-free purification of membrane protein complexes from bacteria: Application to the staphylococcal penicillin-binding protein complex PBP2/PBP2a. Nanotechnology. 2014;25(28).

250. Swainsbury DJK, Scheidelaar S, Van Grondelle R, Killian JA, Jones MR. Bacterial reaction centers purified with styrene maleic acid copolymer retain native membrane functional properties and display enhanced stability. Angew Chemie - Int Ed. 2014;53(44):11803–7.

251. Broecker J, Eger BT, Ernst OP. Crystallogenesis of membrane proteins mediated by polymer-bounded lipid nanodiscs. structure [Internet]. 2017;25(2):384–92. Available from: http://dx.doi.org/10.1016/j.str.2016.12.004

252. Parmar M, Rawson S, Scarff CA, Goldman A, Dafforn TR, Muench SP, et al. Using a

SMALP platform to determine a sub-nm single particle cryo-EM membrane protein structure. Biochim Biophys Acta - Biomembr. 2018;1860(2):378–83.

253. Yang J, Yan R, Roy A, Xu D, Poisson J, Zhang Y. The I-TASSER suite: Protein structure and function prediction. Nat Methods [Internet]. 2014;12(1):7–8. Available from: http://dx.doi.org/10.1038/nmeth.3213

254. Guéguinou M, ChantÔme A, Fromont G, Bougnoux P, Vandier C, Potier-Cartereau M. KCa and Ca2+ channels: The complex thought. Biochim Biophys Acta - Mol Cell Res [Internet]. 2014;1843(10):2322–33. Available from: http://dx.doi.org/10.1016/j.bbamcr.2014.02.019

255. Scheidelaar S, Koorengevel MC, van Walree CA, Dominguez JJ, Dörr JM, Killian JA. Effect of polymer composition and pH on membrane solubilization by styrene-maleic acid copolymers. Biophys J. 2016;111(9):1974–86.

256. Basak P, Debnath T, Banerjee R, Bhattacharyya M. Selective binding of divalent cations toward heme proteins. Front Biol (Beijing). 2016;11(1):32–42.

257. Gewering T, Januliene D, Ries AB, Moeller A. Know your detergents: A case study on detergent background in negative stain electron microscopy. J Struct Biol [Internet]. 2018;203(3):242–6. Available from: https://doi.org/10.1016/j.jsb.2018.05.008

258. Onwueme KC, Vos CJ, Zurita J, Ferreras JA, Quadri LEN. The dimycocerosate ester polyketide virulence factors of mycobacteria. Prog Lipid Res [Internet]. 2005 Sep;44(5):259–302. Available from: https://linkinghub.elsevier.com/retrieve/pii/S0163782705000299

259. Jain M, Cox JS. Interaction between polyketide synthase and transporter suggests coupled synthesis and export of virulence lipid in *M. tuberculosis*. PLoS Pathog. 2005;1(1):0012–9.

260. Su CC, Li M, Gu R, Takatsuka Y, McDermott G, Nikaido H, et al. Conformation of the AcrB multidrug efflux pump in mutants of the putative proton relay pathway. J Bacteriol. 2006;188(20):7290–6.

261. Eicher T, Seeger MA, Anselmi C, Zhou W, Brandstätter L, Verrey F, et al. Coupling of remote alternating-access transport mechanisms for protons and substrates in the multidrug efflux pump AcrB. Elife [Internet]. 2014;3:e03145. Available from: http://elifesciences.org/content/3/e03145.abstract

262. Seeger MA. Structural asymmetry of AcrB trimer suggests a peristaltic pump

mechanism. Science (80-) [Internet]. 2006 Sep 1;313(5791):1295–8. Available from: http://www.sciencemag.org/cgi/doi/10.1126/science.1131542

263. Bernut A, Viljoen A, Dupont C, Sapriel G, Blaise M, Bouchier C, et al. Insights into the smooth-to-rough transitioning in *Mycobacterium bolletii* unravels a functional Tyr residue conserved in all mycobacterial MmpL family members. Mol Microbiol [Internet]. 2016 Mar;99(5):866–83. Available from: http://doi.wiley.com/10.1111/mmi.13283

264. Schrodinger L. The PyMOL Molecular Graphics System, Version 2.0. 2015.

265. Stover CK, de la Cruz VF, Fuerst TR, Burlein JE, Benson L a, Bennett LT, et al. New use of BCG for recombinant vaccines. Nature. 1991;351(6326):456–60.

266. Du D, van Veen HW, Murakami S, Pos KM, Luisi BF. Structure, mechanism and cooperation of bacterial multidrug transporters. Curr Opin Struct Biol [Internet]. 2015 Aug;33:76–91. Available from: http://dx.doi.org/10.1016/j.sbi.2015.07.015

267. Tsukazaki T, Mori H, Echizen Y, Ishitani R, Fukai S, Tanaka T, et al. Structure and function of a protein export-enhancing membrane component SecDF. Nature [Internet]. 2011;474(7350):235–8. Available from: http://www.ncbi.nlm.nih.gov/pmc/articles/PMC3697915/

268. Elkins CA, Nikaido H. Substrate specificity of the RND-type multidrug efflux pumps AcrB and AcrD of *Escherichia coli* is determined predominantly by two large periplasmic loops. J Bacteriol [Internet]. 2002;184(23):6490–8. Available from: http://www.pubmedcentral.nih.gov/articlerender.fcgi?artid=135441&tool=pmcentrez&rendertype=abstract

269. Jeong H, Kim JS, Song S, Shigematsu H, Yokoyama T, Hyun J, et al. Pseudoatomic structure of the tripartite multidrug efflux pump AcrAB-TolC reveals the intermeshing cogwheel-like interaction between AcrA and TolC. Structure [Internet]. 2016;24(2):272–6. Available from: http://dx.doi.org/10.1016/j.str.2015.12.007

270. Domenech P, Reed MB. Rapid and spontaneous loss of phthiocerol dimycocerosate (PDIM) from *Mycobacterium tuberculosis* grown *in vitro*: implications for virulence studies. Microbiology [Internet]. 2009 Nov 1;155(11):3532–43. Available from: https://www.microbiologyresearch.org/content/journal/micro/10.1099/mic.0.029199-0

271. Choudhuri BS, Bhakta S, Barik R, Basu J, Kundu M, Chakrabarti P. Overexpression and functional characterization of an ABC (ATP-binding cassette) transporter encoded by the genes *drrA* and *drrB* of *Mycobacterium tuberculosis*. Biochem J [Internet]. 2002 Oct

1;367(1):279–85. Available from: http://biochemj.org/lookup/doi/10.1042/bj20020615

272. Wilkens S. Structure and mechanism of ABC transporters. F1000Prime Rep [Internet]. 2015 Feb 3;7(4):426–31. Available from: https://linkinghub.elsevier.com/retrieve/pii/S0959440X04001034

273. Braibant M, Gilot P, Content J. The ATP binding cassette (ABC) transport systems of *Mycobacterium tuberculosis*. FEMS Microbiol Rev. 2000;24(4):449–67.

274. Glass LN, Swapna G, Chavadi SS, Tufariello JM, Mi K, Drumm JE, et al. *Mycobacterium tuberculosis* universal stress protein Rv2623 interacts with the putative ATP binding cassette (ABC) transporter Rv1747 to regulate mycobacterial growth. Salgame P, editor. PLOS Pathog [Internet]. 2017 Jul 28;13(7):e1006515. Available from: https://dx.plos.org/10.1371/journal.ppat.1006515

275. Dianišková P, Korduláková J, Skovierová H, Kaur D, Jackson M, Brennan PJ, et al. Investigation of ABC transporter from mycobacterial arabinogalactan biosynthetic cluster. Gen Physiol Biophys [Internet]. 2011 Sep;30(3):239–50. Available from: http://www.ncbi.nlm.nih.gov/pubmed/21952433

276. Cuthbertson L, Kos V, Whitfield C. ABC transporters involved in export of cell surface glycoconjugates. Microbiol Mol Biol Rev. 2010;74(3):341–62.

277. Sinsimer D, Huet G, Manca C, Tsenova L, Koo MS, Kurepina N, et al. The phenolic glycolipid of *Mycobacterium tuberculosis* differentially modulates the early host cytokine response but does not in itself confer hypervirulence. Infect Immun. 2008;76(7):3027–36.

278. Guilfoile PG, Hutchinson CR. A bacterial analog of the *mdr* gene of mammalian tumor cells is present in *Streptomyces peucetius*, the producer of daunorubicin and doxorubicin. Proc Natl Acad Sci U S A [Internet]. 1991 Oct 1;88(19):8553–7. Available from: http://www.ncbi.nlm.nih.gov/pubmed/1924314

279. Kaur P, Russell J. Biochemical coupling between the DrrA and DrrB proteins of the doxorubicin efflux pump of *Streptomyces peucetius*. J Biol Chem. 1998;273(28):17933–9.

280. Bardarov S, Bardarov S, Hatfull G, Larsen M, Tufariello J, Chan J, et al. Specialized transduction: an efficient method for generating marked and unmarked targeted gene disruptions in *Mycobacterium tuberculosis*, *M. bovis BCG* and *M. smegmatis*. Microbiology [Internet]. 2002 Oct 1;148(10):3007–17. Available from: https://www.microbiologyresearch.org/content/journal/micro/10.1099/00221287-148-

10-3007

281. Larsen MH, Biermann K, Tandberg S, Hsu T, Jacobs WR. Genetic manipulation of *Mycobacterium tuberculosis*. Curr Protoc Microbiol [Internet]. 2007 Nov;6(1):10A.2.1-10A.2.21. Available from: https://currentprotocols.onlinelibrary.wiley.com/doi/abs/10.1002/9780471729259.mc10a02s6

282. Oberto J. SyntTax: a web server linking synteny to prokaryotic taxonomy. BMC Bioinformatics [Internet]. 2013 Dec 16;14(1):4. Available from: BMC Bioinformatics

283. Kanehisa M, Sato Y, Furumichi M, Morishima K, Tanabe M. New approach for understanding genome variations in KEGG. Nucleic Acids Res. 2019;47(D1):D590–5.

284. Madduri K, Hutchinson CR. Functional characterization and transcriptional analysis of the *dnrR1* locus, which controls daunorubicin biosynthesis in *Streptomyces peucetius*. J Bacteriol [Internet]. 1995;177(5):1208–15. Available from: https://www.ncbi.nlm.nih.gov/pubmed/7868593

285. Kaur P, Rao DK, Gandlur SM. Biochemical characterization of domains in the membrane subunit DrrB that interact with the ABC subunit DrrA: Identification of a conserved motif. Biochemistry. 2005;44(7):2661–70.

286. Zhang H, Rahman S, Li W, Fu G, Kaur P. Characterization of a novel domain "GATE" in the ABC protein DrrA and its role in drug efflux by the DrrAB complex. Biochem Biophys Res Commun. 2015 Mar 4;459(1):148–53.

287. Gandlur SM, Wei L, Levine J, Russell J, Kaur P. Membrane topology of the DrrB protein of the doxorubicin transporter of *Streptomyces peucetius*. J Biol Chem. 2004;279(26):27799–806.

288. Li W, Sharma M, Kaur P. The DrrAB efflux system of *Streptomyces peucetius* is a multidrug transporter of broad substrate specificity. J Biol Chem. 2014;289(18):12633–46.

289. Karuppasamy K, Srinivasan P, Ashokkumar B, Tiwari R, Kanagarajadurai K, Prasad R. Partial loss of self-resistance to daunorubicin in *drrD* mutant of *Streptomyces peucetius*. Biochem Eng J [Internet]. 2015;102:98–107. Available from: http://dx.doi.org/10.1016/j.bej.2015.02.017

290. Furuya K, Richard Hutchinson C. The DrrC protein of *Streptomyces peucetius*, a UvrA-like protein, is a DNA-binding protein whose gene is induced by daunorubicin. FEMS

Microbiol Lett [Internet]. 1998 Nov 15;168(2):243–9. Available from: http://doi.wiley.com/10.1016/S0378-1097(98)00432-7

291. Lomovskaya N, Hong SK, Kim SU, Fonstein L, Furuya K, Hutchinson CR. The *Streptomyces peucetius drrC* gene encodes a UvrA-like protein involved in daunorubicin resistance and production. J Bacteriol. 1996;178(11):3238–45.

292. Prija F, Prasad R. DrrC protein of *Streptomyces peucetius* removes daunorubicin from intercalated *dnrI* promoter. Microbiol Res [Internet]. 2017 Sep;202(May):30–5. Available from: http://dx.doi.org/10.1016/j.micres.2017.05.002

293. Zhang H, Pradhan P, Kaur P. The extreme C terminus of the ABC protein DrrA contains unique motifs involved in function and assembly of the DrrAB complex. J Biol Chem. 2010;285(49):38324–36.

294. Cuthbertson L, Kimber MS, Whitfield C. Substrate binding by a bacterial ABC transporter involved in polysaccharide export. Proc Natl Acad Sci. 2007;104(49):19529–34.

295. Gerber S, Comellas-Bigler M, Goetz BA, Locher KP. Structural Basis of Trans-Inhibition in a Molybdate/Tungstate ABC Transporter. Science (80-). 2008 Jul 11;321(5886):246–50.

296. Bi Y, Mann E, Whitfield C, Zimmer J. Architecture of a channel-forming O-antigen polysaccharide ABC transporter. Nature [Internet]. 2018;553(7688):361–5. Available from: http://dx.doi.org/10.1038/nature25190

297. Luo Q, Yang X, Yu S, Shi H, Wang K, Xiao L, et al. Structural basis for lipopolysaccharide extraction by ABC transporter LptB 2 FG. Nat Struct Mol Biol [Internet]. 2017;24(5):469–74. Available from: http://dx.doi.org/10.1038/nsmb.3399

298. Lee J-Y, Kinch LN, Borek DM, Wang J, Wang J, Urbatsch IL, et al. Crystal structure of the human sterol transporter ABCG5/ABCG8. Nature [Internet]. 2016 May 26;533(7604):561–4. Available from: http://dx.doi.org/10.1038/nature17666

299. Yan N, Cao P, Lei J, Qian H, Zhao X, Gong X. Structure of the human lipid exporter ABCA1. Cell [Internet]. 2017;169(7):1228-1239.e10. Available from: http://dx.doi.org/10.1016/j.cell.2017.05.020

300. Ishikawa T, Aw W, Kaneko K. Metabolic interactions of Purine derivatives with human ABC transporter ABCG2: Genetic testing to assess gout risk. Pharmaceuticals. 2013;6(11):1347–60.

301. Janvilisri T, Venter H, Shahi S, Reuter G, Balakrishnan L, Van Veen HW. Sterol transport by the human breast cancer resistance protein (ABCG2) expressed in *Lactococcus lactis*. J Biol Chem. 2003;278(23):20645–51.

302. Taylor NMI, Manolaridis I, Jackson SM, Kowal J, Stahlberg H, Locher KP. Structure of the human multidrug transporter ABCG2. Nature [Internet]. 2017;546(7659):504–9. Available from: http://dx.doi.org/10.1038/nature22345

303. Brown K, Li W, Kaur P. Role of Aromatic and Negatively Charged Residues of DrrB in Multisubstrate Specificity Conferred by the DrrAB System of *Streptomyces peucetius*. Biochemistry [Internet]. 2017 Apr 4;56(13):1921–31. Available from: http://www.ncbi.nlm.nih.gov/pubmed/28272881

304. La Rosa V, Poce G, Canseco JO, Buroni S, Pasca MR, Biava M, et al. MmpL3 is the cellular target of the antitubercular pyrrole derivative BM212. Antimicrob Agents Chemother. 2012;56(1):324–31.

305. Owens CP, Chim N, Goulding CW. Insights on how the *Mycobacterium tuberculosis* heme uptake pathway can be used as a drug target. Future Med Chem [Internet]. 2013 Aug;5(12):1391–403. Available from: http://www.ncbi.nlm.nih.gov/pubmed/23919550

306. Yamaguchi A, Nakashima R, Sakurai K. Structural basis of RND-type multidrug exporters. Front Microbiol. 2015;6(APR):1–19.

307. Kapopoulou A, Lew JM, Cole ST. The MycoBrowser portal: A comprehensive and manually annotated resource for mycobacterial genomes. Tuberculosis [Internet]. 2011;91(1):8–13. Available from: http://dx.doi.org/10.1016/j.tube.2010.09.006

308. Notredame C, Higgins DG, Heringa J. T-coffee: A novel method for fast and accurate multiple sequence alignment. J Mol Biol. 2000;302(1):205–17.

309. Robert X, Gouet P. Deciphering key features in protein structures with the new ENDscript server. Nucleic Acids Res. 2014;42(W1):320–4.

310. Snapper SB, Melton RE, Mustafa S, Kieser T, Jacobs WR. Isolation and characterization of efficient plasmid transformation mutants of *Mycobacterium smegmatis*. Mol Microbiol. 1990;4(11):1911–9.

311. Belisle JT, Mahaffey SB, Hill PJ. Isolation of *Mycobacterium* Species Genomic DNA. In: Parish T, Brown AC, editors. Mycobacteria Protocols Methods in Molecular Biology (Methods and Protocols) [Internet]. Second. Totowa, NJ: Humana Press, Totowa, NJ; 2009. p. 1–12. Available from: https://doi.org/10.1007/978-1-59745-207-6_1

312. Sambrook J, Russell DW. The condensed protocols from Molecular cloning : a laboratory manual. Cold Spring Harbor, N.Y. : Cold Spring Harbor Laboratory Press; 2006. 1–800 p.

313. Parish T, Brown AC. Mycobacteria Protocols [Internet]. Parish T, Brown AC, editors. Methods in molecular biology. Totowa, NJ: Humana Press; 2009. 1–489 p. (Methods in Molecular Biology; vol. 465). Available from: http://link.springer.com/10.1007/978-1-59745-207-6

314. Mangan JA, Sole KM, Mitchison DA, Butcher PD. An effective method of RNA extraction from bacteria refractory to disruption, including mycobacteria. Nucleic Acids Res [Internet]. 1997 Feb 1;25(3):675–6. Available from: http://www.ncbi.nlm.nih.gov/pubmed/9016612

315. Rustad TR, Roberts DM, Liao RP, Sherman DR. Isolation of mycobacterial RNA. In: Parish T, Brown AC, editors. Mycobacteria Protocols Methods in Molecular Biology (Methods and Protocols) [Internet]. Second. Totowa, NJ: Humana Press, Totowa, NJ; 2009. p. 13–22. Available from: https://doi.org/10.1007/978-1-59745-207-6_2

316. Goude R, Parish T. Electroporation of Mycobacteria. In: Parish T, Brown AC, editors. Mycobacteria Protocols Methods in Molecular Biology (Methods and Protocols) [Internet]. Second. Totowa, NJ: Humana Press, Totowa, NJ; 2009. p. 203–15. Available from: https://doi.org/10.1007/978-1-59745-207-6_13

317. Besra GS. Preparation of Cell-Wall Fractions from Mycobacteria. In: Parish T, Stoker NG, editors. Mycobacteria Protocols. New Jersey: Humana Press; 1998. p. 91–101.

318. Moolla N. Construction and Phenotypic Characterization of *Mycobacterium smegmatis* Mutants Deficient in DNA Glycosylases. MSc thesis. 2013.

Appendix 1

Media used routinely:

Luria-Bertani broth (LB):
10 g tryptone, 10 g sodium chloride, 5 g yeast.

Luria-Bertani agar plates (LA):
10 g tryptone, 10 g sodium chloride, 5 g yeast extract, 15 g agar/ litre.

Tryptic soy broth (TSB):
30 g TSB powder and 2 ml glycerol. Supplemented with 0.05% Tween80.

Tryptic soy broth (TSB) agar:
30 g TSB powder, 2 ml glycerol and 15 g agar/ L.

Terrific broth (TB):
47.6 g of TB granules and 4 ml glycerol.

Middlebrook 7H9:
4.7 g 7H9 powder and 2 ml glycerol. Supplemented with 0.05% Tween80 and 100 ml OADC per L.

Middlebrook 7H10:
19 g 7H10 powder and 5 ml glycerol. Supplemented with 100 ml OADC per L.

7H9 Top Agar:
4.7 g 7H9 powder, 2 ml glycerol and 7.5 g agar/ L.

7H9 Basal Agar:
4.7 g 7H9 powder, 2 ml glycerol and 15 g agar/ L.

Media were sterilised by autoclaving at 121°C for 15 min and only when cooled were the specified supplements added.

Appendix 2

Concentrations of antibiotic selection markers used:

Antibiotics (stock concentrations)	***E. coli***	***M. smegmatis***	**BCG**
Kanamycin (50 mg/ml)	100 (µg/ml)	50 (µg/ml)	25 (µg/ml)
Hygromycin (50 mg/ml)	150 (µg/ml)	150 (µg/ml)	50 (µg/ml)

Appendix 3

DNA ladders

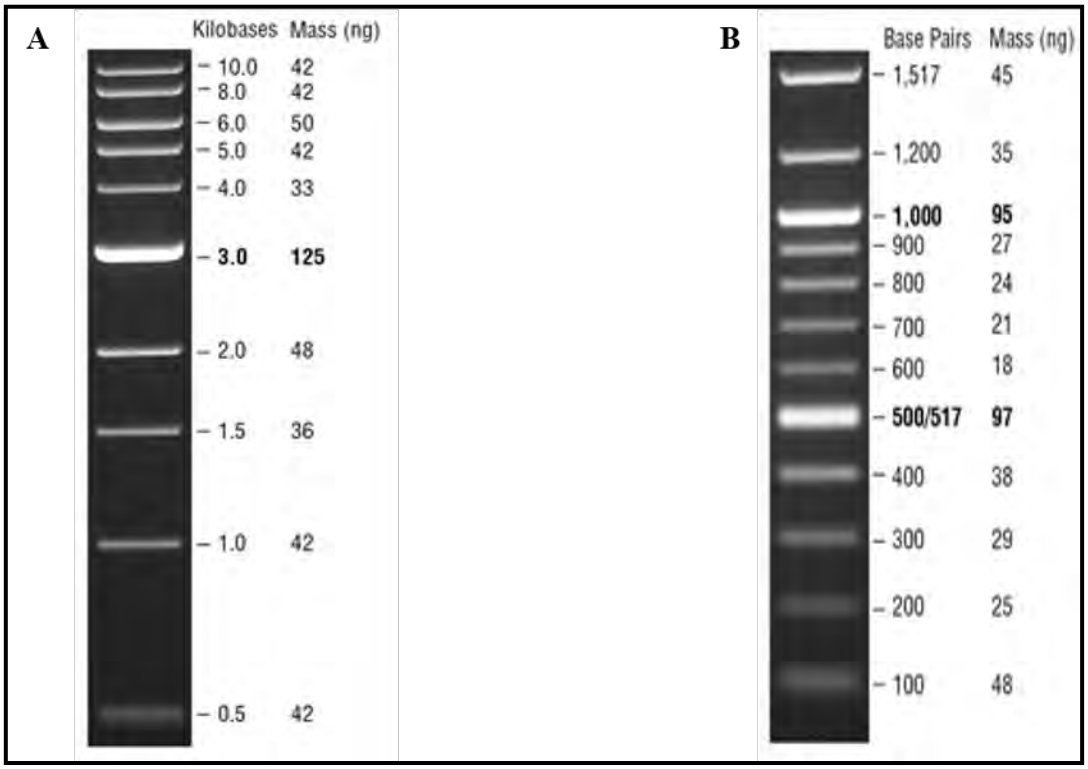

DNA ladders from NEB used to determine the sizes of DNA fragments in agarose gels and Southern blots. **A)** 1 Kbp ladder and **B)** 100 bp ladder. (https://www.neb.com/ accessed 23/06/2019).

Appendix 4

Protein ladders

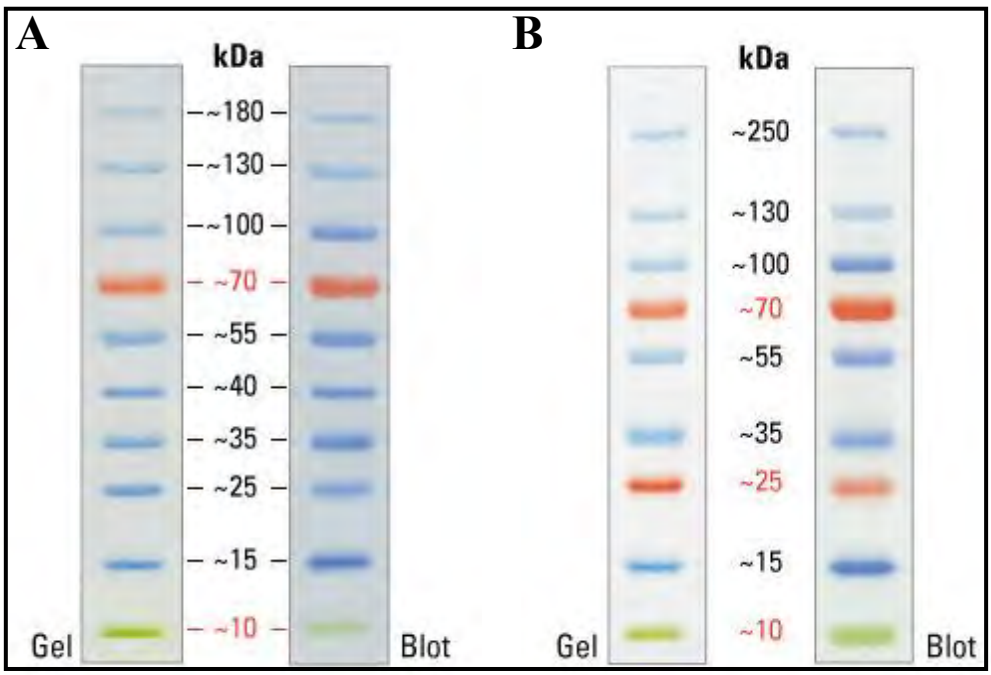

Protein ladders PageRuler™ Prestained Protein Ladder (Thermo scientific) A) and B) were used to determine the sizes of proteins in SDS-PAGE and Western blots (https://www.thermofisher.com/uk/en/home.html accessed 23/06/2019).

Appendix 5

All primers in this study involved in A) gene knockouts of *mmpL7* and *drrABC*, B) restoring *mmpL7, drrAB* and *drrABC* genes, C) generating site-specific substitutions in the *mmpL7* gene, D) generating site-specific deletions in the pMV306::*drrABC* plasmid and E) reverse transcriptase- PCR.

A) Primers (5'-3') involved in the gene knockout construction of *mmpL7* and *drrABC* in *Mycobacterium bovis* BCG. The primer pairs forward (F) and reverse (R) amplify only upstream (Us) and downstream (Ds) regions of the genes. The underlined sequences represent extra bases and italicised sequences indicate endonuclease restriction sites mandatory for cloning purposes while the bold sequences denote overhangs.

ΔmmpL7				**Restriction enzyme**	**Amplicon size (bp)**
Us F	TTTTTTTT*CAC***AAA***G** *TG* GAACGGGCGACTCA GGTTTC	Us R	TTTTTTTT*CAC***TTC***G** *TG* TCGAGGGATTCGGC AGCTTG	*Dra*III (*CACAGGG TG*)	941
Ds F	TTTTTTTT*CAC***AGA***G** *TG* TGGGTGTGCTGGCCT CTTAC	Ds R	TTTTTTTT*CAC***CTT***G** *TG* TTCACGTGCCGTCGA CAAAC		936
Δ*drrABC*				**Restriction enzyme**	**Amplicon size (bp)**
Us F	TTTTTTTT*CAC***AAA***G** *TG* GCCCTTCCCAACGC GCATACC	Us R	TTTTTTTT*CAC***TTC***G** *TG* GCGGCGCACCTTGA AACTCAC	*Dra*III (*CACAGG GTG*)	901
Ds F	TTTTTTTT*CAC***AGA** *GTG* GTCCTCTCTCCGAT GATCGGG	Ds R	TTTTTTTT*CAC***CTT***G** *TG* CTGCCACTCGGTCA GCAGGAT		901

B) Primer pairs (5'-3') forward (F) and reverse (R) involved in the restoring of gene function of mutants generated in this study. Italicised sequences indicate endonuclease restriction sites and underlined sequences denote extra bases mandatory for cloning purposes.

***mmpL7*- C**		**Restriction enzyme**	**Amplicon size (bp)**
F	GAT*AGATCT* AATGCCTAGTCCGGCTGGCCG	*Bgl*II (*AGATCT*)	2763
R	GAT*AAGCTT* TCAACGCCGCCCTGGCGTGG	*Hind*III (*AAGCTT*)	
***drrABC*- C**		**Restriction enzymes**	**Amplicon size (bp)**

F	CATGCATG*TCTAGA* AAGTCCGTTCCGCACTACGGA	*Xba*I (*TCTAGA*)	3316
R	CATGCATG*AAGCTT* CTGGGTGGGTTTCCAAGAGGG	*Hind*III (*AAGCTT*)	
***drrAB*- C**		**Restriction enzymes**	**Amplicon size (bp)**
F1	CATGCATG*TCTAGA* AAGTCCGTTCCGCACTACGGA	*Xba*I (*TCTAGA*)	2558
R1	CATGCATG*GAATTC* AATGCTGTAGAGCCCGCTGTC	*Eco*RI (*GAATTC*)	
F2	CATGCATG*GAATTC* TGGATTCAGCCGTTCGTCGCC	*Eco*RI (*GAATTC*)	385
R2	CATGCATG*AAGCTT* CTGGGTGGGTTTCCAAGAGGG	*Hind*III (*AAGCTT*)	

C) Primer pairs (5'-3') forward (F) and reverse (R) to generate site-specific substitutions in the *mmpL7* gene. The small lettered and bold sequences denote the modification. Primers were designed using the website: http://nebasechanger.neb.com/.

287S		**670R**	
F	AACCATCACC**agc**GCCACCATGCT GGCC	F	TCTCAGCGCC**cgg**TTCGCCGATAC
R	CCGATCGTCAGGACCGCG	R	TTCTTCAGCATCGCCGAC
288T		**673A**	
F	CATCACCGCA**acc**ACCATGCTGG	F	CGATTTCGCC**gcc**ACCGGTGAGG
R	GTTCCGATCGTCAGGACCG	R	GCGCTGAGATTCTTCAGC
292G		**676A**	
F	CACCATGCTG**ggc**GCGCGGCTCG	F	CGATACCGGT**gcc**GGCGGCTTCC
R	GCTGCGGTGATGGTTCCGATCGT CAGG	R	GCGAAATCGGCGCTGAGA
524L		**836D**	
F	CGGCGCGGTC**ctg**CAACTGGACA	F	GTGCGGCGTC**gac**TATCTCGTTGCCG GC
R	CTCATCTGTTCGATTATGGAC	R	GAAGCGAGGACGGCGAAC
610D		**837F**	

F	TGGCGCCGAC**gac**ATCTCCGCGA	F	CGGCGTCCCG**ttc**CTCGTTGCCG
R	GTGGACAGCTCGTTCATGC	R	CACGAAGCGAGGACGGCG
611R		**846A**	
F	CGCCGACCGC**cgg**TCCGCGATATC	F	CAAAGCCGGT**gcc**ATCGCCGACG
R	CCAGTGGACAGCTCGTTC	R	ATGCCGGCAACGAGATAC

D) Primer pairs (5'-3') forward (F) and reverse (R) to generate site-specific deletions in the pMV306::*drrABC* plasmid for the construction of pMV306::*drrBC* and pMV306::*drrAC* plasmids. Primers were designed using the website: http://nebasechanger.neb.com/.

pMV306::*drrBC*	
F	GAATTCGACTCAGACCGCATTACGATGCCG
R	CGGTTCGGAAACAACATCGTAGCC
pMV306::*drrAC*	
F	GAATTCAAGCTGTTTCCGCACTGGATCCAT
R	CACCGTGGTGAGTACTTCACCGTT

E) Primer pairs (5'-3') forward (F) and reverse (R) used for reverse transcriptase- PCR.

Gene	F	R
sigA	TTCGCGCCTACCTCAAACAG	AGGTTGGCTTCCAGCAGATG
mmpL7	ACCACCGAACTGTCGGAATAC	AACGCGCTCATTGTCTGTGTC
drrA	GCTGGCTACGATGTTGTTTCC	GGCATGTACGAGGCTGAATTG
drrB	ACAGATGTGGGTGCTCTATCG	GGCGTGATGTATTGCCCTAAG
drrC	GAGCTTGCACCCACACGTTTG	AATGCTGTAGAGCCCGCTGTC

Appendix 6

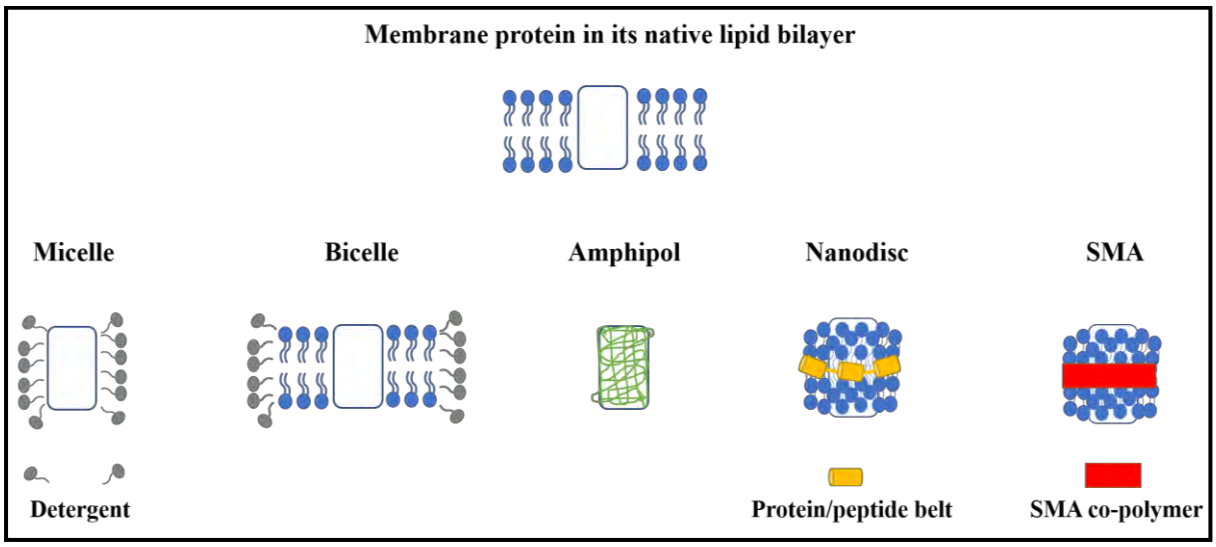

Artificial membrane bilayer mimetics. Detergents replace the native lipid bilayer and form micelle structures while bicelles are mixtures of detergent and phospholipids. Amphipols represent amphiphilic polymers that trap and stabilise membrane proteins, and nanodiscs consist of helical proteins/peptides that encapsulate membrane proteins forming disc-shaped particles extracted with detergent. Styrene-maleic acid (SMA) co-polymers insert into the membrane and scaffold the membrane protein in its native lipid bilayer also forming disc-shaped particles [Adapted from (239)].

Appendix 7

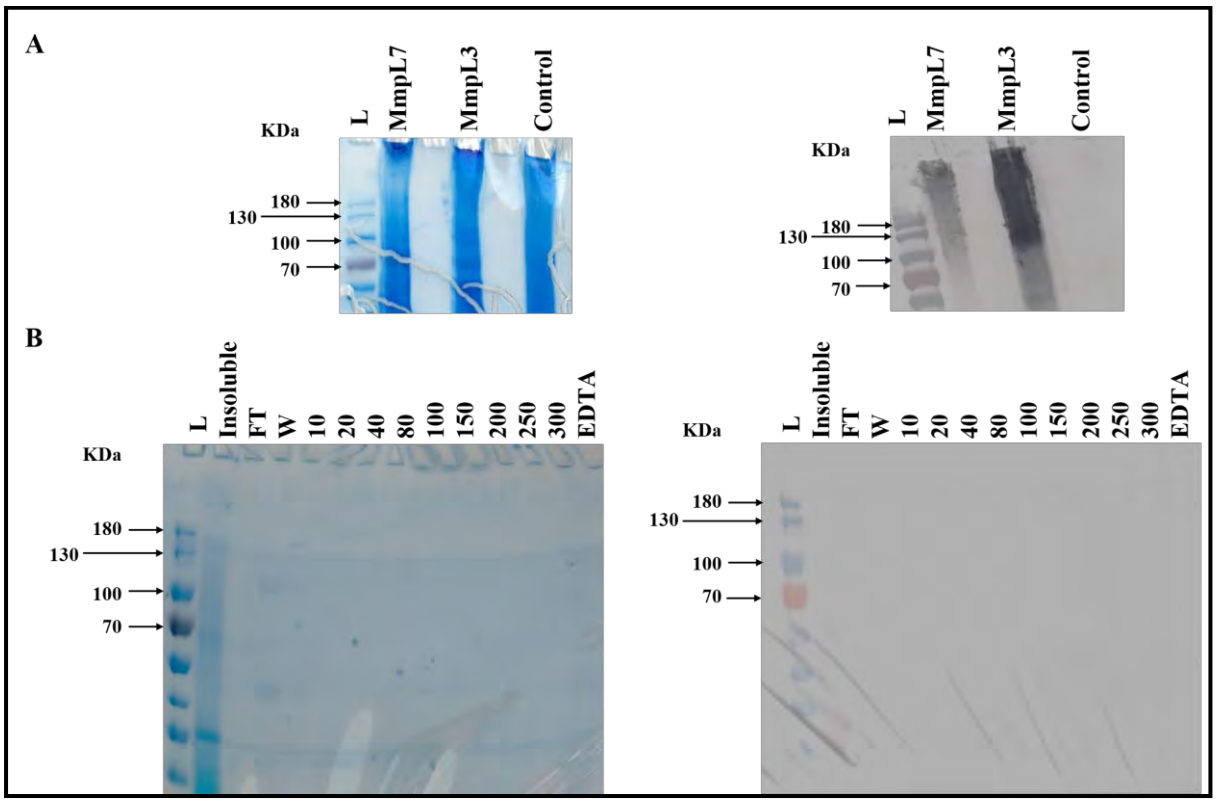

The control strain showing: A) Protein expression of the membrane fraction as compared to MmpL3 and MmpL7 and B) IMAC purification with varying imidazole concentrations. Membrane material was from 1 L cultures. Left panels represents the total protein on SDS-PAGE while the right panels show His-tagged proteins on the Western blot. Imidazole concentrations (mM) are shown as 10, 20, 40, 80, 100, 150, 200, 250 and 300. L represents the protein ladder; FT is the flow through; W is the wash and EDTA represents the 'strip' of the column.

Appendix 8

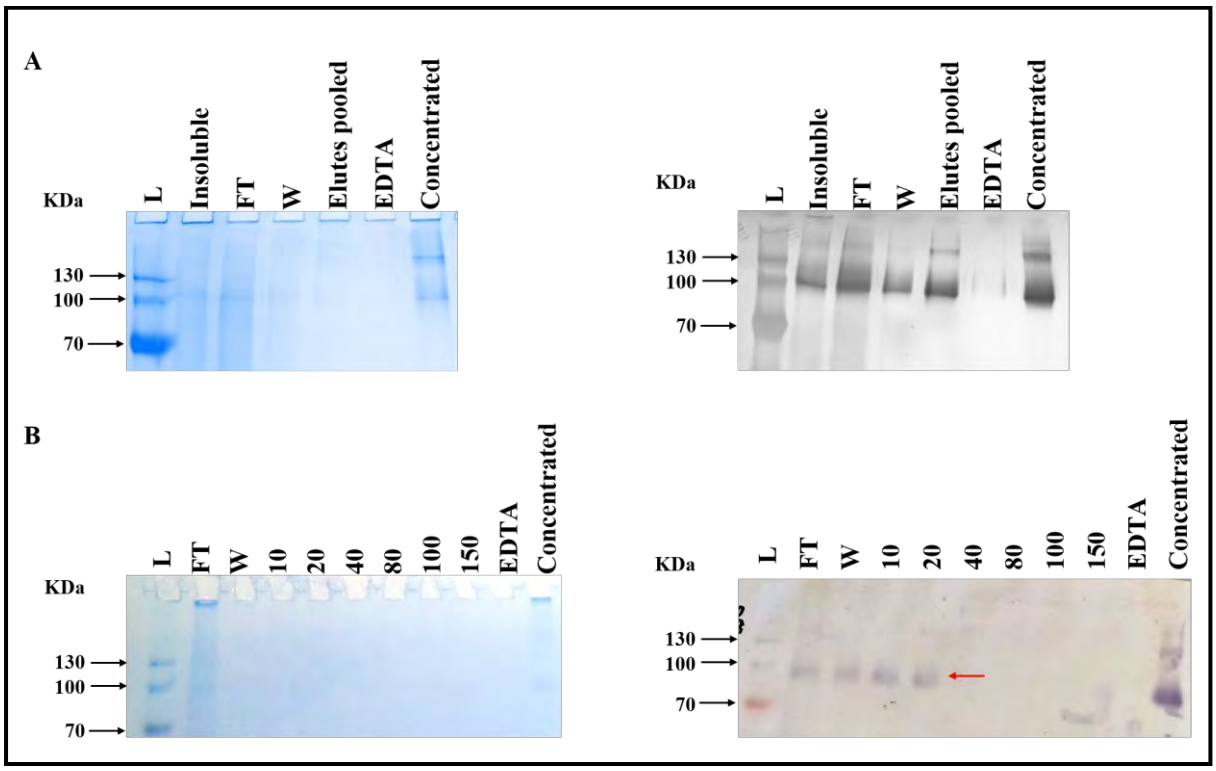

MmpL3 IMAC purification analysed by Native-PAGE/ Western blots over 3 days. A) day 2, B) day 3. Membrane used was from 1 L culture. Red arrow indicates MmpL3. Membrane used was from 1 L culture. Left panels represents the total protein on Native-PAGE while the right panels shows His-tagged proteins on the Western blot. Imidazole concentrations (mM) are shown as 10, 20, 40, 80, 100, 150. L represents the protein ladder; FT is the flow through; W is the wash and EDTA represents the 'strip' of the column. Concentrated indicates that all imidazole eluates were pooled together and concentrated.

Appendix 9

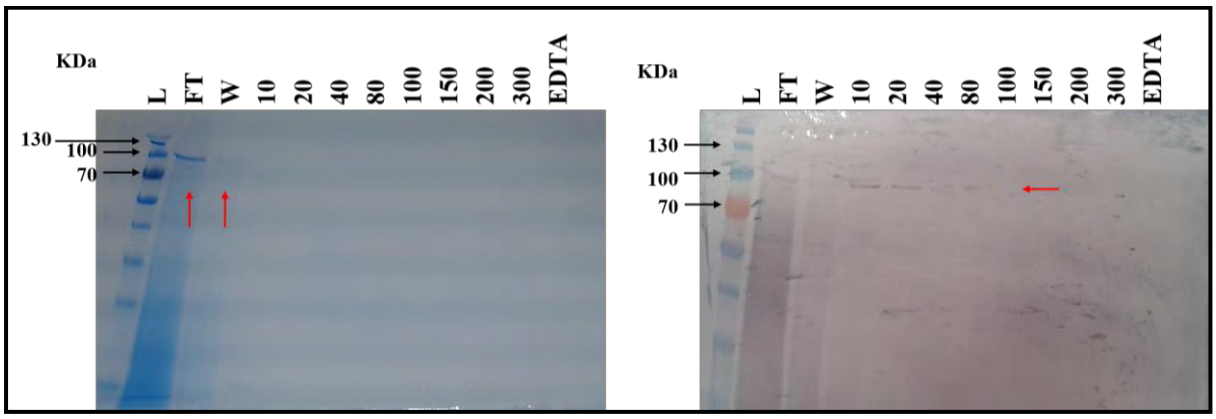

MmpL7 IMAC purification using SMA. Membrane used was from 1 L culture. Left panels represents the total protein on SDS-PAGE while the right panels shows His-tagged proteins on the Western blot. Imidazole concentrations (mM) are shown as 10, 20, 40, 80, 100, 150, 200 and 300. L represents the protein ladder; FT is the flow through; W is the wash and EDTA represents the 'strip' of the column. Red arrow indicates MmpL7.

Appendix 10

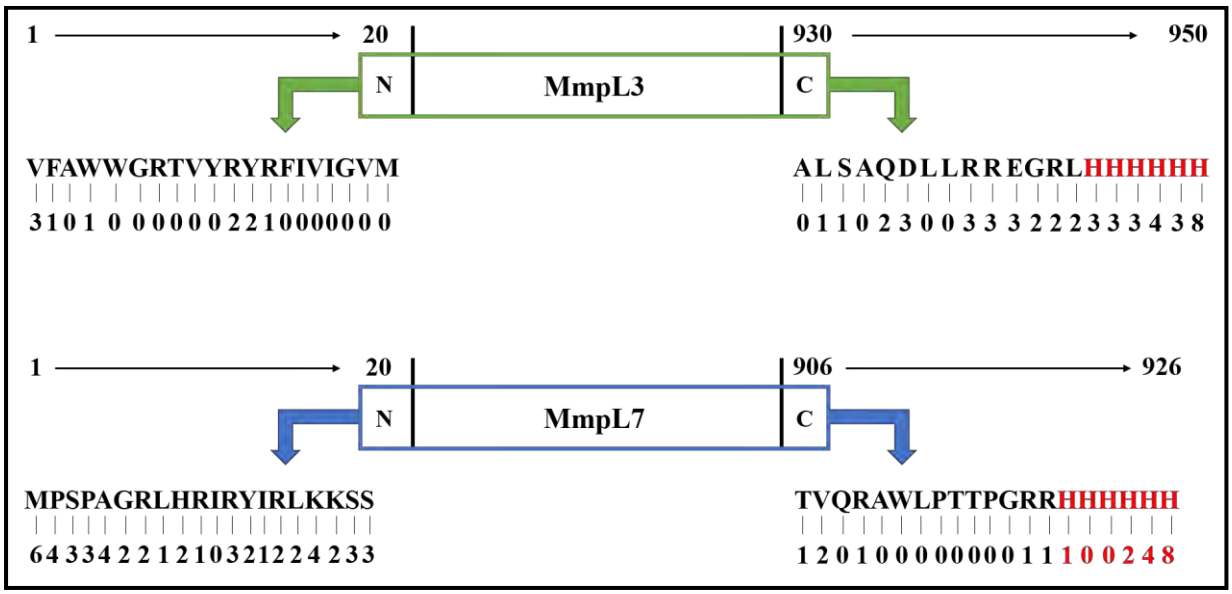

Predicted solvent accessibility of MmpL3 and MmpL7 models. Calculated by the I-TASSER server (253) only showing the N and C terminals, where 0 indicates a buried residue and 9 denotes a highly exposed residue and the His tag is highlighted in red with the corresponding scores.

Appendix 11

A pair of primers (5'-3') forward (F) and reverse (R) to extend the C terminal His tag to twelve His residues and include a TEV site in pET26b:MmpL7. The small lettered and bold sequences denote the modification. These primers were designed by the NEBaseChanger tool (http://nebasechanger.neb.com/).

MmpL7 12HIS/TEV				
F	CACCACCACCACCACCAC**cac caccaccaccaccac**TGAGATCCGG CTGCCTAA**caaagcccgaaaggaag ctg**	R	GGATTGGAAGTACAAGTTCT CCTCGAGTGCGGCCGCAAGC TTACGCCGCCCCTGGCGTGG TCGGAAGC	8065 bp amplicon

Appendix 12

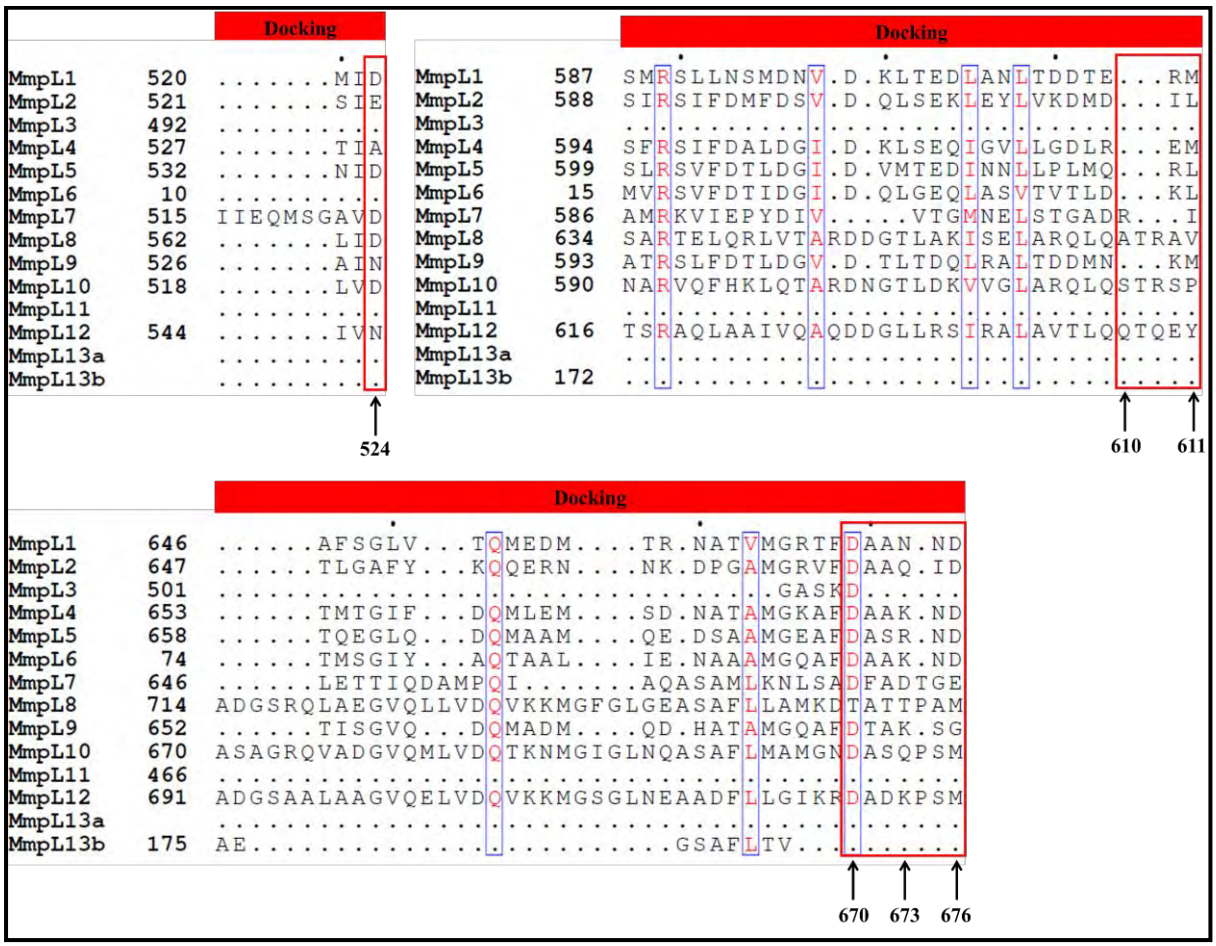

Multiple sequence alignment (MSA) comparing the MmpL7 periplasmic domain 2 (PD2) with other MmpL proteins in Mtb. The arrow and the amino acid indicated MmpL7 residues investigated in this study.

Appendix 13

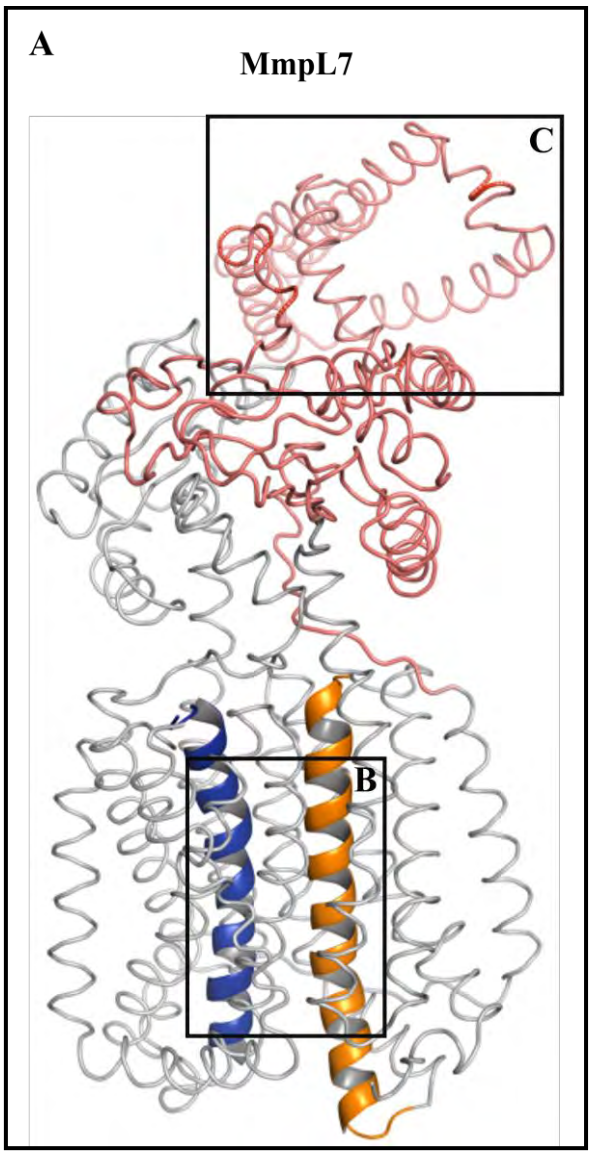

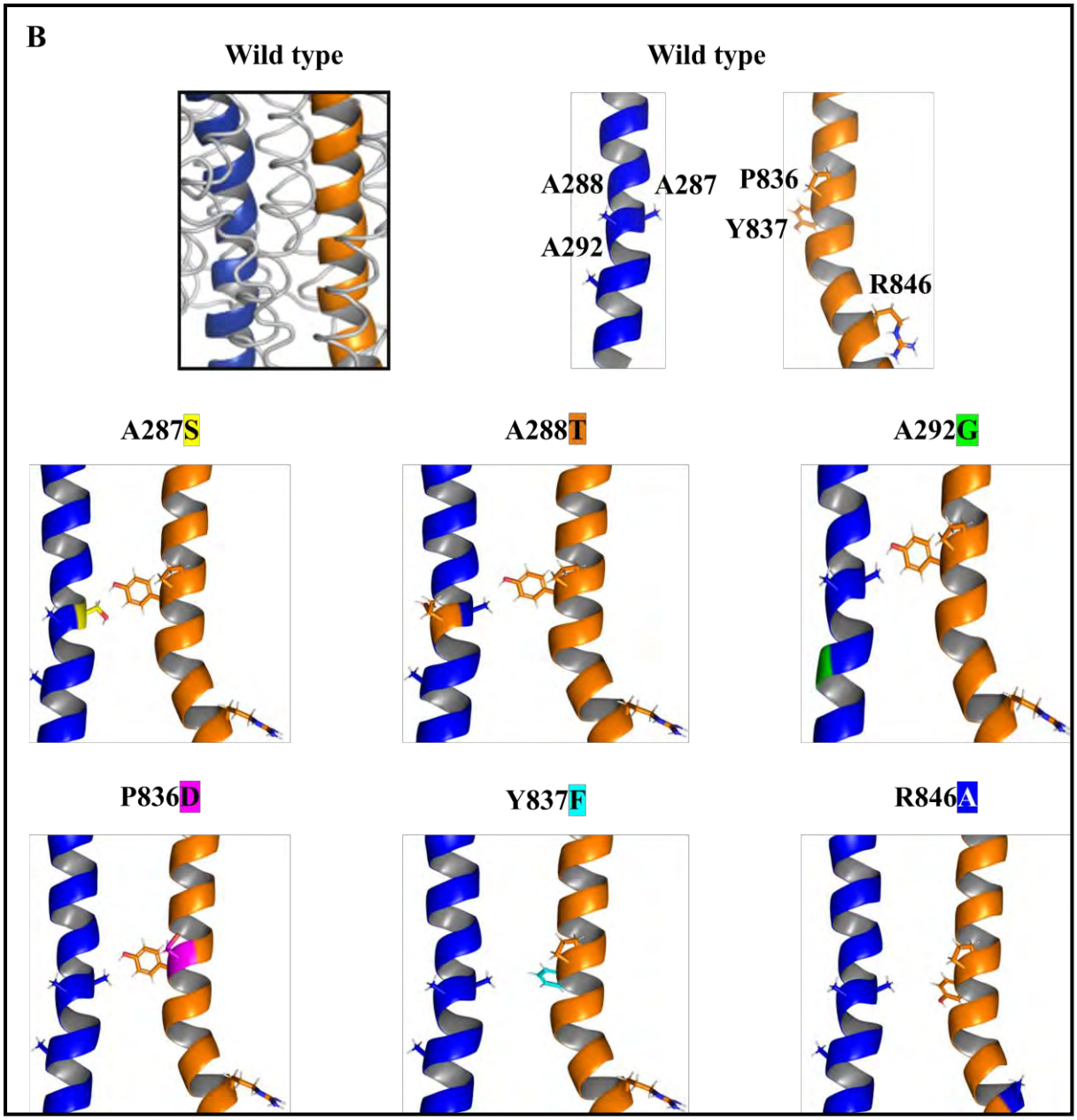
B
Wild type
Wild type
A288
A287
A292
P836
Y837
R846
A287S
A288T
A292G
P836D
Y837F
R846A

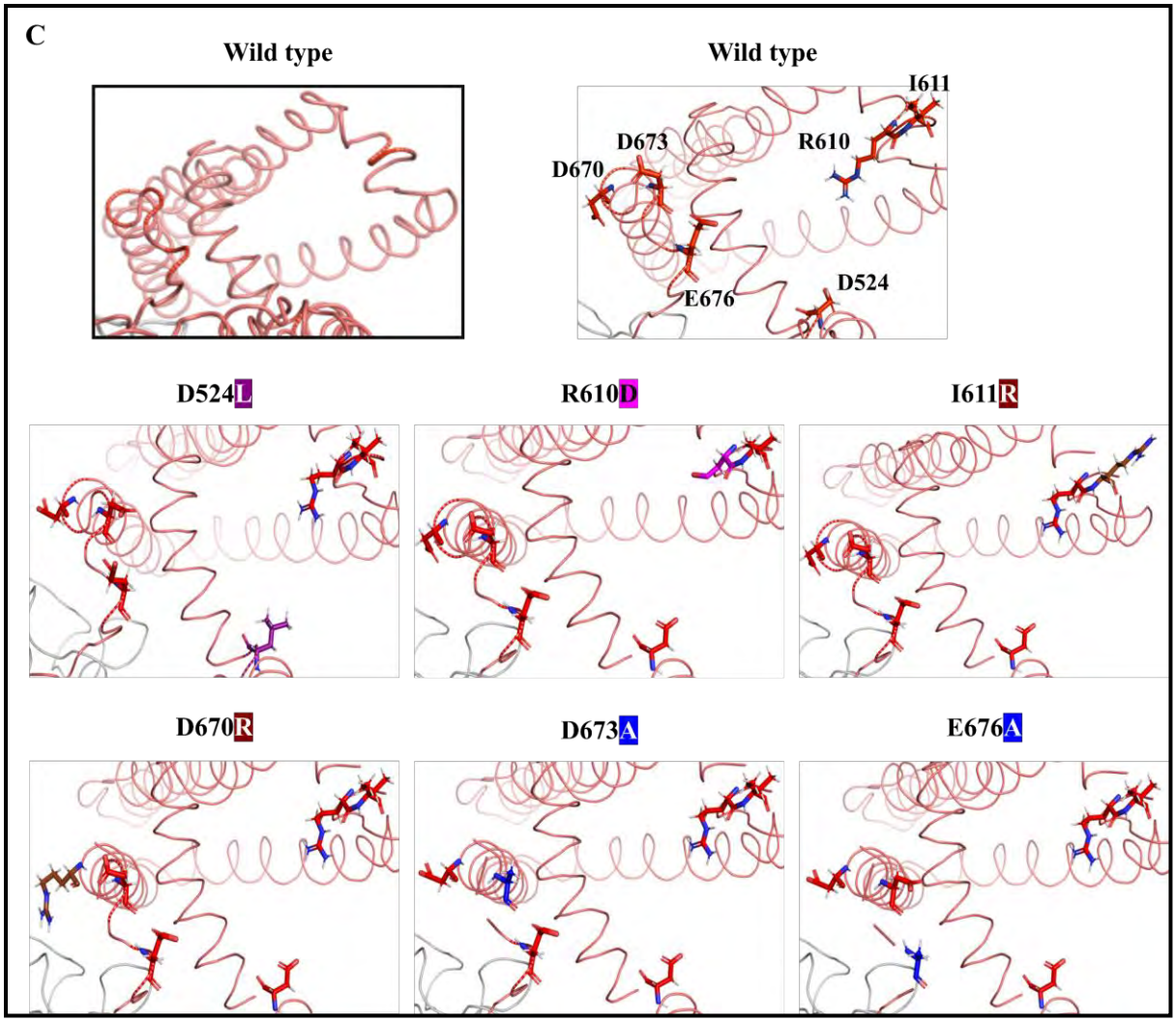

The site-specific modification of single residues in MmpL7. A) MmpL7 homology model highlighting the TM and PD2 regions probed in this study. B) Individual residues in TM4/10 targeted for modification. C) Individual residues in PD2 targeted for modification. The model in ribbons coloured in grey, and only features of interest such as TM4/10 and PD2 were depicted in cartoon and coloured blue/orange and deep salmon respectively. All the modified residues are coloured.

Appendix 14

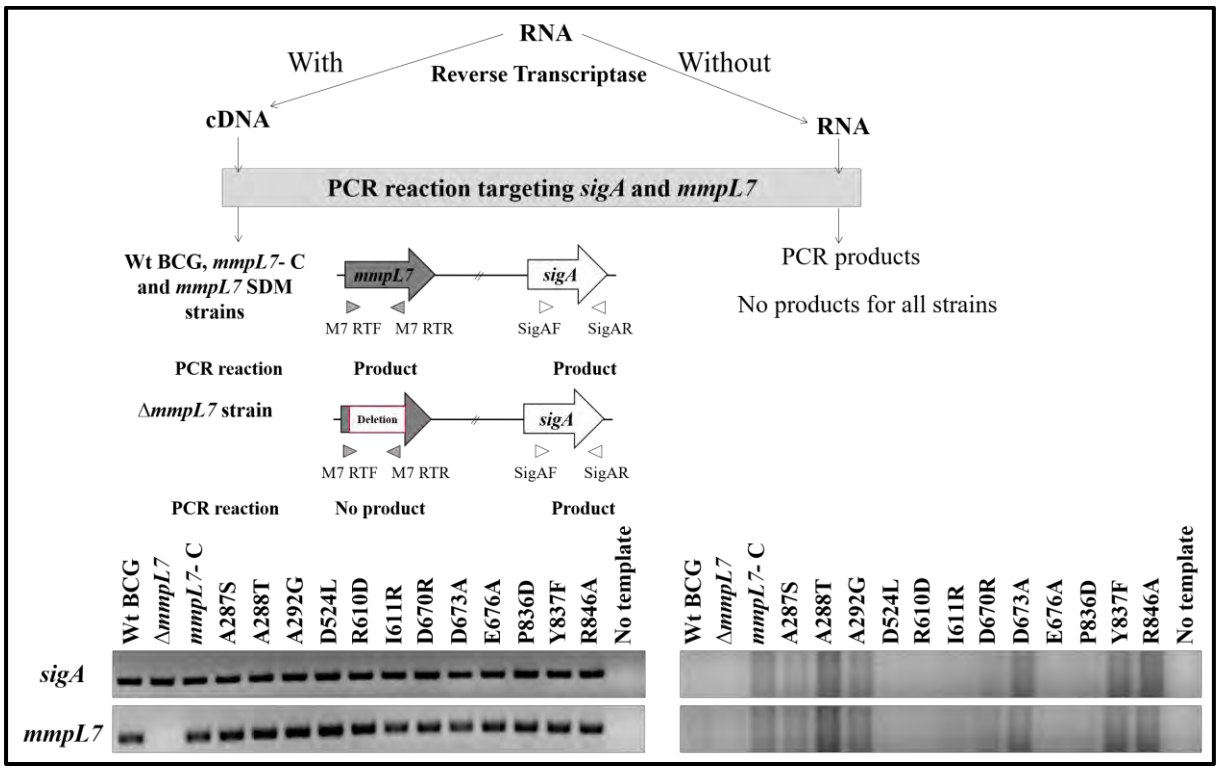

Reverse transcriptase- PCR analysis to confirm *mmpL7* expression. The upper panel illustrates the approach used in this study performed, as described in Chapter 6. The lower panel indicates the expression of the *mmpL7* gene in the wild type (Wt) BCG, the Δ*mmpL7* mutant and the thirteen *mmpL7* complemented strains as compared to the expression of the housekeeping gene *sigA* as a positive control. Two negative controls were used to detect DNA contamination, no reverse transcriptase samples and a no template control. [Presented as in (318)].

Appendix 15

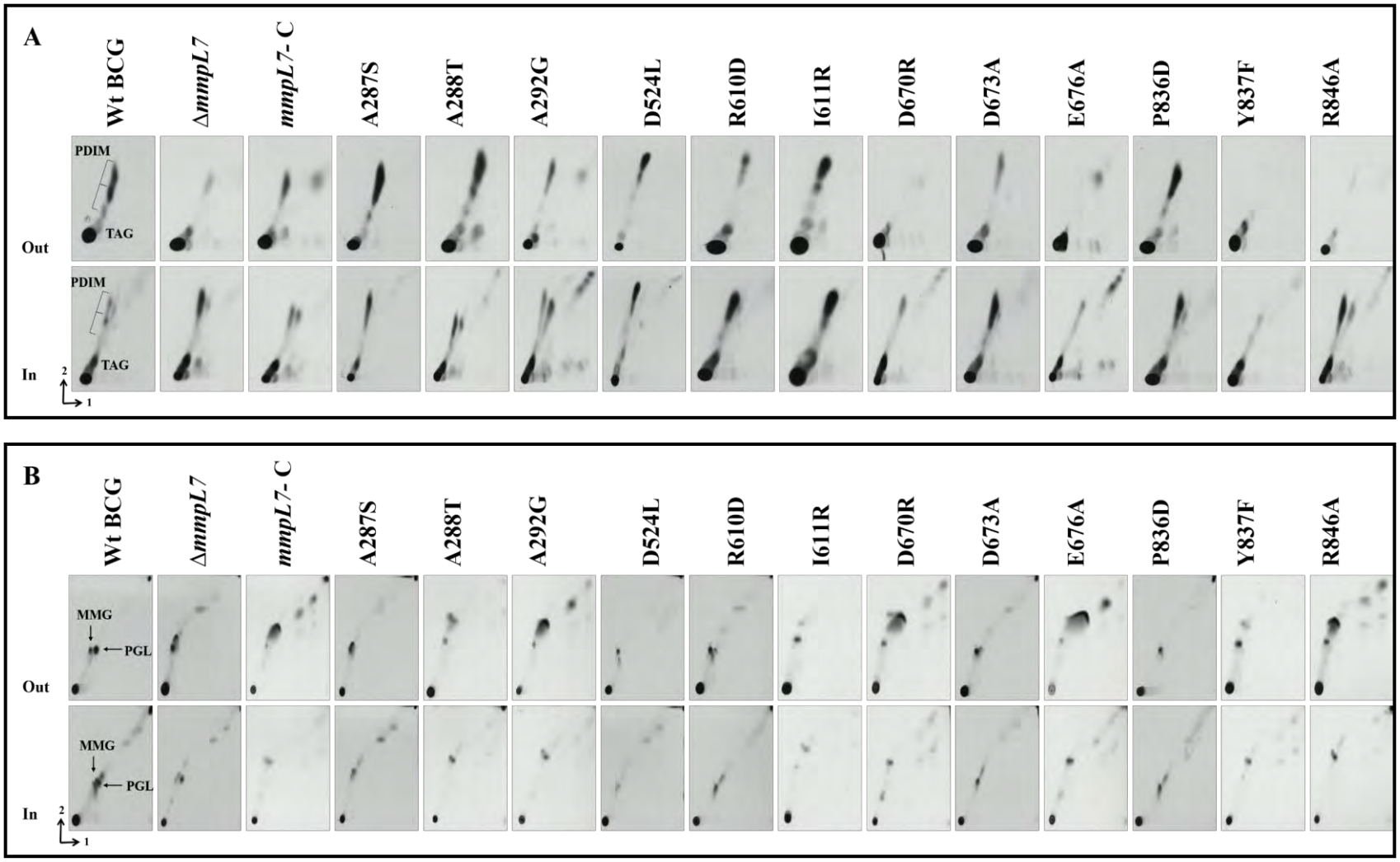
A
Wt BCG
ΔmmpL7
mmpL7- C
A287S
A288T
A292G
D524L
R610D
I611R
D670R
D673A
E676A
P836D
Y837F
R846A
PDIM
TAG
Out
In
2
1
B
MMG
PGL

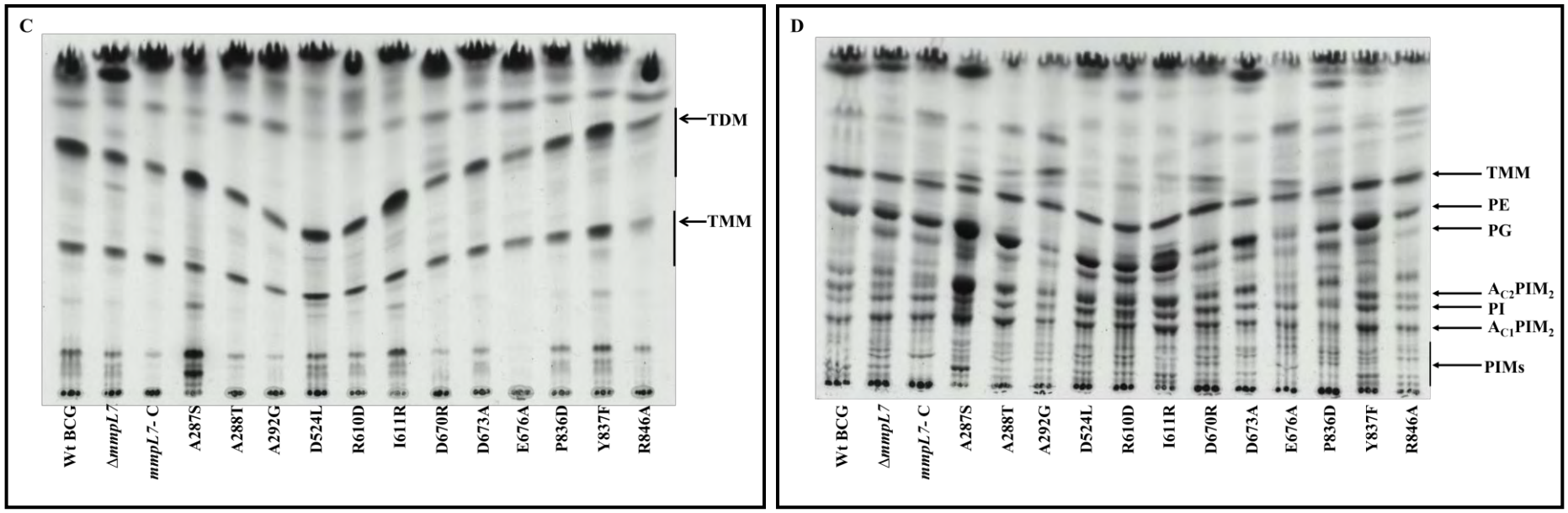

[^{14}C]-acetate analysis of *mmpL7* SDM mutants. A) PDIM, B) PGL, C) Total apolar and D) Polar lipids. Autoradiography of [^{14}C]-acetate labelled lipids from Wild type (Wt), Δ*mmpL7* Mutant and the 13 *mmpL7* complemented strains. Apolar and polar lipids were extracted from the culture filtrate (Out) and intracellular lipids (In). For PDIM/PGL analysis, apolar lipids were separated using Systems A/C on 2D TLC. Intracellular total apolar and polar lipids were separated using chloroform: methanol: water (80:20:2 v/v) and chloroform: methanol: water: ammonium hydroxide (65:25:3.6:0.5 v/v) respectively on TLC (1D). The three-pointed bracket shows the PDIM species and PGL, TDM, TMM and phospholipids are all depicted by an arrow. TAG, triacylglycerol; MMG (monomycolylglycerol); TMM, trehalose monomycolate, TDM, trehalose dimycolate; PE, phosphatidylethanolamine; PG, phosphatidylglycerol; PI, phosphatidylinositol; PIM (phosphatidyl-myo-inositol-mannosides); AcxPIMx, acylated PIM.

Appendix 16

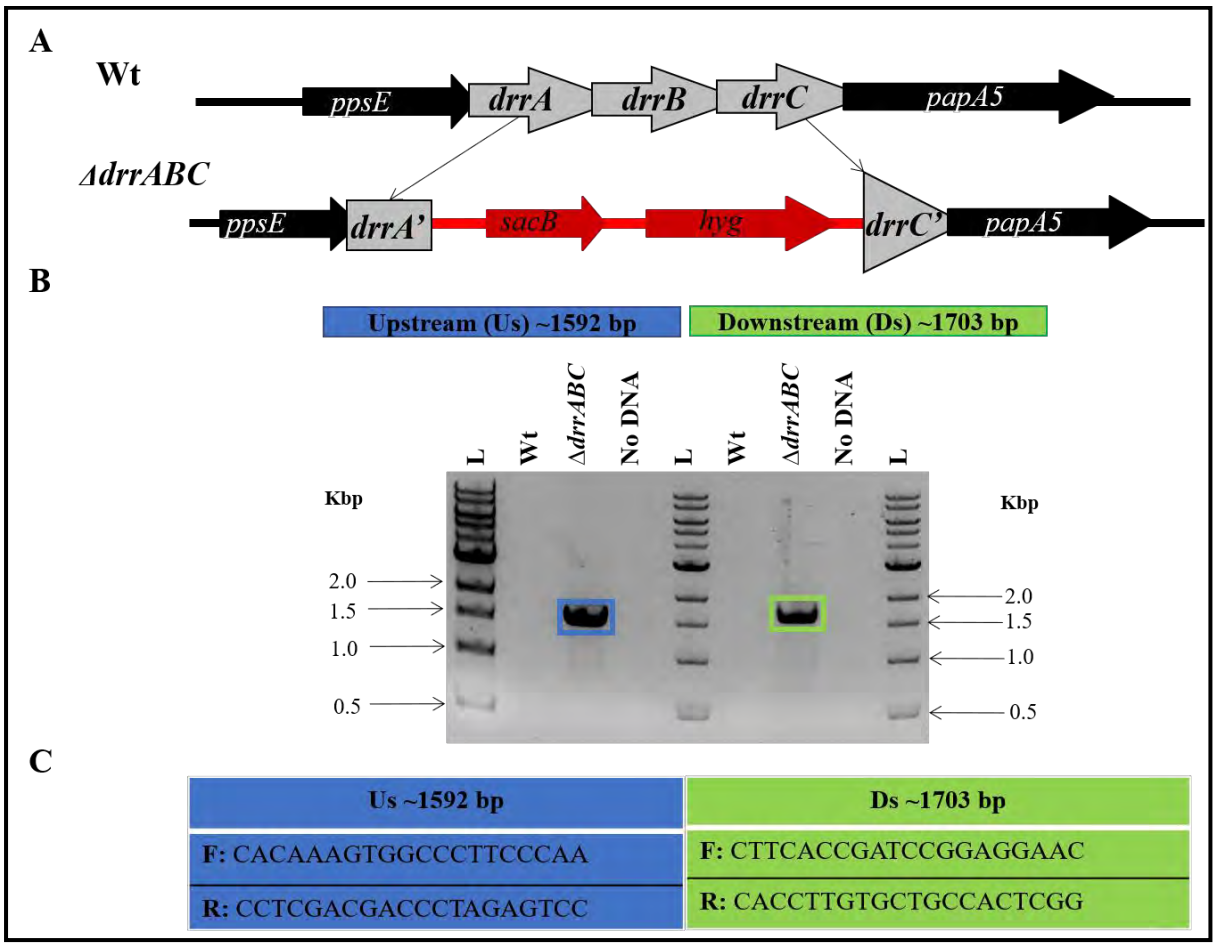

PCR verification of the Δ*drrABC* mutant in BCG. A) Genetic context of *drrABC* in wild type (Wt) BCG and the mutant strains. B) PCR amplification of genomic DNA from the Wt BCG strain and one transductant using C) upstream and downstream primers. No PCR products were expected for Wt BCG and the no DNA template (negative control). Upstream PCR amplicons for the Δ*drrABC* mutant was about 1592 bp and downstream was about 1703 bp as outlined by green and blue boxes.

Appendix 17

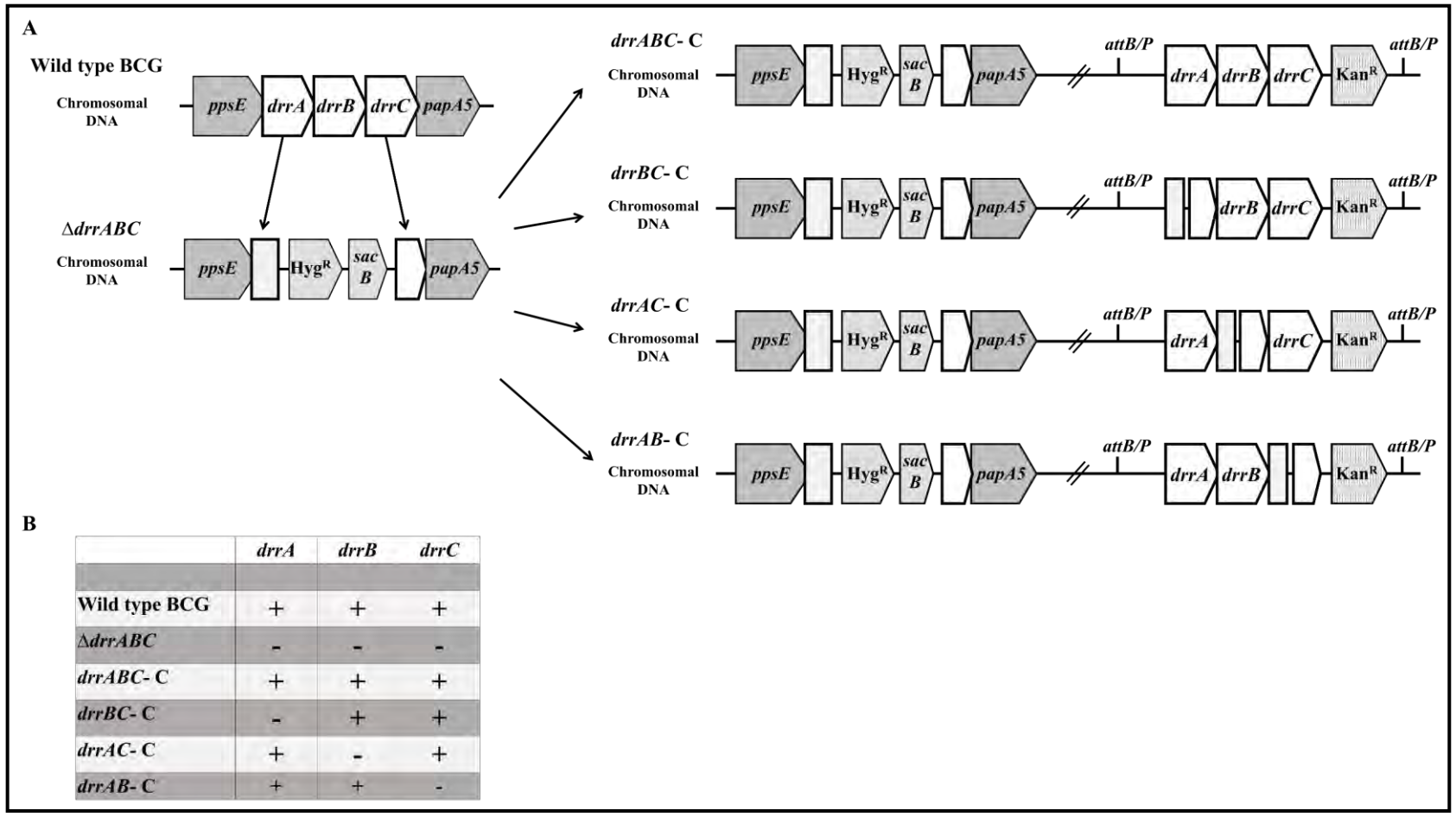

B

	drrA	drrB	drrC
Wild type BCG	+	+	+
ΔdrrABC	-	-	-
drrABC- C	+	+	+
drrBC- C	-	+	+
drrAC- C	+	-	+
drrAB- C	+	+	-

Diagrammatic representation of the A) genetic arrangement of the strains generated in this study with a B) tabularized summary of *drrA/B/C* genes present/ absent in all strains used in Chapter 4.

Appendix 18

A

	DrrB Sp	DrrB Mtb	DrrC Mtb
DrrB Sp	100	24.9	21.32
DrrB Mtb	24.9	100	26.4
DrrC Mtb	21.32	26.4	100

B

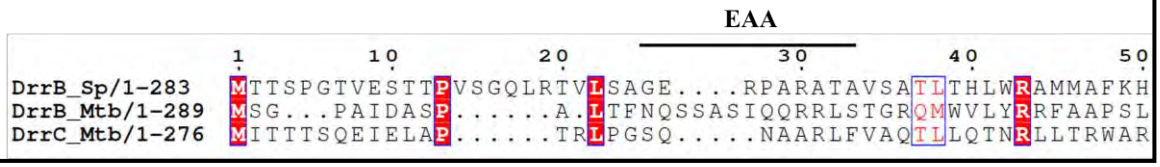

Sequence analysis of mycobacterial DrrB/C with DrrB Sp. A) Percent identity matrix between DrrB/C from Mtb and DrrB from Sp. B) Multiple sequence alignment indicating the EAA motif. Uniprot accession number of each protein, DrrB_Mtb (P9WG23), DrrC_Mtb (P9WG21) and DrrB_Sp (P32011).

Appendix 19

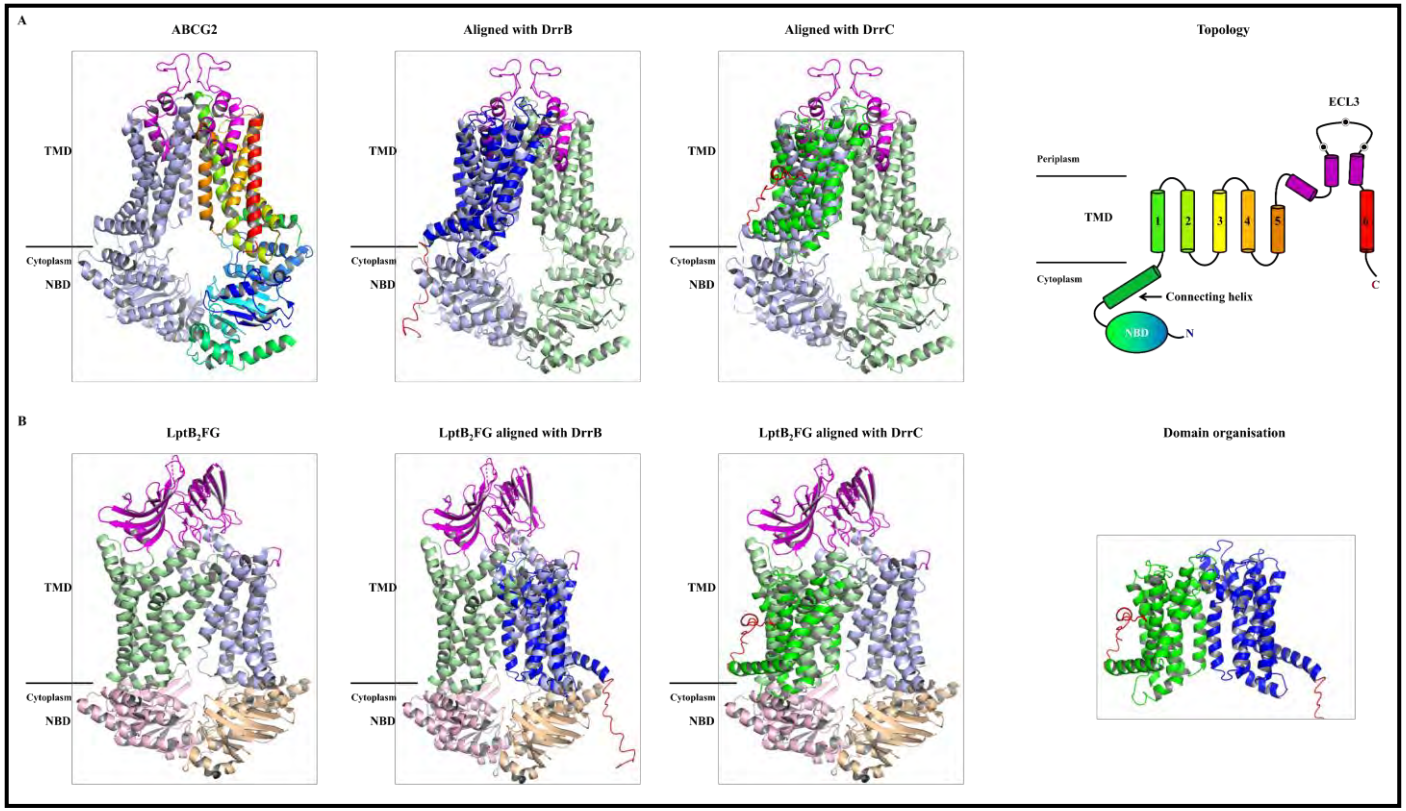

Structural alignments of *in silico* models of DrrB and DrrC each with A) eukaryotic ABCG2 multidrug exporter (5NJ3) and B) prokaryotic lipopolysaccharide transporter $LptB_2FG$ (5X5Y). One half of ABCG2 is coloured in rainbow spectrum starting from the N terminus (blue) to the C terminus (red) that corresponds to the ABCG2 topology. ABCG2 monomers and LptF and LptG are coloured pale green and light blue respectively. LptB that represents the NBD coloured wheat and light pink. The extracellular domains are coloured magenta in ABCG2 and $LptB_2FG$. The black dots in EL3 represent three cysteine residues. Mycobacterial DrrB and DrrC are coloured blue and green respectively, and both the N terminals tails highlighted in red.

Appendix 20

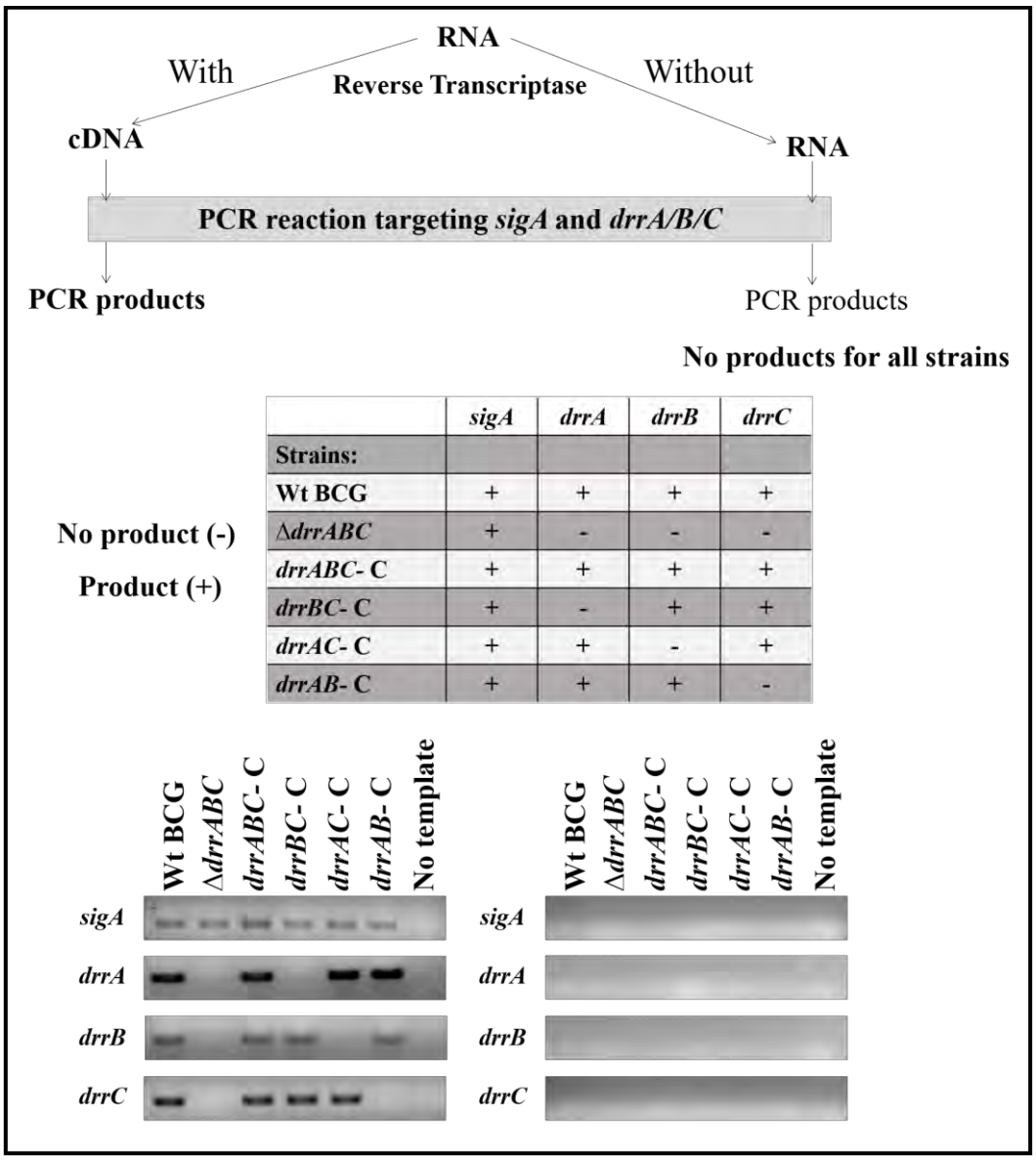

	sigA	*drrA*	*drrB*	*drrC*
Strains:				
Wt BCG	+	+	+	+
Δ*drrABC*	+	-	-	-
***drrABC*- C**	+	+	+	+
***drrBC*- C**	+	-	+	+
***drrAC*- C**	+	+	-	+
***drrAB*- C**	+	+	+	-

Reverse transcriptase- PCR analysis to confirm *drrA*, *drrB* and *drrC* expression. The upper panel illustrates the approach used in this study performed, as described in Chapter 6. The lower panel indicates the expression of individual *drr* genes in the wild type (Wt) BCG, the Δ*drrABC* mutant and the four complemented strains as compared to the expression of the housekeeping gene *sigA* as a positive control. Two negative controls were used to detect DNA contamination, no reverse transcriptase samples and a no template control. [Presented as in (318)].

Appendix 21

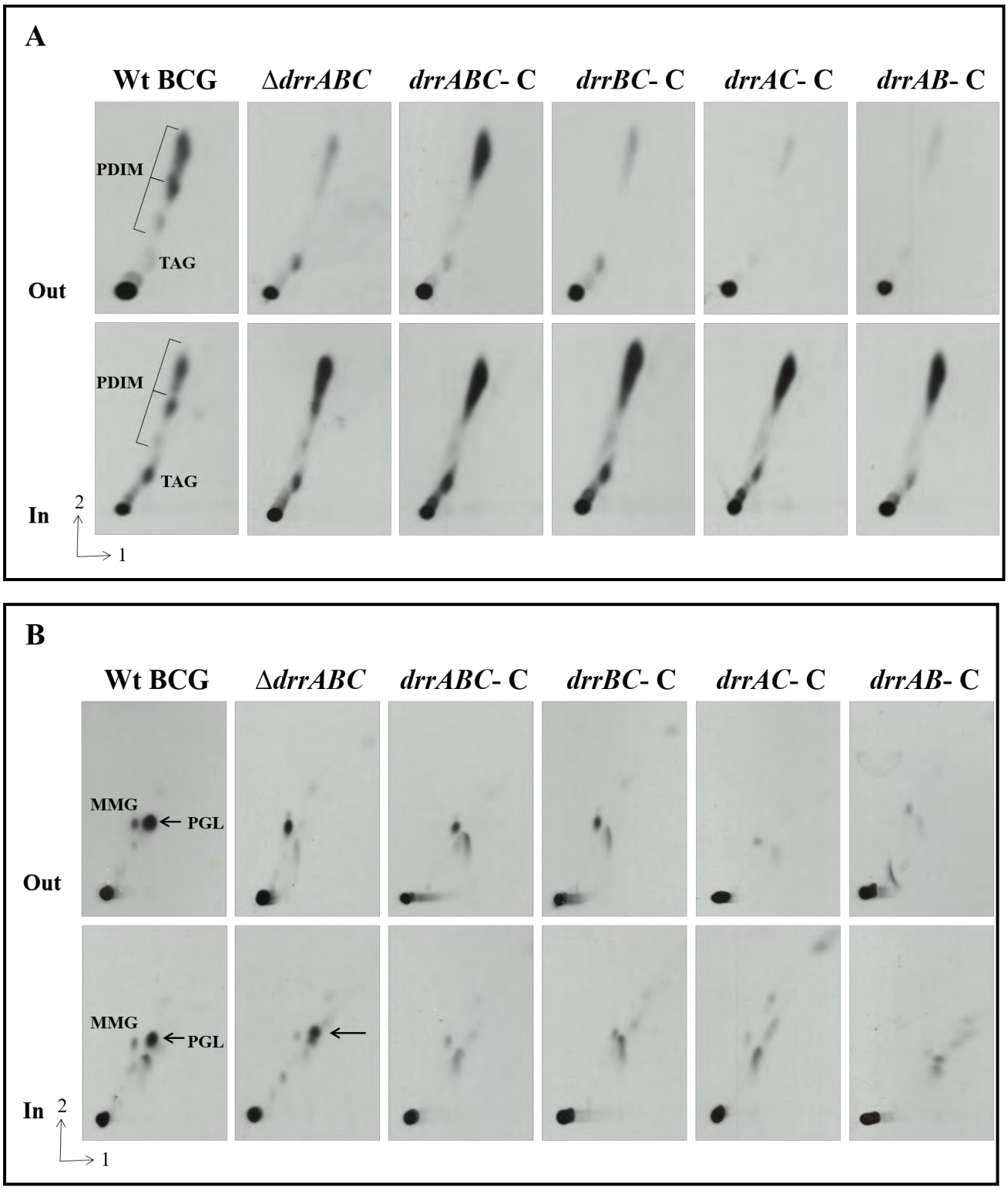
A
Wt BCG
ΔdrrABC
drrABC- C
drrBC- C
drrAC- C
drrAB- C
PDIM
TAG
Out
PDIM
TAG
In
2
1
B
Wt BCG
ΔdrrABC
drrABC- C
drrBC- C
drrAC- C
drrAB- C
MMG
PGL
Out
MMG
PGL
In
2
1

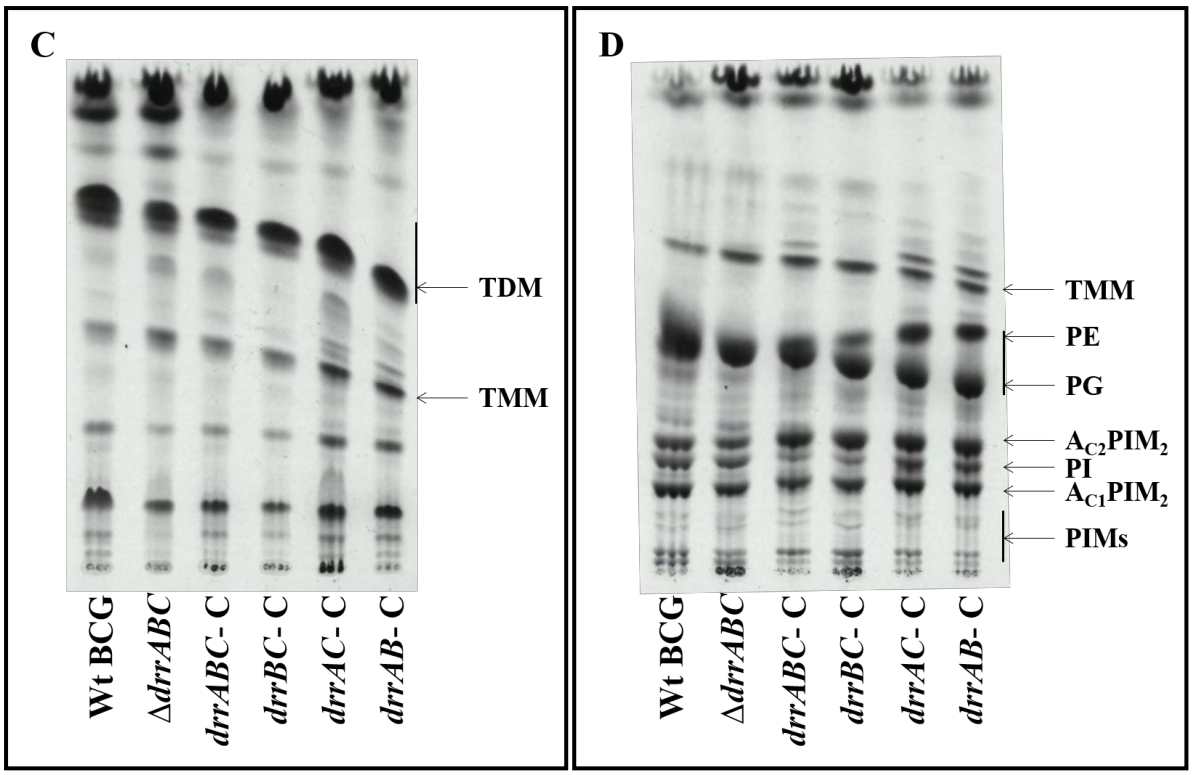

[^{14}C]-acetate analysis of the various *drr* complemented strains. A) PDIM, B) PGL, C) Total apolar and D) Polar lipids. Autoradiography of [^{14}C]-acetate labelled lipids from Wild type (Wt), Δ*drrABC* mutant and the four *drr* complemented strains. Apolar and polar lipids were extracted from the culture filtrate (Out) and intracellular lipids (In). For PDIM/PGL analysis, apolar lipids were separated using Systems A/C on 2D TLC. Intracellular total apolar and polar lipids were separated using chloroform: methanol: water (80:20:2 v/v) and chloroform: methanol: water: ammonium hydroxide (65:25:3.6:0.5 v/v) respectively on TLC (1D). The three-pointed bracket shows the PDIM species and PGL, TDM, TMM and phospholipids are all depicted by an arrow. TAG, triacylglycerol; MMG (monomycolylglycerol); TMM, trehalose monomycolate, TDM, trehalose dimycolate; PE, phosphatidylethanolamine; PG, phosphatidylglycerol; PI, phosphatidylinositol; PIM (phosphatidyl-myo-inositol-mannosides); AcxPIMx, acylated PIM.

Appendix 22

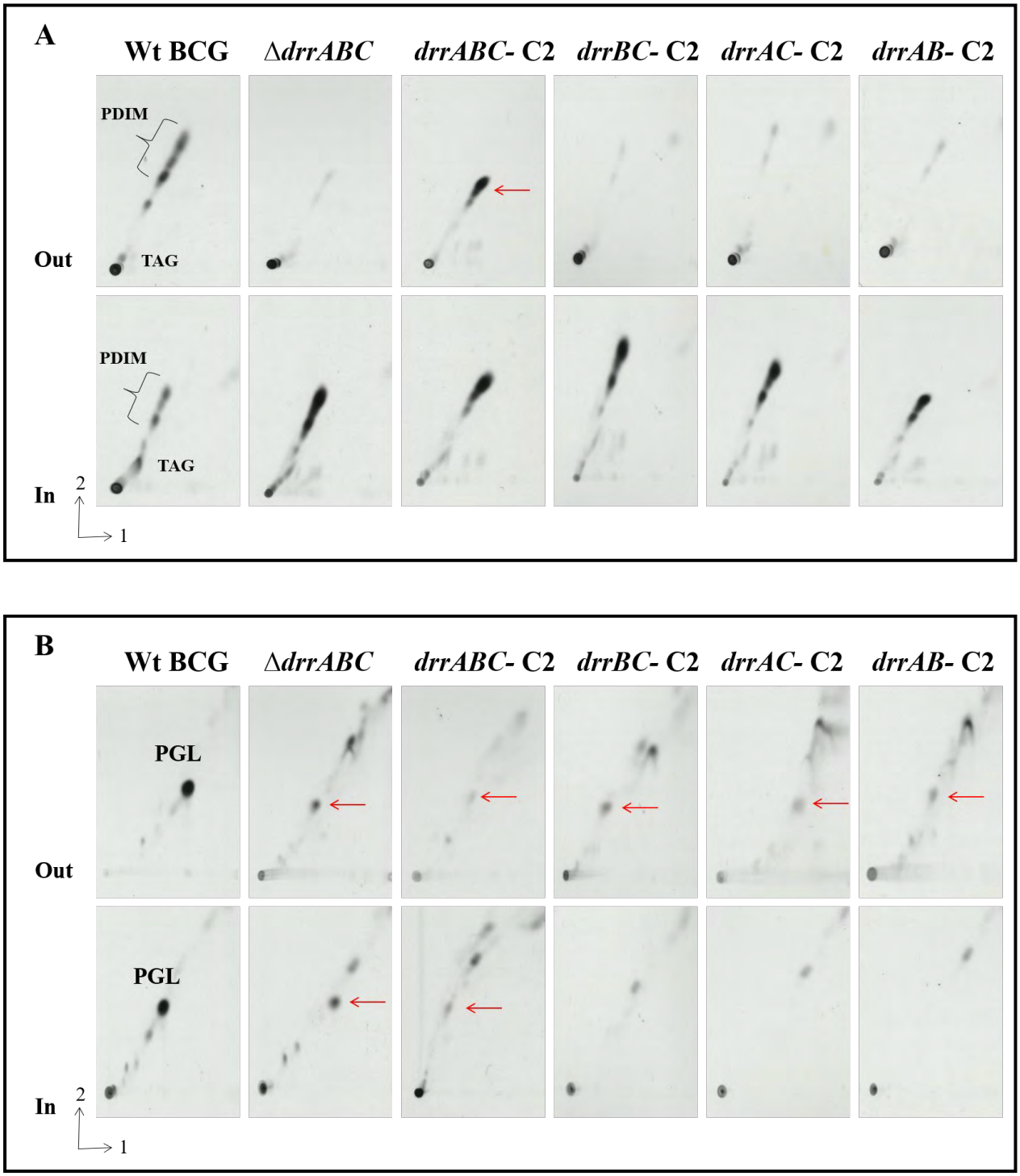

Functional analysis of another set of *drr* complemented strains. A) PDIM and B) PGL. 2D TLC autoradiography of [^{14}C]-propionate labelled lipids from Wild type (Wt), Δ*drrABC* mutant and another set of 4 complemented strains (C2). Apolar lipid extracts from the culture filtrate (Out) and intracellular lipids (In) were separated using System A/C. The three-pointed bracket shows the PDIM species while the arrow depicts the presence of PGL.